Author:
Rowsell, Ben J S

Title:
Iron-Catalysed Cross-Couplings of Organoboron Reagents

Iron-Catalysed Cross-Couplings of Organoboron Reagents

Benjamin J. S. Rowsell

A thesis submitted to the University of Bristol in accordance with the requirements for the award of the degree of Doctor of Philosophy in the Faculty of Science.

School of Chemistry

May 2022

Abstract

Transition metal-catalysed cross-coupling reactions are a powerful method for the formation of new C–C bonds. Whilst palladium-based catalysts are ubiquitous in these reactions, they have some disadvantages compared to more earth abundant metals. Palladium is scarce, and thus expensive, while its extraction is environmentally deleterious. Due to these reasons, there has been an array of efforts to replace palladium with cheap, sustainable, and non-toxic earth abundant metals, such as iron.

Iron-catalysed cross-coupling reactions have been well developed over the last 20 years and in particular Kumada and Negishi type reactions have had a large amount of success. However, organozinc reagents are moisture sensitive, stannanes are highly toxic, and Grignard reagents have a limited functional group tolerance. Due to these reasons, organoboron cross-coupling partners have become a focal point of metal-catalysed cross-coupling reactions.

There have been significant developments in iron-catalysed Suzuki aryl-alkyl cross-coupling reactions, but limited success where this is applied to biaryl formation. The work discussed in Chapter 2 describes the development and optimisation of an iron-catalysed Suzuki biaryl cross-coupling reaction. Compared to previously reported iron-catalysed Suzuki biaryl cross-coupling reactions, the work described does not require the use of a directing group. Building on the development of the iron-catalysed Suzuki biaryl cross-coupling reaction, the work discussed in Chapter 3 describes an in-depth mechanistic study of the reaction, where a simplified and tentative mechanism is proposed.

The transition metal-catalysed carboboration of alkenes is an elegant and effective way to difunctionalise a cheap and abundant starting material, namely alkenes. The process allows for the formation of up to two stereocentres, and not only forms highly desirable C–C bonds, but also installs a boron group that can be used for further functionalisation and diversification. Whilst palladium-, nickel-, and copper-catalysed carboboration of alkenes have been widely reported, only one example of an iron-catalysed carboboration of alkenes has been reported so far. The work discussed in Chapter 4 describes the development and optimisation (through OVAT and DoE approaches) of an iron-catalysed carboboration of alkenes. The functional group tolerance of the reaction is also investigated through a robustness screen and a substrate scope.

Acknowledgments

First of all, I'd like to thank Robin for being a fantastic supervisor and for giving me the opportunity to work on a fascinating project over the last few years. He has enabled me to grow as a research chemist and learn a lot about myself, whilst also providing me with the necessary support to succeed throughout my time in his group.

I'd also like to thank all the past and present members of the Bedford group for their friendship over the last few years. Thanks to Harry and Stephen for their mentorship when I first joined the group. Thanks to Mattia, Sanita, and Wilko for being outstanding lab mates and for all the great memories. Joe and Michael have been excellent additions to the group and have provided plenty of energy around the lab. It has also been a pleasure to work with all the visiting students over the years, particularly Gavin and Soneela. Thanks to the Bower, Pringle, and Russell groups for their friendship during my time in Bristol.

In addition to this, I must thank the Bristol Chemical Synthesis CDT. The 2017 cohort are an amazing group of people and I'm very grateful for the long-lasting friendships and all the hours we have spent together.

My time at CatSci would not have been possible without Jonathan Mosely and Alan Steven, both I must sincerely thank for giving me the chance to work at a fantastic company. The whole of the CatSci team were so welcoming and I learnt a lot during my short time there. In particular, thanks to Charlotte Dalton for all of her guidance and support during my time working with her. Hopefully our paths will cross again in the future.

One of the highlights of my time at Bristol has been the teaching and outreach activities that I have been involved in. For this I'd like to thank Karen Parrish and Tim Harrison. The outreach that is done by Bristol ChemLabS is truly amazing and the enthusiasm that Tim has for outreach is genuinely unmatched. It is clear and obvious the benefit that outreach has and the enjoyment the students have when they visit, without Tim this would not be possible.

Most importantly, I would like to thank all my family and friends for their support during my PhD, and Eliza, for her support and encouragement, what you have done for me can never be thanked enough!

Author Declaration

I declare that the work in this dissertation was carried out in accordance with the requirements of the University's Regulations and Code of Practice for Research Degree Programmes and that it has not been submitted for any other academic award. Except where indicated by specific reference in the text, the work is the candidate's own work. Work done in collaboration with, or with the assistance of, others, is indicated as such. Any views expressed in the dissertation are those of the author.

Benjamin J. S. Rowsell

University of Bristol

May 2022

Abbreviations

%oS	percentage of standard yield	**(*R*,*R*)-QuinoxP***	(*R*,*R*)-2,3-Bis(tert-butylmethylphosphino)quinoxaline
1,8-dppn	1,8-bis(diphenylphosphino)naphthalene	**2-MeTHF**	2-methyltetrahydrofuran
6Mes	1,3-bis(2,4,6-trimethylphenyl)-3,4,5,6-tetrahydropyrimidin-1-ium-2-ide	**6Pr**	1,3-bis(2,6-diisopropylphenyl)-3,4,5,6-tetrahydropyrimidin-1-ium-2-ide
7Mes	1,3-dimesityl-4,5,6,7-tetrahydro-1H-1,3-diazepin-3-ium-2-ide	**8Mes**	1,3-dimesityl-3,4,5,6,7,8-hexahydro-1,3-diazocin-1-ium-2-ide
Ac	acetyl	**acac**	acetylacetonate
Add	additive recovery	**AQ**	8-aminoquinoline amide
aq.	aqueous	**Ar**	aryl
BHT	butylated hydroxytoluene	**BINAP**	2,2′-Bis(diphenylphosphino)-1,1′-binaphthalene
bipy	2,2-bipyridine	**Bn**	benzyl
br	broad	**Bu**	butyl
cat.	catalyst	**CEP**	calculated Tolman electronic parameter
cis-dppe	*cis*-1,2-Bis(diphenylphosphino)ethylene	**Cp**	cyclopentadienyl
Cp*	1,2,3,4,5-pentamethylcyclopentadienyl	**CPME**	cyclopentyl methyl ether
Cy	cyclohexyl	**Cy-Xantphos**	9,9-Dimethyl-4,5-bis(dicyclohexylphosphino)xanthene
d	doublet	**DCE**	1,2-dichloroethane
dcype	1,2-(dicyclohexylphosphino)ethane	**depe**	1,2-(diethylphosphino)ethane
DEPT	Distortionless enhancement by polarization transfer	**DFT**	density functional theory
dipp	2,6-diisopropylphenyl	**DMA**	dimethylacetamide
DME	dimethoxyethane	**DMF**	dimethylformamide
dmpe	1,2-(dimethylphosphino)ethane	**DMSO**	dimethylsulfoxide
DoE	design of experiments	**dpbz**	1,2-(diphenylphosphino)benzene
dppe	1,2-(diphenylphosphino)ethane	**dppp**	1,3-(diphenylphosphino)propane
dppt	3,4-(diphenylphosphino)thiophene	**dtbbpy**	4,4′-Di-*tert*-butyl-2,2′-dipyridyl
dvtms	1,3-divinyltetramethyldisiloxane	**E**	electrophile
e.r.	enantiomeric ratio	**EI**	electron ionisation

EPR	electron paramagnetic resonance	**eq.**	equivalents
ESI	electrospray ionisation	**Et**	ethyl
GC	gas chromatography	**GCMS**	gas chromatography mass spectrometry
h	hour	**HMDS**	bis(trimethylsilyl)amide
HMPA	hexamethylphosphoramide	**HRMS**	high resolution mass spectrometry
ICP-MS	inductively coupled plasma mass spectrometry	**IMe·HCl**	1,3-dimethylimidazolium chloride
IMes	1,3-bis-(2,4,6-trimethylphenyl)imidazol-2-ylidene	**IMes·HCl**	1,3-dimesitylimidazolium chloride
IMes^{Me}·HCl	1,3-dimesityl-4,5-dimethylimidazolium chloride	**INap·HCl**	1,3-bis(2,7-diisopropylnaphthalen-1-yl)imidazolium chloride
^{i}Pr	*iso*-propyl	**IPr**	1,3-bis-(2,6-diisopropylphenyl)imidazol-2-ylidene
IPr·HCl	1,3-bis(2,6-diisopropylphenyl)imidazolium chloride	**IR**	infra-red
IXyl(2,6)·HCl	1,3-(2,6-dimethylphenyl)imidazolinium chloride	***J***	coupling constant
k	rate constant	**L**	ligand
M	molar	**m/z**	mass to charge ratio
M$^+$	parent molecular ion	**Me**	methyl
MeCN	acetonitrile	**Mes**	mesityl
mM	millimolar	**mol**	mole
MS	mass spectrometry	**MTBE**	methyl tert-butyl ether
NBP	*N*-Butyl-2-pyrrolidone	**NHC**	*N*-heterocyclic carbenes
NMP	*N*-Methyl-2-pyrrolidone	**NMR**	nuclear magnetic resonance
NPs	nanoparticles	**Nu**	nucleophile
OVAT	one variable at a time	**p**	pentet
P(Cy)$_3$	tricyclohexylphosphine	**P(^{t}Bu)$_3$**	tributylphosphine
PEG	poly(ethylene glycol)	**phen**	phenanthroline
Pin	pinacol	**ppb**	parts per billion
PPh$_3$	triphenylphosphine	**ppm**	parts per million
q	quartet	**rds**	rate determining step
rt	room temperature	**s**	singlet
SciOPP	spin-control-intended *ortho*-phenylene bisphosphine	**SIMes**	1,3-bis-(2,4,6-trimethylphenyl)imidazol-2-ylidene

SIMes·HCl	1,3-Bis(2,4,6-trimethylphenyl)imidazolinium chloride	**SIPr**	1,3-bis-(2,6-diisopropylphenyl)imidazol-2-ylidene
SIPr·HCl	1,3-(2,6-diisopropylphenyl)imidazolinium chloride	**SIXyl(3,5)·HCl**	1,3-(3,5-dimethylphenyl)imidazolinium chloride
t	triplet	**TASF**	tris(dimethylamino)sulfonium difluorotrimethylsilicate
TBAB	tetrabutylammonium bromide	***t*Bu-Xantphos**	9,9-Dimethyl-4,5-bis(di-*tert*-butylphosphino)xanthene
TEAB	tetraethylammonium bromide	**Temp.**	temperature
TEMPO	2,2,6,6-Tetramethylpiperidinyloxyl	**Tf**	triflate
THF	tetrahydrofuran	**TLC**	thin layer chromatography
TMAB	tetramethylammonium bromide	**TMEDA**	*N*,*N*-tetramethylethylenediamine
TMS	trimethylsilane	**Tol**	tolyl
tpy	terpyridine	**trans-dppe**	*trans*-1,2-Bis(diphenylphosphino)ethylene
VTNA	variable time normalisation analysis	**X**	halide
Xantphos	4,5-Bis(diphenylphosphino)-9,9-dimethylxanthene	**XAS**	X-ray absorption spectroscopy
δ	chemical shift		

Contents

Chapter 1 Introduction

1.1 Methodology of Cross-Coupling Reactions

Transition-metal catalysed reactions have transformed the field of chemistry and have been developed into a near indispensable tool for synthetic chemists. Heterogeneous catalysts can often be found in many industrial applications, such as the Haber-Bosch process, due to the ease of catalyst separation and recyclability.[1] However, the use of homogeneous catalysis allows for unique catalyst design through the facile alteration of the catalyst's steric and electronic properties. Homogeneous transition metal-catalysed carbon-carbon bond formation has become key to a vast array of syntheses and is exploited in many fields, such as the pharmaceutical and agrochemical industries (Scheme 1.1).[2]

$$R-X \quad + \quad R'-M \quad \xrightarrow{\text{transition metal catalyst}} \quad R-R'$$

R, R' = sp, sp^2, sp^3 carbon
X = halide or pseduohalide
M = Mg, Zn, Sn, Al, B, Si etc.
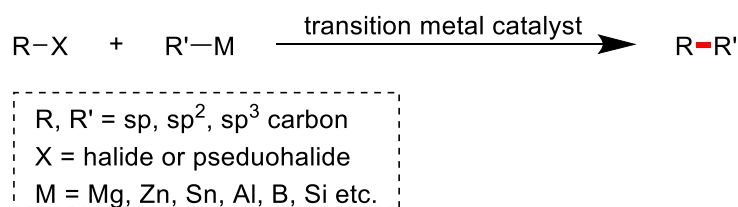
Scheme 1.1 – General scheme for cross-coupling of two different organic fragments using a transition metal catalyst.

The ability to form new C–C bonds using organohalides and an organometallic reagent in the presence of a sub-stoichiometric transition metal catalyst has changed the way chemists approach syntheses. The importance of transition metal catalysis, in particular palladium-catalysed cross-coupling, was highlighted in 2010 when Heck, Suzuki, and Negishi were awarded the Chemistry Nobel Prize.[3] Over the past 150 years, highly significant breakthroughs have occurred in the field of transition metal catalysis. Initial success was seen with copper and nickel, this was followed by palladium, which took over the field, and more recently research has also been focussed on iron-catalysis (Figure 1.1).
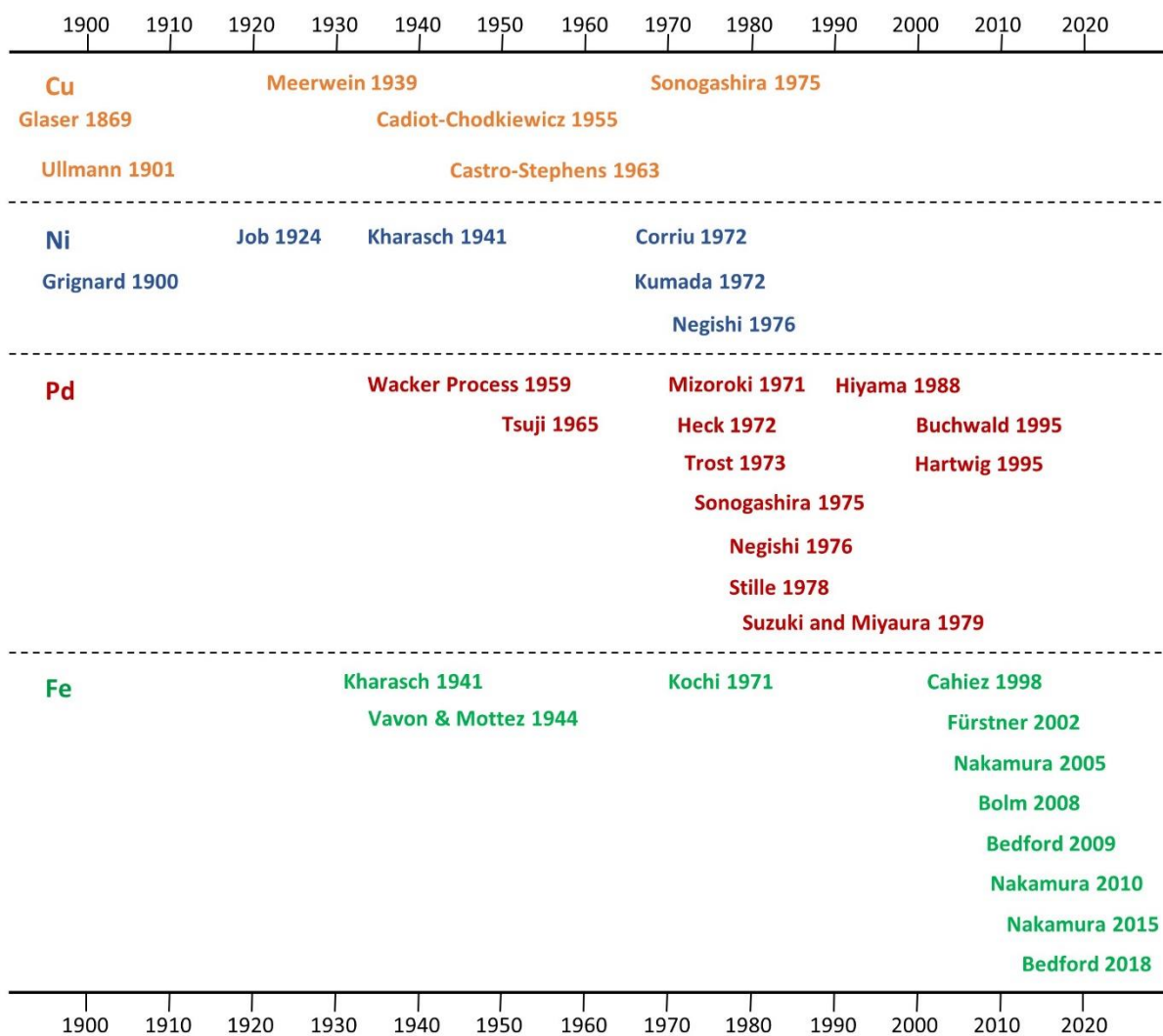
Figure 1.1 – Timeline of important breakthroughs in transition metal-catalysed cross-coupling reactions.

1.1.1 The Origin of Cross-Coupling Reactions

The seminal research published by Glaser in 1869 showed that by using stoichiometric amounts of copper he was able to homo-couple metallic acetylides, this was the first example of any metal mediated coupling (Scheme 1.2).[4,5] This work then went on to inspire future work on copper-catalysed coupling reactions; including the dimerization of 2-bromo and 2-chloronitrobenzene, promoted using super-stoichiometric amounts of copper by Ullmann in 1901 (now known as the Ullmann reaction, Scheme 1.2).[6] It is important to note that the dimerization occurred at the C-X bonds rather than unfunctionalized carbons. Ullman developed this further by using sub-stoichiometric amounts of copper to catalyse C–O bond formation.[7] However, limitations of the early work in this field included the requirement for large amounts of metal to promote the reaction, and the reactions were limited to homo-coupling.
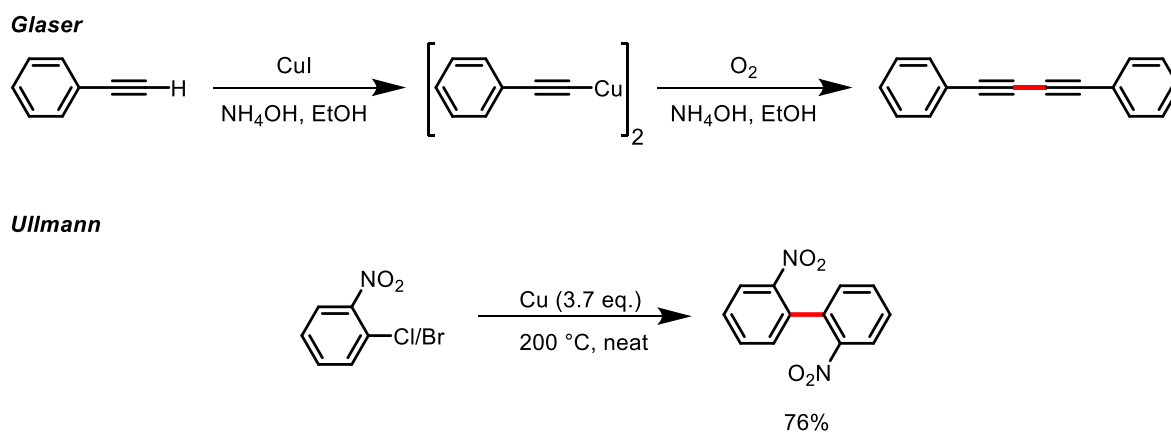
Scheme 1.2 – Early reports of metal promoted reactions: Glaser coupling[4] and Ullmann reaction.[6]

Although Job reported a $NiCl_2$ catalysed C–C bond formation in the reaction of phenylmagnesium bromide with CO, C_2H_4 and C_2H_2 in 1923, it went mostly unrecognised with the award for the first examples of C–C cross-coupling instead being given to Kharasch.[8,9] In the 1940's, Kharasch published several papers reporting transition metal-catalysed $C(sp^2)$-$C(sp^2)$ coupling using aryl Grignard reagents with organic halides. Kharasch then went on to show that he was able to cross-couple phenylmagnesium bromide with both bromobenzene and vinyl bromide to form biphenyl and styrene respectively using different metal halide salts. The key development was that two different organic groups were coupled together, unlike previous examples (Scheme 1.3).[10,11]
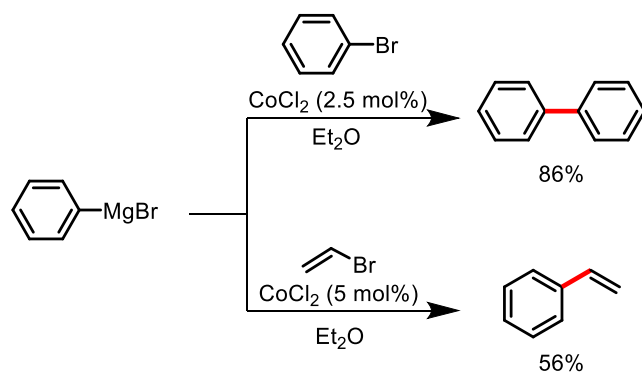
Scheme 1.3 – Co-catalysed cross-coupling demonstrated by Kharasch.[10,11]

Kharasch showed that transition metals could catalyse cross-coupling in the formation of new C–C bonds. However, the catalytic systems that both Kharasch and Meerwein then went on to publish, struggled with selectivity, with large amounts of homo- and cross-coupling observed in both cases.[12,13] This issue was later overcome in 1972 by both Corriu and Kumada who independently reported nickel-catalysed cross-coupling of aryl and alkenyl halides with Grignard reagents (Scheme 1.4).[14–16]
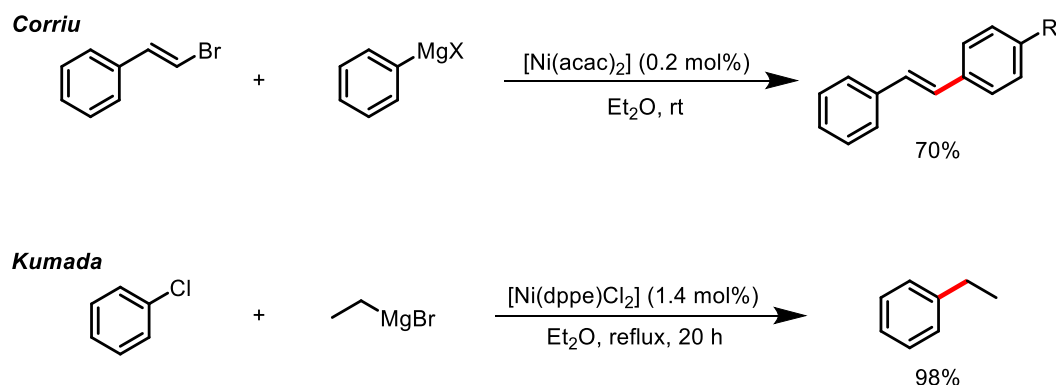
Scheme 1.4 – Ni-catalysed cross-coupling of aryl and alkenyl halides with Grignard reagents reported by Corriu[14] and Kumada.[15]

5

1.1.2 The Development and Takeover of Palladium-Catalysed Cross–Coupling Reactions

In 1968 Heck published seven papers using palladium catalysts to form new C–C bonds using arylmercury compounds, kickstarting the interest in the use of palladium catalysts.[17–23] In 1972 Heck published the coupling of styrene and iodobenzene, now known as the Heck reaction (Scheme 1.5).[24] With palladium shown to be a highly active catalyst, it began to overshadow and replace the other transition metal catalysts used at the time, namely nickel and copper. Palladium demonstrated several advantages over nickel and copper, including its ability to be used under much milder conditions than copper in acetylene cross-couplings.[25] This later led to the well-known Sonogashira reaction (Scheme 1.5).[26] In comparison, the nickel-catalysed cross-coupling of organomagnesium or organolithium reagents with organic halides led to a series of unwanted side reactions, whereas palladium was much more predictable and reliable.[27,28]

Heck

PdCl$_2$ (1 mol%)

KOAc, MeOH, 120 °C

1.25 eq.

75%

Sonogashira

[PdCl$_2$(PPh$_3$)$_2$] (0.5 mol%)

CuI (1 mol%)
Et$_2$NH, rt, 3 h

90%
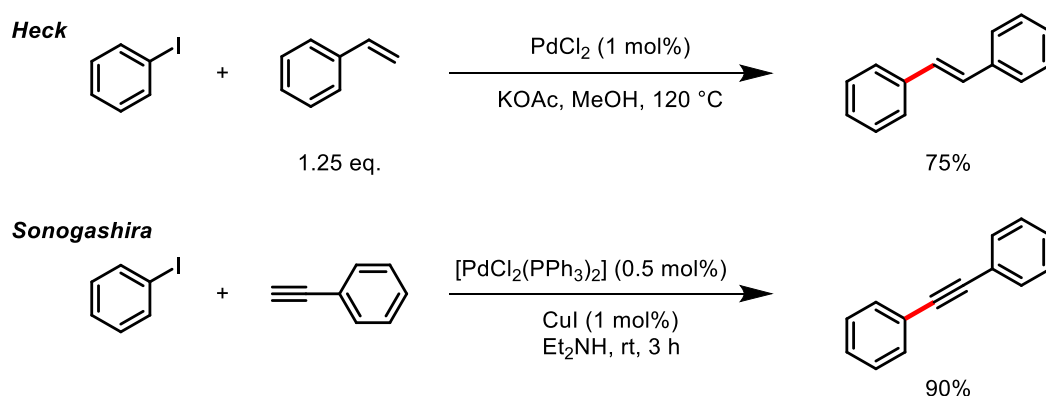
Scheme 1.5 – Examples of the Heck reaction[24] and the Sonogashira reaction.[26]

With palladium at the forefront of catalysis at this time, it paved the way to a new range of cross-coupling partners. This was due to the desire to use less electropositive metals as the organometallic species, to afford greater functional group tolerance for application in a greater number of syntheses. This led to the Stille and Negishi reactions where organostannanes and organozinc reagents were used as coupling partners respectively (Scheme 1.6).[29,30] These reactions suffered some drawbacks; the organozinc reagents utilised by Negishi were air and moisture sensitive, and therefore required special inert atmosphere handling techniques. Stille's use of organostannanes were also undesirable due to the high toxicity of tin reagents. Both of these factors limited their much-desired application in industrial processes. To take palladium-catalysed cross-coupling reactions further into the field of organic synthesis, a non-toxic, air and moisture stable cross-coupling partner with a large functional group tolerance was required.
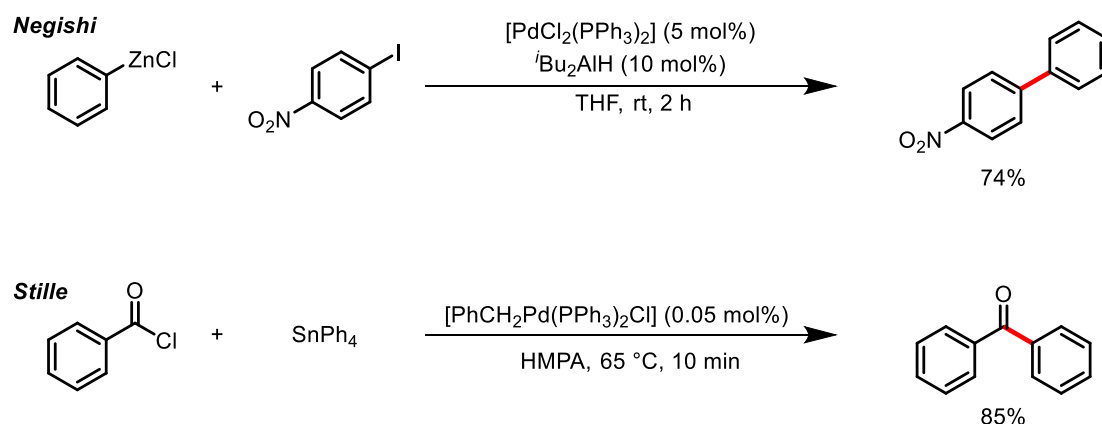
Scheme 1.6 – Examples of the Negishi reaction[30] **and the Stille reaction.**[29]

This led to the discovery of cross-coupling organoboron reagents in the presence of a palladium catalyst by Suzuki (Scheme 1.7).[31,32] This met all of the requirements above but had one minor issue; the polarity of the C–B bond was much lower compared to that of the other organometallics mentioned. This meant that a stoichiometric amount of a base, such as alkoxides, was required to activate the organoboron nucleophile. An example of an even more benign cross-coupling partner was discovered by Hiyama using organosilicon reagents (Scheme 1.7).[33]
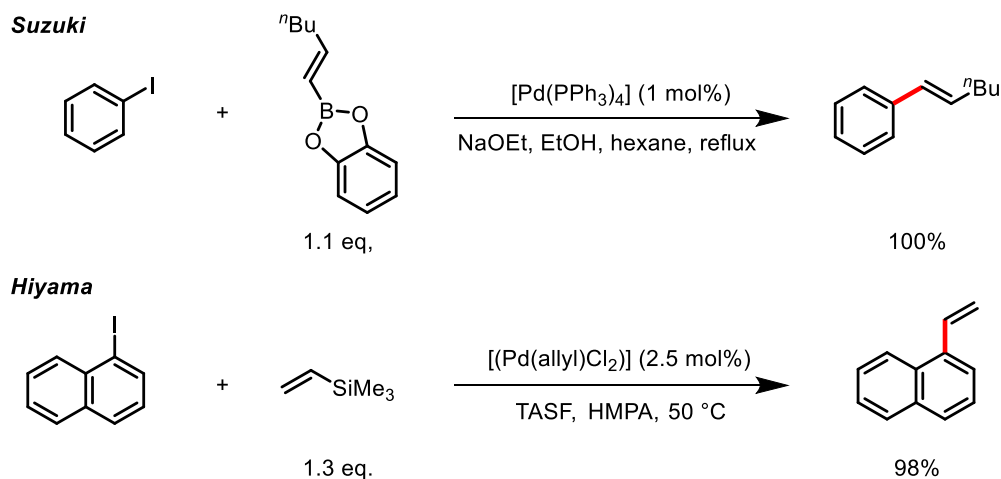
Scheme 1.7 – Examples of the Suzuki reaction[32] **and the Hiyama reaction.**[33]

Today, the Suzuki cross-coupling reaction remains a powerful synthetic tool to form new C–C bonds, in both academic and industrial procedures. A survey has reported that of all C–C bond forming reactions used in the pharmaceutical industry, 40% were Suzuki couplings and in second, with 18%, were Sonogashira couplings.[34] Highlighting the importance of palladium-catalysed cross-coupling reactions in the modern world. The Suzuki reaction has been exploited in a large

range of syntheses and has been demonstrated to be scalable and cost effective in the synthesis of intermediates for pharmaceuticals or fine chemicals (selected examples, Figure 1.2).[2,35]

Pfizer – CI-1034
Endothelin antagonist

Pfizer – Kinase inhibitor

OTBN – key intermediate
for sartan-class drugs
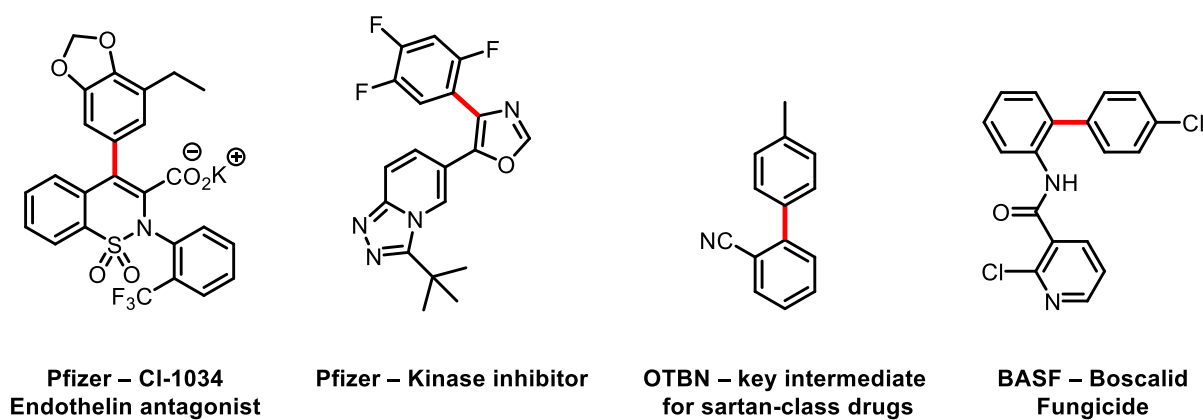
BASF – Boscalid
Fungicide

Figure 1.2 – Key industrial compounds synthesised *via* a Suzuki reaction.

1.1.3 Replacing Precious Metals in Catalysis

There is no doubt that palladium catalysts have played an exceptionally important role in synthesis as we know it today. The ability to form C–C bonds under mild conditions and with a wide functional group tolerance is highly sought after and although palladium-catalysed cross-coupling reactions offers this, there are some drawbacks. Palladium has a very low abundance in the Earth's crust (in the region of parts per trillion). Therefore, palladium is very difficult to extract and the mining of it is environmentally deleterious.[36] The low natural abundance of palladium and its use in competitive industries, such as the automotive and electronic sectors, results in it being a very expensive. Currently palladium costs £55 per gram, to put this into perspective gold costs £47/g (prices as of 31/03/22).[37] Another concern with the use of palladium is its high toxicity.[38] The pharmaceutical industry heavily relies on palladium to form new C–C bonds and therefore it requires that the products are highly purified to remove any remaining palladium. A pharmaceutical drug intended for oral consumption by humans must have a palladium concentration no higher than 10 ppm.[39] This therefore requires palladium-catalysed reactions to be carried out very early on in the synthesis, to allow thorough purification, or to use other routes altogether. This has the potential to increase the length and cost of the overall syntheses of pharmaceutical products. With these issues highlighted, it is essential to offer alternatives to these precious metal catalysts. Earth abundant metals have recently come to the forefront of metal catalysed cross-coupling reactions to offer an alternative to palladium. There has been an increased use of nickel, copper, and more recently cobalt based catalysts (Scheme 1.8).[40–42]
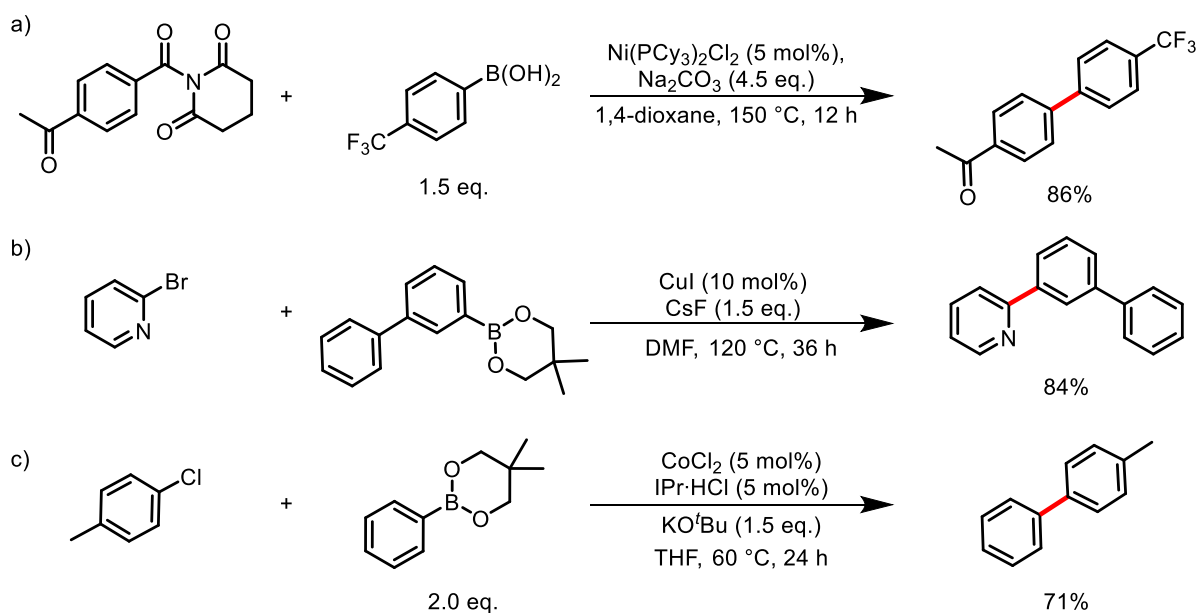
Scheme 1.8 – Examples of the alternative metal catalysed Suzuki reactions; Ni[40] (a) Cu[41] (b) and Co[42] (c).

Iron is an exceptional candidate, as an earth abundant metal, that could be used as an alternative to palladium in C–C bond formation. Iron has been used extensively in other areas of catalysis, including as a heterogeneous catalyst in the Haber-Bosch process.[1] Although iron-catalysed cross-coupling reactions were first discovered in 1944, they had mostly been overlooked until relatively recently (Figure 1.3).[43] Iron is the 4th most abundant element in the Earth's crust, it is exceptionally cheap (£0.00011/g of iron ore, price as of 31/03/22)[37] and in most cases is toxicologically benign.[38] Iron can also access a range of oxidation states (-2 to +6) and can undergo two electron transfers, classically seen with palladium catalysis, or single electron transfers.[44] The reasons stated not only make iron an ideal alternative to palladium but can also potentially allow for exciting and novel chemistry to be discovered.
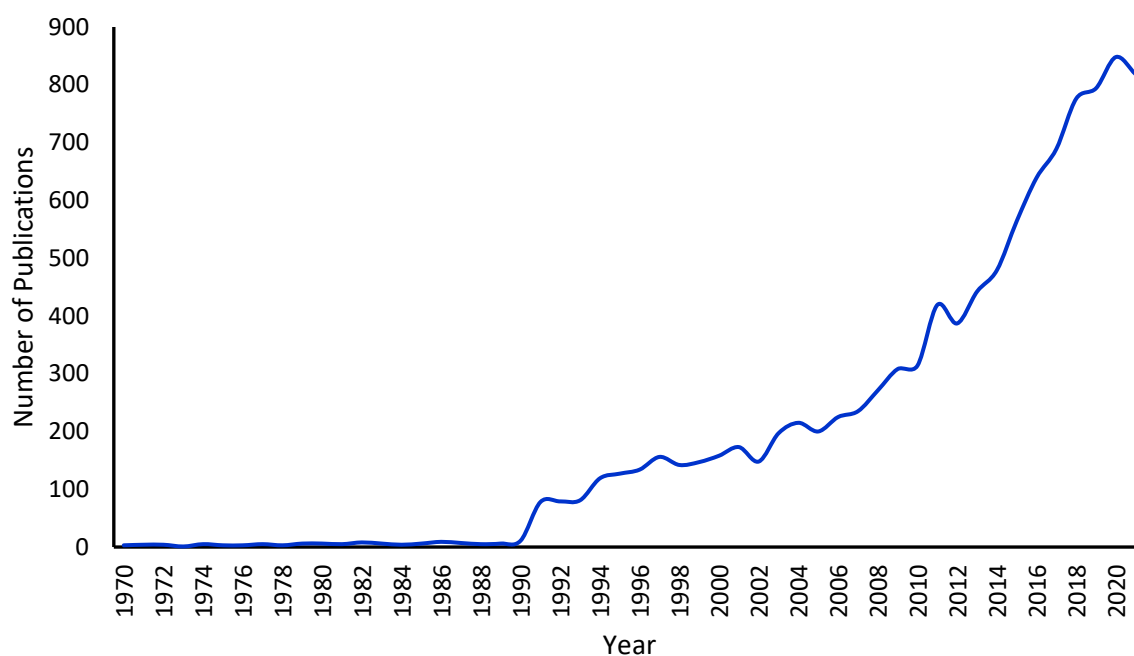

Figure 1.3 – The number of publications related to iron catalysis over time. Data gained from searching *iron catalysis* in *articles* per year using Web of Science (accessed 25/03/22).
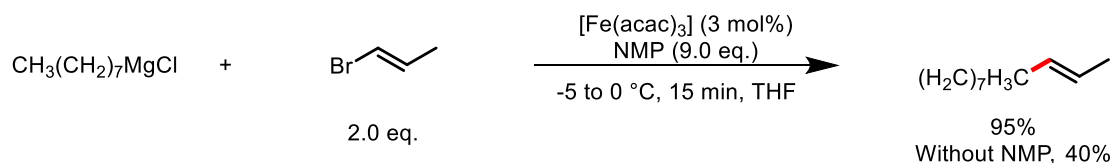
1.1.4 Iron-Catalysed Cross-Coupling Reactions

The first reported use of iron as a catalyst in a cross-coupling reaction was by Vavon and Mottez in 1944.[43] This was followed by Kochi in 1971,[45] who described the use of simple iron halide salts to cross-couple alkenyl halides with Grignard reagents (Scheme 1.9). Although this work was published before the nickel-catalysed work of Kumada and Corriu,[14,15] the academic interest was with nickel- and palladium-based catalysis instead due their success. This resulted in a dormant period for iron-catalysed cross-coupling reactions. It was not until Cahiez and Fürstner published their work on iron-catalysed cross-coupling reactions and showed that it was synthetically viable, that iron-catalysis received more attention from a wider audience (Scheme 1.9).[46,47] In 1998 Cahiez showed that using *N*-methyl-2-pyrrolidine (NMP) as a co-solvent suppressed the unwanted side reactions between Grignard reagents and alkenyl halides.[46] In this work Cahiez built upon Kochi's iron-catalysed Kumada-type reactions, and demonstrated a greater functional group tolerance, including esters, nitriles and ketones. Later, Fürstner also used NMP as a co-solvent to enable the iron-catalysed cross-coupling of alkyl or aryl Grignard reagents with aryl or heteroaryl chlorides, the reaction was able to proceed under very mild conditions and tolerate a large number of functional groups.[47] These reports outlined the exciting prospects of iron-catalysed cross-coupling reactions as they were able to use cheap, abundant, and benign iron salts to cross-couple with aryl chlorides.
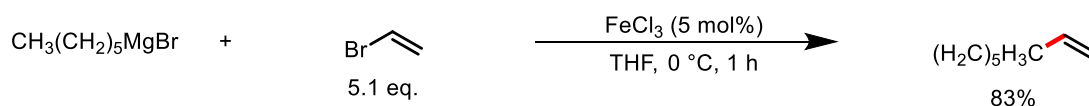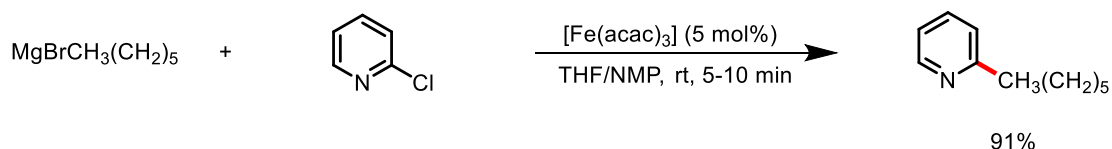

Scheme 1.9 – Early examples of iron-catalysed cross-coupling reactions; Kochi,[45] Cahiez,[46] and Fürstner.[47]

Developments from this early work led to a range of iron-catalysed Kumada, Negishi, and Suzuki reactions. Iron-catalysed Kumada cross-coupling of aryl Grignard reagents with alkyl halides only produced small quantities of the alkene side products from β-elimination.[48] Neidig has also reported that when NHC ligands are used, the amount of β-elimination observed changes dependent on the bulk of the ligand.[49] Specifically, the bulk of the 'wingtips' on the NHC are important to the stabilisation of Fe(II) species. When IPr or SIPr are used an Fe(II) species is able to be isolated, whereas when IMes and SIMes were used, a reduced Fe(0) species was instead isolated. Comparatively, in palladium catalysis, β-elimination can occur rapidly and leads to larger quantities of undesired side products.[50] A variety of examples of iron-catalysed Kumada cross-couplings have been published by numerous groups, including Hayashi,[51] Nakamura,[52] Fürstner,[53] and Bedford (Scheme 1.10).[48,54]
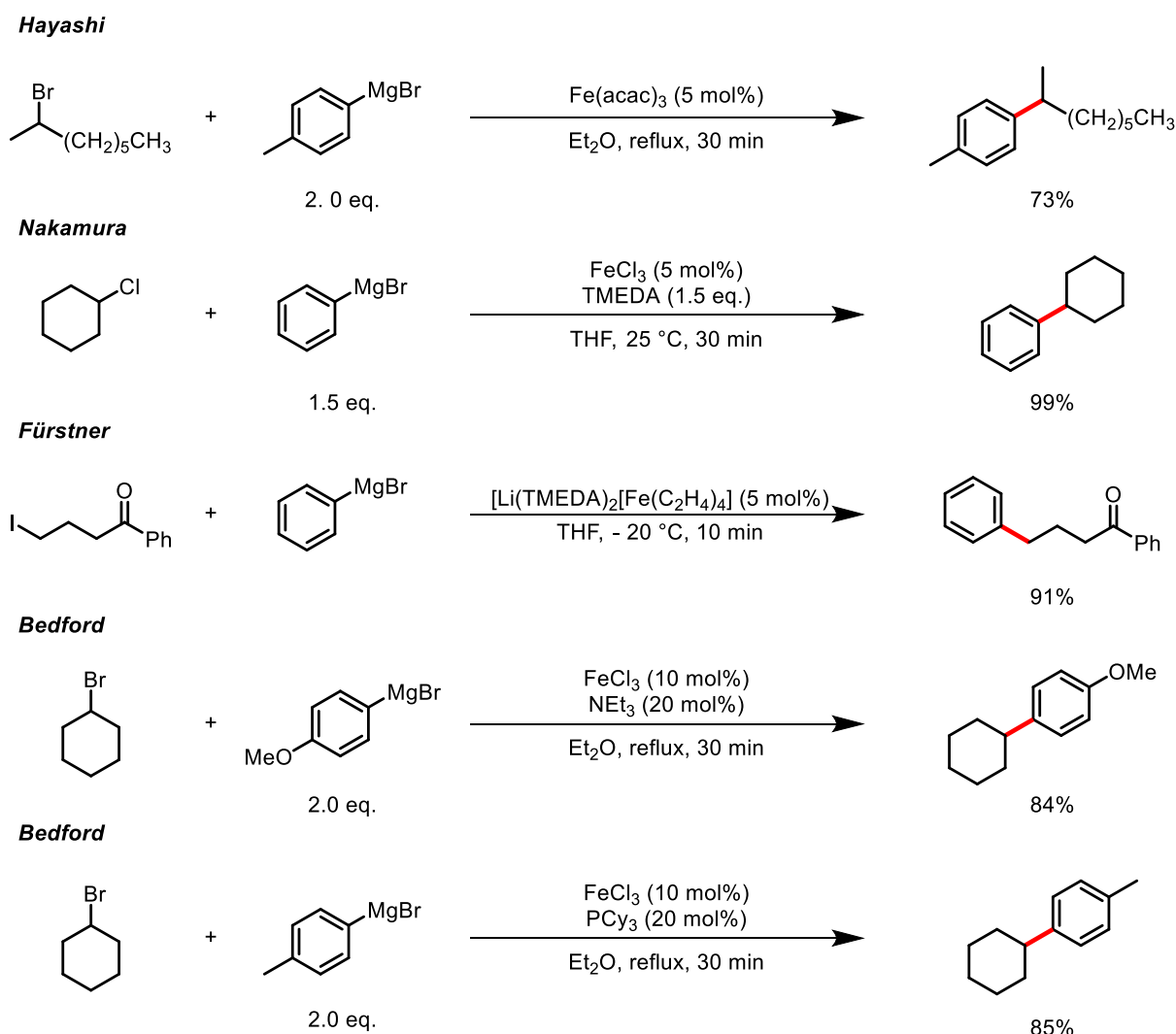
Scheme 1.10 – Examples of iron-catalysed Kumada cross-coupling reactions.

Further developments of iron-catalysed Kumada reactions utilising flow conditions,[55,56] additives such as alkoxide magnesium salts,[57] low catalyst loadings (as low as 0.025 mol%),[58] and new ligand designs[59,60] have since been reported. For example, Neidig recently developed a catalytic system for Kumada couplings using simple dilithium diamide ligands.[60] Noting that tetramethylethylenediamine (TMEDA) is susceptible to ligand displacement and the subsequent Fe species is susceptible to over-transmetallation, Neidig hypothesised that this ligand type is ideal due to the ease of synthesis and the fact that the driving force of formation of the lithium halide salt could promote complexation to the starting iron salt. The iron pre-catalyst was competent in the cross-coupling of aryl Grignard reagents with alkyl electrophiles or alkyl Grignard reagents with aryl electrophiles. The former is not possible to couple when NMP is employed, and therefore this represents the first step towards a potential universal ligand for iron-catalysed Kumada cross-coupling reactions. The reason for the observed reactivity is believed to be due to the stronger coordination of the ligand compared to TMEDA. This coordination prevents over-transmetallation and the formation of a triarylferrate dimer,[61] which has been shown to be unreactive with alkyl bromides.[61]
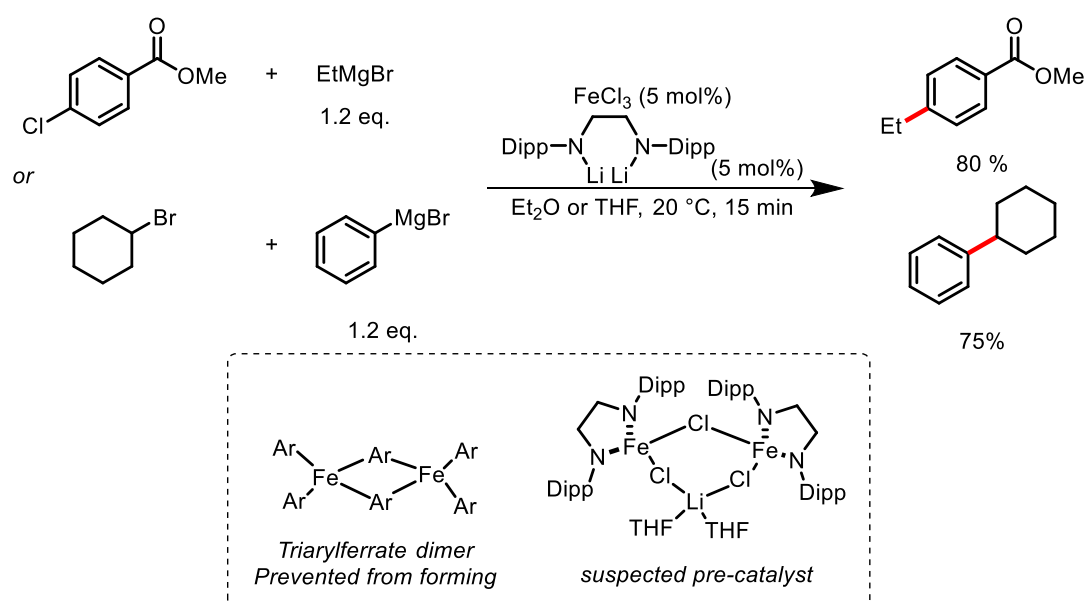
Scheme 1.11 – Iron-catalysed Kumada cross-coupling reaction using a dilithium diamide ligand.[60]

With the iron-catalysed cross-coupling reactions of Grignard reagents in Kumada type reactions seemingly solved, the next goal within the field was to turn to softer nucleophiles with the hope of increasing the functional group tolerance. Early on Fürstner showed that trialkylzincates were effective reagents.[47] This was later followed by Nakamura, who showed that $FeCl_3$ could be used

to catalyse reactions between alkyl halides and diarylzinc reagents, in the presence of TMEDA.[62] Further work by Bedford showed that the need for TMEDA could be replaced with diphosphine ligands such as 1,2-bis(diphenylphosphino)benzene (dpbz) and bis(diphenylphosphino)ethane (dppe) (Scheme 1.12).[63] Pringle also created a system with the diphosphine ligand bis(diarylphosphino)thiophene which was even more active than dppe and dpbz.[64]
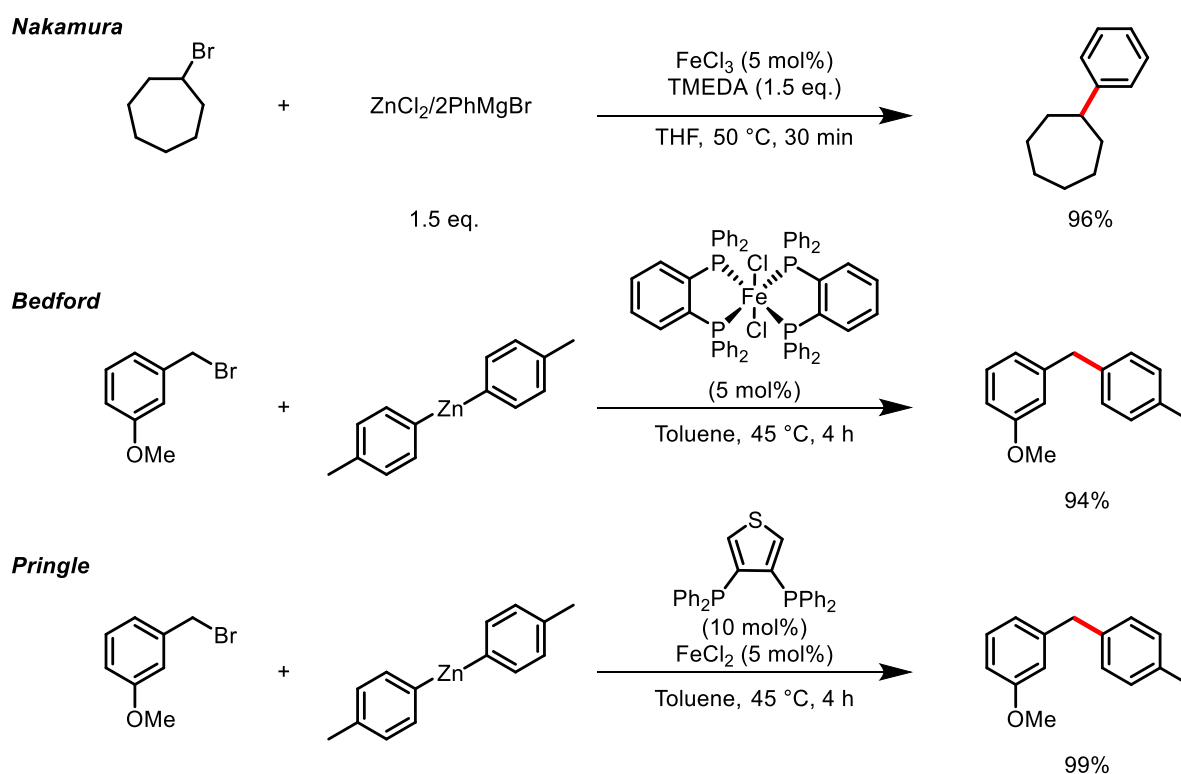
Scheme 1.12 – Examples of iron-catalysed Negishi reactions by Nakamura,[62] Bedford,[63] and Pringle.[64]

Along with iron-catalysed Kumada and Negishi cross-coupling reactions, iron-catalysed Heck,[65–69] Sonogashira,[70–76] aluminium Negishi-type,[77–79] and Hiyama[80] couplings have also been reported (Scheme 1.13). However, these reactions are limited and are not as well developed as iron-catalysed Kumada, Negishi, and Suzuki cross-couplings (discussed in Section 1.1.5).

Iron-catalysed Heck Reaction

Fe(OTf)$_2$ (5 mol%)

TBPB (3.0 eq.)
1,4-dioxane, 50 °C, 2 h

3.0 eq.

62%

Iron-catalysed Sonogashira Reaction

FeCl$_3$ (15 mol%)
dmeda (30 mol%)

Cs$_2$CO$_3$, PhMe, 135 °C, 72 h

1.5 eq.

68%

Iron-catalysed aluminium-Negishi Reaction

FeCl$_2$(dppbz)$_2$ (3 mol%)

THF, 80°C, 48 h

1.2 eq.

94%

Iron-catalysed Hiyama Reaction

FeCl$_2$ (10 mol%), PCy$_3$ (40 mol%)
CuF$_2$ (3.0 eq.), TBAB (1.0 eq.)

Zn (2.0 eq.), TMSCl (30 mol%)
PhMe/MTBE, 120 °C, 24 h

4.0 eq.

54%

Scheme 1.13 – Examples of iron-catalysed Heck,[69] Sonogashira,[71] Negishi,[78] and Hiyama[80] type reactions.

As the Suzuki reaction is one of the most used C–C bond forming processes, there is a high demand to produce an iron-catalysed reaction that utilises non-toxic organoboron reagents as cross-coupling partners. This was first shown to be an achievable target by Bedford, who used bench-stable tetraarylborate salts to arylate benzyl halides (Scheme 1.14).[81] However, unlike the previous examples of iron-catalysed Negishi and Kumada type reactions this required the use of a co-catalytic organozinc reagent to aid the transmetallation of the alkyl group from the borate to the iron centre. Although this stood as a great example to show that iron-catalysed Suzuki cross-couplings could be achieved, it had a limited scope as there were few ways to vary the tetraarylborates.
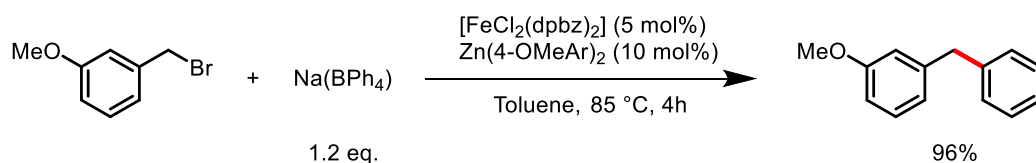
Scheme 1.14 – Iron-catalysed cross-coupling of benzyl halides with tetraorganoborates.[81]

With the precedence of an iron-catalysed Suzuki type reaction demonstrated by Bedford, Nakamura built upon this work and employed an aryl boronic acid pinacol ester activated with alkyl lithium reagents (Scheme 1.15).[82] These are readily synthesised, and this opened the door to a wide range of cross-coupling partners and a large substrate scope. This also required the use of a co-catalyst, and Nakamura showed that 20 mol% loading of $MgBr_2$ was the optimum.
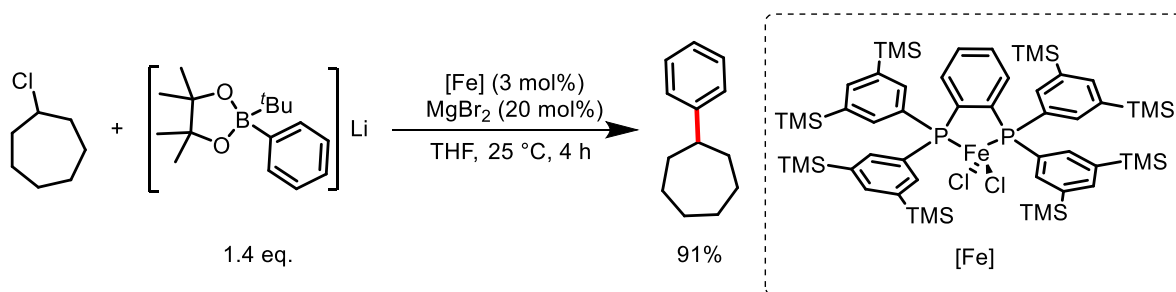
Scheme 1.15 – Iron-catalysed cross-coupling reaction of ^{t}BuLi activated boronates by Nakamura.[82]

Later, Bedford expanded the scope of the organoboron coupling partner by discovering that tetraorganoborates could be used in the iron-catalysed Suzuki reaction.[79] In this example the most effective system used $FeCl_2$ and dpbz alongside a zincate as a co-catalyst. Nakamura showed that formation of alkyl-alkyl bonds was possible using an iron catalyst; *iso*-propylmagnesium chloride-activated trialkylboranes were used to cross-couple with unactivated alkyl halides using an [Fe(acac)$_3$]/Xantphos catalyst system (Scheme 1.16).[83] Unlike the previous examples, this reaction did not require the co-catalytic metal halide, as it was reported that magnesium salts were formed in the activation of the trialkylborane.
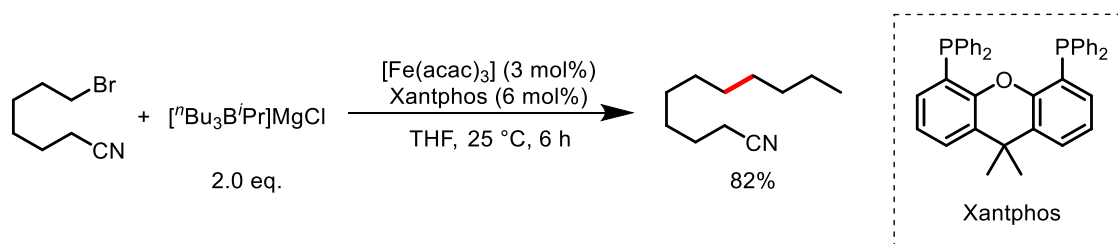
Scheme 1.16 – Iron-catalysed alkyl-alkyl Suzuki cross-coupling.[83]

Byers has since reported three papers on iron-catalysed Suzuki cross-coupling reactions between alkyl halides and unactivated aryl boronic esters.[84–86] The latest publication reveals the utilisation of an air-stable iron(III) pre-catalyst (Scheme 1.17).[86] Despite the benefits of low cost and toxicity, iron pre-catalysts are not widely employed compared to their palladium and nickel counterparts due to their deactivation upon exposure to moisture and air. The ability to overcome this barrier and achieve cross-coupling is a highly desirable feature in iron-based pre-catalysts. Although the reaction is still air and moisture sensitive, the fact that Byers' pre-catalyst is air stable and highly competent at cross-coupling is a huge advancement in the field of iron-catalysed cross-couplings. Prior to Byers' reports, alkyl lithium activated boronates have been required to achieve cross-coupling. The products of these are air and moisture sensitive and require the use of highly hazardous alkyl lithium reagents. Here Byers shows that lithium amide bases can be used in conjunction with boronic esters. Byers reports that the bidentate amine ligands coordinate strongly to iron which results in less ligand dissociation and therefore prevents aggregation of iron. Thus, allowing for a longer lifetime of the catalyst and therefore greater yielding reactions under milder conditions. The use of the anionic ligands and amide bases makes the transmetallation to iron easier, allowing the reaction to proceed without the need for activated boronate species. The reaction also did not require the magnesium additives, previously crucial to catalysis.[82,87] A disadvantage of this procedure was that it was only applicable to C–C bond formation of an alkyl- to an aryl-group; biaryl cross-coupling was not achieved under these mild conditions.
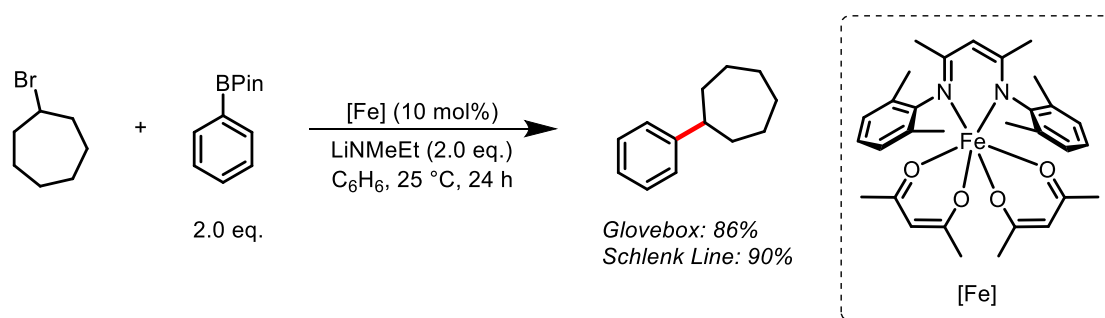
Scheme 1.17 – Air stable iron pre-catalyst used in the synthesis of alkyl-aryl products.[86]

In 2015 Nakamura reported the first enantioselective iron-catalysed Kumada cross-coupling reaction.[88] Nakamura has since developed the first enantioselective iron-catalysed Suzuki coupling.[89] The method employed used a catalyst combination of $FeCl_2$ with (*R*,*R*)-QuinoxP* to couple lithium aryl boronates (used in previous syntheses) with *tert*-butyl α-bromopropionate to synthesise optically active α-aryl propionic acids, including examples of nonsteroidal anti-

inflammatory drugs (Scheme 1.18). The key ligand requirements included the use of a *P*-chiral ligand that contained an electron deficient quinoxaline backbone; this reached yields up to 98% and an e.r. up to 88:12. Although the enantioselectivity could be improved in the future, this highlights a significant progression in iron-catalysed Suzuki reactions and makes the field even more pharmaceutically relevant, as the industry is constantly looking to incorporate stereogenic centres into its drug design.[90] Since Nakamura's discovery, Byers has developed an iron-catalysed enantioselective Suzuki cross-coupling reaction of benzyl chlorides and unactivated aryl-boronic pinacol esters, with e.r. up to 99:1.[91]
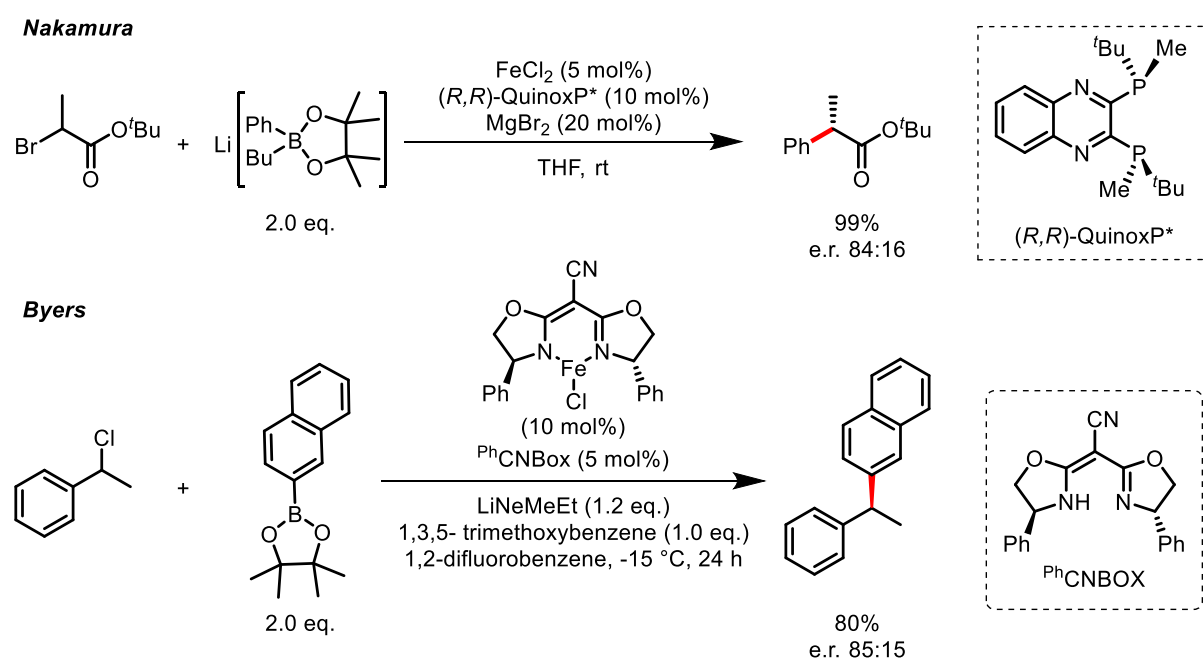
Scheme 1.18 – Examples of an enantioselective iron-catalysed Suzuki cross-coupling reactions by Nakamura[89] and Byers.[91]

The examples shown are the latest developments in alkyl-aryl iron-catalysed Suzuki cross-coupling reactions. However, most of these rely on activated boronate species and alkyl lithium reagents, both of which are moisture and air sensitive, and alkyl lithium reagents can also be pyrophoric. Bench stable boronic esters and acids used alongside alkoxide bases are so far ineffective, but Byers has shown that lithium amide bases can be used. Protocols for iron-catalysed aryl-aryl Suzuki cross-couplings are very limited, with full activity only seen when a directing group is employed (see Section 2.1 for full discussion). Thanks to the pioneering work described throughout this section, success has been seen with scaled up iron-catalysed cross-coupling reactions and in the synthesis of medicinally relevant compounds.[92] For example, Tewari was able to use an iron-

catalysed Kumada reaction on a multikilogram scale to synthesise cinacalet HCl (a calcimimetic agent).[93]
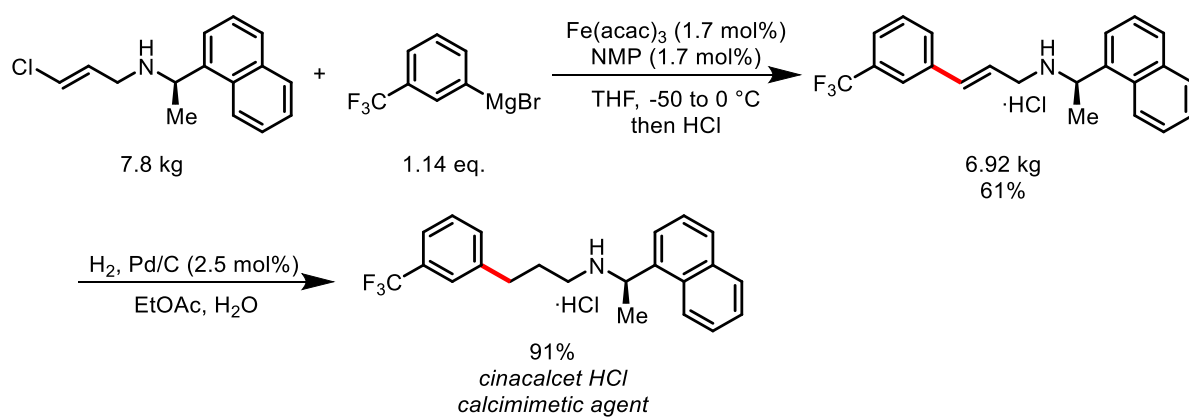
Scheme 1.19 – Synthesis of cinacalcet HCl using and iron-catalysed Kumada coupling as a key step.[93]

1.2 Mechanistic Investigations of Iron-Catalysed Cross-Coupling Reactions

The mechanism behind palladium-catalysed cross-coupling reactions is well documented and understood (Figure 1.4). As palladium has a low energy barrier between Pd(0) and Pd(II), it can readily go between these oxidation states throughout the catalytic cycle. The Pd(0) species, formed *in situ* in the reaction mixture, is able to oxidatively insert into the C–X bond to form a Pd(II) species. This species can then react with the organometallic coupling partner in a transmetallation step, adding the unit to the Pd(II) and releasing the halide to form a metal salt as the side product. The final step is reductive elimination; this releases the cross-coupled product and in turn regenerates the Pd(0) species.[94]
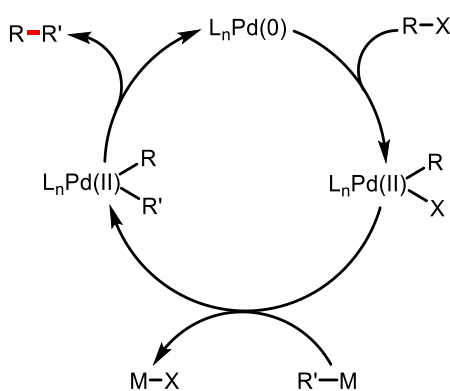

Figure 1.4 – Accepted catalytic cycle for palladium-catalysed cross-coupling reactions.

However, the level of understanding regarding iron-catalysed cross-coupling reactions is not at the same stage as palladium-catalysed cross-coupling reactions. Many iron species are paramagnetic as well as being thermally, air, and moisture sensitive, making species very hard to study.[44] As stated, palladium can only readily go between the 0 and +2 oxidation sates, in a two-electron transfer. Iron can readily go between -2 and +6 oxidation states *via* either single or two electron transfers, immediately making any mechanism harder to understand and investigate.[44] Single electron transfers using iron-catalysts were observed when Nakamura reacted both the *cis* and *trans*-1-bromo-4-tert-butylcyclohexane in an iron-catalysed cross-coupling reaction to find that only the more stable trans-arylated product formed, suggesting the mechanism progressed *via* a radical species (Scheme 1.20).[52] This work was later followed up by Bedford; a radical clock experiment was performed on (bromomethyl)cyclopropane, this resulted in formation of the ring opened 4-phenylbutene rather than the ring closed (cyclopropylmethyl)benzene (Scheme 1.20).[48] This suggested that an alkyl radical was formed *via* single electron transfers, rather than the classical two electron transfers in the oxidative addition step.
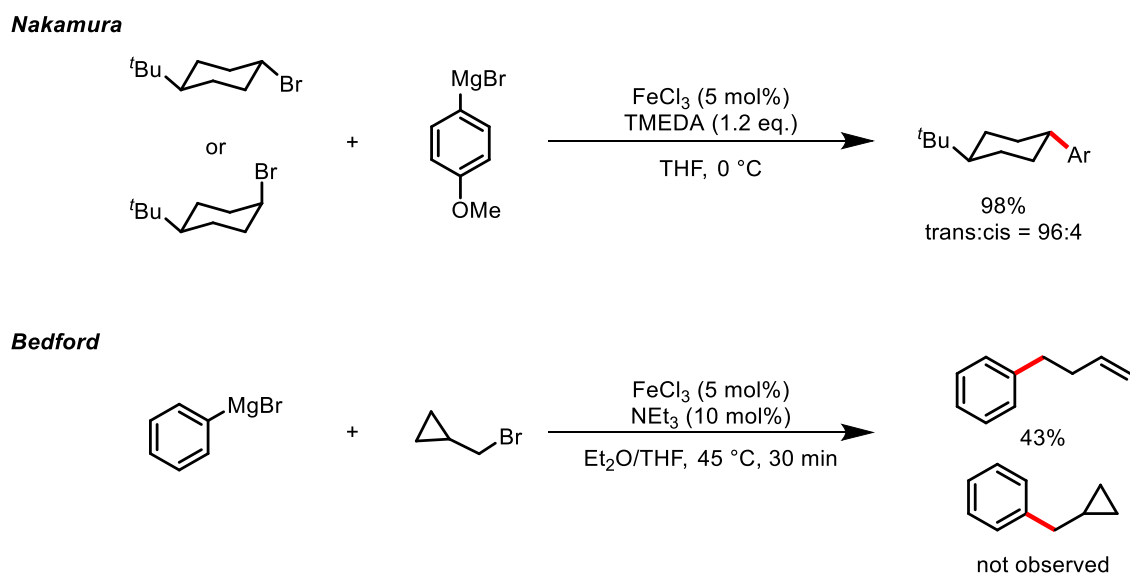
Scheme 1.20 – Radical probe reactions by Nakamura[52] and Bedford.[48]

It is widely accepted that the lowest oxidation state of palladium in cross-coupling reactions is 0. Based on this, and the knowledge of the redox reactions of palladium, the catalytic cycle can be built. However, in the case of iron, Fe(-II), Fe(-I), Fe(0), Fe(I) and Fe(II) have all been proposed as the lowest oxidation state for cross-coupling reactions.[95] This makes it very difficult to suggest a generic mechanistic model for iron-catalysed cross-coupling reactions.

Fe(-II) was suggested as the lowest oxidation state of iron by Fürstner when Grignard reagents were coupled to alkyl halides.[47] This was based on Bogdanovic's work where he formed Fe(MgX)$_2$ complexes from Mg(0), alkyl halide and FeCl$_2$ in a ratio of 25:4:1.[96] The catalytic cycle proposed was based on an Fe(-II)/Fe(0) manifold (Figure 1.5).[47] However, this relied on the excess of Mg(0) to access Fe(-II) and so is not representative of common cross-coupling reactions.
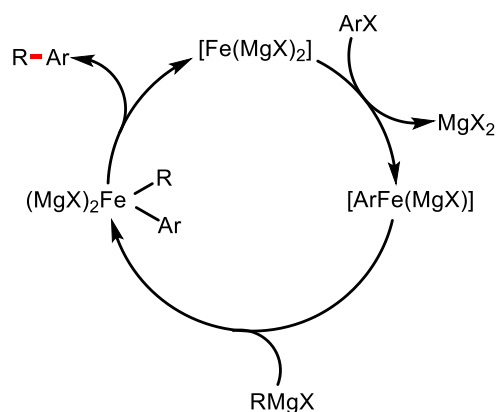
Figure 1.5 – Fürstner's proposed Fe(-II)/Fe(0) cycle.[47]

Building on these observations, Fürstner set out to show Fe(-II) was the lowest oxidation sate of iron in the catalytic cycle. To do this, Fürstner and co-workers prepared the Fe(0), Fe(I), Fe(II) and Fe(III) species with cyclopentadienyl (Cp) or 1,2,3,4,5-pentamethylcyclopentdienyl (Cp*) ligands (Figure 1.6).[97] When subsequently trialled in a cross-coupling reaction of phenylmagnesium bromide and methyl-4-bromocrotonate, all of these species were outperformed by an Fe(-II) complex (Figure 1.6). From this Fürstner concluded that Fe(-II) must be the lowest oxidation state in the catalytic cycle. However, what Fürstner failed to consider was that the Cp or Cp* ligands used are not commonly exploited in iron-catalysed cross-coupling reactions and therefore an accurate interpretation cannot be drawn from the experiments. Additionally, he failed to use an Fe(-II) species with a Cp ligand, making it inconsistent with the testing parameters. Also, if his theory was correct then the most active Cp-Fe species should have been the Fe(0) complex, but instead it was the least active. Since this work, there has been very little evidence to show that the lowest oxidation state of iron in the catalytic cycle is -2.
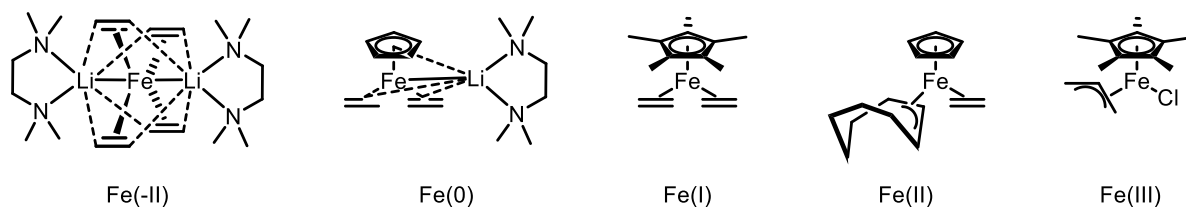

Figure 1.6 – Fürstner's model iron complexes with a range of oxidation states.[97]

Another proposed lowest oxidation state of iron is 0. Fe(0) is accessible under many catalytic conditions, often when reduced to Fe(0), nanoparticles (NPs) have been seen rather than homogeneous complexes. Fe(0) NPs stabilised by poly(ethylene glycol), synthesised by Bedford

and co-workers, are catalytically active.[98] It remains unknown whether the catalysis takes place on the NP surface or not; it is possible that these NPs instead act as an off-cycle reservoir for a soluble cycle. Evidence for this was given by Bedford who showed that the dropwise addition of NPs to an alkyl bromide resulted in the formation of a homogeneous solution and the loss of NPs.[99] Although this evidence does not prove that the NPs are not the catalyst, it could suggest that an organo-iron complex with an oxidation state higher than 0 is formed. Lefèvre has also suggested that Fe(0) may be the active species in the coupling of aryl Grignard reagents with (hetero)aryl halides, when the electrophile is less easily reduced.[100] In this case an Fe(0) species is formed from the reduction of an $[Ar_3Fe^{II}]^-$ species, which can then undergo a two electron oxidative addition with the less easily reduced electrophiles. The oxidative addition products using 2-chloropyridine (2-PyCl) and chloropentafluorobenzene (C_6F_5Cl) in the presence of MesMgBr, $[Mes_2(2-Py)Fe^{II}]^-$ and $[Mes_2(C_6F_5)Fe^{II}]^-$, were characterised making the Fe(0)/Fe(II) proposal feasible. However, Lefèvre also noted, more easily reduced electrophiles were still able to readily undergo single electron transfers and thus, an Fe(II)/Fe(III) cycle, as previously reported.[82]
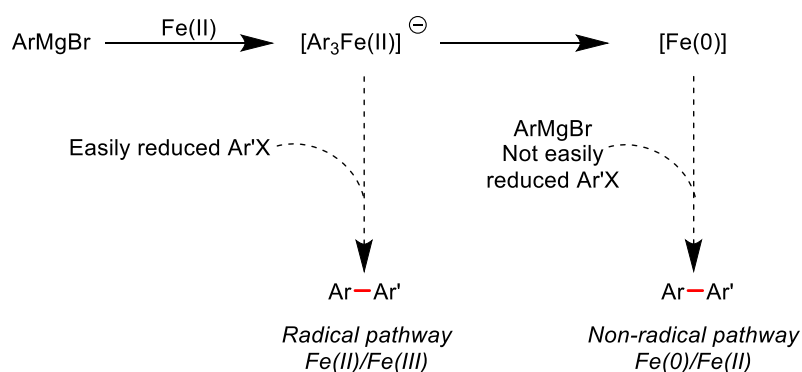
Scheme 1.21 – Suggested Fe(II)/Fe(III) and Fe(0)/Fe(II) mechanisms suggested by Lefèvre.[100]

The suggested lowest oxidation state of iron in most investigations is greater than Fe(0), with Fe(I) being both readily formed and catalytically active. Kochi identifies Fe(I) as the lowest oxidation state after observing an $S = \frac{1}{2}$ species (low spin Fe(I)) in the EPR spectrum of iron halide salts with methylmagnesium bromide, and thus proposed an Fe(I)/Fe(III) cycle (Figure 1.7).[101] Neidig later revealed that the $S = \frac{1}{2}$ species discovered by Kochi was an iron cluster $[MgCl(THF)_5][Fe_8Me_{12}]$ (Figure 1.7).[102] When this species was then trialled in the cross-coupling reaction it produced very low yields of the cross-coupled product, and therefore the active species in Kochi's reaction is still unknown.
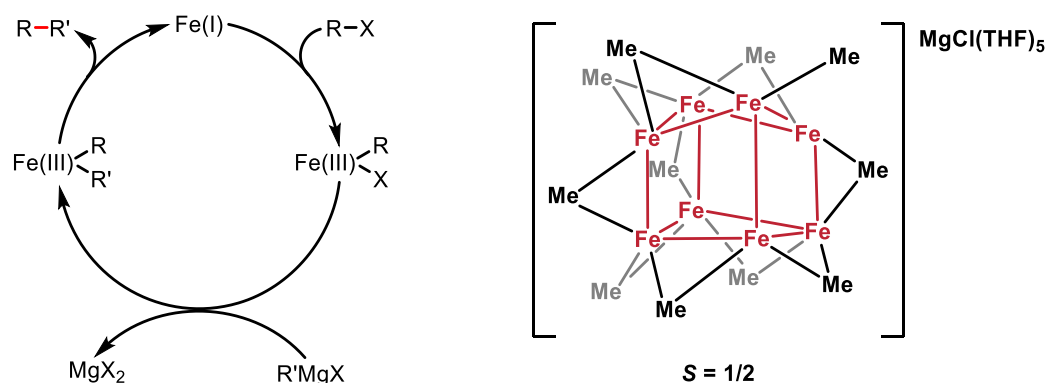
Figure 1.7 – Proposed Fe(I)/Fe(III) cycle by Kochi[101] and identity of observed $S = \frac{1}{2}$ species.[102]

Research into the field has progressed for the investigation of cross-coupling systems that use bidentate phosphine ligands such as dpbz and dppe. An added benefit of investigating these systems is that smaller, more representative nucleophilic reagents can be investigated. When reacting $FeCl_2(dpbz)_2$ with a diarylzinc reagent in a Negishi type reaction, Bedford found that the iron is reduced to an oxidation state lower than +1, but that the bulk oxidation state of iron during the most productive cross-coupling was +1.[103] With these results, Bedford and co-workers isolated complexes **1**–**3** as proposed intermediate species (Figure 1.8). All three complexes were found to be low spin ($S = \frac{1}{2}$) with the unpaired electron to be predominantly on the iron (determined through EPR spectroscopy and DFT calculations). All three complexes were competent pre-catalysts for the Negishi reaction, with **1** showing the same kinetic profile as $FeBr_2(dpbz)_2$ for cross-coupling. Fe(I)-phosphine containing complexes were also identified in samples removed from catalytic reactions.

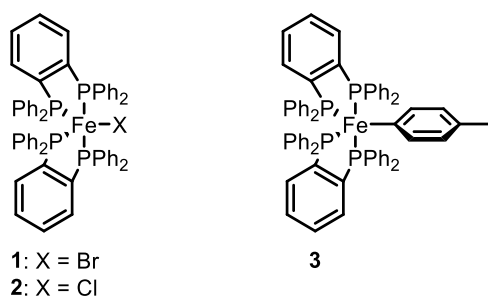**1**: X = Br
2: X = Cl

3

Figure 1.8 – Bedford's reported Fe(I) complexes.[103]

It is also thought that perhaps that Fe(II) is the lowest possible oxidation state of an iron species in a range of transformations. This was seen with an $[Fe(Mes)_3]^-$ species where an Fe(II) ate species is formed. It is possible to synthesise Fe(II) ate complexes from smaller Grignard reagents, but

these are often found to be thermally unstable and disproportionate when warmed.[99,104] Similarly to Fe(I) complexes mentioned previously, bidentate diphosphine ligands are able to form stable Fe(II) complexes that are also active in catalysis. Nakamura has made use of a specially designed 'spin-control-intended *ortho*-phenylene bisphosphine' ligand (SciOPP) in a variety of reactions to stabilise Fe(II) and promote it in cross-coupling reactions.[76,82,105] The phosphine binds strongly to the iron centre and with its steric bulk prevents coordination of more than one ligand. Nakamura proposes the mechanism based on an Fe(II)/Fe(III) cycle (Figure 1.9).[82] This is based mainly on the theory of single electron transfers and radical formation, with results backed up by radical probe experiments and a lack of biphenyl production (showing that it was not reduced lower than Fe(II)).
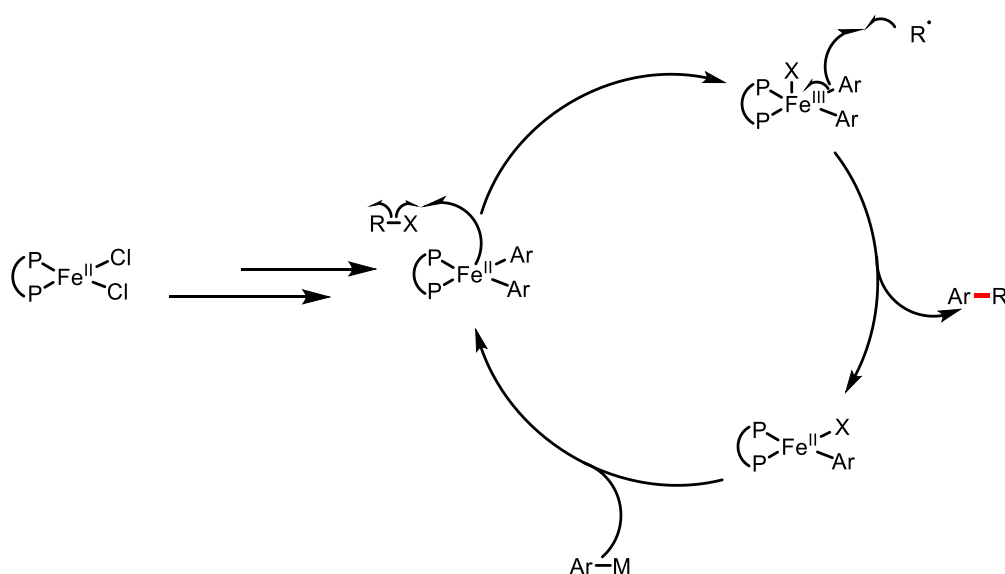
Figure 1.9 – Proposed Fe(II)/Fe(III) cycle by Nakamura.[82]

These findings have been further corroborated by Neidig, by carrying out *in situ* spectroscopic techniques along with the syntheses, isolation and reactions of monoarylated and biarylated SciOPP- containing organoiron complexes (Figure 1.10).[106,107] Reaction of FeCl$_2$(SciOPP) with mesitylmagnesium bromide forms complex **4** which then reacts with primary alkyl halides to produce **6**, and also affords the cross-coupled product. When smaller phenyl nucleophiles were investigated, both complexes **5** and **7** were formed in solution, but kinetic investigations show that monoarylated **7** is the most reactive species.[106,107] Neidig has also further backed up these findings by proposing that the same mechanism is also likely for the iron-catalysed alkynylation of alkyl halides.[108]
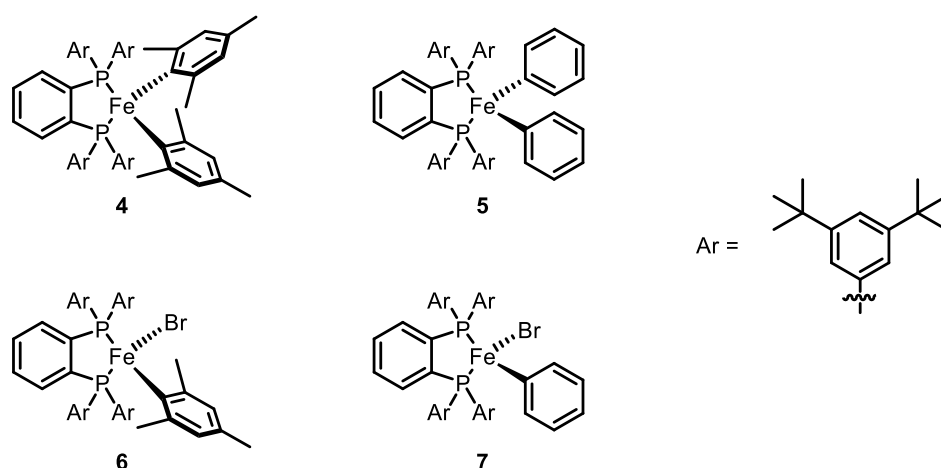
Figure 1.10 – Fe(II)SciOPP complexes investigated by Neidig.[106,107]

Nakamura also believed that +2 was the lowest oxidation state of iron in an iron-catalysed cross-coupling of aryl chlorides with alkyl Grignard reagents (Scheme 1.22).[109] In this case it is thought that the iron undergoes 2 electron transfer processes and thus is oxidised from +2 to +4 in the catalytic cycle. This proposed cycle was corroborated by X-ray absorption spectroscopy and DFT calculations.
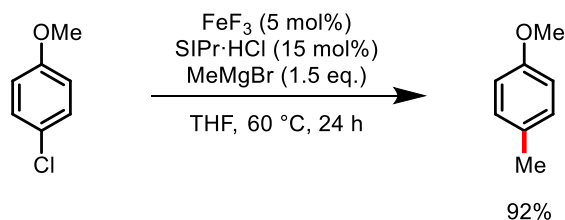
Scheme 1.22 – Iron-catalysed Kumada cross-coupling.[109]

Initially Nakamura conducted a radical probe experiment in which he predicted that if a radical process were taking place, a cyclisation product would form. Instead, the aromatic methylation product formed quantitatively without observation of any cyclisation products (Scheme 1.23).[109]
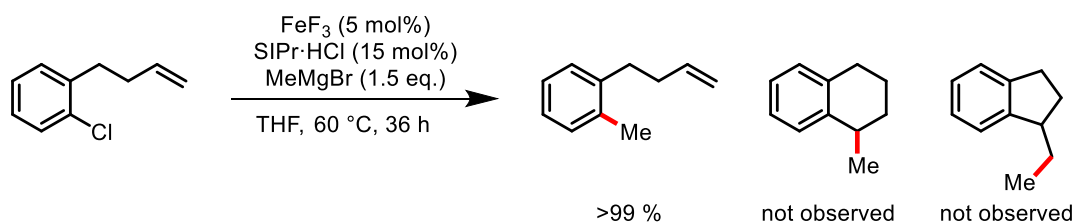
Scheme 1.23 – Radical probe experiment determining 2 electron process.[109]

Further to this, Nakamura hypothesised that iron is initially reduced by the Grignard reagent from Fe(III) to Fe(II).[109] By reacting the pre-catalyst with RMgX, a difluorido organoferrate(II) intermediate forms, this can then readily take part in the oxidative addition of aryl chloride giving Fe(IV). This intermediate can then undergo reductive elimination to give the cross-coupled product. To confirm the formation of the organoferrate(II) intermediate, a stoichiometric reaction was undertaken with its solution phase analysed by XAS analysis. A reaction mixture was prepared by mixing $FeF_3 \cdot 3H_2O$ (0.06 mmol) and a large excess of SIPr (7.0 eq.) and Me_3SiCH_2MgCl (12 eq.) in THF (80 °C, 1 h). Subsequent treatment of the reaction mixture with an aryl chloride (0.06 mmol) resulted in the cross-coupling reaction proceeding to give the corresponding product in 74% yield. Prior to the addition of the aryl chloride, synchrotron XAS analysis was undert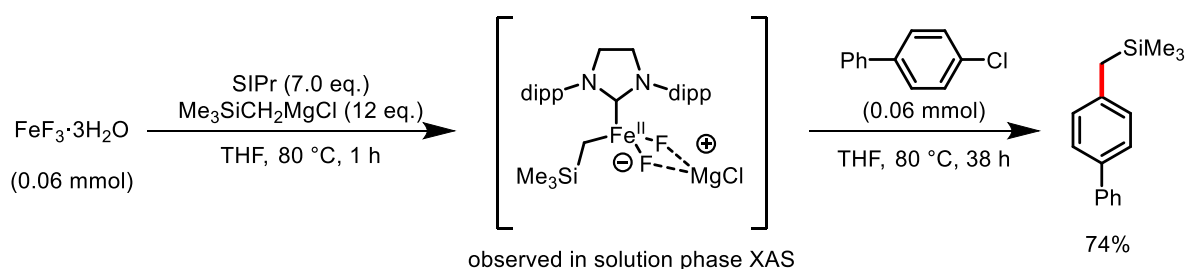aken. This resulted in the identification of a high spin ($S = 2$) difluorido organoferrate (II) intermediate (Scheme 1.24).[109]

Scheme 1.24 – Synthesis of Fe(II) intermediate and use in cross-coupling.[109]

The reaction also had a strong fluoride dependence; when a lack of fluoride was present in the reaction, a lack of reactivity was observed. This could be restored when an additional fluoride source, KF, was added to the reaction when premixed with $FeCl_3$. As fluoride ligands are less easily displaced than chloride and bromide ligands, it was suggested that the iron-NHC complex is formed *in situ* and is prevented from reducing to oxidation states lower than +2. From these results, the Fe(II)/Fe(IV) mechanism was proposed. This result and the resulting catalytic cycle were further corroborated by DFT calculations. However, although the use of iron fluoride systems as a pre-catalyst can form highly active catalytic systems, the mechanistic insights cannot be applied more widely due to the non-innocence of the fluoride ligand compared to other halides.[109]

A further complication, compared to palladium-catalysed cross-coupling reactions, is the role of the ligand and additives, as they are not always coordinated to the iron centre during the catalysis. It has been noted before that the ligand or additive can act to suppress unwanted side reactions

rather than promote cross-coupling. Nakamura noted this with his use of TMEDA in an iron-catalysed Kumada cross-coupling reaction.[52] The mechanism of this reaction was then investigated by Nagashima, using bromooctane and mesitylmagnesium bromide as the test reaction.[110] Use of a bulkier and more sterically hindered Grignard reagent resulted in a lower yield of the cross-coupled product. However, this allowed for isolation of an organo-iron species that had been previously thought of as too unstable to isolate. Nagashima was able to isolate complexes **8** and **9** which were then tested in a variety of reactions. When **8** was reacted with 2.0 eq. of bromooctane, **9** was formed which resulted in a yield of 76% of the cross-coupled product. Compound **9** was then reacted with mesitylmagnesium bromide to afford **8**. The final observation was that **9** reacted much slower with bromooctane than **8**, and therefore the catalytic cycle shown was proposed (Figure 1.11).[110]
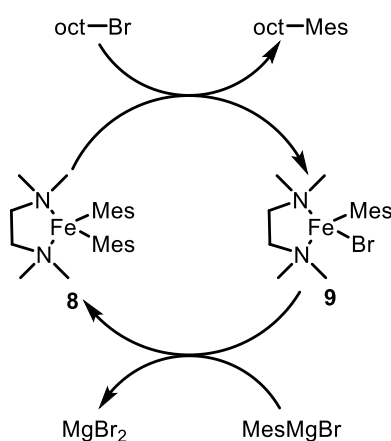
Figure 1.11 – Catalytic cycle with complexes 8 and 9.[110]

Bedford later showed that when either $FeCl_2$ or $FeCl_3$ was mixed with 8.0 eq. of mesitylmagnesium bromide and TMEDA, the only species observed by NMR was a homoleptic Fe(II) ate species [Fe(Mes)$_3$], **10**.[99] The homoleptic species proved to be competent in catalysing the cross-coupling of bromooctane and also reacted much faster than species **8**. This led to the conclusion that TMEDA acted to stabilise off-cycle species and prevented catalyst decomposition (Figure 1.12).
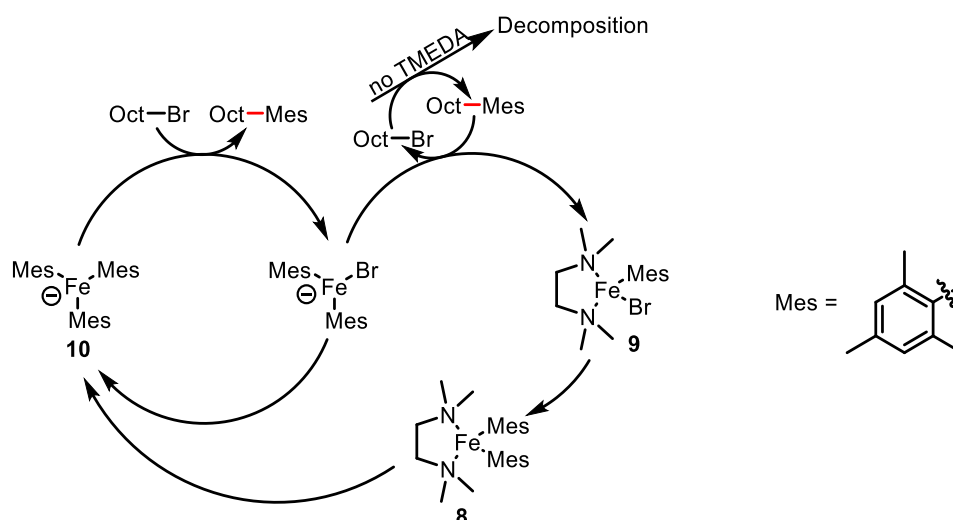
Figure 1.12 – Revised catalytic cycle for cross-coupling of bromooctane and MesMgBr.[99]

However, Neidig has recently published an investigation on the role of TMEDA in coupling of alkyl halides with phenyl and ethyl Grignard reagents.[111] Neidig argues that the use of MesMgBr with TMEDA is unrepresentative of the behaviour of TMEDA in cross-couplings with PhMgBr (often MesMgBr performs very poorly compared to PhMgBr), along with slow nucleophile addition protocols that are widely employed.[112] Therefore, homoleptic ferrate species, such as **10**, may not form in reactions when PhMgBr is employed. The reaction was studied using X-ray diffraction, ^{57}Fe Mössbauer and EPR spectroscopy, and kinetic studies. The study found that TMEDA does coordinate to iron in the primary catalytic cycle with PhMgBr or EtMgBr; through freeze-quenched ^{57}Fe Mössbauer spectroscopy, TMEDA ligated monomeric iron species were observed. A possible Fe(II)/Fe(III)/Fe(I) manifold is suggested for the catalytic cycle (Figure 1.13).
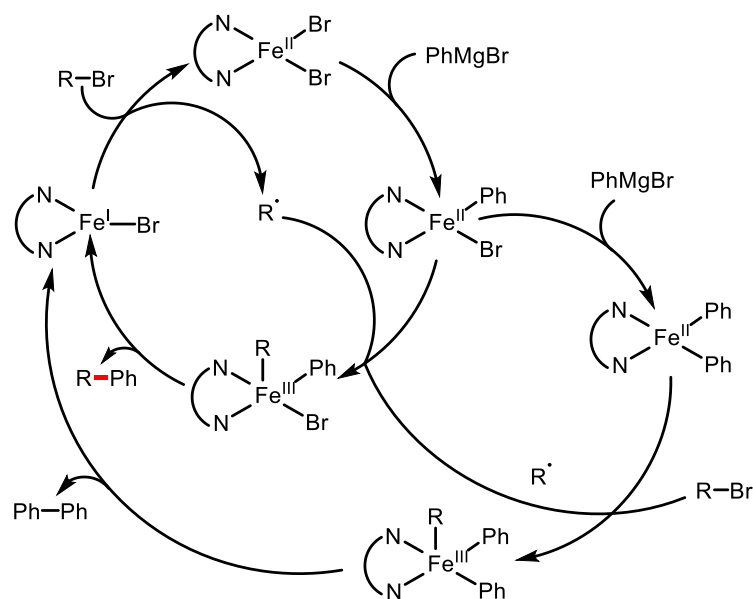
Figure 1.13 – Role of TMEDA in an iron-catalysed Kumada reaction.[111]

Another commonly employed additive in iron-catalysed cross-coupling reactions is NMP, which also acts to supress unwanted side reactions. When NMP is used as a co-solvent or ligand it was initially thought that NMP-Fe species can form. This was demonstrated by Holland, who reacted 3.0 eq. of $FeCl_2(THF)_{1.5}$ with 8.0 eq. NMP to form a species containing two iron complexes.[113] This species was also found be a successful catalyst in a Kumada cross-coupling reaction. However, it was later found by Neidig, using *in situ* spectroscopy, that these types of species were not formed in the catalytic system. Instead, when reacting [Fe(acac)₃] with methylmagnesium bromide in THF and NMP, homoleptic Fe(II) ate $[FeMe_3]_2[Mg(NMP)_6]$ is formed as the major species.[114] The conclusion is that the NMP interacts and stabilises magnesium cations rather than the iron (Figure 1.14).
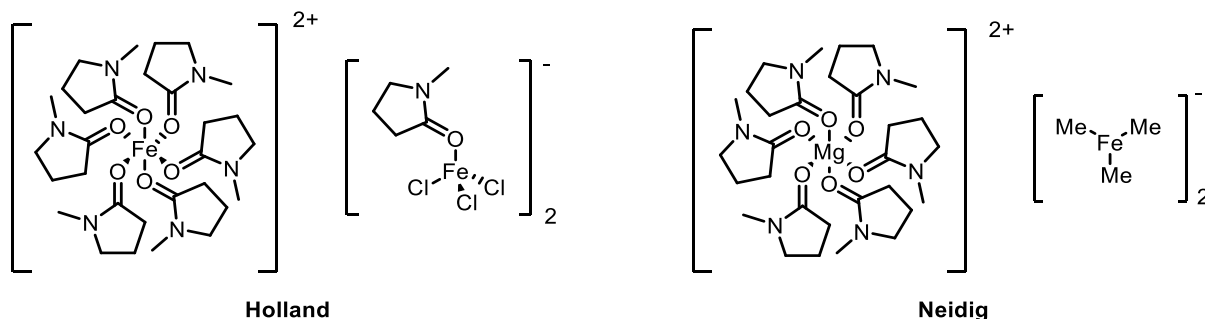
Figure 1.14 – Iron and NMP species reported by Holland[113] **and Neidig.**[114]

A further complication to understanding iron-catalysed cross-coupling reactions is understanding the role of the ligand. It is commonly believed that the ligand coordinates to the metal, forming a catalytically active species. However, this is not always the case. Bedford recently published a mechanistic study into an iron-catalysed Negishi reaction.[115] It was found that the reaction was highly dependent on the diphosphine ligand, although the ligand did not appear to be coordinated to the iron during catalysis. Instead, it was thought that the diphosphine ligands were coordinated to the zinc. Bedford proposed the formation of an Fe-Zn intermediate, which is crucial for the activity rather than just iron (Scheme 1.25). As our mechanistic understanding currently trails behind the existing methodology, results like these only complicate things further.
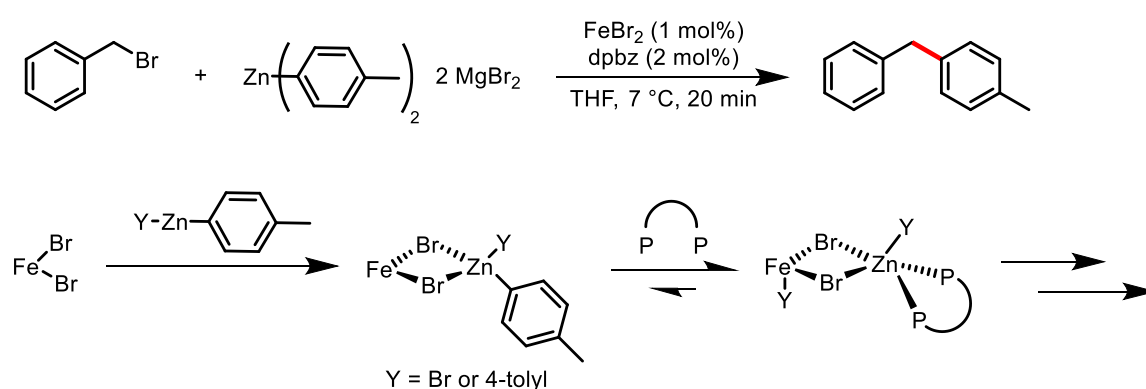

Scheme 1.25 – Bedford's iron-catalysed Negishi reaction finding diphosphine ligand does not coordinate to iron.[115]

Another issue seen in iron-catalysed cross-coupling reactions is the lack of selectivity, with homo-coupling of the nucleophile and/or the electrophile often being observed.[116] This is noticeable in Kumada type couplings where aryl Grignard reagents are used in reactions with alkyl halides that undergo single electron transfers in an Fe(II)/Fe(III) catalytic manifold.[117]

It is commonly believed that to prevent homo-coupling, transmetallation must be controlled to ensure only one aryl unit is transmetallated to form an Fe(II) species.[107,118,119] One way to achieve this is believed to be through slow addition of the Grignard to the reaction mixture[112] or through the use of strong σ-donating additives to perturb multiple transmetallation steps.[120,121] However, Lefèvre has since reported that a singly arylated Fe(II) species, although catalytically active, does not prevent homo-coupling of the Grignard.[116] Instead, it is reported that fluoride anion additives are able to prevent homo-coupling, by controlling the transmetallation degree of Fe(III)

intermediates formed later in the catalytic process. Therefore, fine control of the Fe(III) coordination sphere is imperative to control the selectivity of the reaction.

Although mechanistic investigations of iron-catalysed cross-coupling reactions have predominantly focussed on Kumada type couplings, there have also been limited investigations on Suzuki type reactions (see Section 3.1 for full discussion). All of these findings presented above demonstrate how difficult it is to not only study the mechanism behind iron-catalysed cross-coupling reactions, but also to understand and suggest new mechanisms. These current findings suggest that there is not just one robust and generic cycle, but rather a range of different cycles dependant on the reaction conditions.

1.3 Research Aims

The overall aim of the project was to find more sustainable routes to key organic motifs seen in an array of pharmaceutical, agrochemical, and fine products; as well as to expand our knowledge of iron-catalysed reactions. Although the field of iron catalysis continues apace, there are still many unknowns and further progress is required.

After Kochi's seminal report there was a dormant period where palladium catalysis took centre stage.[45] However, since the 2000's, thanks in particular to the work of Bedford, Fürstner, Nakamura, and Neidig, great strides have been made in iron-catalysed cross-coupling reactions. Iron-catalysed Kumada, Negishi, and Suzuki cross-coupling reactions have been widely published; there is now comparative success when compared to the respective palladium catalysed reaction (particularly with Kumada couplings). However, there has been very limited success with iron-catalysed Suzuki biaryl cross-coupling reactions; with the field-leading example requiring a directing group to achieve the desired result.[87] The aim of the work described in Chapter 3 was to remove the dependency of this directing group, and thus create an iron-catalysed Suzuki biaryl cross-coupling reaction that can cross-couple simple aryl halides.

Due to the relatively low stability of iron complexes, the range of accessible oxidation states, and potential radical processes, studying iron-catalysed reactions can be challenging. Although many mechanistic investigations have been undertaken for iron-catalysed reactions, there is a clear lack of consensus for the reactive pathways. However, understanding the mechanism behind chemical reactions is crucial to the development of synthetic methodologies. Therefore, the aim of the work described in Chapter 4 was to study the mechanism behind the iron-catalysed Suzuki biaryl cross-coupling reaction described in Chapter 3. The result of this study will hopefully aid further reaction development and provide more insights into the field in general.

The carboboration of alkenes is an elegant route to difunctionalise alkenes, whilst also installing a reactive centre that can be further functionalised. The reaction also has the benefit of creating a chiral centre which is highly sought after, particularly in pharmaceutical products. Whilst there are plentiful examples catalysed by copper, nickel, and palladium, there is only one example in the literature catalysed by iron (alkenylboration by Koh).[122] As discussed in the introduction, iron has many benefits over the other metals mentioned. Therefore, the aim of the work described in Chapter 5 was to create an iron-catalysed alkylboration of alkenes.

Chapter 2 Iron-Catalysed Suzuki Biaryl Cross-Coupling Reaction

2.1 Introduction

Biaryl motifs are widely seen in the structures of many pharmaceutical, agrochemical, and conducting materials and thus, synthetic routes to their formation are highly sought after.[123] The most routinely used methodology to synthesise this motif, by chemists working in both academia[124] and industry,[2] is the pallad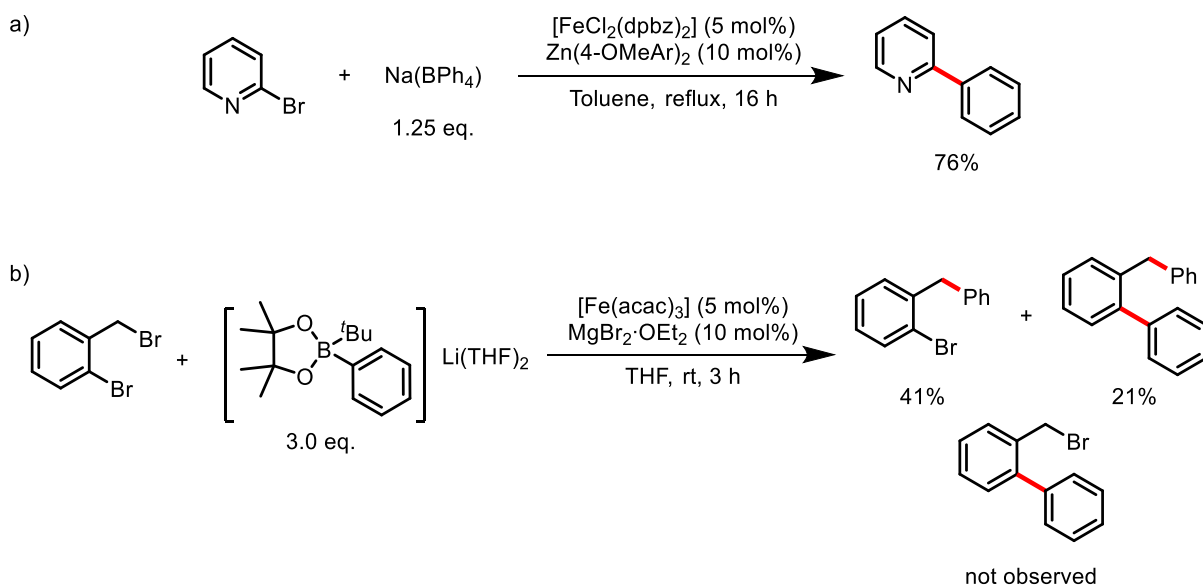ium-catalysed Suzuki biaryl cross-coupling (Scheme 2.1). This reaction has been extensively exploited in the synthesis of a wide range of commercial products.[125,126] The use of a mild boron nucleophile allows for a high functional group tolerance when compared to other cross-coupling reactions; for example, Kumada cross-coupling reactions use Grignard reagents which are incompatible with groups such as aldehydes and ketones. Palladium can also be used in very low loadings as the catalysts have very high activity, with loading levels of ppm or even ppb.[127,128] Whereas first-row transition metals often require greater loadings to perform Suzuki biaryl cross-coupling reactions, the lowest reported loadings of nickel, copper, cobalt, and iron are 0.5 mol%,[129] 2 mol%,[130] 5 mol%,[42] and 10 mol%,[87] respectively. However, there are some major disadvantages associated with palladium, including its high price, toxicity, and environmentally deleterious effects. Consequently, attention has turned towards methodologies that require cheaper and more sustainable metal catalysts. Whilst there has been success with the development of nickel-[40,129,131], copper-[132–134] and cobalt-[42,135,136] based catalysts, there has been only limited success with iron-based catalysts in Suzuki biaryl cross-couplings.
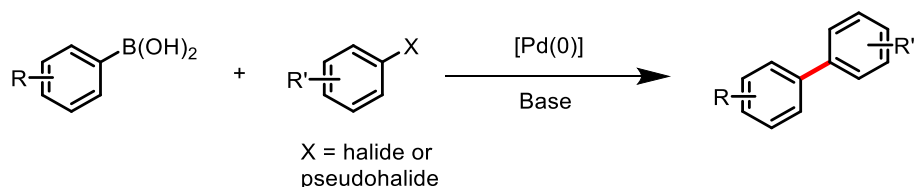
Scheme 2.1 – General scheme for palladium-catalysed Suzuki biaryl cross-coupling.

The first example of an iron-based catalyst used in a Suzuki biaryl cross-coupling was reported by Bedford in 2009, where a mixed iron-zinc catalyst was utilised to cross-couple tetraarylborates with 2-bromopyridines (Scheme 2.2a).[81] Whilst the reaction worked with milder conditions to cross-couple benzyl bromides (toluene, 85 °C, 4 h), to perform the reaction with 2-bromopyridines harsher conditions were required in order to maximise conversion (toluene, reflux, 16 h). The scope was limited due to the lack of tetraarylborates available. The second example, also reported by Bedford and published in 2015, showed that coupling 2-halobenzyl halides with ^{t}BuLi activated aryl boronates using an Fe(acac)$_3$ catalyst and a magnesium co-catalyst led to the formation of

small amounts of diarylated product along with the expected singly arylated product (Scheme 2.2b).[104] Selective cross-coupling at the aryl position was unachievable.

a)

b)

Scheme 2.2 – a) Fe-Zn-catalysed Suzuki biaryl cross-coupling.[81] b) Iron-catalysed Suzuki biaryl cross-coupling of 2-halobenzylhalides.[104]

This result led Bedford to believe that issues of the activation of the aromatic C–X bond could be overcome by utilising a π-coordinating directing group. Following on from this, work published in 2018 described an iron-catalysed substrate-directed Suzuki biaryl cross-coupling (Scheme 2.3).[87] Here, the group used a pyrrole amide directing group on the aryl halide to π-coordinate to the iron-catalyst and direct it to the aromatic C–Cl bond and facilitate insertion. The use of the directing group on the aryl halide allowed the biaryl cross-coupling to occur under relatively mild conditions, with alkyl lithium-activated arylboronic acid pinacol esters.
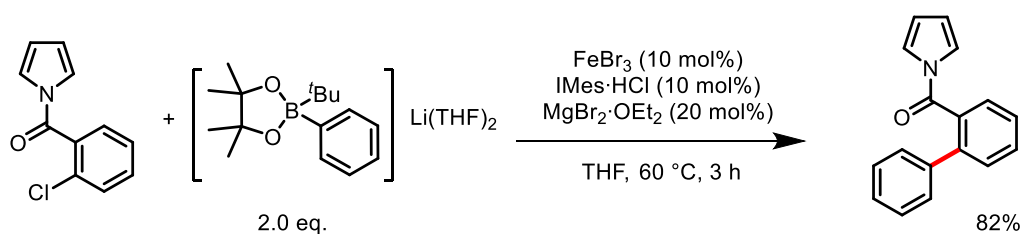
Scheme 2.3 – Substrate-directed iron-catalysed Suzuki biaryl cross-coupling.[87]

The substrate-directed approach unequivocally shows that an iron-catalysed Suzuki biaryl cross-coupling is an obtainable reaction. However, there are issues with the current methodology that

must be addressed before it can be widely used by chemists. Firstly, all the examples shown require the use of a co-catalyst (either zinc or magnesium salts). Secondly, bench stable boronic esters and acids used alongside activating agents such as alkoxide bases are so far ineffective. Alkyl lithium-activated boronic esters, which are not only air and moisture sensitive themselves, but are synthesised using pyrophoric alkyl lithium reagents, are not suitable on an industrial scale. Finally, the requirement of a directing group is likely to limit many syntheses, especially if the directing group cannot be easily installed and removed from the aryl halides; even if it could, this adds additional steps which would further limit their industrial applicability. Therefore, the initial aim of the work described below was to see if the transformation could be achieved in the absence of a directing group.

2.2 Reaction Optimisation

Considering the issues mentioned in Section 2.1, in order to improve the methodology, it was decided to attempt to remove the use of the directing group. Therefore, we were curious to see the effect of removing the pyrrole amide directing group on the aryl halide and just use a simple aryl halide, chlorobenzene, under the same reaction conditions. Chlorobenzene was reacted with ^{t}BuLi activated 4-methoxyphenylboronic acid pinacol ester (**11**), using a pre-catalyst combination of FeBr$_3$ (10 mol%), IMes·HCl (10 mol%), and MgBr$_2$·OEt$_2$ (20 mol%) in THF at 60 °C and was left overnight (Scheme 2.4). This preliminary reaction gave a cross-coupled conversion of 11%, along with the formation of 4,4'-dimethoxybenzene (**14**, homocoupling of the nucleophile) in 16% conversion. When the temperature was raised to 80 °C, conversion of the cross-coupled product increased to 24%. The yield of the undesired nucleophile homo-coupled product, 4,4'-dimethoxybiphenyl, also increased to 20%, showing the reaction was not as selective as was hoped (Scheme 2.4). Despite the low selectivity and the poor yield of the cross-coupled product compared to that obtained with the use of a directing group on the aryl halide, this result demonstrated the catalytic nature of this system. It was concluded that, with further catalyst design and optimisation, the issues previously noted with activation of the C–X bond could be overcome and a synthetically viable method for iron-catalysed Suzuki biaryl cross-couplings could be reached.
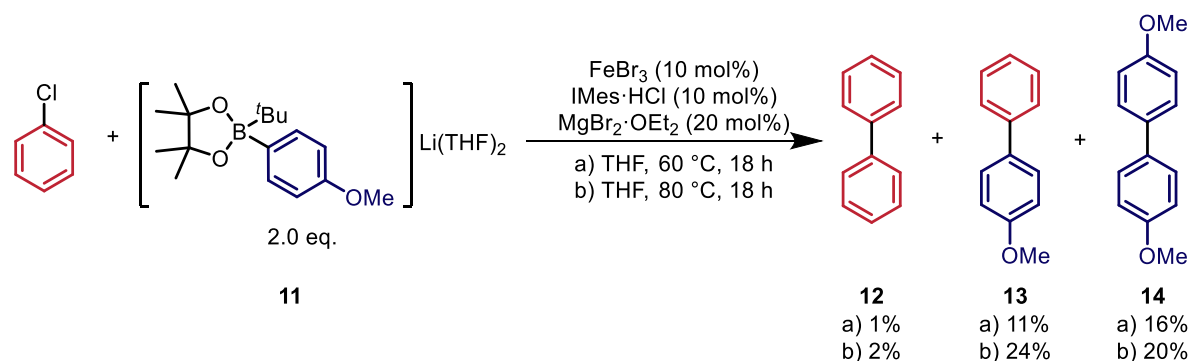
Scheme 2.4 – Non-directed iron-catalysed Suzuki biaryl cross-coupling reaction. Yield determined by GC using dodecane as an internal standard.

2.2.1 Aryl Halide Screen

With the initial data in hand, the first part of the optimisation involved screening a range of simple aryl halides to find the easiest C–X bond to activate under the current reaction conditions. Fluorobenzene, bromobenzene, and iodobenzene gave very little of the desired product, but the homo-coupled product **14** was still produced in relatively high yields (Table 2.1, entries 1, 3 & 4). Phenyl triflate gave the second highest conversion to the cross-coupled product, but also gave comparatively higher yields of the homo-coupled product (Table 2.1, entry 5), whereas phenyl carbamate yielded virtually no product (Table 2.1, entry 6). As phenols are readily available and conversion to triflates an easy transformation, the ability to cross-couple using triflates as the electrophile is a welcomed option. The results show that chlorobenzene is by far the most reactive of the aryl halides and pseudo halides, with cross-coupling yields of 24%. This is not surprising as iron pre-catalysts often show a greater reactivity cross-coupling with chlorides over other halides and pseudohalides.[47,52,61,82,87,91] Yields of biphenyl (**12**), resulting from the homo-coupling of aryl halides, remained very low throughout.

Table 2.1 – Effect of changing halide on aryl halide.

Entry	ArylX	12, % Yield	13, % Yield	14, % Yield
1	C_6H_5F	< 1	1	9
2	C_6H_5Cl	2	24	20
3	C_6H_5Br	< 1	3	11
4	C_6H_5I	< 1	2	8
5	C_6H_5OTf	1	13	24
6	$C_6H_5OCONH_2$	< 1	<1	1

Conditions: aryl halide (0.1 mmol), 11 (0.2 mmol), FeBr₃ (0.01 mmol), IMes·HCl (0.01 mmol), MgBr₂·OEt₂ (0.02 mmol), THF (1.5 mL), 80 °C, 18 h. Yield determined by GC using dodecane as an internal standard.

Palladium tends to be less efficient at cross-coupling aryl chlorides compared to aryl bromides and iodides, although there are some examples where this has been improved.[137–140] However, aryl chlorides are far more widely available and cheaper than their bromide and iodide counterparts. Therefore, the ability to cross-couple aryl chlorides using an iron-catalyst is advantageous. This would offer a great alternative route to chemists in the future.

2.2.2 Ligand and Pre-Catalyst Screen

With the best aryl halide candidate found, the next step in the optimisation was a ligand screen. Previous work directed towards iron-catalysed cross-coupling reactions has shown that phosphine[63,82,88,118,141–143] and NHC[120,144–151] ligands work particularly well. Bidentate diphosphine ligands have been proven to work in a range of different iron-catalysed reactions and often give high yields. However, when these were trialled in the reaction, they all gave yields of ≤ 5% of the cross-coupled product (Table 2.2, entries 1–12). Even dppe and dpbz, along with SciOPP, which had previously shown to have very high activity in iron-catalysed cross-coupling reactions,[84,103,108] provided very little turnover and resulted in a low yielding reaction. It was thought that the low activity could be due to over-coordination of the iron centre using bidentate ligands, forming homoleptic iron-phosphine species rather than a catalytically active heteroleptic species. Thus, monodentate phosphine ligands were then trialled. Triphenylphosphine, tricyclohexylphosphine, and tri-*tert*-butylphosphine were all trialled in the reaction. Like the bidentate diphosphine ligands, the monodentate ligands showed very poor reactivity. The highest yield of cross-coupled product was 4% (Table 2.2, entries 13–15).

Table 2.2 – Effect of varying phosphine ligand.
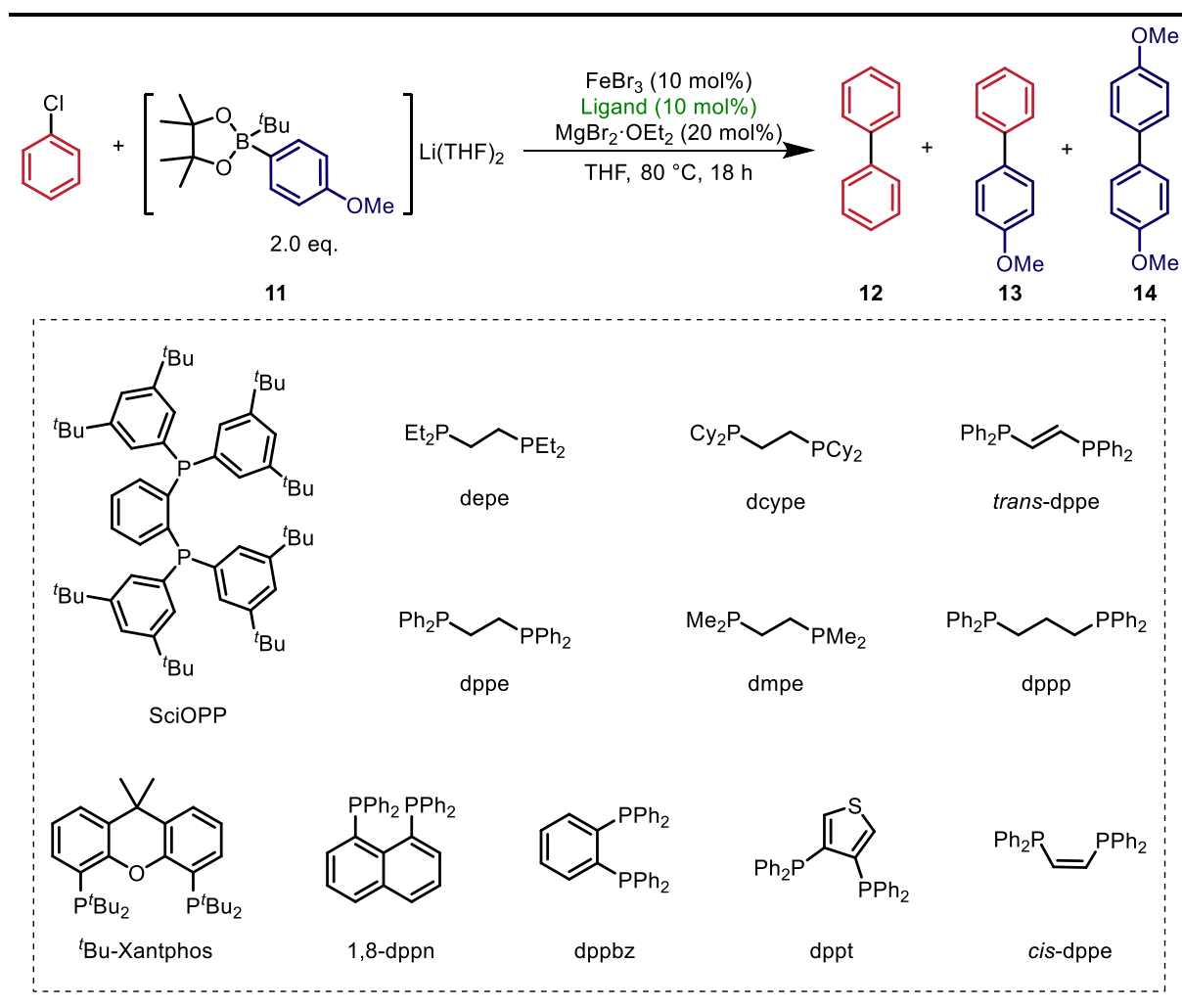
Entry	Ligand	12, % Yield	13, % Yield	14, % Yield
1	depe	1	3	14
2	dcype	1	2	10
3	*trans*-dppe	2	5	17
4	*cis*-dppe	3	5	16
5	dppe	2	5	21
6	dmpe	1	3	13
7	dppp	1	4	23
8	*t*Bu-Xantphos	1	2	8
9	SciOPP	2	3	15

10	1,8-dppn	2	3	16
11	dppbz	1	3	17
12	dppt	2	3	13
13	PPh$_3$	2	4	11
14	P(Cy)$_3$	1	2	12
15	P(^{t}Bu)$_3$	2	3	17
16	N/A	1	3	13

Conditions: chlorobenzene (0.1 mmol), 11 (0.2 mmol), FeBr$_3$ (0.01 mmol), ligand (0.01 mmol), MgBr$_2$·OEt$_2$ (0.02 mmol), THF (1.5 mL), 80 °C, 18 h. Yield determined by GC using dodecane as an internal standard.

The phosphine ligands did not perform better than the IMes·HCl originally used, which is also the optimal ligand for the substrate directed iron-catalysed Suzuki cross-coupling reaction,[87] so it was decided to investigate more NHC precursors. NHCs are better σ-donors and poorer π-acceptors than phosphines yet can be obtained as air-stable salts. Additionally, the free carbene can form stable metal-carbon bonds to both high-valent and low-valent metals. The appeal of NHCs lies in their wide structural versatility, as their electronic and steric properties can be altered by changing substituents on or within the heterocyclic ring.[152] These ligands also showed high activity in iron-catalysed Kumada cross-coupling reactions in work previously reported by Bedford, Nakamura and Duong.[120,151,153] A range of NHC precursors with differing steric and electronic properties were synthesised according to Scheme 2.5.[154]
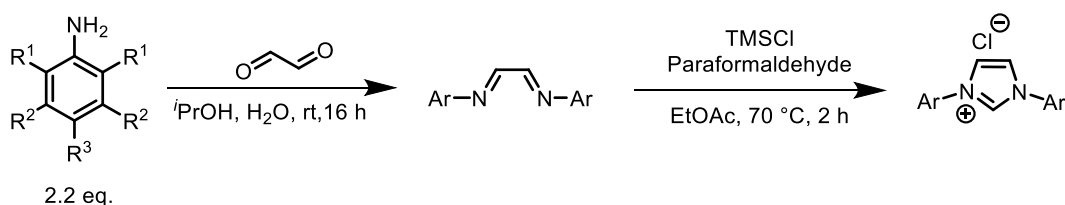
Scheme 2.5 – General synthesis of NHC salts

When comparing the results of SIPr·HCl to IPr·HCl (Table 2.3, entries 1 & 2), and SIMes·HCl to IMes·HCl (Table 2.3, entries 3 & 4), there is a clear trend that the saturated NHC precursor forms a less active catalyst than the unsaturated one. To determine whether this was more of an electronic factor (aromatic vs non-aromatic) or a steric issue, IMes^{Me}·HCl was trialled in the

reaction (Table 2.3, entry 9). If additional steric bulk on the heteroaryl of the saturated NHC precursors was preventing reactivity, then the use of IMes[Me]·HCl would result in a further decrease in yield. However, the yield (10%) was greater than that of SIPr·HCl and SIMes·HCl. Therefore, the improved reactivity between IMes·HCl and SIMes·HCl is likely to be due to the aromaticity in the heteroaryl group. Increasing the bulk in the 2- and 4-position of the aryl groups from methyl to isopropyl groups (IMes·HCl and IPr·HCl, Table 2.3, entry 3 & 1) led to a decrease in the activity of the catalysts with the yield dropping from 24 to 3%. The additional steric bulk of the isopropyl groups is substantial in NHCs, it has previously been shown that the synthesis of bis(IPr)Fe complexes has not been possible whereas the synthesis of bis(IMes)Fe complexes is possible (Scheme 2.6).[155,156] The percent buried volumes (%V_{bur}) have been calculated by Clavier and Nolan for a variety of NHC-metal complexes.[157] This parameter describes the bulkiness of the NHC ligand by the total percentage of a sphere that is occupied by the ligand. In the cases of IMesAuCl and IPrAuCl the %V_{bur} is 36.5 and 44.5 respectively. This could help to explain that the additional bulk in IPr·HCl could block active sites on the iron catalyst as the volume of space it occupies is much greater, thus preventing aryl groups coordinating and preventing product formation.
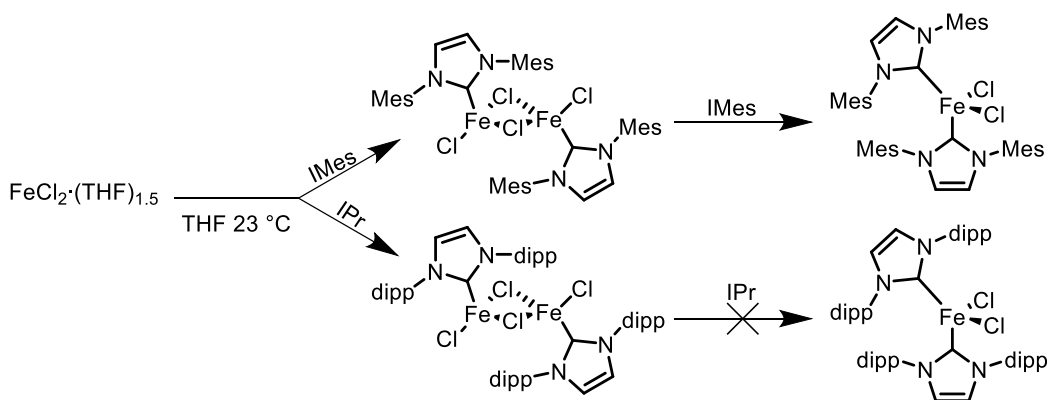
Scheme 2.6 – Synthesis of NHC-Fe complexes by Tonzetich.[155]

In 2007, Grubbs used NHC ligands in a ruthenium-catalysed ring closing metathesis.[158] One of the key findings was that moving the steric bulk from the 2,6-positions of the aryl group on the NHC to the 3,5-positions resulted in a significant increase in yield (from 31% in 24 h to 90% in 1.5 h).[158] However, when SIXyl(3,5)·HCl was trialled in the iron-catalysed Suzuki biaryl cross-coupling reaction it led to a complete loss of reactivity (Table 2.3, entry 5). Attempts to synthesise IXyl(3,5)·HCl have not been successful, and a literature procedure has not been reported.

With the issue of the competitive homo-coupling of the nucleophile still present, it was thought that a much bulkier NHC precursor could be used to prevent over-coordination of the aryl units transferred from the boronate nucleophile. Originally synthesised by the Nolan group,[159] an NHC precursor bearing naphthalene units, INap·HCl, could provide the answers required to decrease the competitive formation of the homo-coupled product. When this ligand was later trialled in the system, it resulted in very low yields of the cross-coupled product (3%) and low yields of the homo-coupled product (4%) (Table 2.3, entry 8). This suggested that it could have been too bulky and therefore was severely impeding the coordination of aryl groups and significantly reducing the yields. On the other end of the sterics scale, IMe·HCl was synthesised and trialled in the reaction, this also resulted in a significant reduction in cross-coupling (Table 2.3, entry 12).

Increasing or decreasing the loading of IMes·HCl resulted in a decrease in catalyst activity (Table 2.3, entries 10 & 11). When the loading was decreased to 5 mol%, the yield dropped to 14%. When it was increased to 20 mol%, the yield dropped to 3%. The additional IMes·HCl in the reaction mixture could be leading to the formation of catalytically inactive bis(NHC)Fe-complex. Reducing the loading, which also reduced cross-coupling, would not provide the necessary amount of ligand to form as much of the catalyst compared to when 10 mol% is used. The free carbene, IMes, was also trialled in the reaction and gave very similar yields to IMes·HCl, showing that the NHC precursor salts have equal activity to the free carbene (Table 2.3, entry 12). Therefore, as the salts are air stable and easier to handle, their use was continued. However, it was later found that the free NHC ligand was more active than the salt (discussed in Chapter 3).

Table 2.3 – Effect of varying NHC ligand.
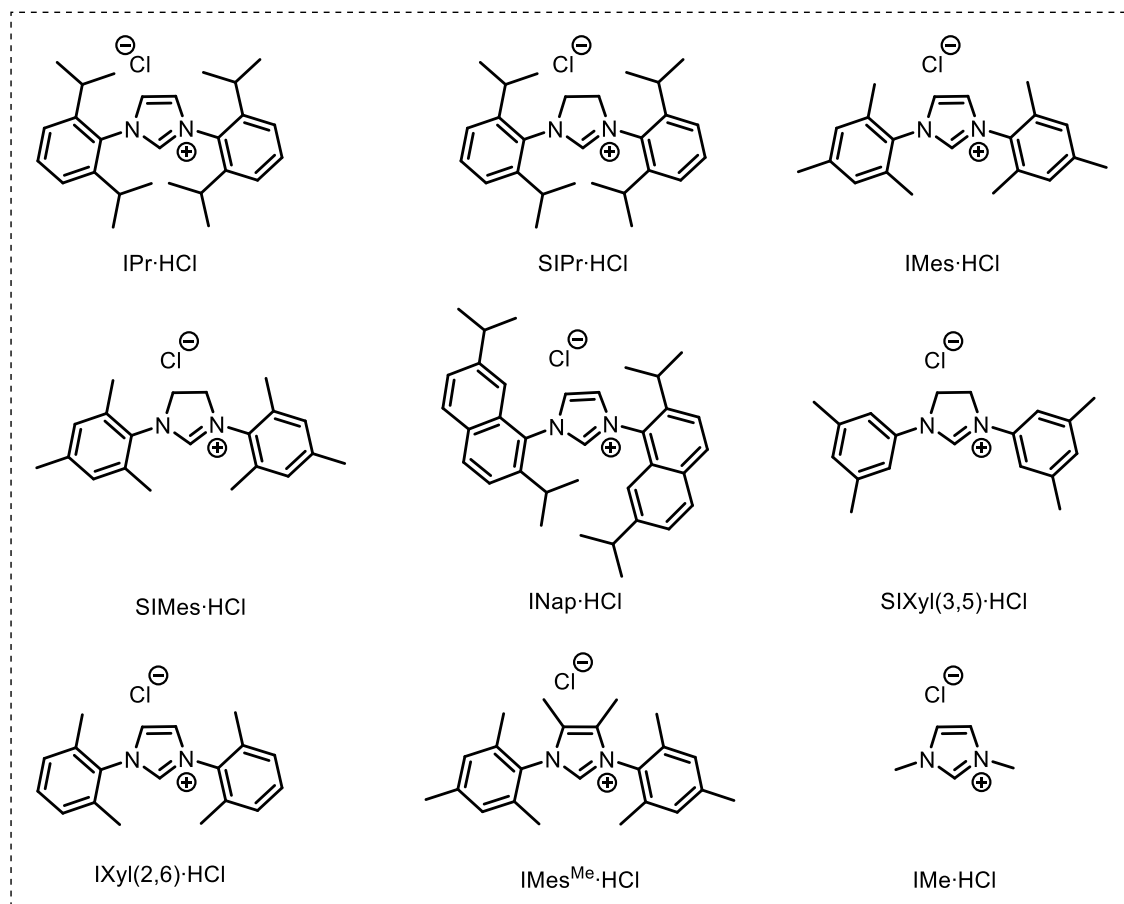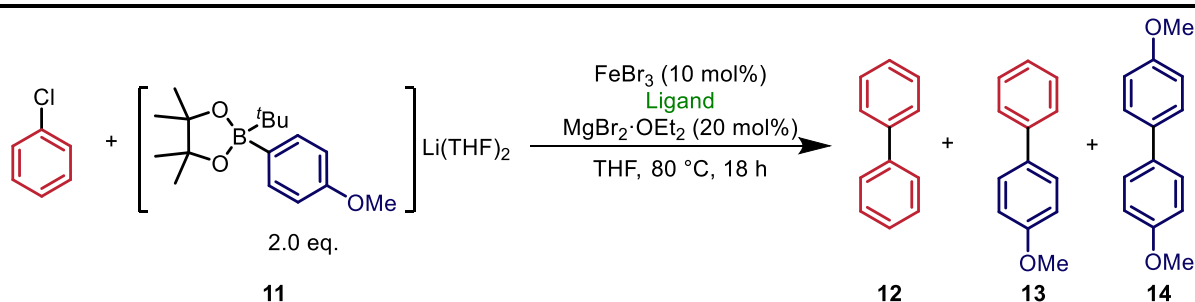
Entry	Ligand	12, % Yield	13, % Yield	14, % Yield
1	IPr·HCl (10 mol%)	< 1	3	11
2	SIPr·HCl (10 mol%)	< 1	2	11
3	IMes·HCl (10 mol%)	2	24	20
4	SIMes·HCl (10 mol%)	< 1	7	12
5	SIXyl(3,5)·HCl (10 mol%)	< 1	2	12
6	IXyl(2,6)·HCl (10 mol%)	1	10	16

7	IMe·HCl (10 mol%)	1	1	1
8	INap·HCl (10 mol%)	1	3	4
9	IMes^{Me}·HCl (10 mol%)	1	10	9
10	IMes·HCl (5.0 mol%)	2	14	15
11	IMes·HCl (20 mol%)	< 1	3	11
12	IMes (10 mol%)	3	25	19

Conditions: chlorobenzene (0.1 mmol), 11 (0.2 mmol), FeBr$_3$ (0.01 mmol), ligand (0.01 mmol), MgBr$_2$·OEt$_2$ (0.02 mmol), THF (1.5 mL), 80 °C, 18 h. Yield determined by GC using dodecane as an internal standard.

With the greatest yield of cross-coupled product **13** still only 24%, it was thought that ring expanded NHC ligands might be able to form much more active species under the reaction conditions. Ring expanded NHC iron complexes were reported in 2016 by Ingleson and ring expanded NHCs have since been used in iron-catalysis.[160] Previously exploited by Duong and Huynh in iron-catalysed cross-coupling reactions of arylmagnesium reagents and aryl chlorides, ring expanded NHCs have shown good activity, in particular 7Mes·HBr led to the greatest activity.[161] In some cases, these ligands have displayed superior activity compared to the five-membered ring NHCs. Studies by Buchmeiser, Hermann, Cavell, and others believe this to be due to a wider N–C–N bond angle.[162–164] This results in a higher degree of sp-hybridisation at the carbene centre, leaving the lone pair of electrons in a more diffuse orbital with greater p-character. With the additional carbons in the ring, it also induces a greater positive inductive effect and results in a more strongly donating carbene. As IMes·HCl showed the greatest activity, the ring expanded NHCs 6Mes, 7Mes, and 8Mes were synthesised, along with 6Pr (Scheme 2.7).
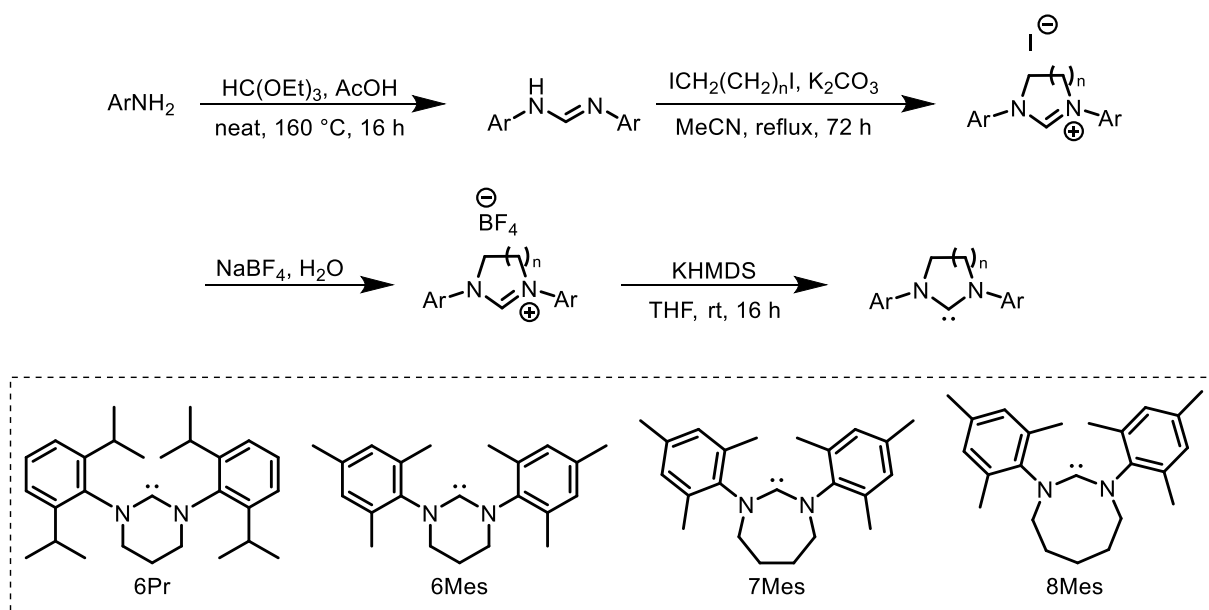
Scheme 2.7 – General synthesis of ring expanded NHCs.

These ligands turned out to give poor conversions, and it was found that the larger the ring, the lower yield of the cross-coupled product (Table 2.4). This could be due to the greater donating ability of the ring expanded NHCs leading to formation of a stronger bond to iron, preventing any reactivity. Another argument could be due to the enlarged N–C–N angle bringing the N-substituents closer to the carbene carbon, leading to greater steric bulk around the metal centre causing extra steric crowding from the mesityl groups around the iron, preventing coordination of the cross-coupling partners.[161]

Table 2.4 – Effect of varying ring expanded NHC ligand.

Entry	Ligand	12, % Yield	13, % Yield	14, % Yield
1	6Pr	1	5	18
2	6Mes	1	7	15

| 3 | 7Mes | 1 | 6 | 20 |
| 4 | 8Mes | 1 | 5 | 16 |

Conditions: chlorobenzene (0.1 mmol), 11 (0.2 mmol), FeBr₃ (0.01 mmol), ligand (0.01 mmol), MgBr₂·OEt₂ (0.02 mmol), THF (1.5 mL), 80 °C, 18 h. Yield determined by GC using dodecane as an internal standard.

Next, we investigated the effect of changing the iron salt on the reaction. In the substrate directed iron-catalysed Suzuki biaryl cross-coupling reaction, Bedford found $FeBr_3$ to be the best candidate,[87] it was hypothesised that the boronate nucleophile reduces the iron species before it enters the cycle, potentially forming an Fe(I) or Fe(II) species. Therefore, the screen was initiated with $FeBr_3$ which yielded 24% of the cross-coupled product. In previously reported iron-catalysed cross-coupling reactions others have suggested alternate iron sources were better and could also suppress any homo-coupling. As homo-coupling of the nucleophile has been a persistent issue it was decided to explore this further. Nakamura reported that use of a fluoride salt, such as FeF_3, could suppress homo-coupling in a reaction between aryl halides and aryl Grignard reagents.[120,165] It was hypothesised that the fluoride coordinates strongly to the iron centre, limiting the number of anionic aryl ligands from the Grignard reagent to one, and thus limiting any homo-coupling. Further to this, Duong used $Fe(OTf)_2$ to catalyse the cross-coupling of aryl chlorides and tosylates with aryl Grignard reagents.[166] In this case, it was proposed that the non-coordinating triflate anion could retard the transmetallation step, suppressing the homo-coupling pathway. With these hypotheses in mind, a range of iron halide salts were then screened (Table 2.5). $FeCl_3$ and FeF_3 gave slightly lower yields of the cross-coupled product compared to $FeBr_3$, 19 and 18% respectively (Table 2.5, entries 7–9). Alongside the cross-coupled product, these reactions also yielded relatively large amounts of the homo-coupled product, **14** (17 and 18%). As it was hypothesised that the Fe(III) species was being reduced to an Fe(II) species by the boronate, putting a preformed Fe(II) species straight into the reaction mixture could increase the rate of reaction. This could outcompete the formation of **14** and lead to a greater yield of **13**. When FeF_2, $FeCl_2$, $FeBr_2$, FeI_2, $Fe(CH_3CO_2)_2$, and $Fe(OTf)_2$ were trialled in the reaction, they all led to a reduction in yield of the cross-coupled product **13** by at least 10% (Table 2.5, entries 1–6); the most active was $Fe(OTf)_2$ which resulted in 15% yield of the cross-coupled product. In all cases, the formation of the homo-coupled product outcompeted the formation of the cross-coupled product and gave greater yields. Decreasing the loading of $FeBr_3$ to 5 mol% led to a reduction in formation of **13** to 1% and increasing the loading to 15 and 20 mol% also lead to a decrease in yield of **14** to 11% (Table 2.5, entries 10–12).

Table 2.5 – Effect of varying iron salt.

Entry	Fe Source (mol%)	12, % Yield	13, % Yield	14, % Yield
1	FeF_2	3	10	15
2	$FeCl_2$	2	11	16
3	$FeBr_2$	3	14	18
4	FeI_2	3	11	18
5	$Fe(CH_3CO_2)_2$	3	14	15
6	$Fe(OTf)_2$	3	15	18
7	FeF_3	2	18	17
8	$FeCl_3$	2	19	18
9	$FeBr_3$	2	24	20
10	$FeBr_3$ (5)	< 1	1	1
11	$FeBr_3$ (15)	1	11	13
12	$FeBr_3$ (20)	1	11	12

Conditions: chlorobenzene (0.1 mmol), **11** (0.2 mmol), Fe salt (0.01 mmol, unless otherwise stated), IMes·HCl (0.01 mmol), MgBr₂·OEt₂ (0.02 mmol), THF (1.5 mL), 80 °C, 18 h. Yield determined by GC using dodecane as an internal standard.

The NHC-FeCl₂ dimers (NHC = IMes or IPr), originally synthesised by Tonzetich, have also shown to have catalytic properties and have been utilised in the coupling of aryl and alkyl halides with alkyl and aryl Grignard reagents.[155,167] As the initial optimisation results have shown a reliance on IMes·HCl and it is proposed that the boronate may reduce Fe(III) to Fe(II), it was thought that the active iron species could be similar to the dimer. Therefore, pre-forming the iron dimer **15**, and using it in the reaction could increase cross-coupling as the catalytically active species is already formed and does not require an initial pre-catalytic step. This might also decrease the

homo-coupling of the nucleophile, as the initial reduction of iron would not be necessary. However, when trialled in the reaction the yield of **13** decreased to 15%.
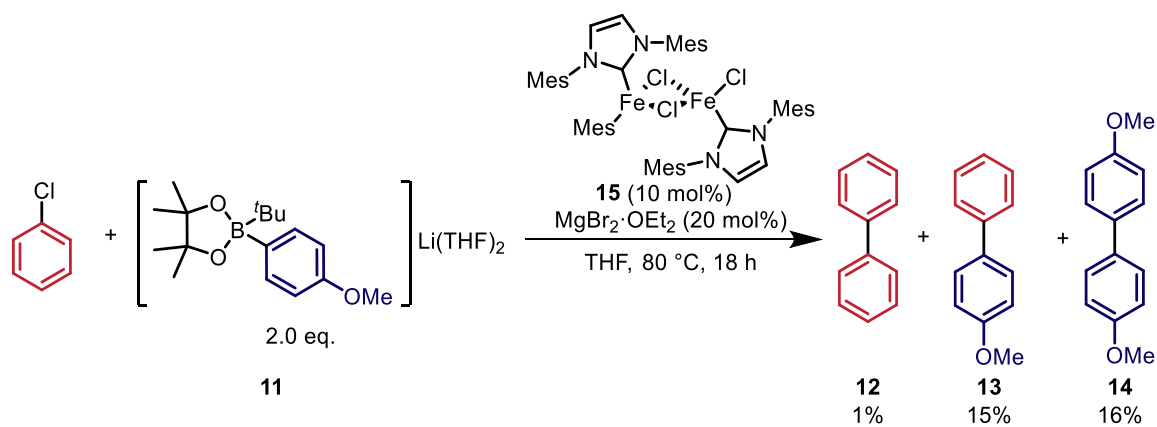
Scheme 2.8 – Effect of using IMesFeCl₂ dimer (15) in the reaction. Conditions: chlorobenzene (0.1 mmol), 11 (0.2 mmol), 15 (0.01 mmol), MgBr₂·OEt₂ (0.02 mmol), THF (1.5 mL), 80 °C, 18 h. Yield determined by GC using dodecane as an internal standard.

2.2.3 Boronic Ester Screen

The most common diol used in the synthesis of boronic esters for Suzuki cross-coupling reactions is pinacol. This is due to it being very stable, relatively cheap, and commercially available. However, there have been significant results found with other diols, often leading to formation of 6 membered rings in the boronic ester backbone. Duong and co-workers used a neo-pentyl glycol derived boronic ester to cross-couple with heteroaryl halides using a cobalt catalyst, with 31 examples and yields up to 93% (Scheme 2.9).[135] The six membered boronic ester was activated by potassium methoxide base rather than the more commonly used organolithium reagents. Although the reaction worked using heteroaryl chlorides (mainly pyridines), it struggled to cross-couple aryl halides that do not contain a heteroatom. Bedford has since reported a cobalt-catalysed Suzuki biaryl cross-coupling reaction that also employs alkoxide bases and can couple simple aryl chlorides (Scheme 2.9).[42]
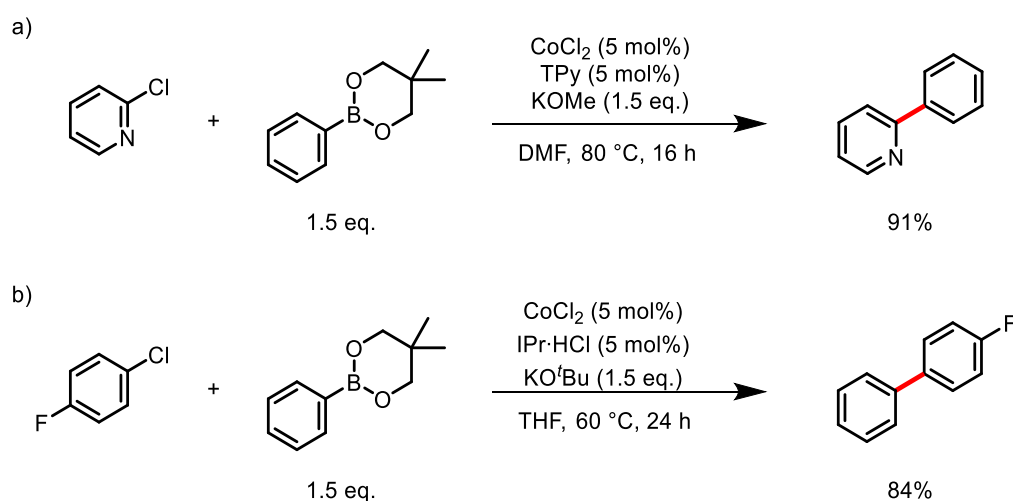

Scheme 2.9 – Cobalt-catalysed Suzuki biaryl cross-couplings using neopentyl glycol backbone on boronic ester: a) Duong,[135] b) Bedford.[42]

Intrigued by Duong's and Bedford's findings, a range of boronic esters with different sized rings and different substituents were synthesised with the hope that these might provide greater reactivity. These boronic esters were then activated with ^{t}BuLi, rather than the alkoxide salts that have been used in cobalt-catalysed Suzuki biaryl cross-couplings, and trialled in the reaction (Table 2.6). The results obtained show that the most active boronate was that derived from pinacol, and the other boronates showed very limited activity (Table 2.6, entry 1). A notable result came from the boronate derived from 2,4-pentanediol (Table 2.6, entry 4). Although this boronate was not very reactive, only forming 9% cross-coupled product, the formation of the homo-coupled

product was suppressed to less than 1%. This showed that it is possible to 'switch off' formation of the homo-coupled product. Moving from ^{t}BuLi to ^{n}BuLi resulted in a complete loss of reactivity, showing that less nucleophilic organolithium reagents cannot be used at this stage (Table 2.6, entry 8).
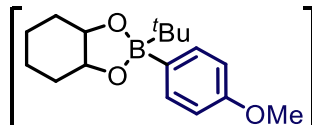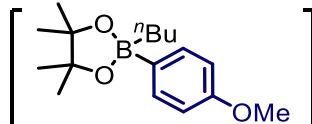
Table 2.6 – Effect of changing boronic ester backbone on the reaction.
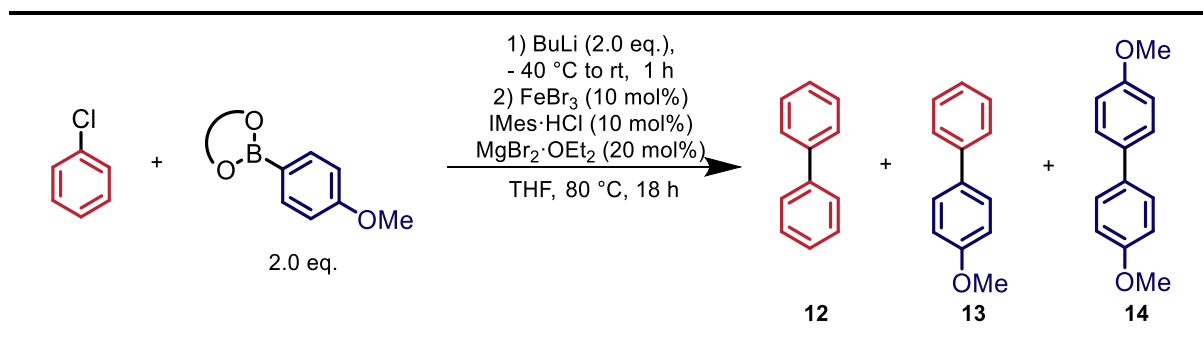
Entry	Boronate formed *in situ*	12, % Yield	13, % Yield	14, % Yield
1		2	21	16
2		< 1	5	14
3		< 1	3	7
4		1	9	< 1
5		< 1	1	2
6		< 1	< 1	2

|				
7	[structure: cyclohexane-fused dioxaborolane with ^{t}Bu and 4-OMe-phenyl]Li(THF)$_2$	< 1	< 1	< 1
8	[structure: pinacol boronate with ^{n}Bu and 4-OMe-phenyl]Li(THF)$_2$	< 1	< 1	< 1

Conditions: chlorobenzene (0.25 mmol), boronic ester (0.5 mmol), BuLi (0.5 mmol), FeBr$_3$ (0.025 mmol), IMes·HCl (0.025 mmol), MgBr$_2$·OEt$_2$ (0.05 mmol), THF (3.0 mL), 80 °C, 18 h. Yield determined by GC using dodecane as an internal standard.

2.2.4 Temperature and Solvent Screen

It was previously shown that a decrease in the reaction temperature from 80 °C to 60 °C led to a decrease in yield of **13** to 11%, which showed that the reaction is temperature dependent. As the boiling point of THF is 66 °C, a change in solvent was needed to investigate whether further increases in temperature would increase the yield of the reaction. A solvent with very similar properties to THF but with a greater boiling point is 2-MeTHF. Use of 2-MeTHF as the solvent allowed greater reaction temperatures to be reached. When reacted at external temperatures of 80, 90 and 100 °C, gradual increases in yield were observed from 25%, 29% to 35% (Figure 2.1).
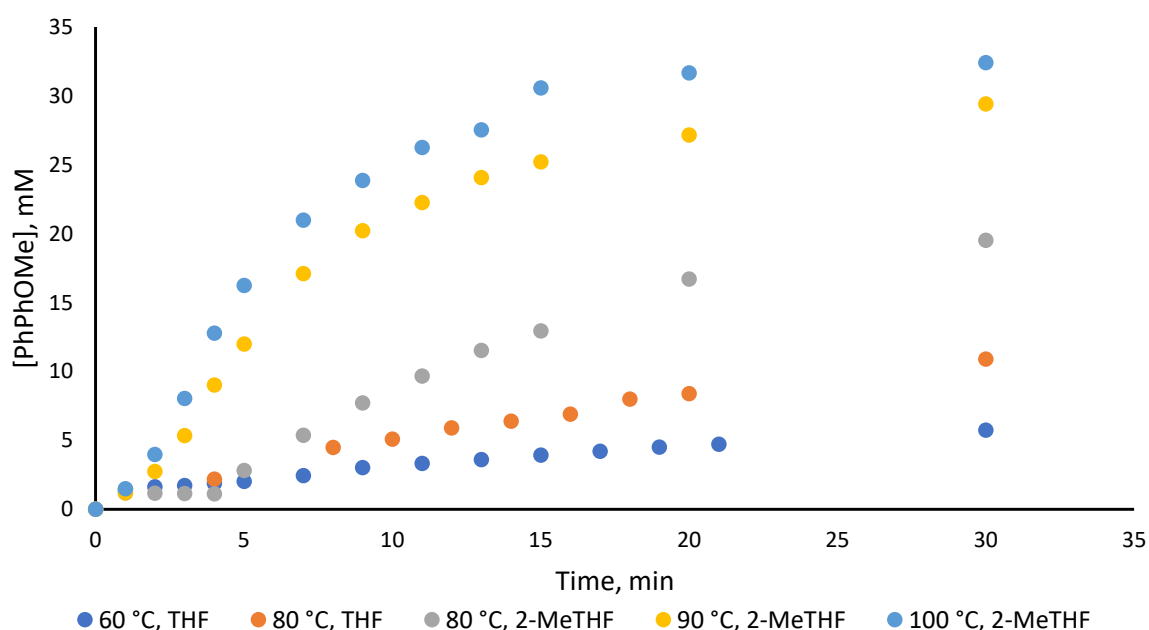

Figure 2.1 – Temperature dependence of reaction using THF and 2-MeTHF. Conditions: chlorobenzene (1.0 mmol), 11 (2.0 mmol), FeBr₃ (0.1 mmol), IMes·HCl (0.1 mmol), MgBr₂·OEt₂ (0.2 mmol), solvent (10 mL). Yield determined by GC using dodecane as an internal standard.

With these positive results in hand, the next logical step was to screen a range of other polar and aprotic solvents, with greater boiling points than THF and 2-MeTHF (Table 2.7). The solvent and temperature that gave highest yield (45%) was a 1:1 mixture of 2-MeTHF and 1,4-dioxane at 100 °C (Table 2.7, entry 6). Using either 2-MeTHF or 1,4-dioxane, at external temperatures of 100 °C and at 110 °C respectively, decreased the yields to 36 and 35% respectively (Table 2.7, entries 5 & 7). Use of 1,4-dioxane led to issues with the solubility of the reaction mixture, whereas solubility in 2-MeTHF was not an issue but greater temperatures could not be reached. Therefore, the combination of the two allowed for elevated reaction temperatures and full dissolution of the

reaction mixture. Changing the ratio of 2-MeTHF and 1,4-dioxane to 2:1 or 1:2 led to a decrease in cross-coupling (Table 2.7, entries 17 & 18). Another notable solvent used was pyridine where a yield of 41% was obtained (Table 2.7, entry 10). A reduction in yield was seen when toluene was used; this is likely to be due to poor solubility of the metal salts, although toluene has successfully been employed as a solvent in other iron-catalysed reactions (Table 2.7, entry 16).[81,82] When the polarity of the solvent was increased further to incorporate solvents such as DMF, DMA, MeCN, and DMSO the reactivity was almost completely shut down (Table 2.7, entries 8, 9, 13–15). Although the yields of the cross-coupled product have increased significantly with the change of solvent and temperature, the yield of **14** only increased slightly to 24% when a 1:1 mixture of 2-MeTHF and 1,4-dioxane was used. These results show that without a directing group on the aryl halide substrate, much harsher conditions are required to achieve cross-coupling.

Table 2.7 – Effect of temperature and solvent on reaction.
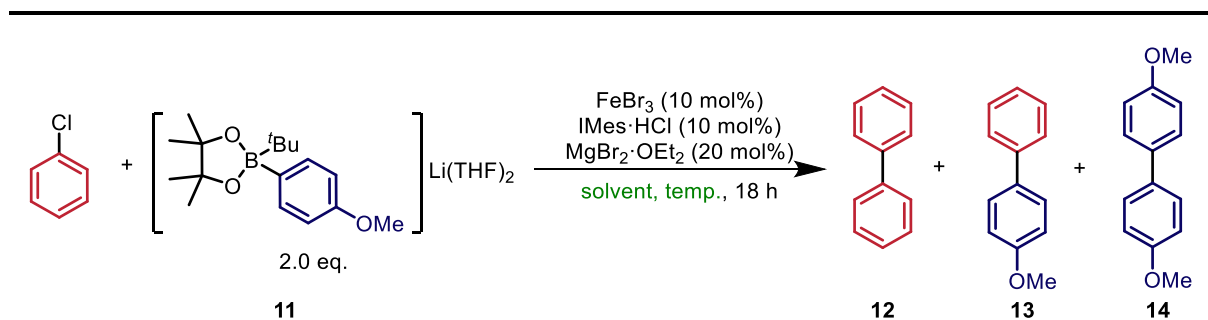
Entry	Solvent	External Temperature, °C	12, % Yield	13, % Yield	14, % Yield
1	THF	60	1	11	16
2	THF	80	2	24	20
3	2-MeTHF	80	3	27	20
4	2-MeTHF	90	4	32	23
5	2-MeTHF	100	5	36	25
6	2-MeTHF:1,4-dioxane (1:1)	100	6	45	24
7	1,4-dioxane	110	5	35	28
8	DMF	155	<1	19	3
9	DMF	125	<1	3	1
10	Pyridine	110	7	41	20
11	DME	85	2	17	23

| 12	DCE	85	<1	1	19
13	MeCN	80	<1	1	2
14	DMA	120	<1	1	2
15	DMSO	120	1	2	2
16	Toluene	110	7	25	25
17	2-MeTHF:1,4-dioxane (1:2)	100	6	33	24
18	2-MeTHF:1,4-dioxane (2:1)	100	5	39	28

Conditions: chlorobenzene (0.25 mmol), 11 (0.5 mmol), FeBr$_3$ (0.025 mmol), IMes·HCl (0.025 mmol), MgBr$_2$·OEt$_2$ (0.05 mmol), solvent (3.0 mL), 18 h. Yield determined by GC using dodecane as an internal standard.

2.2.5 Additive Screens

In the proposed mechanism of the substrate-directed iron-catalysed Suzuki biaryl cross-coupling reaction, it is hypothesised that the initial step involves the reduction of Fe(III) to form an Fe(II) species and in this step the homo-coupled product is formed.[87] This leaves a lower concentration of the boronate able to be involved in the cross-coupling thus potentially reducing yields. It was thought that an external sacrificial reducing agent could be used for this role to reduce the iron, so the active catalytic species could be formed without an initial reaction with the boronate. Thus, this could increase the cross-coupling and decrease homo-coupling of the nucleophile. A range of reducing agents were screened including Grignard reagents and hydride reagents (Table 2.8). Of those screened, four were found to increase the yield: ^{n}BuLi, MeMgBr, $NaBH_4$ and $LiAlH_4$ (Table 2.8, entries 2, 7, 10 & 11). The greatest yields were observed with MeMgBr and $LiAlH_4$, where both gave 55% of the cross-coupled product. MeMgBr was viewed as the preferred option as the yield of homo-coupled product was 33%, whereas for $LiAlH_4$ it was 44%. Although the nucleophilic homo-coupling was also increased, the use of an initiator in the reaction was advantageous. It could be that the other Grignard reagents were not able to reduce the Fe(III) *in situ* and instead formed iron species that were not catalytically active. Neidig previously reported that reaction of $FeCl_3$ with MeMgBr in THF at low temperatures produced a tetramethyliron(III) ferrate complex, $[FeMe_4]^-$.[102,168] The crystal structure of this distorted square-planar ferrate complex contains a noncoordinating $[MgCl(THF)_5]^+$ countercation. This ferrate was shown to react further upon warming to 0 °C to form a $[Fe_8Me_{12}]^-$ cluster with the same noncoordinating countercation. This cluster has been shown to be a reactive and a catalytically relevant species. Although $FeCl_3$ was used rather than $FeBr_3$, and the $[Fe_8Me_{12}]^-$ species was shown to be extremely temperature dependent, with the likelihood of forming at 100 °C being very low, a test reaction without IMes·HCl present was carried out. This resulted in a reduction of yield to 7% of cross-coupled product. This shows that an iron-IMes species is likely to be catalytically active, and it is unlikely that an $[Fe_8Me_{12}]^-$ cluster is.

The loading of the reducing agent was also investigated for MeMgBr, and 10 mol% proved to be the best yielding for the cross-coupled product (Table 2.8, entries 7, 12 & 13). This is in a ratio of 1:1 with $FeBr_3$ and IMes·HCl. When the loading was changed to 5 or 15%, the yield of cross-coupled product decreased. This was also the case for the homo-coupled product. It was later found, and is discussed in Chapter 3, that the role of MeMgBr was to deprotonate IMes·HCl rather than to reduce an iron species.

Table 2.8 – Effect of using a reducing agent on reaction.
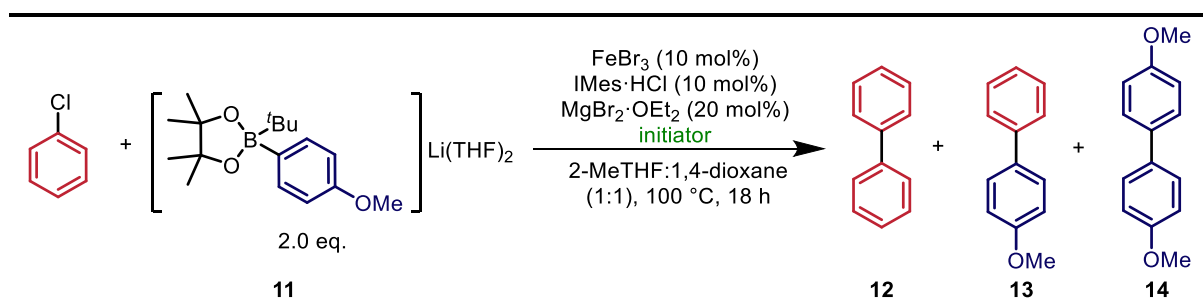
Entry	Reducing Agent	mol%	12, % Yield	13, % Yield	14, % Yield
1	None	0.0	6	45	24
2	^{n}BuLi	10	11	49	17
3	^{n}BuMgCl	10	5	37	20
4	TolylMgBr	10	6	46	30
5	EtMgCl	10	4	36	22
6	1,3-dioxane-2-yl-ethyl magnesium chloride	10	5	41	31
7	MeMgBr	10	8	55	33
8	EtMgBr	10	4	40	28
9	NaHBEt$_3$	10	3	26	22
10	NaBH$_4$	10	5	51	44
11	LiAlH$_4$	10	6	55	40
12	MeMgBr	5.0	9	54	32
13	MeMgBr	15	6	42	26

Conditions: chlorobenzene (1.0 mmol), 11 (2.0 mmol), FeBr$_3$ (0.1 mmol), IMes·HCl (0.1 mmol), MgBr$_2$·OEt$_2$ (0.2 mmol), 2-MeTHF:1,4-dioxane (1:1) (12 mL), 100 °C, 18 h. Yield determined by GC using dodecane as an internal standard.

Previous work done by Neidig and Nakamura, as well as others, has shown that additives such as TMEDA and NMP[46,47,62,110,113,114,169] can act to stabilise species in the catalytic system and result in higher yielding reactions. Although, efforts have been made to replace NMP in iron-catalysed

reactions, with less toxic O-coordinating ligands.[170,171] The role of the additive is not well known and has been shown in some examples to not even interact with iron species, but it is thought to stabilise catalytically active species. One of the most common additives used is NMP and thus was trialled under the reaction conditions with and without MeMgBr (Table 2.9, entries 3–10). As the literature reports a variety of loadings of NMP, we opted to screen a range of 10–100 eq. of NMP with respect to FeBr$_3$. The general trend shows that as the loading of NMP increases, both the yield of cross-coupled product and the activity of the catalyst decreases. This could be due to NMP coordinating to an iron species in solution and stopping the catalytically active iron species from forming, and therefore inhibiting the reaction.

TMEDA was also trialled as an additive in the reaction (Table 2.9, entries 11–18). A range of eq. of TMEDA with respect to FeBr$_3$ were used both in the presence and absence of MeMgBr. Excluding what appears to be an anomaly with 10 eq. of TMEDA with respect to FeBr$_3$, it appears that addition of TMEDA to the reaction mixture shuts the reaction down and leads to very low yields of the cross-coupled product. This is potentially due to TMEDA coordinating to any iron species that are formed in the reaction mixture and rendering them catalytically inactive or it could be coordinating to the MgBr$_2$, preventing it from playing a role in the cycle.[99]

Table 2.9 – Effect of using additives in the reaction.

Entry	Additive	Eq. (with respect to FeBr₃)	MeMgBr, mol%	12, % Yield	13, % Yield	14, % Yield
1	/	/	10	6	55	33
2	/	/	0.0	6	45	24
3	NMP	10	10	3	19	24
4	NMP	20	10	2	18	20
5	NMP	50	10	2	16	20

6	NMP	100	10	2	12	19
7	NMP	10	0.0	3	25	22
8	NMP	20	0.0	3	12	21
9	NMP	50	0.0	1	9	15
10	NMP	100	0.0	1	12	16
11	TMEDA	1.0	10	1	12	14
12	TMEDA	2.0	10	1	5	13
13	TMEDA	5.0	10	1	4	11
14	TMEDA	10	10	1	30	25
15	TMEDA	1.0	0.0	1	6	13
16	TMEDA	2.0	0.0	1	6	11
17	TMEDA	5.0	0.0	1	7	13
18	TMEDA	10	0.0	1	5	11

Conditions: chlorobenzene (1.0 mmol), 11 (2.0 mmol), FeBr$_3$ (0.1 mmol), IMes·HCl (0.1 mmol), MgBr$_2$·OEt$_2$ (0.2 mmol), MeMgBr (0.1 or 0 mmol), additive, 2-MeTHF:1,4-dioxane (1:1) (12 mL), 100 °C, 18 h. Yield determined by GC using dodecane as an internal standard.

Co-catalysts, such as MgBr$_2$, AlBr$_3$ and ZnBr$_2$, have been commonly employed in iron-catalysed cross-coupling reactions and play a crucial role in catalyst activity.[62,63,82,89] The role of the co-catalyst is debated, with some suggestions that the metal acts as a transmetallating agent as the aryl unit released from the boronate is able to coordinate to it before being transferred to the iron.[79,81] Bedford and co-workers have proposed that instead of the metal playing a role in transmetallation, it instead acts as a halide donor with formation of an iron-halide species and aids oxidative addition.[87]

The most commonly employed co-catalysts are bromide salts, but chloride salts have also shown good reactivity. In almost all cases the bromide salts outperformed their chloride counterparts (Table 2.10). MgBr$_2$·OEt$_2$ proved to be the best halide salt resulting in 55% formation of cross-coupled product and 33% formation of the homo-coupled product (Table 2.10, entry 4). When the loading of MgBr$_2$·OEt$_2$ was either decreased or increased to 10 or 25 mol% the yield of **13** also decreased to 46 and 49% respectively (Table 2.10, entries 20 & 21). However, the amount of **14**

produced stayed fairly constant no matter the loading of $MgBr_2 \cdot OEt_2$, indicating that the homo-coupling of the nucleophile is potentially independent of $MgBr_2 \cdot OEt_2$. $ZnBr_2$ and $AlBr_3$, did not perform well with yields of 2% and 19% of **13** respectively (Table 2.10, entries, 5 & 6). Ammonium salts, tetraethylammonium bromide (TEAB) and tetrabutylammonium bromide (TBAB), worked well in the reaction producing yields of 50 and 51% of **13** respectively (Table 2.10, entries 8 & 9). In most cases the production of **14** remains relatively high. These results indicate that in this system the co-catalyst perhaps acts in a similar role to that shown in the substrate directed iron-catalysed Suzuki reaction rather than as a transmetallating agent reported by others.[79,81]

Table 2.10 – Effect of using different halide salts in the reaction.
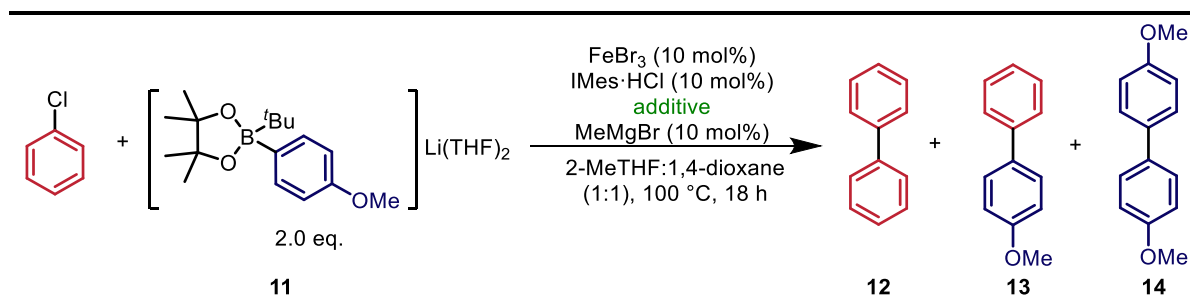
Entry	Co-catalyst (mol%)	12, % Yield	13, % Yield	14, % Yield
1	LiBr (20)	4	37	27
2	NaBr (20)	4	37	28
3	KBr (20)	3	39	31
4	MgBr₂ (20)	6	55	33
5	AlBr₃ (20)	2	19	20
6	ZnBr₂ (20)	1	2	17
7	TMAB (20)	5	34	23
8	TEAB (20)	4	50	36
9	TBAB (20)	6	51	30
10	LiCl (20)	3	30	24
11	NaCl (20)	2	16	25
12	KCl (20)	4	35	27
13	MgCl₂ (20)	1	9	11

14	AlCl$_3$ (20)	2	16	21
15	ZnCl$_2$ (20)	1	1	11
16	GaCl$_3$ (20)	1	1	5
17	N[Me$_4$]Cl (20)	5	34	24
18	N[Et$_4$]Cl (20)	4	32	24
19	N[Bu$_4$]Cl (20)	3	20	17
20	MgBr$_2$ (10)	2	46	30
21	MgBr$_2$ (25)	4	49	32
22	N/A	3	36	25

Conditions: chlorobenzene (0.1 mmol), 11 (0.2 mmol), FeBr$_3$ (0.01 mmol), IMes·HCl (0.01 mmol), co-catalyst, MeMgBr (0.01 mmol), 2-MeTHF:1,4-dioxane (1:1) (1.5 mL), 100 °C, 18 h. Yield determined by GC using dodecane as an internal standard.

2.2.6 Additional Optimisation

With the yield of **13** raised from 11% (using the initial conditions used in the substrate-directed iron-catalysed Suzuki biaryl cross-coupling) to 55% during previous optimisation, it was believed that this could be improved even further. One thing that had not yet been investigated was the loading of the boronate **11**. If the MeMgBr used does in fact reduce the iron pre-catalyst, then perhaps a lower loading of **11** would be needed to prevent over reduction of the iron pre-catalyst and increase activity. Alternatively, increasing the loading of **11** might provide the necessary material to lead to greater cross-coupling. Therefore, the loading was varied from 1.0 to 3.0 eq. (Table 2.11). As the loading increased from 1.0 to 2.5 eq., the yield of **13** increased to 61%, but when increased further, the yield dropped. The yield of **14** doubled from 14 to 30% when the loading was increased from 1.0 to 1.8 eq. but then when increased further the yield varied little from 30 to 38%.

Table 2.11 – Effect of changing the loading of 11 on the reaction.

Entry	Eq. of 11	12, % Yield	13, % Yield	14, % Yield
1	1.0	3	21	14
2	1.2	3	24	18
3	1.4	4	32	23
4	1.6	4	35	22
5	1.8	5	44	30
6	2.0	8	55	33
7	2.2	5	56	32
8	2.4	5	58	30
9	2.5	4	61	35
10	2.6	5	52	38

| 11 | 2.8 | 4 | 45 | 36 |
| 12 | 3.0 | 4 | 43 | 34 |

Conditions: chlorobenzene (0.1 mmol), 11, FeBr₃ (0.01 mmol), IMes·HCl (0.01 mmol), MgBr₂·OEt₂ (0.02 mmol), MeMgBr (0.01 mmol), 2-MeTHF:1,4-dioxane (1:1) (1.5 mL), 100 °C, 18 h. Yield determined by GC using dodecane as an internal standard.

The loading of catalytic reagents was then investigated to see if increasing this could improve the yield or if there was an optimum loading that was lower than 10% (Table 2.12). It was found that decreasing the loading to 5 mol% FeBr₃, 5 mol% IMes·HCl, 10% MgBr₂·OEt₂ and 5% MeMgBr decreased the yield of cross-coupled product to 50% and the homo-coupled product to 28% (Table 2.12, entry 1). This is likely to be because there is less catalyst in the reaction and therefore less product formation. Whereas increasing the loading to 15 mol% FeBr₃, 15 mol% IMes·HCl, 30% MgBr₂.OEt₂ and 15% MeMgBr caused a greater decrease in the yield of cross-coupled product to 51%, while the homo-coupled product, **14**, remained at a similar yield (29%) (Table 2.12, entry 2). The decrease in yield here could be due to over saturation of the system or aggregation of iron species resulting in a decrease in catalytic activity.

Table 2.12 – Effect of changing the catalytic reagents loading on the reaction.

Entry	FeBr₃, IMes·HCl & MeMgBr loading, mol%	MgBr₂·OEt₂ loading, mol%	12, % Yield	13, % Yield	14, % Yield
1	5.0	10	5	50	28
2	10	20	4	61	35
3	15	30	6	51	29

Conditions: chlorobenzene (0.1 mmol), 11 (0.25 mmol), FeBr₃, IMes·HCl, MgBr₂·OEt₂, MeMgBr, 2-MeTHF:1,4-dioxane (1:1) (1.5 mL), 100 °C, 18 h. Yield determined by GC using dodecane as an internal standard.

The formation of **14** from the nucleophile homo-coupling was a persistent issue in the reaction optimisation, both for the selectivity of the catalyst and the detrimental effect on the yield of **13**. Therefore, a way to reduce the yield of **14** and if possible, increase the yield of **13** would be beneficial. A potential way to do this might be the slow addition of either the electrophile or nucleophile. Slow addition of the nucleophile would lower the concentration of **11** in the reaction at any one time, compared to the standard addition, and therefore favour cross-coupling over homo-coupling. Slow addition of nucleophiles in iron-catalysed Kumada coupling reactions has proven to reduce nucleophile homo-coupling, where it is argued that it prevents over transmetallation to the iron centre.[112] Conversely, slow addition of the electrophile might also limit the amount of an oxidant in the reaction and could limit the homo-coupling of the nucleophile; prevention of any excess oxidant in the reaction may prevent re-oxidation and formation of an Fe species responsible for the homo-coupling, which could result in further cross-coupling. Standard conditions involve the addition of the electrophile to a Schlenk tube containing a suspension of the other reagents (except boronate **11**) in 1,4-dioxane. This is then followed by rapid addition of a solution of the boronate in 2-MeTHF. To limit any electronic differences between the two aryl units favouring either cross-coupling or homo-coupling of the nucleophile, the electrophile was changed from chlorobenzene to 4-ethoxychlorobenzene. The electrophile and nucleophile were then added dropwise to their separate reaction mixtures over 1 h using a syringe pump (Figure 2.2).
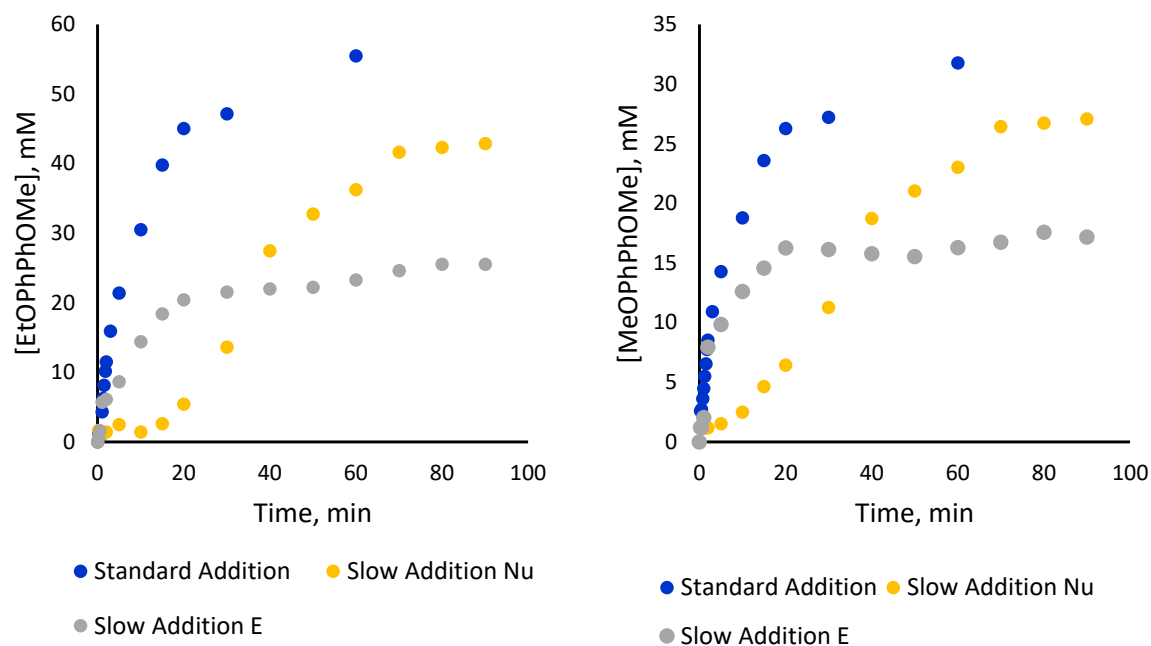
Figure 2.2 – Effect of slow addition of the electrophile (E) and nucleophile (Nu) on the reaction (Left: cross-coupling. Right: homo-coupling). Conditions: 4-ethoxychlorobenzene (0.5 mmol), 11 (1.25 mmol), FeBr₃ (0.05 mmol), IMes·HCl (0.05 mmol), MgBr₂·OEt₂ (0.1 mmol), MeMgBr (0.05 mmol), 2-MeTHF:1,4-dioxane (1:1) (6.0 mL), 100 °C, 1 h. Yield determined by GC using dodecane as an internal standard.

The dropwise addition of the nucleophile to the reaction mixture led to an expected decrease in the rate of formation of 4-methoxy-4'-ethoxybiphenyl with a slight sigmoidal curve, and also a drop in yield to 51% (-10%). The effect on the homo-coupling of the nucleophile was the same, with a slight decrease in yield from 32% to 27%. Overall, the effect of slow addition of the nucleophile had a limited effect on the overall reaction. When the electrophile was added over an hour the effect on the reaction was much greater; both the formation of 4-methoxy-4'-ethoxybiphenyl and 4,4'-dimethoxybiphenyl decreased to 31% and 16% respectively. To conclude, neither the slow addition of either the electrophile or nucleophile improved the result of the reaction, and in fact the slow addition of electrophile significantly hindered the reaction.

A catalyst designed to block the catalytic pathway to the formation of **14** was still desired. The use of the bulkier INap·HCl did not successfully promote cross-coupling, but it did hinder the formation of **14** (Table 2.3). It was hypothesised that the use of a bidentate chelating NHC ligand could improve upon this. The chelating (bis)carbene ligands **16** and **17** were first reported by Arnold in 2016, and were used to support thorium complexes that could undergo further reactions.[172] If **13** and **14** are both formed from a common iron intermediate then these ligands could coordinate to the iron-catalyst and potentially block a coordination site, only allowing for

67

two aryl units on the iron centre. If this was the case, then this could promote cross-coupling over homo-coupling of the nucleophile. Furthermore, iron complexes supported by ligand **17** have been reported by Smith, such as the Fe(I) complex **18** (Figure 2.3).[173]
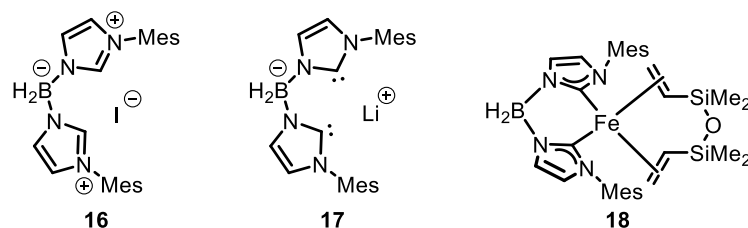

Figure 2.3 – Chelating (bis)carbene ligands (16 and 17) reported by Arnold[172] and the iron complex (8) subsequently published by Smith.[173]

Ligands **16** and **17** were then synthesised according to the literature procedure and subsequently trialled in the reaction.[172] This resulted in diminution of cross-coupling ability and led to a reduction in yield of cross-coupled product **13** to 11 and 10% respectively (Scheme 2.10). The formation of **14** was seemingly unaffected giving yields of 30 and 26% respectively. If the ligand did chelate to the iron, then it could have just blocked a site for the electrophile aryl group rather than the additional biaryl unit from the nucleophile. Or it could be that formation of **13** and **14** occur on independent iron complexes where only the iron species that is involved with cross-coupling was affected. Nonetheless, the use of the ligand was not beneficial.
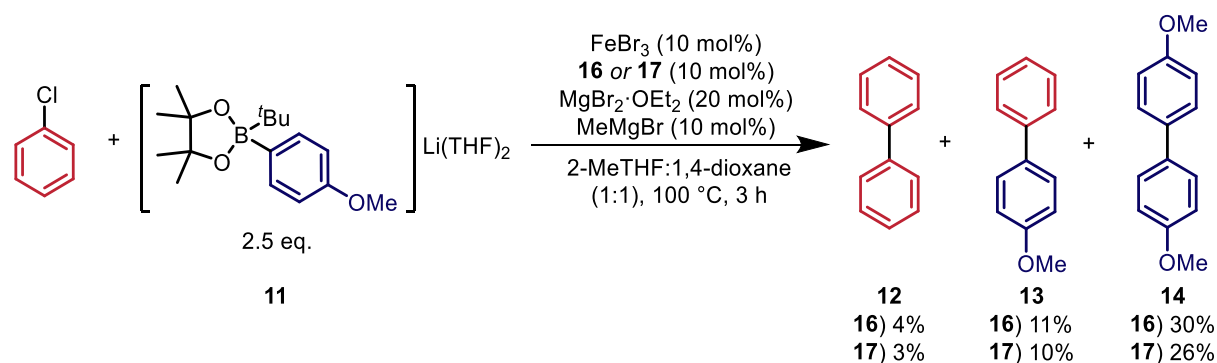
Scheme 2.10 – Effect of using ligands 16 and 17. Conditions: chlorobenzene (0.5 mmol), 11 (1.25 mmol), FeBr$_3$ (0.05 mmol), ligand (0.05 mmol), MgBr$_2$·OEt$_2$ (0.1 mmol), MeMgBr (0.05 mmol), 2-MeTHF:1,4-dioxane (1:1) (6.0 mL), 100 °C, 3 h. Yield determined by GC using dodecane as an internal standard.

It has previously been reported that visible light can been used to promote iron-catalysed cross-coupling reactions.[174] For example, in 2019, Alcázar and Noel published a report on a visible light
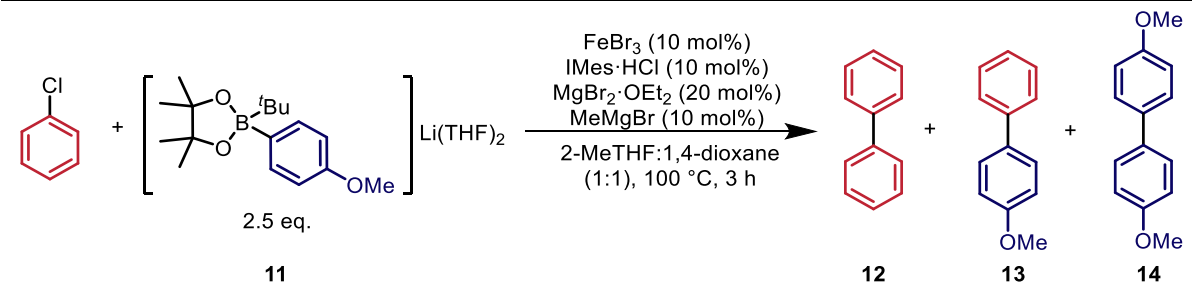
promoted iron-catalysed Kumada cross-coupling reaction in flow (Figure 2.4).[55] Aryl chlorides were coupled with aliphatic Grignard reagents using a continuous-flow, visible-light promoted method at room temperature alongside an Fe(acac)$_3$ (2–10 mol%) and SIPr·HCl (4–30 mol%) catalyst. Under the reaction conditions it was possible to cross-couple 5-chloroindole with CyMgBr on a multigram scale with yields up to 95%. Removing light sources from the reaction conditions resulted in a significant decrease in yields. The group suggest a mechanistic pathway of the reduction of Fe(III) to Fe(I) followed by a light promoted oxidative addition step, which was determined as the rate limiting step. This was then followed by transmetallation and reductive elimination to complete the cycle. These findings were based on kinetic studies used in combination with UV-Vis analysis and DFT calculations.
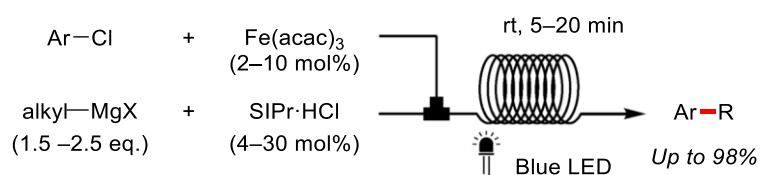
Figure 2.4 – Visible light promoted iron-catalysed Kumada cross-coupling reaction in flow.[55]

It was argued that in the substrate-directed iron-catalysed Suzuki biaryl cross-coupling reaction that the directing group is what was needed for the transformation to occur by aiding oxidative addition overcoming the aryl C–Cl bond. In this case, without the directing group to aid the reaction, overcoming the oxidative addition barrier is much harder, but Alcázar and Noel have shown it is possible to overcome this barrier using blue LED light. Therefore, the reaction was trialled with normal lighting, exposure to blue LED light and in the absence of any light (Table 2.13). There was no change in the reactivity when either light was removed from the reaction or blue LED lights were used and therefore the reaction is not light dependent.

Table 2.13 – Effect of changing the light source on the reaction.

Entry	Lighting	12, % Yield	13, % Yield	14, % Yield
1	Normal lab lighting	8	61	35
2	Blue LED	14	59	32
3	No light	10	61	34

Conditions: chlorobenzene (0.5 mmol), **11** (1.25 mmol), FeBr$_3$ (0.05 mmol), IMes·HCl (0.05 mmol), MgBr$_2$·OEt$_2$ (0.1 mmol), MeMgBr (0.05 mmol), 2-MeTHF:1,4-dioxane (1:1) (6.0 mL), 100 °C, 3 h. Yield determined by GC using dodecane as an internal standard.

When using the boronic ester derived from 2,4-pentanediol it was observed that the yield of **13** dropped to 9% but nucleophile homo-coupling was almost completely shut down (Table 2.6, entry 4). This boronic ester was then trialled under the optimised conditions to see whether the formation of **14** remained limited and whether there would be an increase in formation of **13**. This resulted in a similar outcome to when the boronic ester was originally trialled (Scheme 2.11).
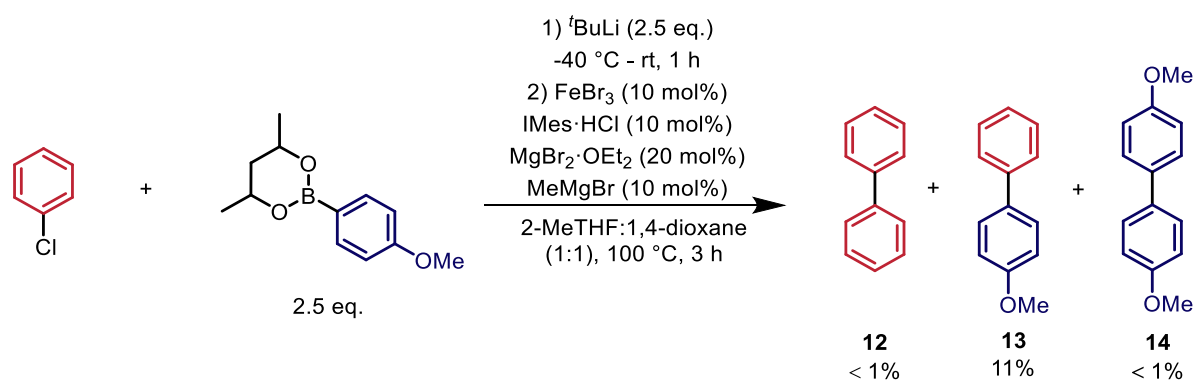
Scheme 2.11 – Effect of using boronic ester derived from 2,4-pentanediol. Conditions: boronic ester (1.25 mmol), ^{t}BuLi (1.25 mmol), chlorobenzene (0.5 mmol), FeBr$_3$ (0.05 mmol), ligand (0.05 mmol), MgBr$_2$·OEt$_2$ (0.1 mmol), MeMgBr (0.05 mmol), 2-MeTHF:1,4-dioxane (1:1) (6.0 mL), 100 °C, 3 h. Yield determined by GC using dodecane as an internal standard.

In conclusion, a viable route to prevent formation of **14** was not found and a mechanistic study is likely to aid the understanding of the selectivity issues (see Chapter 3).

2.3 Determining Whether Iron is Responsible for the Catalytic Behaviour

Replacing palladium in cross-coupling reactions is not easily done, and previously reported 'palladium free' cross-coupling reactions have been retracted[175–179] or disputed.[180–184] Debunking papers[184,185] or matters arising pieces[186–188] have followed these original publications disputing the claims. In some cases it was shown that impurities in glassware or reagents, namely palladium, were actually the catalysts in the reactions not the 'catalyst' the authors originally thought.[189,190] Due to these previous issues and general concerns when publishing a palladium free Suzuki cross-coupling reaction, a series of control experiments were undertaken. Firstly, the reactions were carried out in the absence of the catalytic reagents to ensure that they were all needed in the reaction mixture. Three different sources of $FeBr_3$ from three different suppliers were also trialled in the reaction (Table 2.14, entries 1, 5 & 6). The three different commercially sourced samples of $FeBr_3$ gave almost identical results showing that there is no issue with a certain supplier only leading to positive results. Suggesting that there is not one impurity that catalyses the reaction that is only present in a sample from one supplier. Although, it is likely the synthetic route used by the separate companies is the same. Although $FeBr_2$ was shown to be a poorer pre-catalyst in the earlier screening (Table 2.5), it still did catalyse the reaction and gave both cross-coupled and nucleophile homo-coupled product. As ultra-pure $FeBr_3$ is not commercially available, high purity $FeBr_2$ and standard purity $FeBr_2$ were also trialled in the reaction (Table 2.14, entries 7 & 8). When both 98% and 99.995% purity $FeBr_2$ were trialled under the optimised reaction conditions, they also gave almost identical results (although the yield was, as expected, lower than $FeBr_3$), further indicating that impurities in any component of the reaction mixture are unlikely to be responsible for the observed catalytic reactivity.
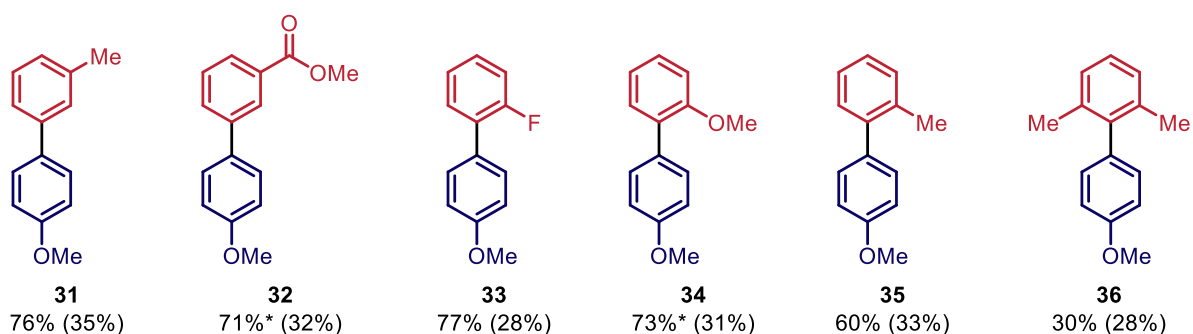
Table 2.14 – Control experiments to show impurities are not the active catalyst.

Entry	Fe salt, purity, supplier	IMes·HCl, mol%	MgBr$_2$, mol%	12, % Yield	13, % Yield	14, % Yield
1	FeBr$_3$, 98.5%, Fluorochem	10	20	4	61	35
2	FeBr$_3$, 98.5%, Fluorochem	10	0	4	40	28
3	FeBr$_3$, 98.5%, Fluorochem	0	20	2	3	13
4	N/A	10	20	<1	<1	<1
5	FeBr$_3$,98%, Aldrich	10	20	6	63	33
6	FeBr$_3$, 98%, Alfa Aesar	10	20	4	59	30
7	FeBr$_2$ 98%, Alfa Aesar	10	20	6	53	33
8	FeBr$_2$ 99.995%, Alfa Aesar	10	20	5	52	33

Conditions: chlorobenzene (0.25 mmol), 11 (0.625 mmol), Fe salt (10 mol% except for entry 4), IMes·HCl, MgBr$_2$·OEt$_2$, MeMgBr (0.025 mmol), 2-MeTHF:1,4-dioxane (1:1) (3.0 mL), 100 °C, 3 h. Yield determined by GC using dodecane as an internal standard.
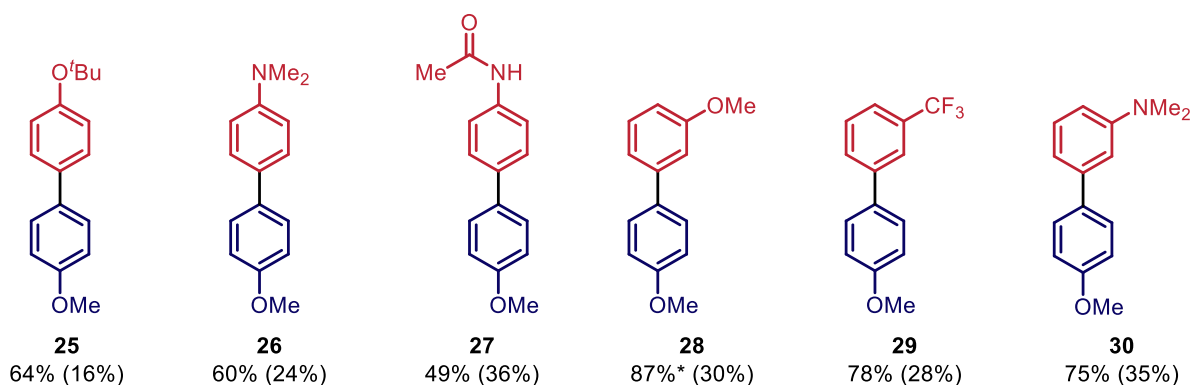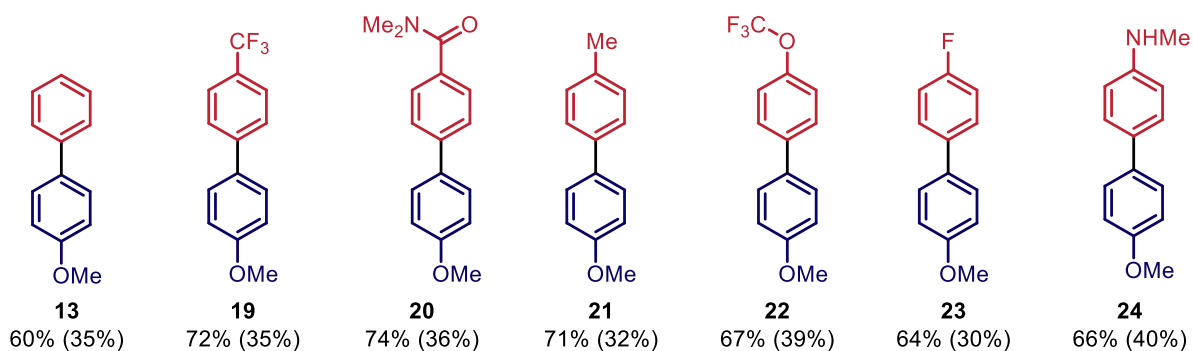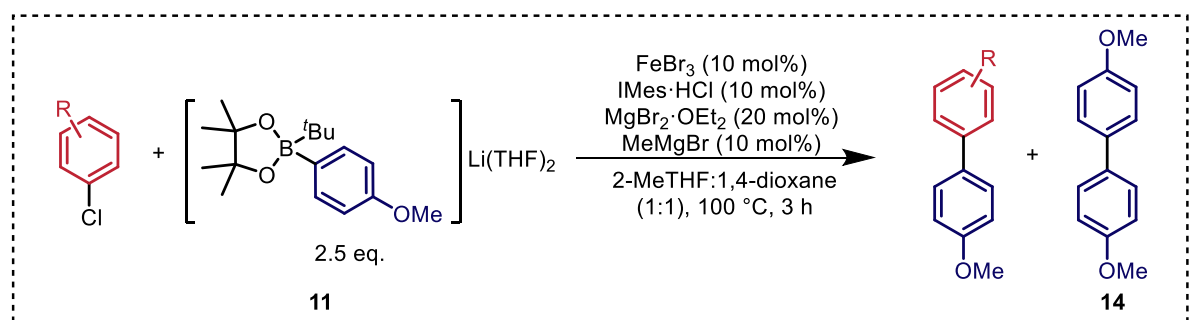
To further demonstrate that it is unlikely that impurities are responsible for the observed results, reaction profiles were taken for the cross-coupling of 4-chlorotoluene and ^{t}BuLi activated phenylboronic acid pinacol ester using FeBr$_3$ (98.5% purity), FeBr$_2$ (98 and 99.995% purity) and FeCl$_3$ (98% and 99.99% purity). The results clearly show that, although FeCl$_3$ and FeBr$_2$ give lower yields of **13** and **14** compared to FeBr$_3$, the observed kinetics seem to be the same regardless of the purity of the iron salt (Figure 2.5). This further suggests that the observed catalytic activity

is likely to be due to the iron rather than an impurity, as one would expect different kinetic data if there was an alternate catalytic species in the lower purity iron salts.
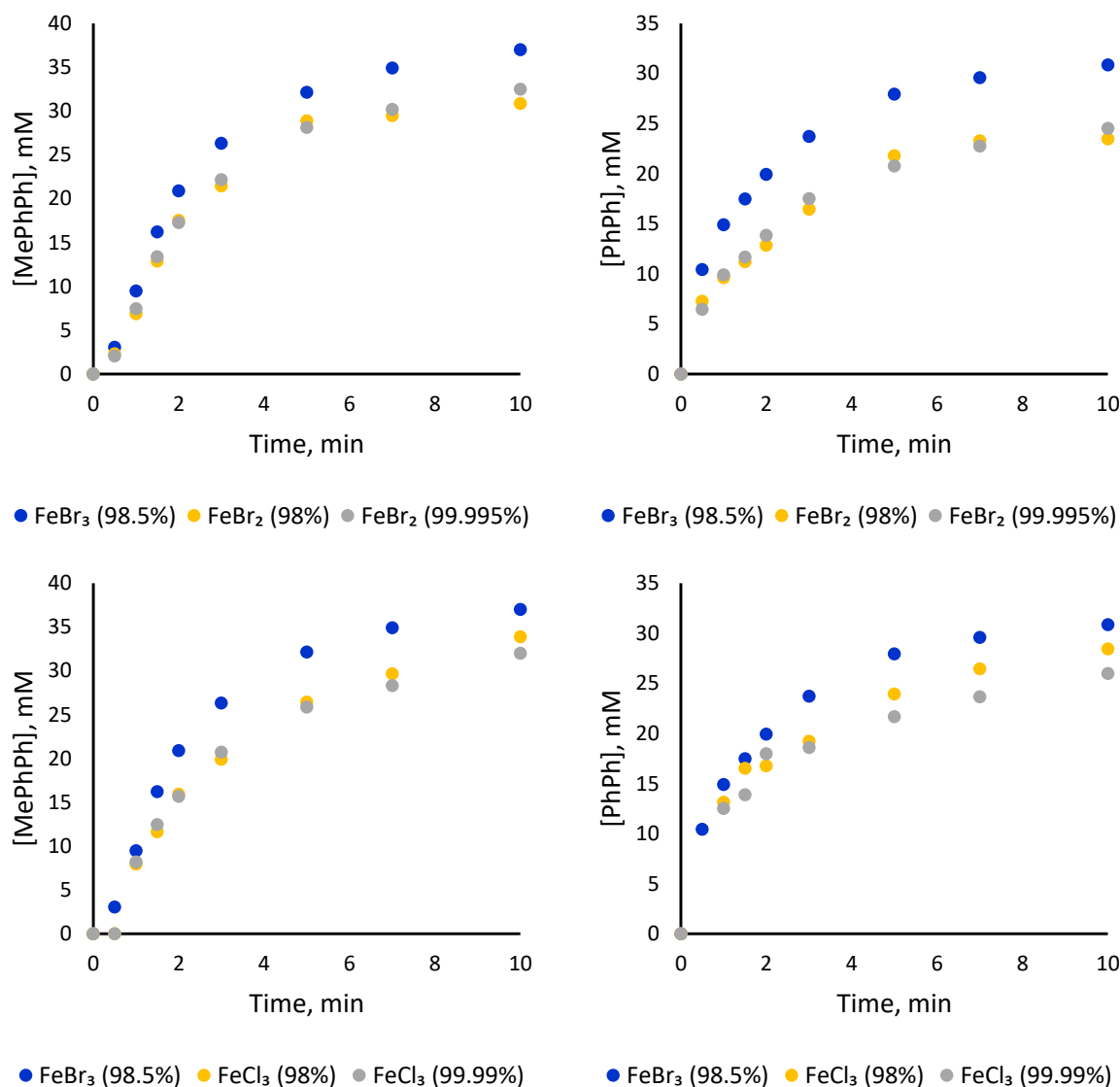
Figure 2.5 – Reaction profiles showing how different purity Fe salts effect the cross-coupling (left graphs) and homo-coupling (right graphs). Conditions: 4-chlorotoluene (0.5 mmol), 11 (1.25 mmol), FeBr₃ (0.05 mmol), IMes·HCl (0.05 mmol), MgBr₂·OEt₂ (0.1 mmol), MeMgBr (0.05 mmol), 2-MeTHF:1,4-dioxane (1:1) (6.0 mL), 100 °C, 3 h. Yield determined by GC using dodecane as an internal standard.

In addition to the data showing the varying yields and kinetic data when different purity iron salts were used, ICP-MS was carried out by Johannes Krieger of Merck Healthcare. Analysis of reaction mixtures catalysed by 98% and 99.995% FeBr₂ showed the samples had relatively high amounts of palladium in them, 2 and 1 ppm respectively. However, analysis of the palladium content in samples of 98% and 99.995% FeBr₂ and 98.5% FeBr₃ showed significantly lower palladium

concentrations; triplicate studies on 100 mg samples of each gave ranges of 23–200, 76–281 and 230–390 ppb respectively. Therefore, palladium impurities in the iron salts only contribute minor amounts to the total palladium content in the reaction mixture. ICP-MS analysis of a reaction mixture prepared in the absence of any iron salt showed a palladium concentration of 2.9 ppm, confirming the main source of palladium as one or more of the other reaction components. Significantly, the lack of catalytic activity in the absence of an iron salt shows that the palladium impurities present are not responsible for the observed catalytic behaviour (Table 2.14, entry 4). In conclusion, it is highly unlikely that the reaction is catalysed by anything other than iron.

2.4 Scope and Limitations

With an optimised system in place for the iron-catalysed Suzuki biaryl cross-coupling, the scope and limitations of the reaction were explored. A range of simple, commercially available aryl chlorides were screened under the optimised reaction conditions (Figure 2.6). The reaction tolerated a variety of groups with yields ranging from 30–74%. In all cases, homocoupling of the nucleophile also occurred (16–40%). In most cases the products were able to be separated by column chromatography, but for some only spectroscopic yields were obtainable (**28**, **32** & **34**). The reaction proceeded without notable preference for either electron donating or withdrawing groups; when either CF_3 (**19** & **29**) or NMe_2 (**26** & **30**) functional groups were used both resulted in good yields. Amides (**20** & **27**), esters (**32**), and secondary amines (**24**) cross-coupled in good yields, allowing for further functionalisation of the biaryl. Fluorinated biaryls are desirable in pharmaceutical products and pleasingly F (**23** & **33**), CF_3 (**19** & **29**), and OCF_3 (**22**) groups led to good conversions. When either 1-chloro-2-fluorobenzene or 1-chloro-4-fluorobenzene were used in the reaction there was exclusive reactivity at the C–Cl bond. This shows that the methodology has the potential to be used in later stage of a synthesis with the fluoro group already installed.

Along with the screening of *p*-substituted aryl chlorides, a few examples of both *m*- and *o*-substituents on the aryl chloride were reacted to see if they could be tolerated. In the case of the *m*-substituted aryl chlorides, they outperformed or performed similarly to their *para* counterparts for both electron withdrawing and donating groups (**28**–**32**). *O*-substituted aryl chlorides also successfully cross-coupled with similar yields to their *p*-substituted counterparts (**33**–**36**). However, in the case of 2-chloro-*m*-xylene, the extra steric bulk around the C–Cl bond led to a significant decrease in yield of the cross-coupled product to 30% (**36**).

13
60% (35%)

19
72% (35%)

20
74% (36%)

21
71% (32%)

22
67% (39%)

23
64% (30%)

24
66% (40%)

25
64% (16%)

26
60% (24%)

27
49% (36%)

28
87%* (30%)

29
78% (28%)

30
75% (35%)

31
76% (35%)

32
71%* (32%)
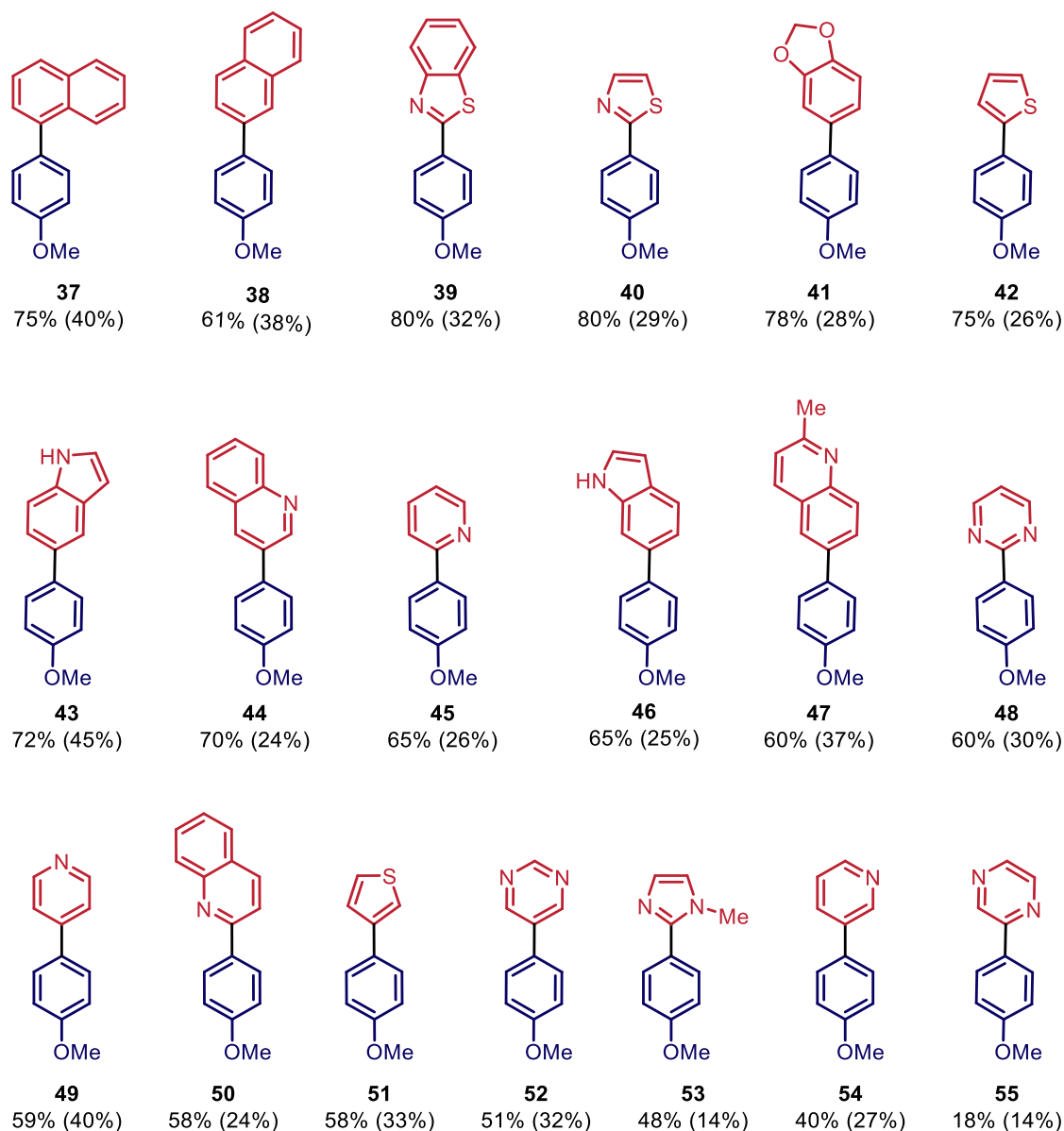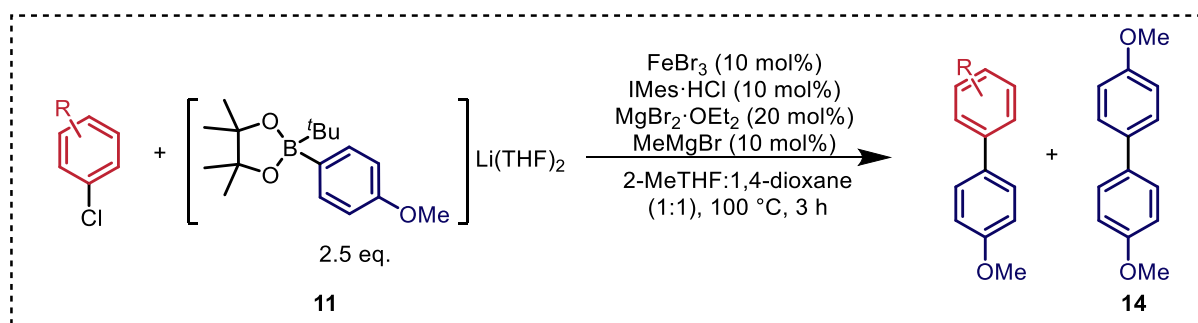
33
77% (28%)

34
73%* (31%)

35
60% (33%)

36
30% (28%)

Figure 2.6 – Scope of aryl chlorides in iron-catalysed Suzuki biaryl cross-coupling reaction. Conditions: aryl chloride (0.5 mmol), 11 (1.25 mmol), FeBr₃ (0.05 mmol), IMes·HCl (0.05 mmol), MgBr₂·OEt₂ (0.1 mmol), MeMgBr (0.05 mmol), 2-MeTHF:1,4-dioxane (1:1) (6.0 mL), 100 °C, 3 h. Isolated yields shown and yield of 14 shown in parentheses. *Unable to isolate, spectroscopic yield determined by ¹H NMR spectroscopy using 1,3,5-trimethoxybenzene as an internal standard.

It has previously been shown by Nakamura that biaryl units, such as those containing naphthyl groups, have greater reactivity than phenyl groups in iron-catalysed borylation reactions (75% and 27% respectively).[191] With this in mind, 1-chloronaphthalene was cross-coupled and gave a yield of 88% (**37**). With this result, other biaryls were subjected to the reaction conditions to see if cross-coupling could be observed (Figure 2.7). Quinolines and indoles were very well tolerated, with yields up to 72% (**43**, **44**, **46**, **47** & **50**). These *N*-containing biaryl units gave very promising results and led to the belief that other heteroaryls could potentially be used in the reaction. Heteroaryls have very high pharmacological importance and activity, and therefore the ability to incorporate them into the motif by the iron-catalysed Suzuki biaryl cross-coupling was highly sought after.[192] Thiazoles (**39** & **40**), thiophenes (**42** & **51**), pyridines (**45**, **49** & **54**), imidazoles (**53**), pyrazine (**55**), and pyrimidines (**48** & **52**) were well tolerated in the reaction with yields up to 82%. This shows that the reaction was able to tolerate a large range of heteroaryls as well as biaryls (Figure 2.7).

37
75% (40%)

38
61% (38%)

39
80% (32%)

40
80% (29%)

41
78% (28%)

42
75% (26%)

43
72% (45%)

44
70% (24%)

45
65% (26%)

46
65% (25%)

47
60% (37%)

48
60% (30%)

49
59% (40%)

50
58% (24%)

51
58% (33%)

52
51% (32%)

53
48% (14%)

54
40% (27%)

55
18% (14%)

Figure 2.7 – Scope of biaryl and heteroaryl chlorides in iron-catalysed Suzuki biaryl cross-coupling reaction. Conditions: aryl chloride (0.5 mmol), 11 (1.25 mmol), FeBr₃ (0.05 mmol), IMes·HCl (0.05 mmol), MgBr₂·OEt₂ (0.1 mmol), MeMgBr (0.05 mmol), 2-MeTHF:1,4-dioxane (1:1) (6.0 mL), 100 °C, 3 h. Isolated yields shown and yield of 14 shown in parentheses.

Disappointingly, there are a few examples of substituents that were not tolerated in the reaction (Figure 2.8). Both nitrile and nitro groups did not lead to any cross-coupling, with only the starting aryl chloride being observed by GCMS. It was hoped that the nitrile would be tolerated as seen in the substrate-directed iron-catalysed Suzuki biaryl cross-coupling; although previously a nitrile group was not tolerated in Bedford's cobalt-catalysed Suzuki cross-coupling.[42,87,136] The intolerance of a nitro group in the reaction could be due to strong electronically withdrawing resonance properties associated with nitro substituents or its ability to form and combine with radical species. The unprotected protic thiol, hydroxyl and amine substituents on the aryl chloride were also unsuccessful in the cross-coupling; only trace amounts of product were observed by GCMS. It has previously been reported that the highly basic nature of the boronates causes any species with potentially acidic protons to be deprotonated and leads to degradation of the boronate, resulting in a lack of cross-coupling. This could be the case here, although it was not seen with all substituents trialled. Neither aldehydes nor ketones were tolerated in the reaction, with only trace amounts of cross-coupled product being seen. These groups are susceptible to nucleophilic addition of the boronate and the product resulting from this arylation was observed in the GCMS. Bromoaryl chlorides were trialled to see if the reactivity was selective to the C–Cl bond and leave the C–Br untouched. If this was the case, then a bromo substituent could be installed for later functionalisation and allow the cross-coupling to occur unhindered. However, when 1-bromo-2-chlorobenzene and 1-bromo-3-chlorobenzene were used, no cross-coupling was observed at either the Cl or Br position with starting material only being seen. This highlights the current limitations of the reaction when considering the type of electrophile that can be used.
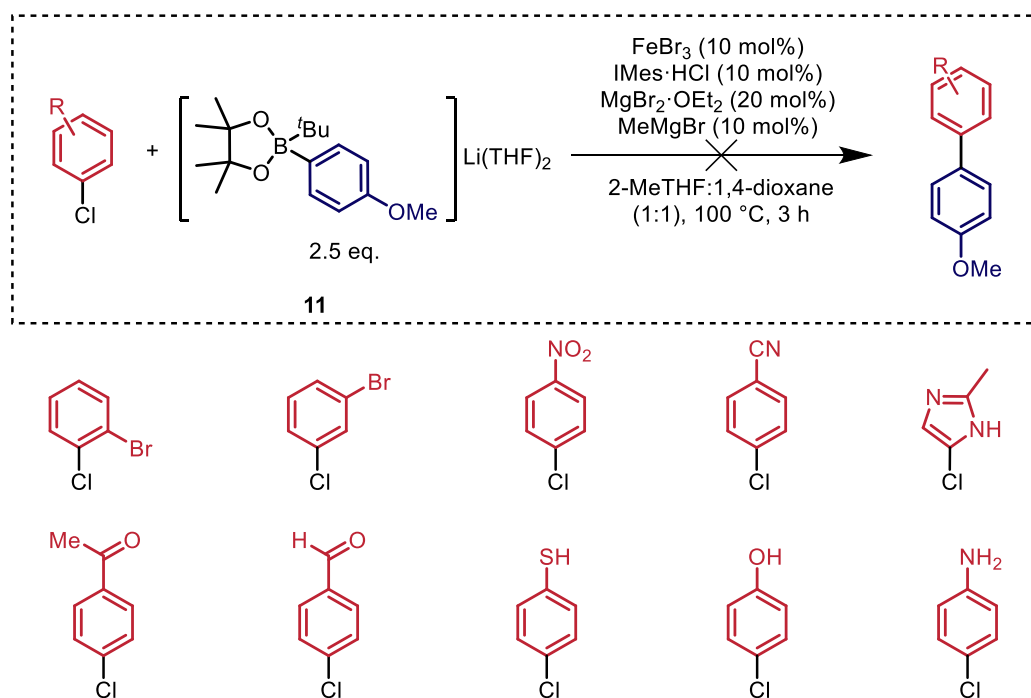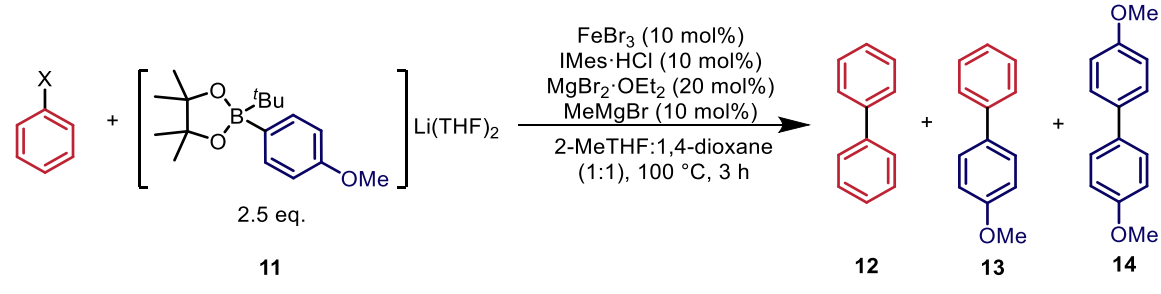
Figure 2.8 – Unsuccessful aryl halide coupling partners in the iron-catalysed Suzuki biaryl cross-coupling. Conditions: 4-chlorotoluene (0.5 mmol), 11 (1.25 mmol), FeBr$_3$ (0.05 mmol), IMes·HCl (0.05 mmol), MgBr$_2$·OEt$_2$ (0.1 mmol), MeMgBr (0.05 mmol), 2-MeTHF:1,4-dioxane (1:1) (6.0 mL), 100 °C, 3 h.

To ascertain the scope and limitations of the reaction conditions on the nucleophile, a range of ^{t}BuLi activated boronic esters were trialled with 4-chlorotoluene (Figure 2.9). The limitations on the nucleophile were far greater than that of the electrophile, with only 9 examples being recorded. However, the reaction did proceed with good yields (up to 81%) for both electron donating and withdrawing groups. Electron donating groups tended to outperform electron withdrawing groups, it is likely to be due to the extra electron donation making the boronate more nucleophilic and therefore better at cross-coupling. To investigate any reactivity based on steric effects, boronates with Me (**61**) and OMe (**63**) groups in the o-position of the aryl ring were trialled in cross-coupling and were successful, albeit in lower yields when compared to the less sterically hindered p-counterparts. In the case of OMe the yield decreased from 71% to 45% (**63**).
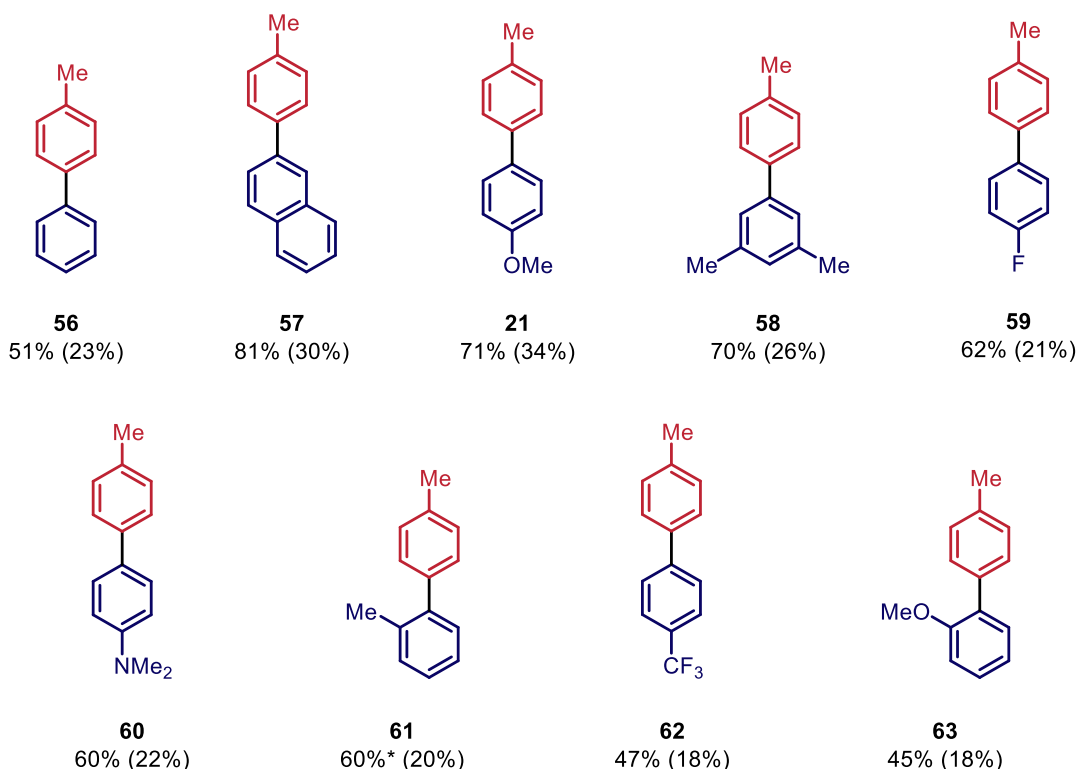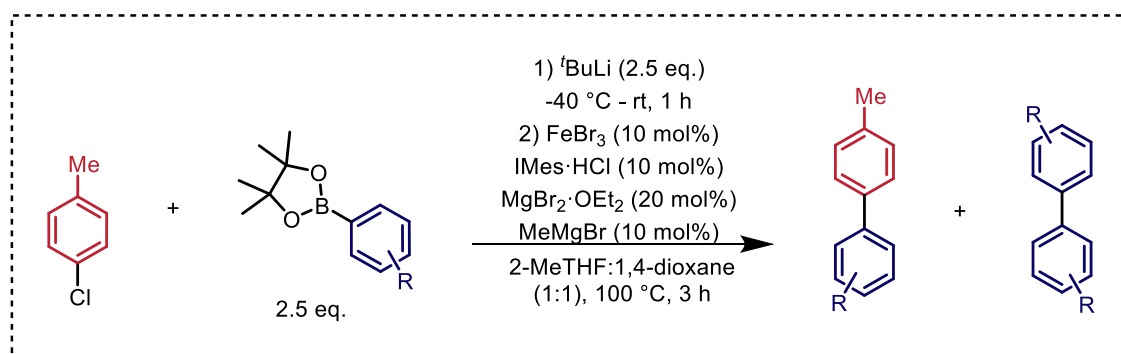
Figure 2.9 – Scope of boronic esters in iron-catalysed Suzuki biaryl cross-coupling reaction. Conditions boronic ester (1.25 mmol), ^{t}BuLi (1.25 mmol), 4-chlorotoluene (0.5 mmol), FeBr$_3$ (0.05 mmol), IMes·HCl (0.05 mmol), MgBr$_2$·OEt$_2$ (0.1 mmol), MeMgBr (0.05 mmol), 2-MeTHF:1,4-dioxane (1:1) (6.0 mL), 100 °C, 3 h. Isolated yields shown, and yield of nucleophile homo-coupling shown in parentheses. *Unable to isolate, spectroscopic yield determined by ^{1}H NMR spectroscopy using 1,3,5-trimethoxybenzene as an internal standard.

The number of functional groups on the nucleophile that were not tolerated were far greater than that of the aryl chloride. Disappointingly, nucleophiles containing heteroaryls were unsuccessful at cross-coupling. Therefore, to incorporate a heteroaryl group it must be installed in the electrophile. Increasing steric bulk around the C–B bond with methyl groups led to loss of reactivity when both the 2,6-phenyl and 2,4,6-phenyl boronic acid pinacol esters were used. One issue that persists is the competitive formation of the undesired homo-coupled product of the

nucleophile. These issues highlight the current limitations of the reaction, as the functional group tolerance is not as broad as hoped, and the catalytic system is not selective enough. Nevertheless, these examples show that the iron-catalysed Suzuki biaryl cross-coupling reaction is achievable.
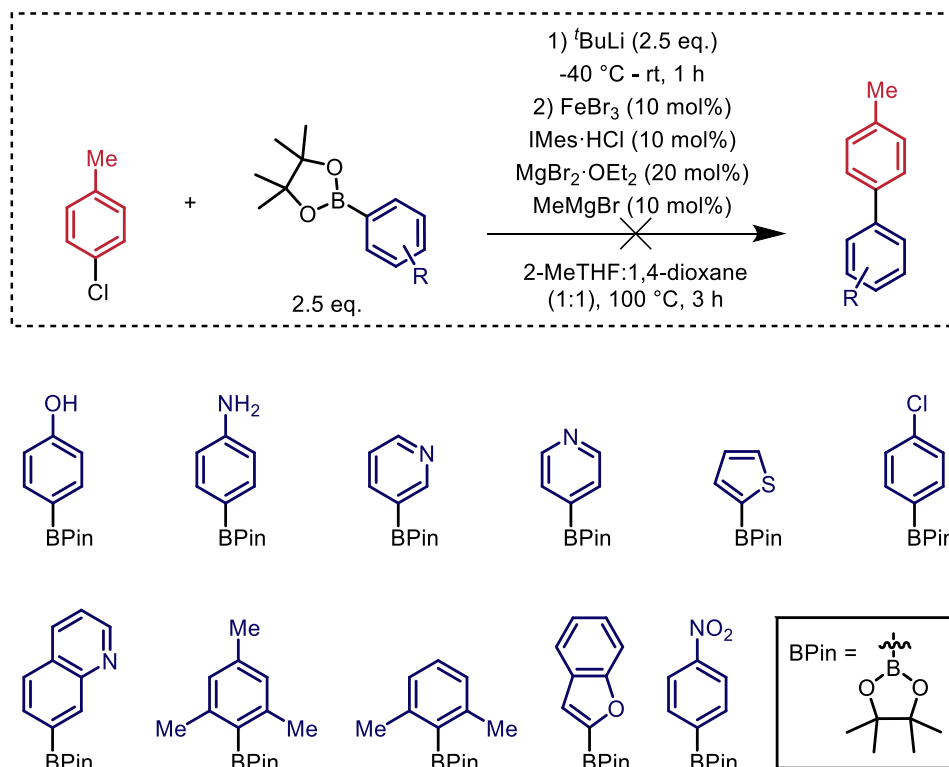
Figure 2.10 – Unsuccessful boronic acid coupling partners in the iron-catalysed Suzuki biaryl cross-coupling. Conditions: boronic ester (1.25 mmol), ^{t}BuLi (1.25 mmol), 4-chlorotoluene (0.5 mmol), FeBr$_3$ (0.05 mmol), IMes·HCl (0.05 mmol), MgBr$_2$·OEt$_2$ (0.1 mmol), MeMgBr (0.05 mmol), 2-MeTHF:1,4-dioxane (1:1) (6.0 mL), 100 °C, 3 h.

In the initial screen of halides and pseudohalides on the electrophile, it was found that chlorobenzene outperformed the other electrophiles but also that phenyl triflate showed that it could be potentially used as an electrophile. The effect of using different halide and pseudohalides was then screened again under the optimised conditions to see if any other aryl halides and pseudohalides could be used (Table 2.15). The results show that while fluoro, bromo, iodo and carbamates remain unsuitable cross-coupling partners, phenyl triflate works almost as well as chlorobenzene. As mentioned previously, due to the lack of reactivity of the fluorobenzene and bromobenzene it was thought that fluoro and bromo groups could be installed in the aryl chloride and would be left unreacted. When the fluoro group was used this was the case, and the corresponding fluoro-biphenyls were synthesised in good yields (**23** & **33**, Figure 2.6). However,

when bromine was incorporated into the aryl chloride, no reactivity was observed at either the C–Cl bond or C–Br bond (Figure 2.8).

Table 2.15 – Effect of Changing halide on aryl halide using optimised conditions.

Entry	ArylX	12, % Yield	13, % Yield	14, % Yield
1	C_6H_5F	< 1	4	9
2	C_6H_5Cl	4	61	35
3	C_6H_5Br	< 1	3	5
4	C_6H_5I	< 1	11	7
5	C_6H_5OTf	8	59	36
6	$C_6H_5OCONH_2$	7	14	7

Conditions: aryl chloride (0.5 mmol), 11 (1.25 mmol), FeBr$_3$ (0.05 mmol), IMes·HCl (0.05 mmol), MgBr$_2$·OEt$_2$ (0.1 mmol), MeMgBr (0.05 mmol), 2-MeTHF:1,4-dioxane (1:1) (6.0 mL), 100 °C, 3 h. Yield determined by GC using dodecane as an internal standard.

With the positive result of using phenyl triflate as a cross-coupling partner, a small screen of aryl triflates was carried out (Figure 2.11). Use of methyl, fluoro, and methyl ester groups gave the cross-coupled products in mediocre yields, all lower than when the corresponding aryl chloride was used. However, in cases where aryl chlorides are not available this still gives an alternative strategy to access the desired biaryl.
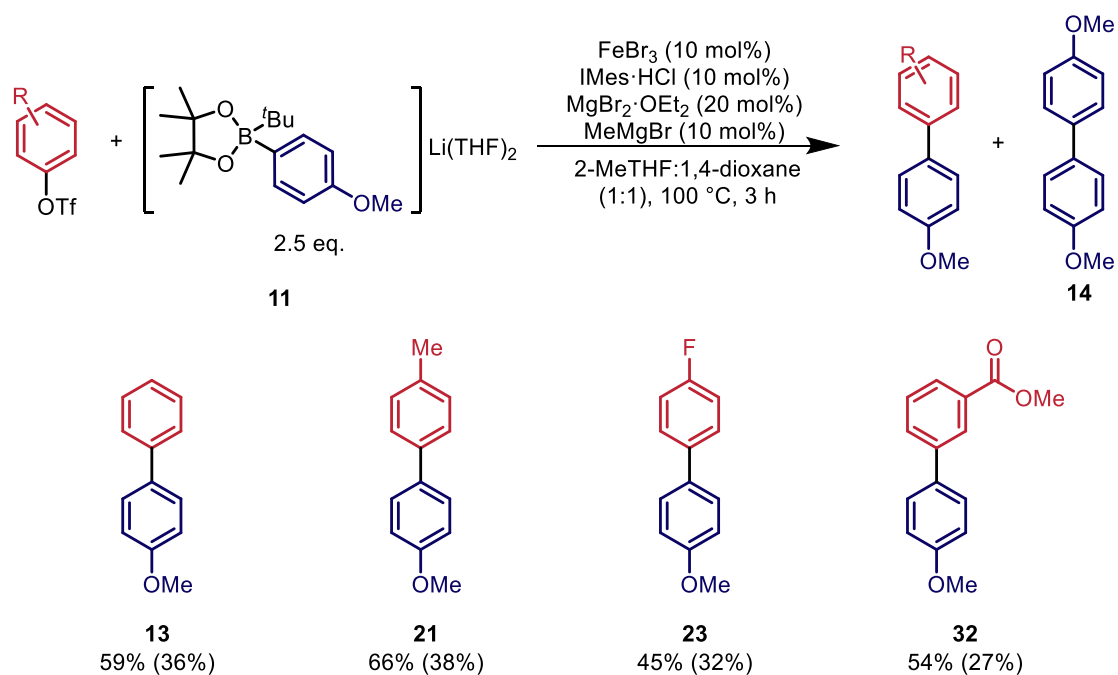
Figure 2.11 – Scope of aryl triflates in iron-catalysed Suzuki biaryl cross-coupling reaction. Conditions: aryl triflate (0.5 mmol), 11 (1.25 mmol), FeBr₃ (0.05 mmol), IMes·HCl (0.05 mmol), MgBr₂·OEt₂ (0.1 mmol), MeMgBr (0.05 mmol), 2-MeTHF:1,4-dioxane (1:1) (6.0 mL), 100 °C, 3 h. Spectroscopic yields shown with yield of 4 shown in parentheses. Determined by ¹H NMR spectroscopy using 1,3,5-trimethoxybenzene as an internal standard.

2.5 Conclusions

In conclusion, it has been demonstrated that the iron-catalysed Suzuki biaryl cross-coupling reaction is achievable without the need for a directing group on either cross-coupling partner. The data show that aryl halide activation can be overcome by employing harsher conditions. The final optimised conditions, using $FeBr_3$ as a pre-catalyst, in combination with the commercially available bench stable IMes·HCl ligand precursor, co-catalytic $MgBr_2·OEt_2$ and MeMgBr as an initiator in 2-MeTHF and 1,4-dioaxane (1:1) at 100 °C, allows for a reasonable functional group tolerance, including an array of heteroaromatic groups. In total, 47 biaryl were synthesised. The ability to incorporate heteroaryls is highly sought after due to the activity of pharmaceutical products when this moiety is present.
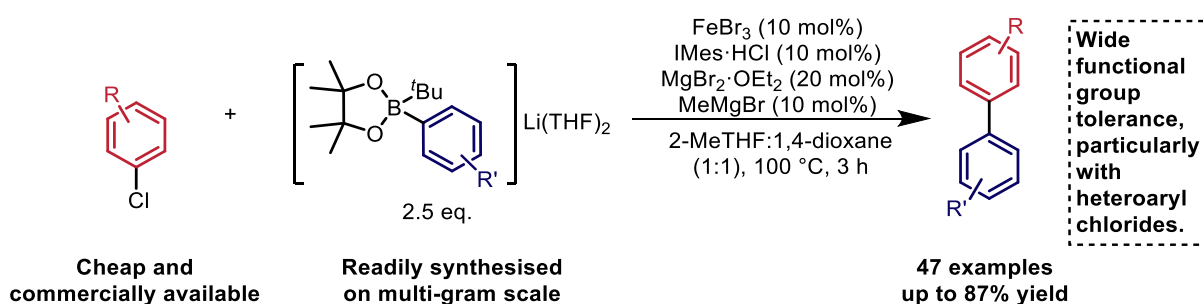
Scheme 2.12 – Summary of iron-catalysed Suzuki biaryl cross-coupling reaction developed.

The added advantage of being able to preferentially cross-couple aryl chlorides over other halides enables this procedure to be viewed as a viable alternative to palladium-catalysed cross-coupling reactions. Throughout the optimisation, there has also been observation of significant homo-coupling of the nucleophile, which shows that there are selectivity issues in the absence of a directing group. However, in almost all cases it was able to be separated from the cross-coupled product by column chromatography, and so this should not deter the use of this methodology when palladium-catalysts are unsuitable or unavailable.

Although the need for a directing group on the aryl halide has been overcome, the greatest limitation so far is the competitive homo-coupling of the boronate nucleophile. Thus, to take this methodology further into the realms of synthetic utility, a way to control the selectivity towards the cross-coupled product needs to be identified. To do this, a mechanistic investigation was undertaken and is discussed in Chapter 3, with the hope that greater understanding of the reaction mechanism will show why the selectivity issues occur and how to promote cross-coupling and shut

down homo-coupling. Greater understanding of the catalytic cycle of this work will not only aid the development of this reaction, but also the general understanding of iron-catalysed cross-coupling reactions. A greater understanding of the mechanism will guide the approach to the synthesis of ligands and a catalytic system to further develop the reaction.

2.6 Future Work

The process currently relies on the boronic ester to be activated with 'BuLi before it can be used in cross-coupling. However, 'BuLi has several safety implications including its pyrophoric nature; this is not appealing to industrial chemists, especially when alkoxide bases used in palladium-catalysed cross-couplings do not have these extreme safety implications. Using 'BuLi also limits the functional group tolerance on the aryl of the nucleophile. Future attempts should focus on moving away from these aggressive bases and move towards alkoxide bases if possible. Byers has shown it is possible to use lithium amide bases in iron-catalysed Suzuki aryl-alkyl cross-coupling reactions, and these may be applicable in biaryl cross-couplings.[84–86] Development of cobalt-catalysed Suzuki biaryl cross-coupling reactions have been able to move away from alkyl lithium bases to alkoxide bases.[42,135] As cobalt and iron can often display similar reactivity, this is promising for the development of iron-catalysed Suzuki reactions using alkoxide bases.

Although a large reaction scope has been completed, it would be exciting to see whether the current methodology could be used in the synthesis of pharmaceutically relevant products. Examples of drug molecules that use a palladium-catalysed Suzuki biaryl cross-coupling include: ruxolitinib,[193,194] rucaparib,[195–197] merestinib,[198,199] abemaciclib[200,201] and lapatinib[202] (Figure 2.12). It would be hugely beneficial if these reactions could be catalysed by iron rather than palladium. To attempt to narrow down which substrates are likely to be successful in the reaction and speed up the process, a robustness screen could be carried out prior to the attempts. A robustness screen, developed by Glorius and discussed in more detail in Chapter 4, involves the introduction of an additive to the reaction mixture and then quantifying the amount of additive and product at the end of the reaction.[203,204] Glorius has since truncated the number of additives down to 15 (Figure 2.13).[205] This gives quick and easy insights into the likely tolerance of functional groups in the reaction.

Ruxolitinib
(myelofibrosis)

Rucaparib
(anticancer, Aproved US)

Merestinib
(anticancer, in Phase II)

Abemaciclib
(anticancer, in Phase III)

Lapatinib
(anticancer)
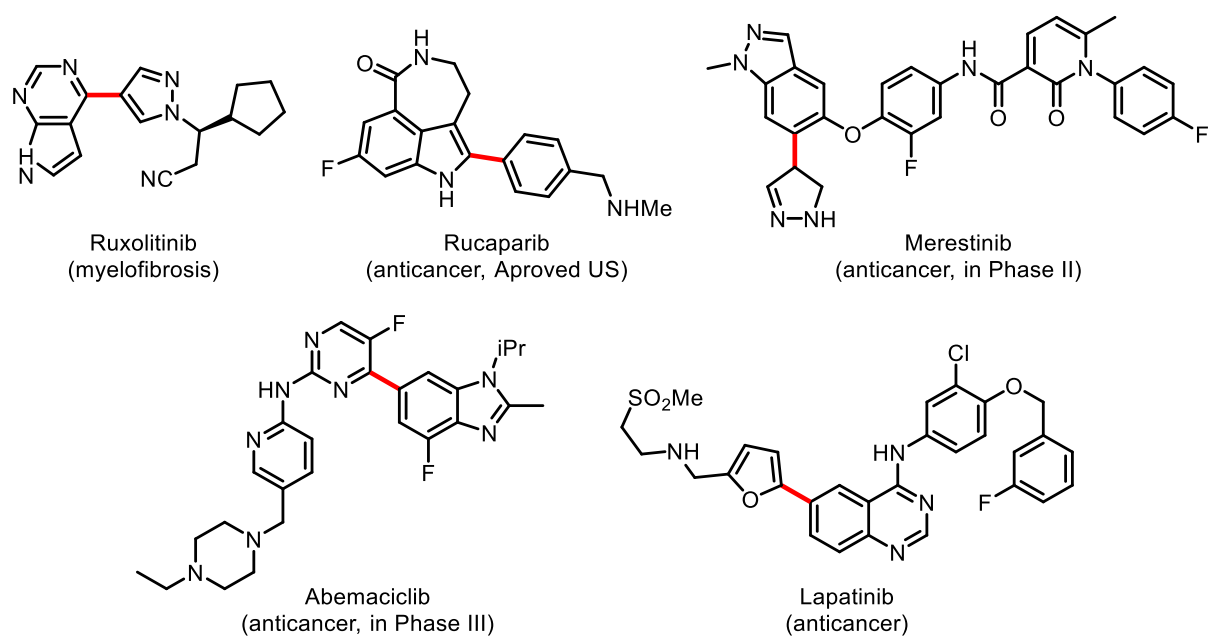
Figure 2.12 – Examples of drug molecules that use the Suzuki reaction (bond formed highlighted in red).
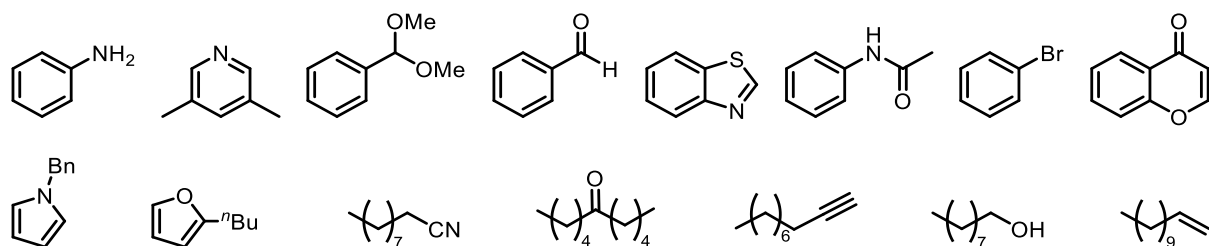
Figure 2.13 – The 15 additives used in a robustness screen developed by Glorius.

Chapter 3 Mechanistic Study of an Iron-Catalysed Suzuki Biaryl Cross-Coupling Reaction

3.1 Introduction

Many mechanistic investigations of iron-catalysed cross-coupling reactions have already been performed, mainly focused on iron-catalysed Kumada type reactions.[47,48,52,99,101,109,110] These investigations are comprised of in-depth studies into the potential oxidation states of catalytically active iron species, whether the reaction proceeds *via* radical pathways, and the roles of ligands, solvents, and additives in the reaction. However, there is no clear consensus of these investigations, with no uniform mechanism for iron to react by in all cross-coupling reactions (see Chapter 1 for full discussion).

Iron-catalysed Suzuki cross-coupling reactions have also been studied. In 2014, Bedford and co-workers undertook mechanistic investigations into the arylation of alkyl, benzyl, and allyl halides with aryl boronates using iron precatalysts.[206] Similarly to the iron-catalysed Kumada studies, bidentate ligands such as dppe and dppp were the most effective. The findings showed that Fe(II) pre-catalysts $FeX_2(dppe)_2$, where X = Cl or Br, were reduced to $Fe(I)X(dppe)_2$ by an aryl boronate species in the presence of $MgBr_2$ (Scheme 3.1). It was thought that the $MgBr_2$ aided transmetallation as it was not required for the reduction of Fe(II), but without it the amount of Fe(I) formed was significantly lower. Further investigation by initial rate studies led to the understanding that the species act as off-cycle resting states for the highly reactive, low coordinate Fe(I) species, which then activates the alkyl halide species.
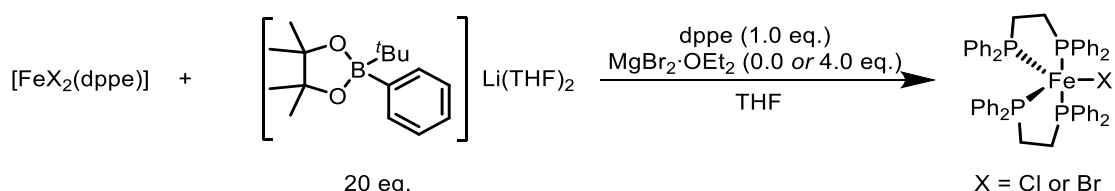
Scheme 3.1 – Production of [FeX(dppe)$_2$] using boronates.[206]

Neidig undertook a mechanistic study into Nakamura's original iron-catalysed Suzuki cross-coupling reaction.[82,107] Although the conditions were similar to Bedford's,[206] one major difference was the use of SciOPP. When $FeCl_2(SciOPP)$ was reacted with an aryl boronate and $MgBr_2$, an Fe(0) complex **64** is formed rather than the Fe(I) complex proposed by Bedford using dppe and dpbz. Although the Fe(0) complex was isolated and accessed in these conditions, using it as a pre-catalyst led to sluggish results with turnover frequencies much lower than expected, thus, its role was determined to be as an off-cycle intermediate, rather than a catalytically active species. Neidig

proposed that instead, the active species in catalysis was a phenylated Fe(II) SciOPP species (Scheme 3.2). The role of the MgBr₂ was still not elucidated but was shown to be crucial for the reaction to occur.
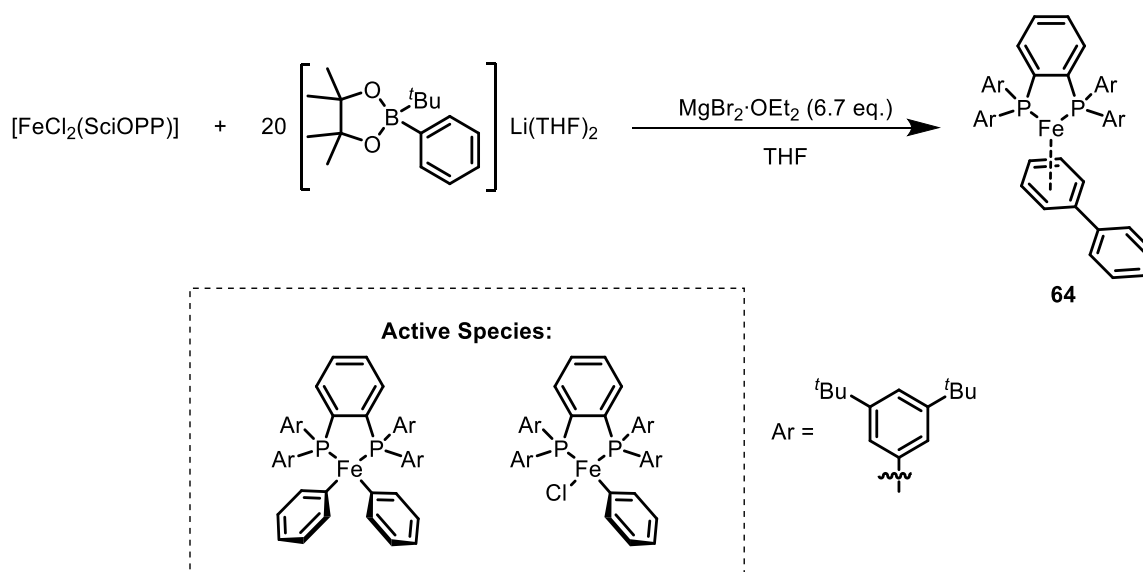
Scheme 3.2 – Reduction to Fe(0) using boronate and the proposed active species in Nakamura's Suzuki reaction.[107]

As alkoxide bases, commonly employed in palladium-catalysed Suzuki reactions, are unable to be used in iron catalysed Suzuki reactions, Ingleson investigated the aryl transfer from the boronate species to the iron complxes.[207] Ingleson found that it was preferred for there to be an alkoxide transfer to the iron from the aryl boronate rather than the aryl. However, when alkyl lithium reagents are used, aryl transfer is achievable.[208] This showed that organometallic reagents such as *t*BuLi are required for the aryl transfer to the iron (Scheme 3.3).
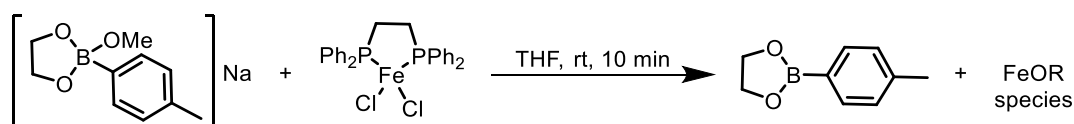
Scheme 3.3 – Alkoxide transfer rather than aryl transfer to iron from boronate.[207]

The only mechanistic investigation into iron-catalysed Suzuki biaryl reactions was that undertaken by Bedford and co-workers into the iron-catalysed substrate directed Suzuki biaryl cross-coupling reaction (Figure 13).[87] Bedford proposed that the iron is transiently π-coordinated to the pyrrole amide directing group and guided into the C–Cl bond, *via* the formation of amino ketyl radicals.

Interestingly, they found that rather than acting as a transmetallating agent as shown previously, co-catalyst $MgBr_2$ instead coordinates to the iron complex to form an activated species (Figure 3.1).
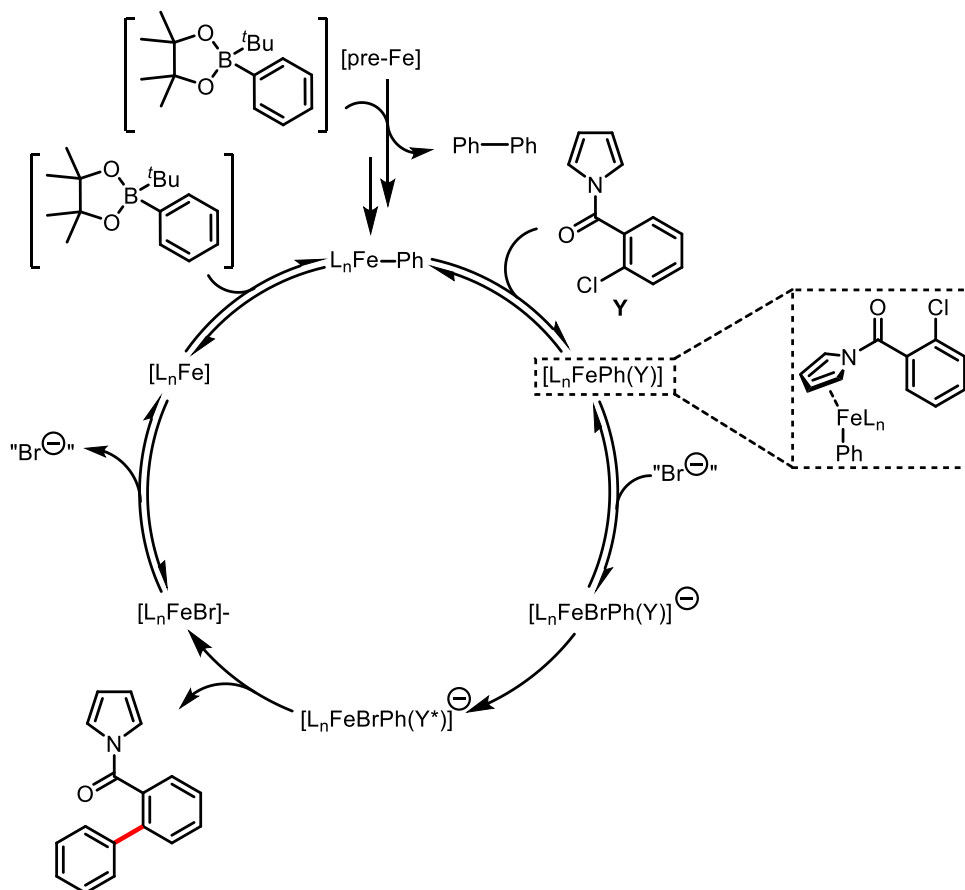
Figure 3.1 – Proposed catalytic cycle of the substrate directed iron-catalysed Suzuki cross-coupling reaction.[87]

Having optimised the reaction conditions for the iron-catalysed Suzuki biaryl cross-coupling (Chapter 2), the next step was to investigate the mechanism of the catalytic reaction (Scheme 3.4). Along with the desired cross-coupled product, homo-coupling of the nucleophile was also observed in relatively high yields (up to 40%). Attempts to inhibit the formation of **14** were unsuccessful in the reaction optimisation; a mechanistic study would hopefully elucidate the lack of reaction selectivity and therefore allow for further reaction development. As well as the selectivity issue, the roles of $MgBr_2$ and MeMgBr were not fully understood from the reaction optimisation studies alone. Understanding their roles in the reaction would further aid the reaction development. Furthermore, as there have been very few reported iron-catalysed Suzuki biaryl

cross-coupling reactions,[81,87,104] there is a need to improve the understanding of the reaction as well as possible, potentially to provide insights to further improve the methodology.
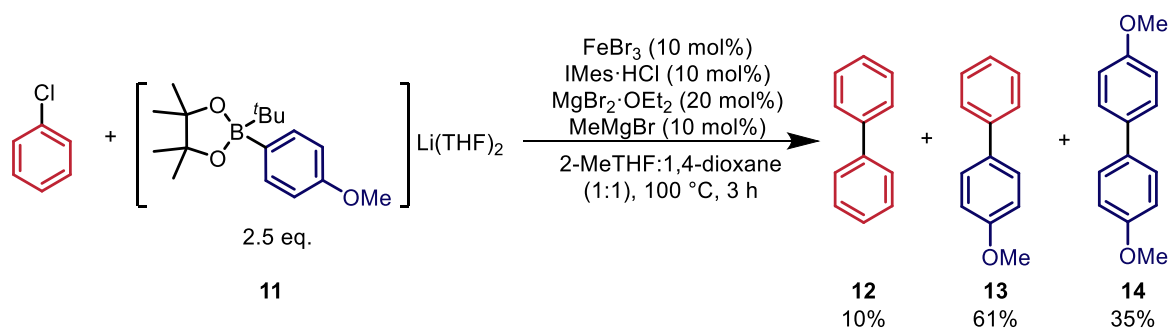
Scheme 3.4 – Optimised conditions for iron-catalysed Suzuki biaryl cross-coupling reaction.

3.2 Determining the Role of MeMgBr in the Reaction

Boronate species, such as **11**, have been reported to be able to reduce iron pre-catalysts to form catalytically active iron species, for example an Fe(II) pre-catalyst to an Fe(0) species.[87] When this happens, the homo-coupled nucleophile, in this case **14**, is formed. One potential way to reduce homo-coupling of the nucleophile could be to use a sacrificial reducing agent to reduce the iron pre-catalyst *in situ* before the boronate is added to the reaction mixture. Not only could this reduce the amount of nucleophile homo-coupling, but it would provide additional reactant to form the cross-coupled product. Grignard reagents have been shown to be able to reduce iron species *in situ* to form an active catalytic iron species.[55,101,109,110,209] During the optimisation studies in Chapter 2, it was found that the addition of MeMgBr not only led to an increase in cross-coupling but also to an increase in homo-coupling of the nucleophile (Section 2.5.2). This result suggests that MeMgBr is not acting as a reducing agent in this reaction, it could instead be that it acts as a base to deprotonate the NHC salt. To investigate this, reactions were performed with the free carbene, IMes, in the presence and absence of MeMgBr (Table 3.1, entries 3 & 4). The results show that using IMes with or without MeMgBr give the same result as when IMes·HCl is used in conjunction with MeMgBr. These results make it highly likely that the role of MeMgBr is to deprotonate IMes·HCl, allowing for an active IMes-Fe species to form. Bedford has previously reported that the boronate is basic enough to deprotonate IMes·HCl,[87] in this case as the MeMgBr is added to the reaction mixture before the boronate. The MeMgBr, therefore, deprotonates IMes·HCl forming a catalytically active IMes-Fe species which allows for greater catalytic activity once the boronate is added.

Table 3.1 – Determining the role of MeMgBr.
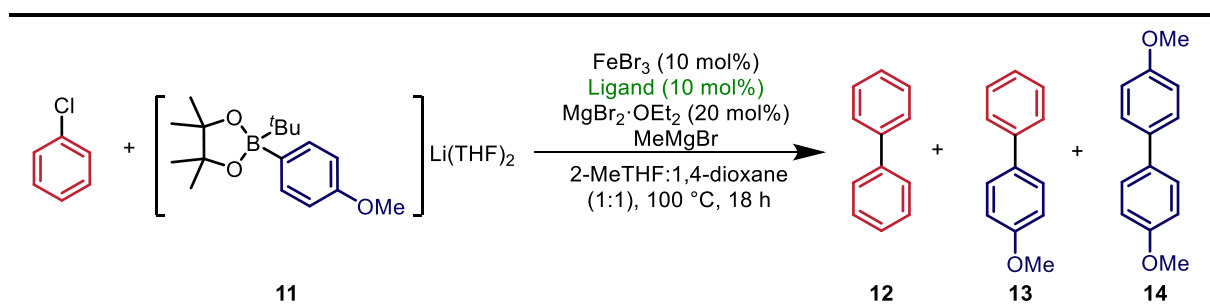
Entry	Ligand	MeMgBr, mol%	12, % Yield	13, % Yield	14, % Yield
1	IMes·HCl	0.0	6	45	24
2	IMes·HCl	10	4	61	35
3	IMes	0.0	5	62	36
4	IMes	10	7	61	38

Conditions: chlorobenzene (0.5 mmol), **11** (1.25 mmol), FeBr$_3$ (0.05 mmol), IMes·HCl or IMes, MgBr$_2$·OEt$_2$ (0.1 mmol), MeMgBr, 2-MeTHF:1,4-dioxane (1:1) (6.0 mL), 100 °C, 3 h. Yield determined by GC using dodecane as an internal standard.

3.3 Determining the Bulk Oxidation State of Iron in the Reaction

There is much debate about what the lowest oxidation state of iron is in iron-catalysed reactions, with -2, 0, +1 and +2 all being suggested.[95,97,98,103,105] Kochi has shown that MeMgBr was able to reduce Fe(III) halide salts to Fe(I) pre-catalysts.[101] Nakamura has suggested that the use of Grignard reagents reduces Fe(III) to catalytically active Fe(II) species.[147] It has also been reported that boronate species are able to reduce iron complexes to as low as Fe(0).[87] Iron species with varying oxidation states supported by NHC ligands have also been reported in the literature.[155,160,210–215]

To elucidate the lowest kinetically relevant bulk oxidation state of iron in the reaction and to determine the catalyst activation process, electrophile free reactions were conducted. Omission of the electrophile from the reaction means that there is not an oxidant present in the reaction. Therefore, any iron that is reduced by the boronate cannot be reoxidised to continue catalysis. By monitoring the amount of 4,4'-dimethoxybiphenyl (**14**) formed in the absence of an oxidant, we can deduce what the bulk oxidation state of iron in the reaction is (Figure 3.2). This does not necessarily correspond to the absolute oxidation state of the active catalyst, as it could be an average oxidation state of several species. However, it is still a good indicator of the potential oxidation state of the catalytically actives species that are kinetically relevant. When the electrophile is omitted from the reaction mixture approximately, 0.06 mmol of **14** is formed. As the formation of **14** is a two-electron reductive process and 0.05 mmol of $FeBr_3$ is used, this suggests that Fe(III) is reduced to Fe(I) (a 2-electron reductive process occurring once per iron centre). Comparison of the 4,4'-dimethoxybiphenyl production when MeMgBr is present to when it is absent shows that the rate of formation is significantly quicker (roughly 2x) when MeMgBr is present (Figure 3.2). This further suggests that a 'cleaner' pre-catalyst is formed more rapidly in the presence of MeMgBr.
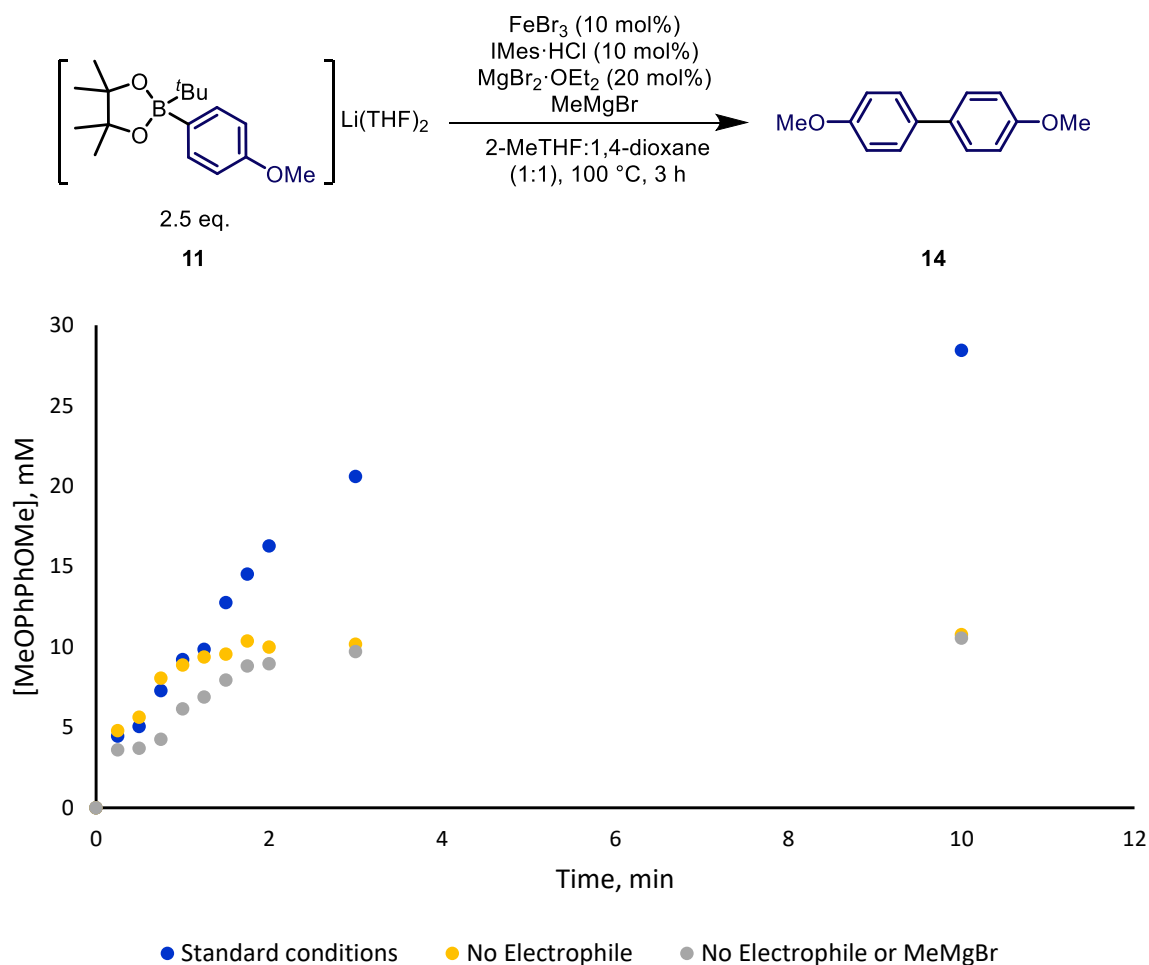
Figure 3.2 – Determining the bulk oxidation state of iron in the reaction. Conditions: chlorobenzene (0.5 mmol or 0.0 mmol), 11 (1.25 mmol), FeBr₃ (0.05 mmol), IMes·HCl (0.05 mmol), MgBr₂·OEt₂ (0.1 mmol), MeMgBr (0.05 mmol or 0.0 mmol), 2-MeTHF:1,4-dioxane (1:1) (6.0 mL), 100 °C, 3 h. Yield determined by GC using dodecane as an internal standard.

When the electrophile is omitted from the reaction, formation of **14** plateaus after approximately 45 seconds, where approximately 0.05 mmol of **14** is formed. When comparing this to the standard cross-coupling reaction where the electrophile is included, there is a short induction period of approximately 45 seconds for the formation of **13** (Figure 3.3). The induction period could therefore be accounted for by the need for iron to be reduced to a catalytically active species before cross-coupling can occur (Figure 3.3).
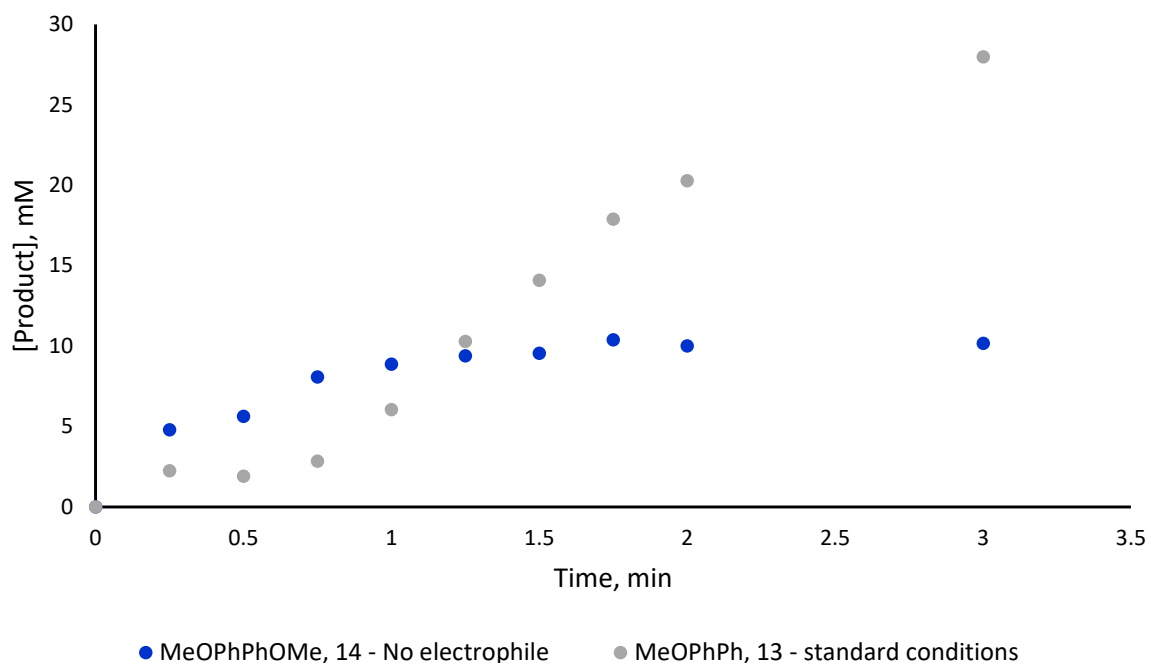
Figure 3.3 – Observing the induction period of cross-coupling reaction and bulk oxidation state of iron in the reaction. Conditions: chlorobenzene (0.5 mmol or 0.0 mmol), 11 (1.25 mmol), FeBr$_3$ (0.05 mmol), IMes·HCl (0.05 mmol), MgBr$_2$·OEt$_2$ (0.1 mmol), MeMgBr (0.05 mmol), 2-MeTHF:1,4-dioxane (1:1) (6.0 mL), 100 °C, 3 h. Yield determined by GC using dodecane as an internal standard.

To confirm whether the reductive process observed is the same as the catalyst activation process, a catalytic reaction was set up where the electrophile was added after the reductive process had occurred. In the standard reaction set up, the boronate was added as the final reaction component, but in this case, chlorobenzene was added to the reaction mixture 1 min 50 secs after the boronate was added (Figure 3.4). The reaction profile shows that in the opening minute of the reaction homo-coupling occurs until approximately 10 mM of **14** is formed, this then plateaus until the electrophile is added. Once the electrophile is added, **14** continues to be produced. The reaction profile also shows that cross-coupling starts immediately without an induction period. This data strongly suggests that the reaction requires an initial catalyst activation where Fe(III) is reduced to Fe(I).
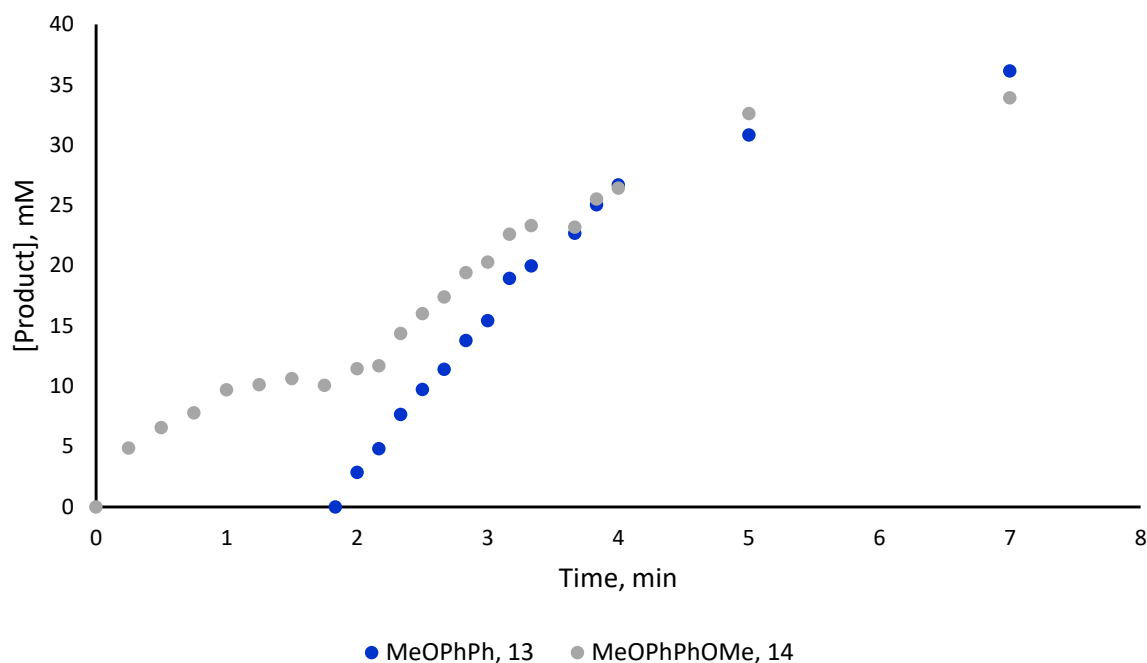
Figure 3.4 – Effect of adding the electrophile 1 min and 50 sec after the boronate. Conditions: chlorobenzene (0.5 mmol), 11 (1.25 mmol), FeBr₃ (0.05 mmol), IMes·HCl (0.05 mmol), MgBr₂·OEt₂ (0.1 mmol), MeMgBr (0.05 mmol), 2-MeTHF:1,4-dioxane (1:1) (6.0 mL), 100 °C, 3 h. Yield determined by GC using dodecane as an internal standard.

Although the bulk oxidation state of iron has been shown to be Fe(I), it may not represent the lowest possible thermodynamically accessible oxidation state under the reaction conditions. Boronate species have been reported to be able to reduce iron species to oxidation states as low Fe(0).[87] When assessing the reaction mixture by ^{1}H-NMR spectroscopy, the IMes-iron(0) complex (**65**) reported by Tatsumi was not observed.[213] However, Tatsumi reported that this species could only be isolated in low yields from the reduction of FeCl₂ and IMes with KC₈. Various attempts were made to observe the species **65** using **11** as a reducing agent and in the presence and absence of MgBr₂ and MeMgBr, but **65** was never observed (Scheme 3.5).
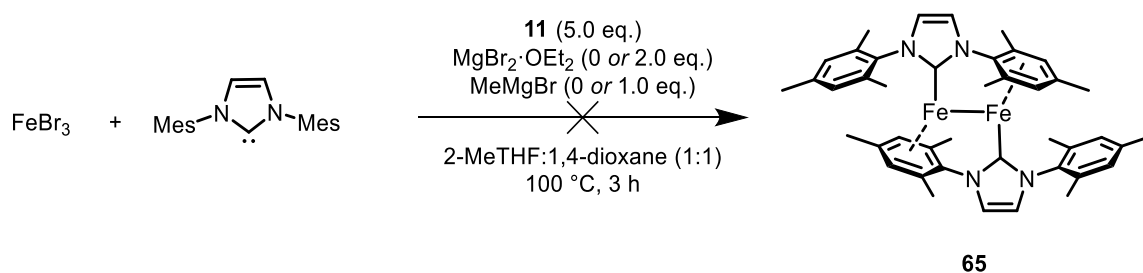
Scheme 3.5 – Synthesis of Fe(0) complex by Tatsumi.[16]

Deng reported that IMes-Iron(0) species **66** could be synthesised when dvtms was also employed in the reaction mixture, using Na/Hg as the reducing agent (Scheme 3.6).[217]
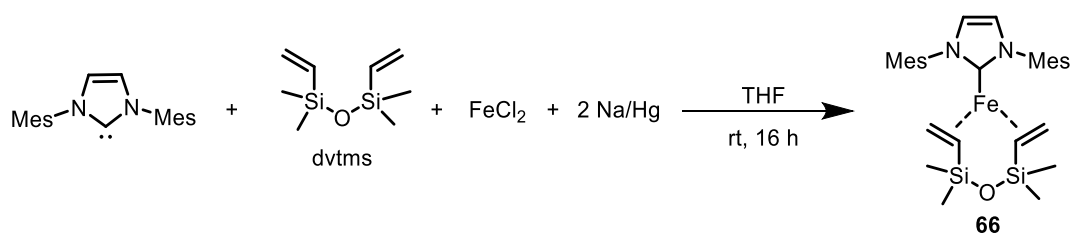
Scheme 3.6 – Synthesis of Fe(0) complex stabilised with dvtms.[217]

^{1}H-NMR analysis of the reaction of FeCl$_2$ and IMes with **11** in the presence of dvtms showed evidence that **66** was present in the reaction mixture (Scheme 3.7 and Figure 3.5). Using FeBr$_3$, instead of FeCl$_2$, also led to the observation of **66** in the reaction mixture. IMes·HCl was also used instead of IMes, and **66** was observed. This shows that the boronate is basic enough to deprotonate the NHC salt in accordance by a previous report by Bedford.[87] Incorporation of MeMgBr and MgBr$_2$ into the reaction mixture also led to formation of **66**, demonstrating that they are not needed in the reduction process. When **11** was excluded from the reaction and MeMgBr was used in excess, **66** was not observed which shows that the boronate is required to reach oxidation states as lows as Fe(0).
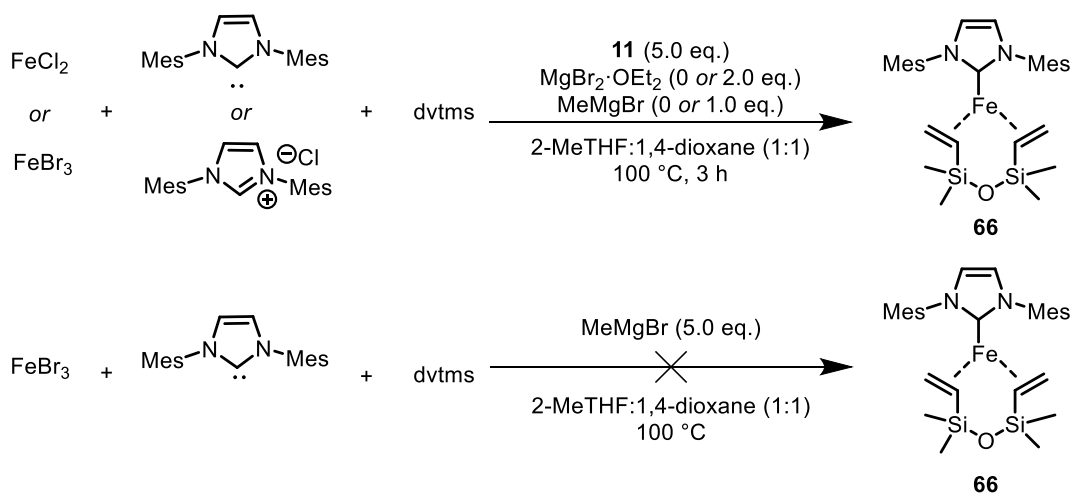
Scheme 3.7 – Formation of 66, by reduction of FeCl$_2$ and FeBr$_3$ using 11. 66 was not formed when MeMgBr used instead of 11.
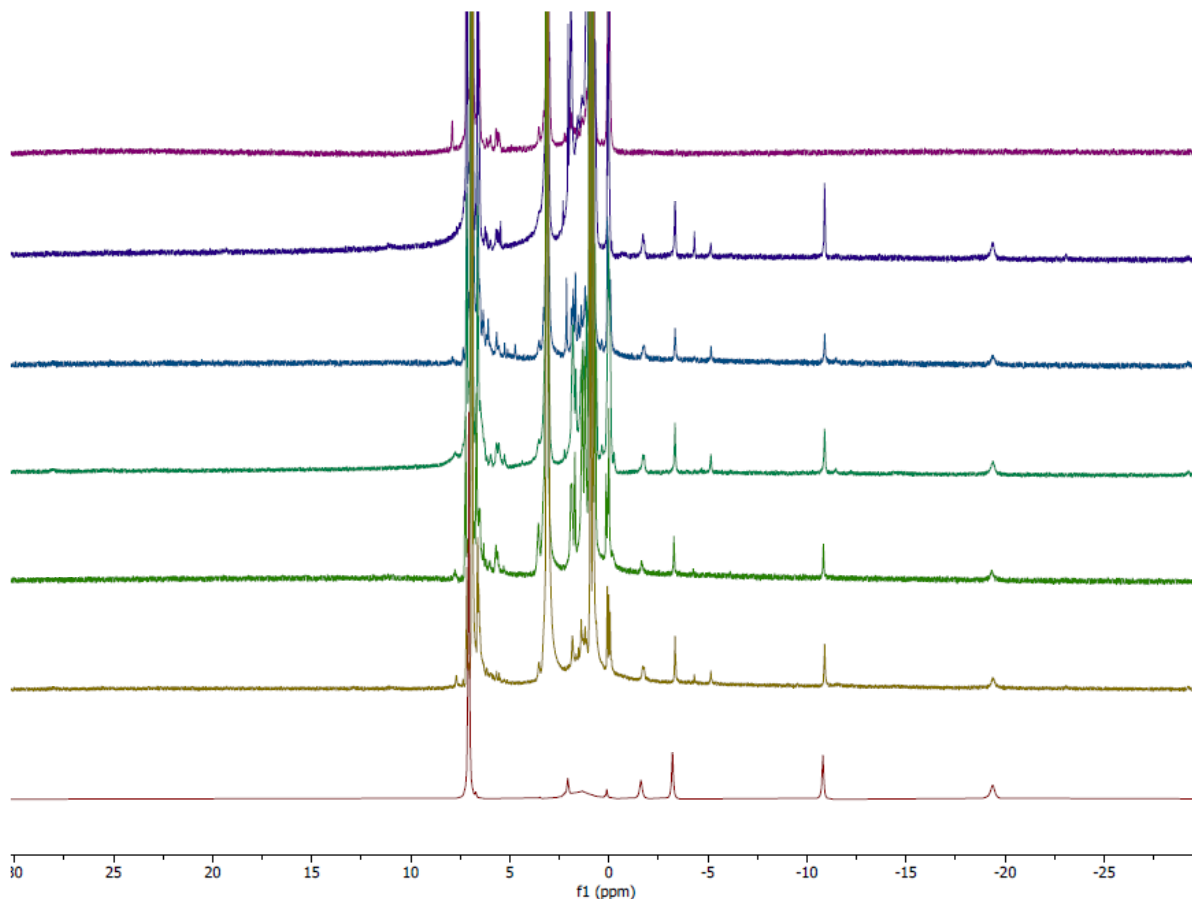
Figure 3.5 – ¹H-NMR spectra of 66 observed under various conditions. a) sample synthesised according to Deng,[217] b) 66 observed by FeCl₂, IMes and 11, c) 66 observed by FeBr₃, IMes and 11, d) 66 observed by FeBr₃, IMes, MgBr₂, MeMgBr and 11, e) 66 observed by FeBr₃, IMes·HCl, and 11, f) 66 observed by FeBr₃, IMes·HCl, MgBr₂, MeMgBr and 11, g) 66 not observed when 11 excluded from reaction but MeMgBr used instead.

From monitoring the reaction of FeBr₃, IMes·HCl, MgBr₂, MeMgBr, dvtms and **11** over time, it was observed that **66** forms after one minute and is still present after an hour in the reaction mixture (Scheme 3.8 and Figure 3.6).
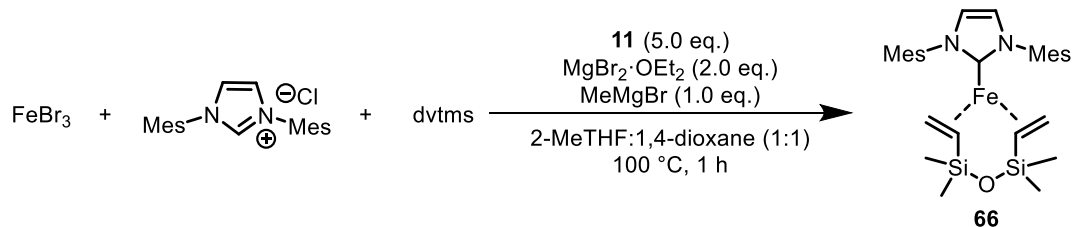
Scheme 3.8 – Synthesis of 66, by reduction of FeBr₃, in the presence of dvtms, with 11. Conditions: 11 (0.25 mmol), FeBr₃ (0.05 mmol), IMes·HCl (0.05 mmol), MgBr₂·OEt₂ (0.1 mmol), MeMgBr (0.05 mmol), dvtms (0.05 mmol) 2-MeTHF:1,4-dioxane (1:1) (2.0 mL), 100 °C, 1 h.
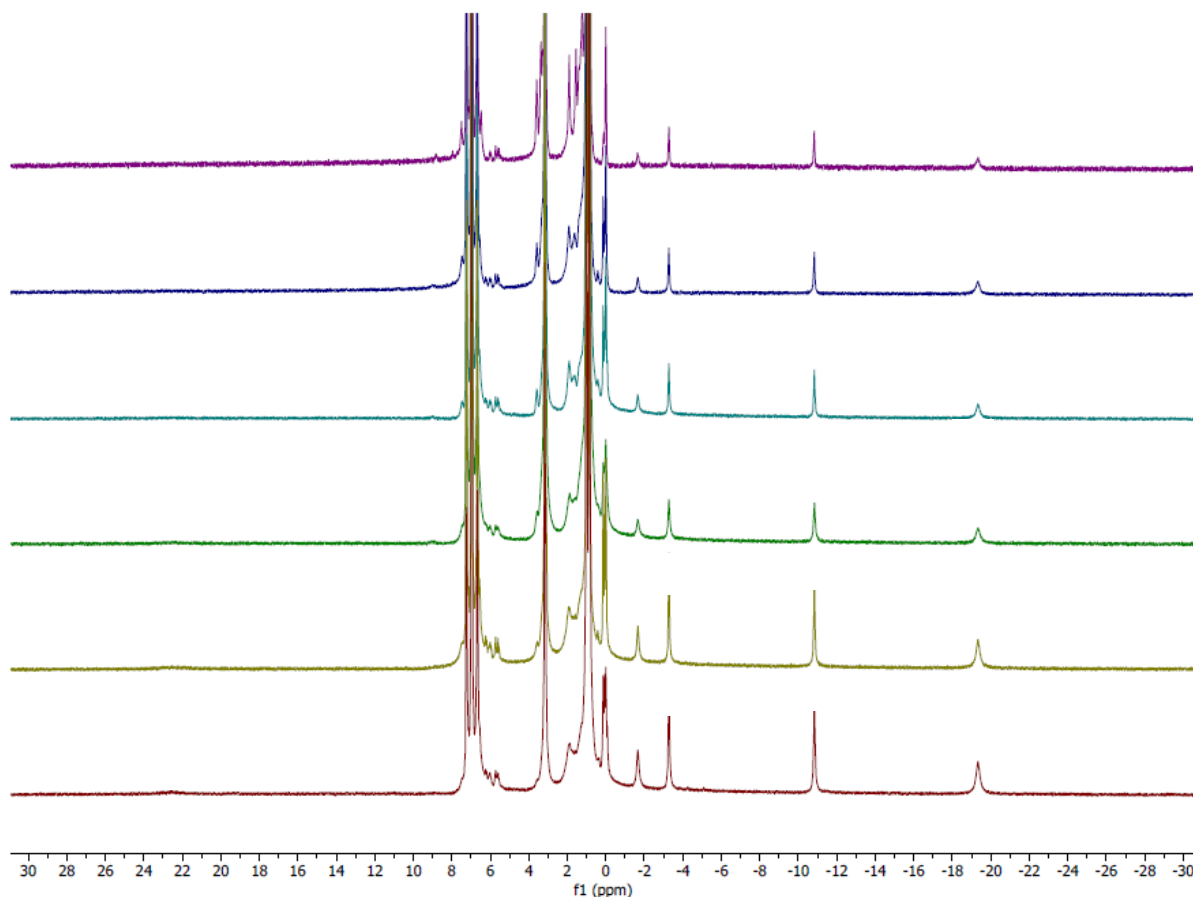
Figure 3.6 – ¹H-NMR spectra of Fe(0) complex being observed over various times. a) 60 min, b) 30 min, c) 20 min, d) 10 min, e) 5 min, f) 1 min.

Trialling **66** in the reaction as the pre-catalyst resulted in a 58% yield of **13** (Scheme 3.9). However, this does not necessarily mean that an Fe(0) species is the active catalyst, but that Fe(0) is obtainable under the reaction conditions and that it could be a thermodynamically stable resting state rather than a kinetically relevant catalytic intermediate.
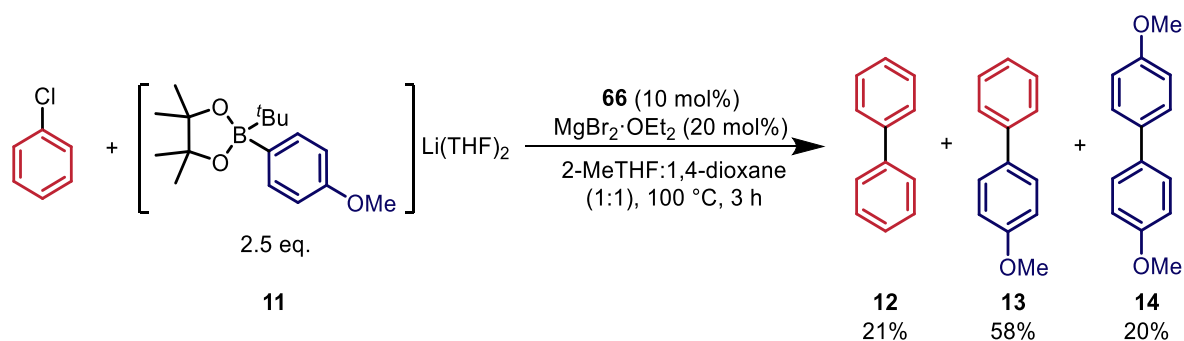
Scheme 3.9 – Use of 66 in the standard catalytic reaction. Conditions: chlorobenzene (0.5 mmol), 11 (1.25 mmol), 66 (0.05 mmol), IMes·HCl (0.05 mmol), MgBr₂·OEt₂ (0.1 mmol), MeMgBr (0.05 mmol), 2-MeTHF:1,4-dioxane (1:1) (6.0 mL), 100 °C, 3 h. Yield determined by GC using dodecane as an internal standard.

3.4 Determining the Phase of the Reaction

Bedford has previously shown that iron nanoparticles (NPs) can catalyse the cross-coupling of alkyl halides with aryl Grignard reagents.[98] NPs were also observed in the cross-coupling of alkyl, benzyl, and allyl halides with arylboronic esters when the ligand was removed from the reaction (Scheme 3.10).[206] In the coupling of benzyl bromide, NPs were formed after the cross-coupling had occurred but with other coupling partners (*e.g.*, alkyl bromides or benzyl chlorides) NPs formed much earlier in the reaction. They also noted an induction period in the reaction, which was concurrent with a colour change of the solution, from pale yellow to black, indicative of iron NPs forming.
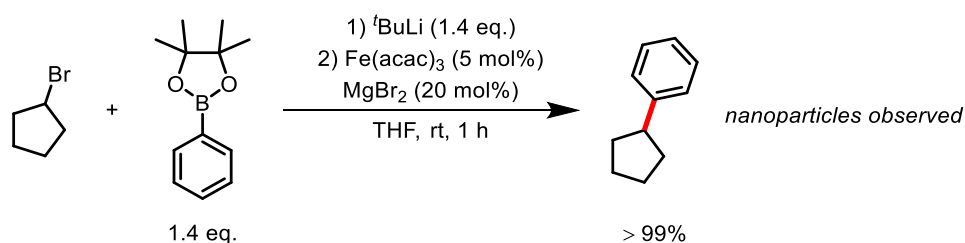
Scheme 3.10 – 'Ligand free' cross-coupling of alkyl bromides with aryl boronic esters and the observation of Fe NPs.[206]

With dvtms in the reaction mixture, Fe(0)IMes species are observed. However, without dvtms acting as a trapping agent, it is conceivable that any Fe(0) species that form could aggregate to form iron NPs. On addition of the boronate the reaction mixture also changes colour from a pale orange to black after approximately 45 seconds, which could suggest NP formation.

Polyethylene glycol (PEG) has been shown to stabilise metal NPs by preventing aggregation and, therefore, keeping catalytic activity and selectivity high.[218] Palladium NPs have been used to promote a vast array of cross-coupling reactions.[219,220] Iron NPs supported by PEG have also been prepared[221,222] and used in catalysis,[223,224] including a cross-coupling reaction.[98]

To investigate whether iron NPs were responsible for the observed catalytic activity, PEG was added to the reaction mixture. If iron NPs participate in the catalysis, it was anticipated that the addition of PEG could result in increased catalytic activity due to the formation of PEG stabilised iron NPs. Incorporation of PEG in the reaction resulted in almost complete shut down of the

reactivity (Table 3.2), which indicates that iron NPs may not be responsible for the catalytic activity, but still could be present in the reaction mixture.

Table 3.2 –The effect of adding PEG to the reaction.

Entry	Eq. of PEG	12, % Yield	13, % Yield	14, % Yield
1	0.0	6	61	32
2	1.0	0	1	2
3	2.0	0	1	1
4	5.0	1	1	1
5	10	1	1	0

Conditions: chlorobenzene (0.5 mmol), 11 (1.25 mmol), FeBr$_3$ (0.05 mmol), IMes·HCl (0.05 mmol), MgBr$_2$·OEt$_2$ (0.1 mmol), MeMgBr (0.05 mmol), PEG, 2-MeTHF:1,4-dioxane (1:1) (6.0 mL), 100 °C, 3 h. Yield determined by GC using dodecane as an internal standard.

The mercury drop test was originally introduced to probe whether reaction mixtures in platinum-group catalysis occur under a homogeneous or heterogeneous regime, and the method has been exploited in selective poisoning tests in iron catalysis.[225] However, there is a lack of consensus as to whether the mercury drop experiment is as effective for determining the homogeneity of iron-catalysed processes compared to platinum group metals. Iron is one of the few metals that does not form amalgams with mercury, so the hypothesis of the mercury drop experiment does not really align with iron catalysis. However, it has been shown to inhibit the reactivity of previously reported iron-catalysed reactions.[226] To further investigate whether metal NPs were playing a role in the catalysis, a mercury drop experiment was undertaken (Figure 3.7). Any platinum-group metal NPs present in the reaction mixture would amalgamate, forming mercury alloys. If it were platinum-group metal NPs that were the catalytically active species in the reaction, this would lead to a significant decrease in reactivity and a decrease in the formation of the cross-coupled product. In this experiment, mercury was added after 1.75 minutes and little to no change in reactivity was

observed, the product was formed with the expected yield. This could indicate that metal NPs are not formed as the catalytically active species, and that the catalyst is homogeneous in this reaction. However, it could also indicate that iron NPs are forming in the reaction mixture and that the Hg drop test does not work in this example.
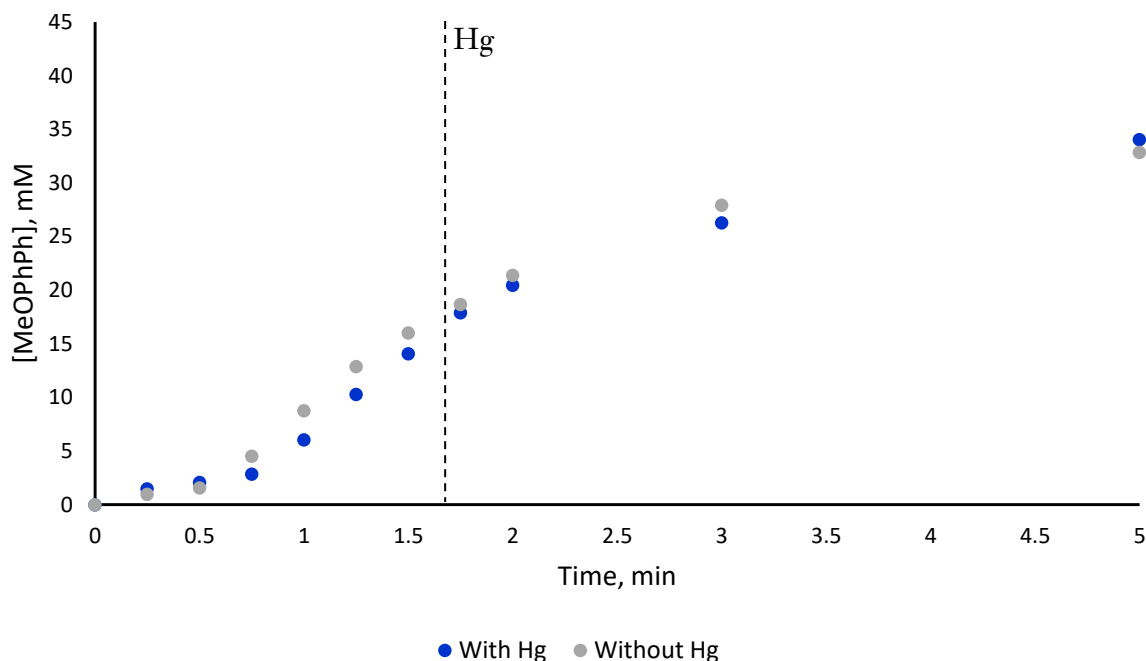
Figure 3.7 – Effect of adding Hg to the reaction mixture. Conditions: chlorobenzene (0.5 mmol), 11 (1.25 mmol), FeBr$_3$ (0.05 mmol), IMes·HCl (0.05 mmol), MgBr$_2$·OEt$_2$ (0.1 mmol), MeMgBr (0.05 mmol), 2-MeTHF:1,4-dioxane (1:1) (6.0 mL), 100 °C, 3 h. Yield determined by GC using dodecane as an internal standard.

Finally, the synthesis of pre-formed PEG-supported iron NPs, reported by Bedford,[98] were used in the reaction and this only led to a yield of 5% of cross-coupled product. These combined results, along with the high ligand dependence of the reaction (without IMes·HCl in the reaction, cross-coupling decreases to 3% and nucleophile homo-coupling decreases to 12%) indicate that the formation of catalytically active iron NPs does not occur and that homogeneous intermediates are responsible for the catalytic activity.

3.5 Kinetic Investigations

Reaction kinetic analysis can be used to work out the order with respect to a reactant in a reaction and to determine the rate equation, as well as determining the linear free-energy relationships (LFER), and reaction activation parameters. With these insights, the rate determining step (rds) of the reaction may be deduced, potentially leading to further developments in catalyst design and improvement of reaction conditions. For these reasons, reaction kinetic analysis has become a powerful and widespread tool to study the mechanism of many reactions. As the reaction is relatively unselective between cross-coupling and nucleophile homo-coupling, the orders with respect to reactants, LFER, and activation parameters were calculated for both.

To determine the reaction orders, the initial rates method was used. For the pre-catalyst, variable time normalisation analysis (VTNA) was also used to help determine the order. The initial rates method involves changing the concentration of one of the reagents and monitoring the concentration of product in the early stage of the reaction to calculate the initial rate (typically up to 10% conversion). A logarithmic plot of concentration vs rate is then produced and the order with respect to a reactant is determined from the gradient.[227] VTNA is a way to graphically interrogate the kinetic data to determine the order of a reactant; it has been argued that it is easier, quicker, and potentially more accurate to analyse the data using VTNA than the initial rates method.[228] Reaction profiles of differing concentrations of the reactant (A) are required. However, in comparison to initial rates, the whole plot is used rather than just the initial section. The data is then overlayed and unless the order with respect to A is zero, the plots at varying concentrations will not overlay using the time axis. Instead, it must be replaced by the time integral of the concentration of A raised to the correct power, α (Equation 3.1). α is determined by changing the number until the best overlay of data is visually observed and this is then the order in that reactant. As long as the product formation, time, and reactant consumption can be measured then the data can be analysed quickly by any spreadsheet software. The VTNA method works by normalising the time between each pair of data points by averaging the concentration of these points and thus removes the kinetic effect of that reactant from the reaction profile.[228]

$$\int_{t=0}^{t=n} [A]^a dt = \sum_{t=1}^{n} \left(\frac{A_i + A_{i-1}}{2} \right)^\alpha (t_i - t_{i-1})$$

Equation 3.1 – Normalisation of the time scale. Where t = time, A = concentration in reactant A, and α = priori unknown (order with respect to A)

3.5.1 Orders of Reaction for the Cross-Coupled Product, 13

3.5.1.1 Order in FeBr₃-IMes·HCl Pre-Mix

First investigated by the initial rates method was the effect of the pre-catalyst, FeBr$_3$-IMes·HCl, on the reaction (Figure 3.8). From varying the concentration of FeBr$_3$ and IMes·HCl and then measuring the formation of 4-methoxybiphenyl, a positive correlation between pre-catalyst loading and initial rate was observed between 4.2 mM (5 mol%) and 12.5 mM (15 mol%) loading. However, when the loading was further increased to 16.7 mM (20 mol%), a decrease in initial rate was observed.
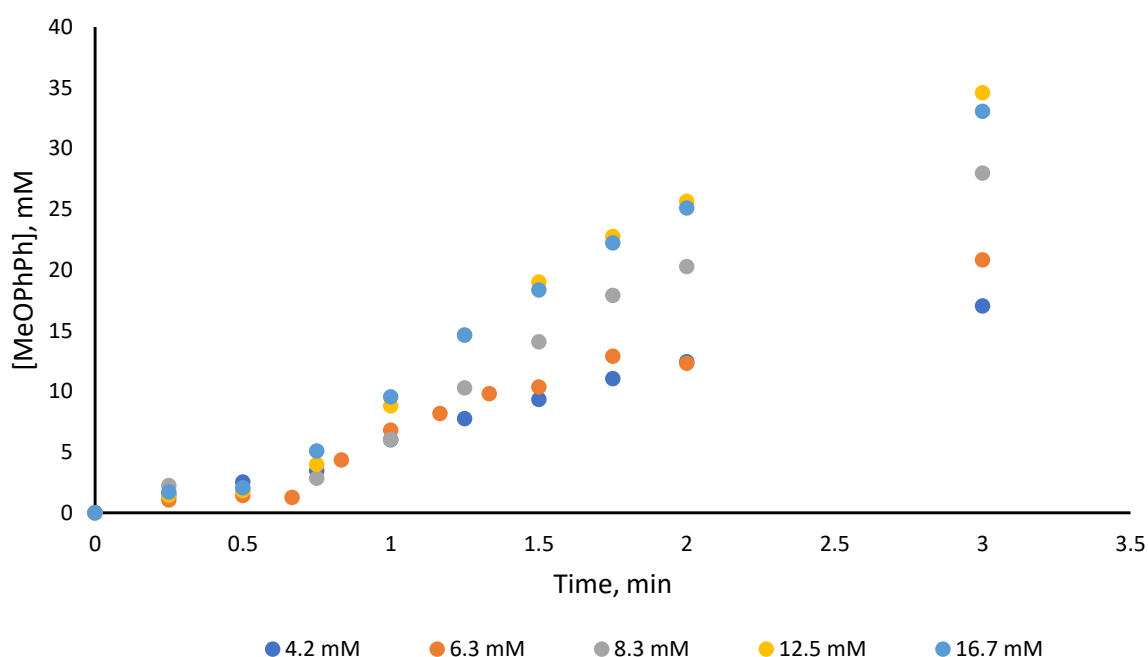
Figure 3.8 – Concentration-time plots for the formation of 4-methoxybiphenyl at varying concentrations of FeBr$_3$-IMes·HCl. Conditions: chlorobenzene (0.5 mmol), 11 (1.25 mmol), FeBr$_3$, IMes·HCl, MgBr$_2$·OEt$_2$ (0.1 mmol), MeMgBr (0.05 mmol), 2-MeTHF:1,4-dioxane (1:1) (6.0 mL), 100 °C, 3 h. Yield determined by GC using dodecane as an internal standard.

Plotting the logarithm of the concentration of pre-catalyst against the logarithm of initial rate, the order with respect to pre-catalyst for the cross-coupling reaction can be obtained from the gradient of the plot (Figure 3.9). In this case the gradient is 0.978, suggesting that the cross-coupling reaction is 1st order with respect to pre-catalyst up to 12.5 mM (15 mol%). When the loading of pre-catalyst is further increased to 16.7 mM (20 mol%), the initial rate decreased, potentially indicating that the system became saturated and catalytically inactive aggregates are formed. The

first order dependence with respect to pre-catalyst shows that it is involved in the rds on the reaction mechanism.
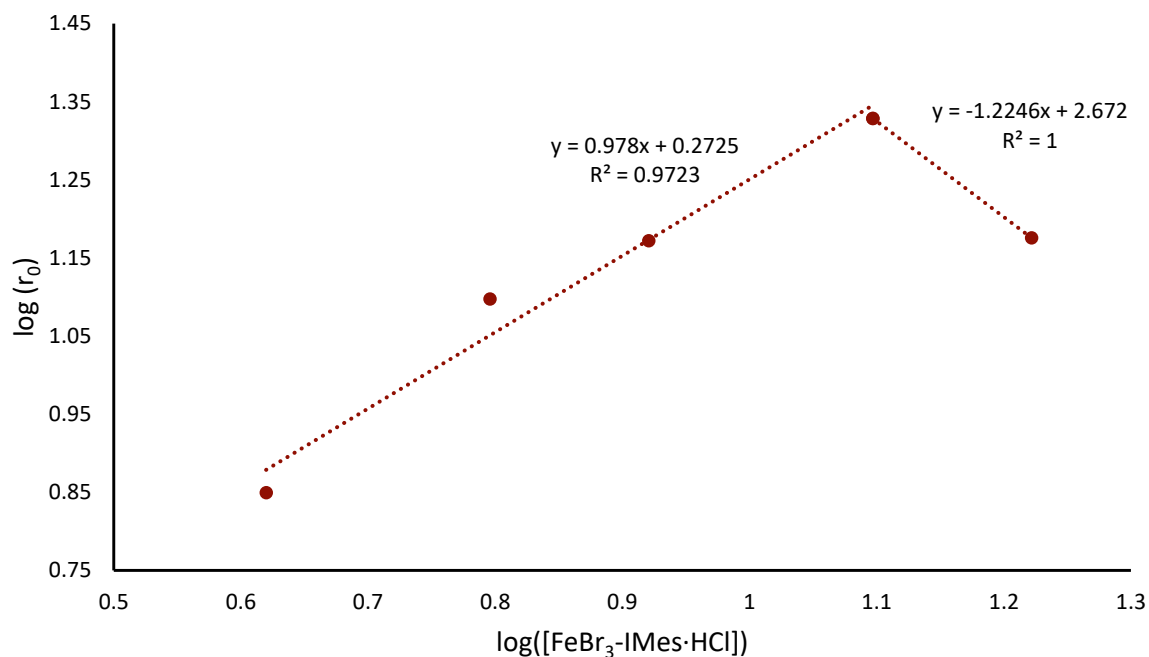
Figure 3.9 – Determination of the order of reaction with respect to FeBr₃-IMes·HCl by initial rates method.

An alternate approach to analyse and interpret reaction kinetics, is by Variable Time Normalisation Analysis (VTNA).[228] Described by Burés, VTNA involves overlaying the data points from different reactions against the variable normalisation of the time scale, when the data overlays that is the order of the reaction with respect to that reactant (see start of Section 3.5 for fuller explanation of the normalised time scale). VTNA uses the data from all points in the reaction, rather than just the initial stage, and therefore can be seen as a more accurate way to analyse the reaction. To use VTNA to analyse a reaction, the concentrations of product and reactant must be known at each time point. In this reaction, neither the concentration of chlorobenzene (poor burning in GC-FID) nor boronate **11** (air and moisture sensitive) could be accurately determined by GC. Therefore, VTNA could only be used to determine the order with respect to pre-catalyst where the concentration can be assumed to be constant.

The order determined with respect to pre-catalyst by the initial rates method was 1 between 4.2 mM (5 mol%) and 12.5 mM (15 mol%). However, when analysed by VTNA there is not an overlay of data when the order is set to 1 (Figure 3.10). In fact, there is no clear overlay of the plots when

all the concentrations of pre-catalyst are used at any order. However, Burés reports that only two plots are needed, as a minimum, to determine the order in a reactant.[229] Therefore, taking the two data points that are closest to each other, the order with respect to pre-catalyst was determined between these two concentrations (Table 3.3). This shows a change in order in pre-catalyst depending on the concentrations that are used. Therefore, suggesting that the order in pre-catalyst may not be simply described as first order.

Table 3.3 – Summary of order in pre-catalyst at varying concentrations.

Entry	Concentration 1, mM	Concentration 2, mM	Observed order
1	4.2	6.3	0.45
2	6.3	8.3	0.75
3	8.3	12.5	0.45
4	12.5	16.7	0
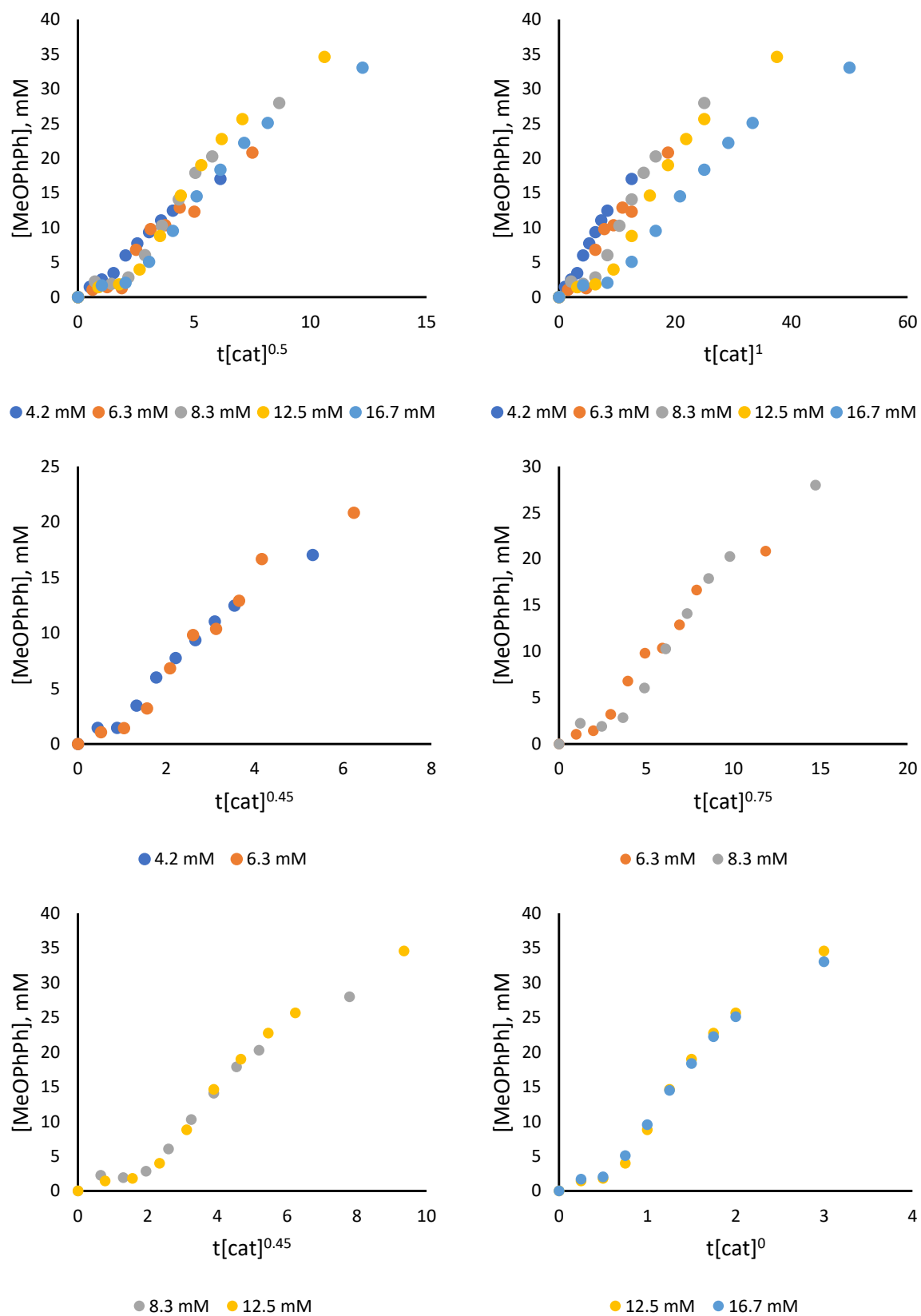
Figure 3.10 – VTNA for the formation of 13, with varying concentrations of pre-catalyst.

The initial rates method depends on the maximum rate at the start of the reaction to determine the order in a reactant. In the reaction profiles for the formation of 4-methoxybiphenyl, a clear induction period is seen for all concentrations of pre-catalyst. In these cases, the induction period can be omitted and corrected for (Figure 3.11). When this data is analysed by VTNA there is still not a clear overlay of data when the order in pre-catalyst is set to 1, although the data collected when 16.7 mM (20 mol%) of pre-catalyst is omitted gives a much better overlay. Again, two data sets with the next highest concentration of pre-catalyst were used to determine the order in pre-catalyst at these concentration points (Table 3.4). The orders obtained when VTNA is used strongly suggest that an order of 1 in pre-catalyst (as determined by initial rates) may not be an accurate way to describe the cross-coupling reaction and that the order is dependent on the pre-catalyst concentration.

Table 3.4 – Summary of order in pre-catalyst at varying concentrations.

Entry	Concentration 1, mM	Concentration 2, mM	Observed order
1	4.2	6.3	0.75
2	6.3	8.3	1
3	8.3	12.5	0.6
4	12.5	16.7	-0.75
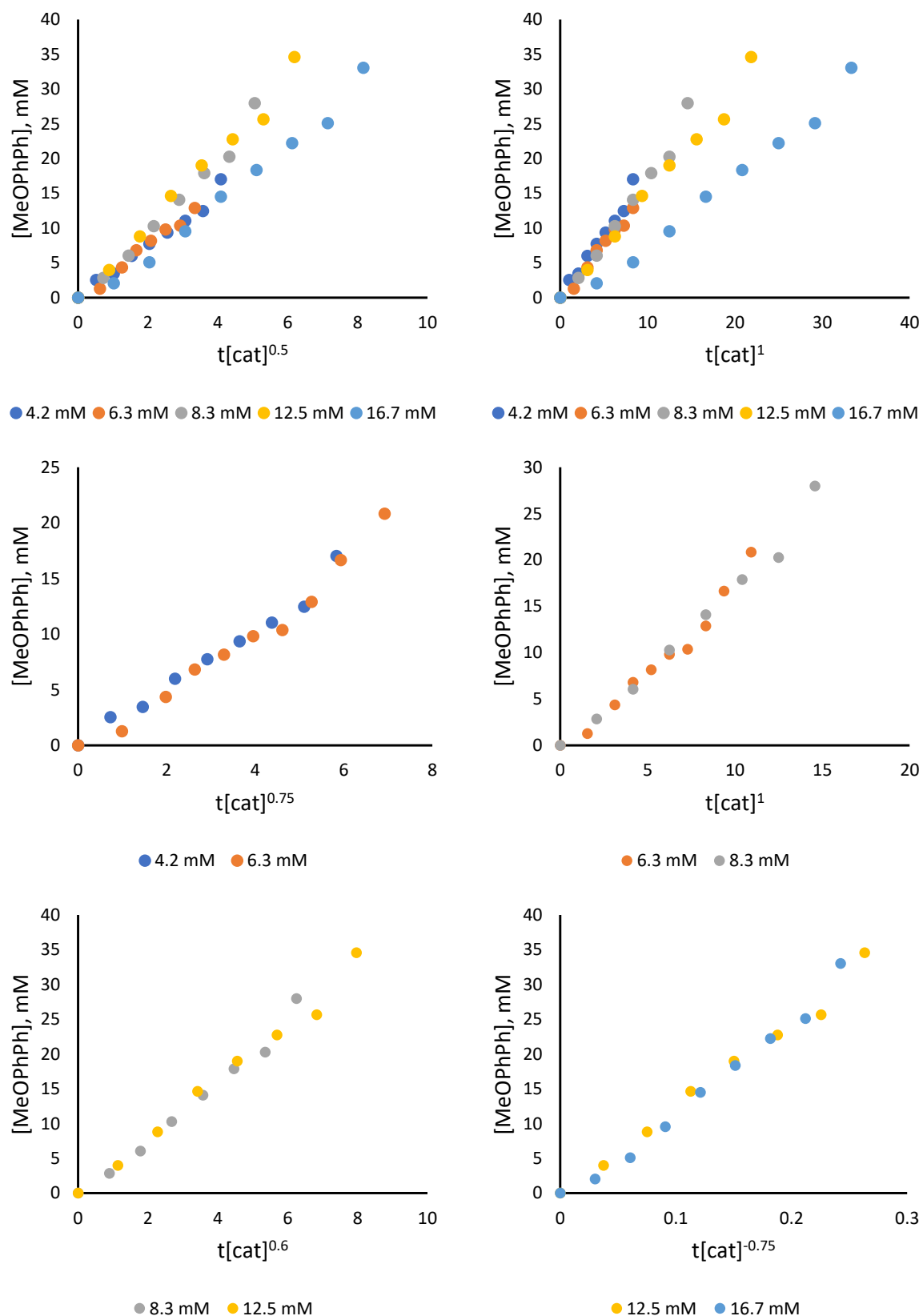
Figure 3.11 – VTNA (corrected for induction period) for the formation of 13, with varying concentrations of pre-catalyst.

VTNA works best when there is a short induction period and a longer set of data points.[228] Therefore, with these data sets, VTNA might not be an accurate way to determine the order in pre-catalyst. However, VTNA does suggest that there is a change in order in pre-catalyst dependent on the concentration of pre-catalyst. A better way to interpret the data might be to use the initial rates method but to use three continuous points to assess the order in these concentration ranges and see the changes over the complete data set (Figure 3.12). When the data is analysed this way, we see an initial order in pre-catalyst of 1, that drops to 0.77 and then becomes zero order at the highest concentrations.

The change in order observed when the data is assessed this way could suggest that there is a series of finely balanced equilibria in the reaction mixture where any change in concentration of pre-catalyst shifts these equilibria and thus changes the observed order in pre-catalyst. It could also suggest that there are two competing pathways (cross-coupling and homo-coupling), where different concentrations favour different pathways.
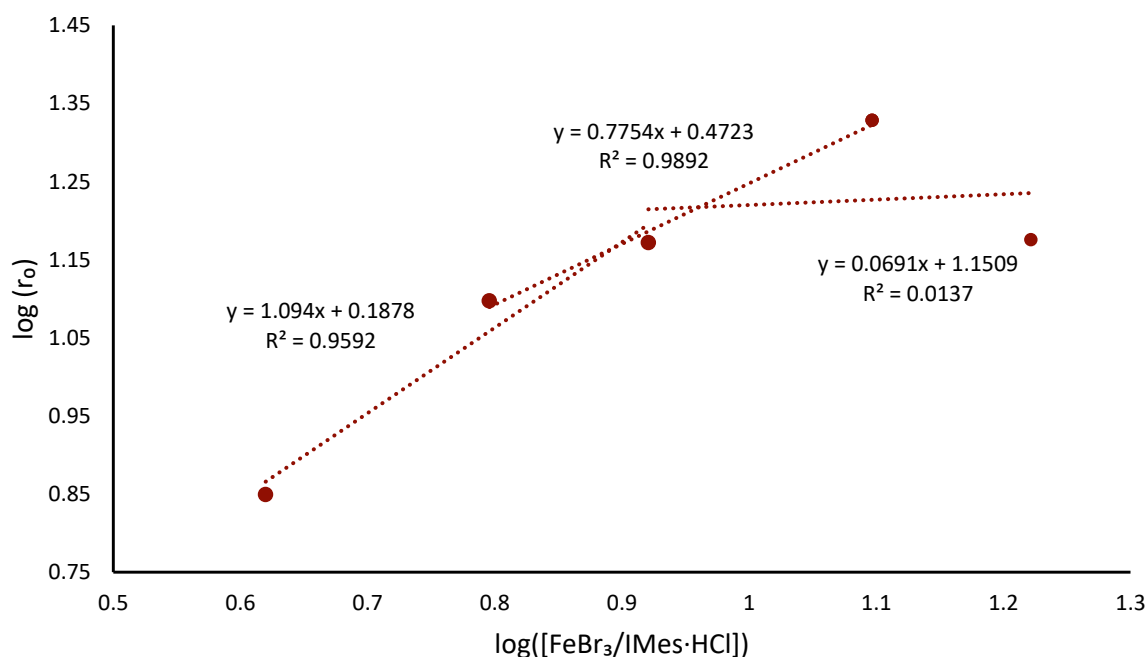
Figure 3.12 – Determination of the order of reaction in FeBr₃-IMes·HCl by initial rates method and using three continuous points at a time.

3.5.1.2 Order in Electrophile, Chlorobenzene

Next the effect of changing the concentration of the electrophile on the initial rate of the cross-coupling reaction was investigated. A positive dependence of initial rate on chlorobenzene concentration is observed (Figure 3.13).
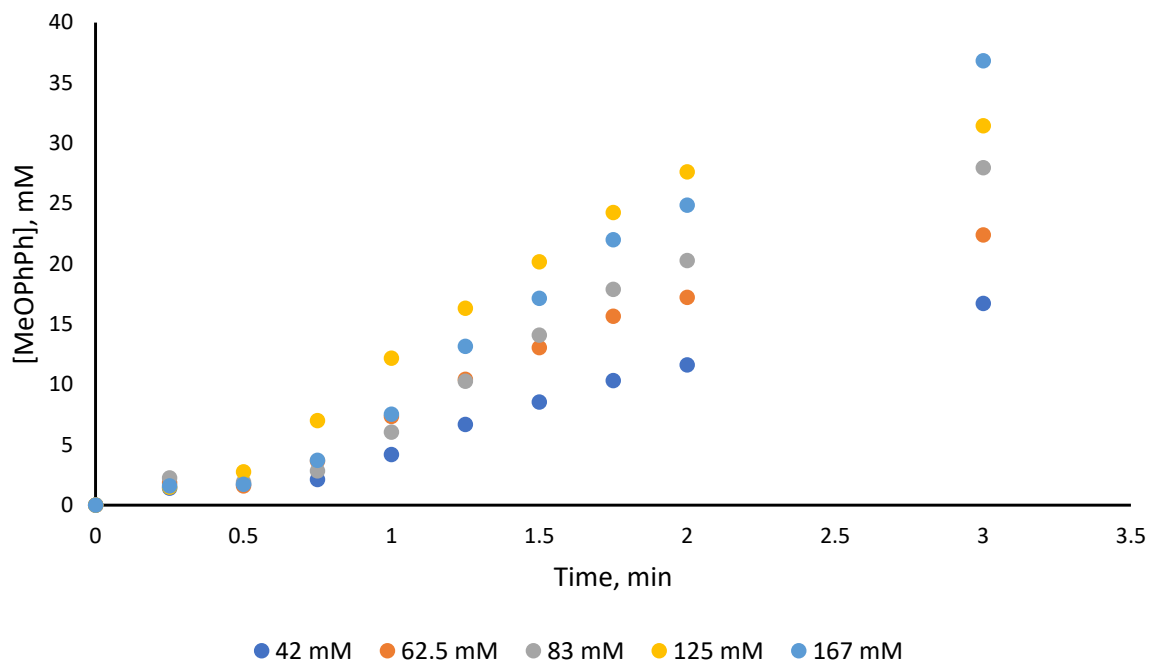
Figure 3.13 – Concentration-time plots for the formation of 4-methoxybiphenyl at varying concentrations of chlorobenzene. Conditions: chlorobenzene, 11 (1.25 mmol), FeBr$_3$ (0.05 mmol), IMes·HCl (0.05 mmol), MgBr$_2$·OEt$_2$ (0.1 mmol), MeMgBr (0.05 mmol), 2-MeTHF:1,4-dioxane (1:1) (6.0 mL), 100 °C, 3 h. Yield determined by GC using dodecane as an internal standard.

An excellent fit was observed when the logarithm of electrophile concentration is plotted against the logarithm of initial rate, up to 125 mM (Figure 3.14). Here, the experimentally determined reaction order in electrophile is 0.7, up to 125 mM. The positive value demonstrates that the electrophile could be involved in the rds of the reaction, but the non-integer value suggests that a more complex reaction mechanism is in place, potentially involving an equilibrium step in the reaction mechanism.
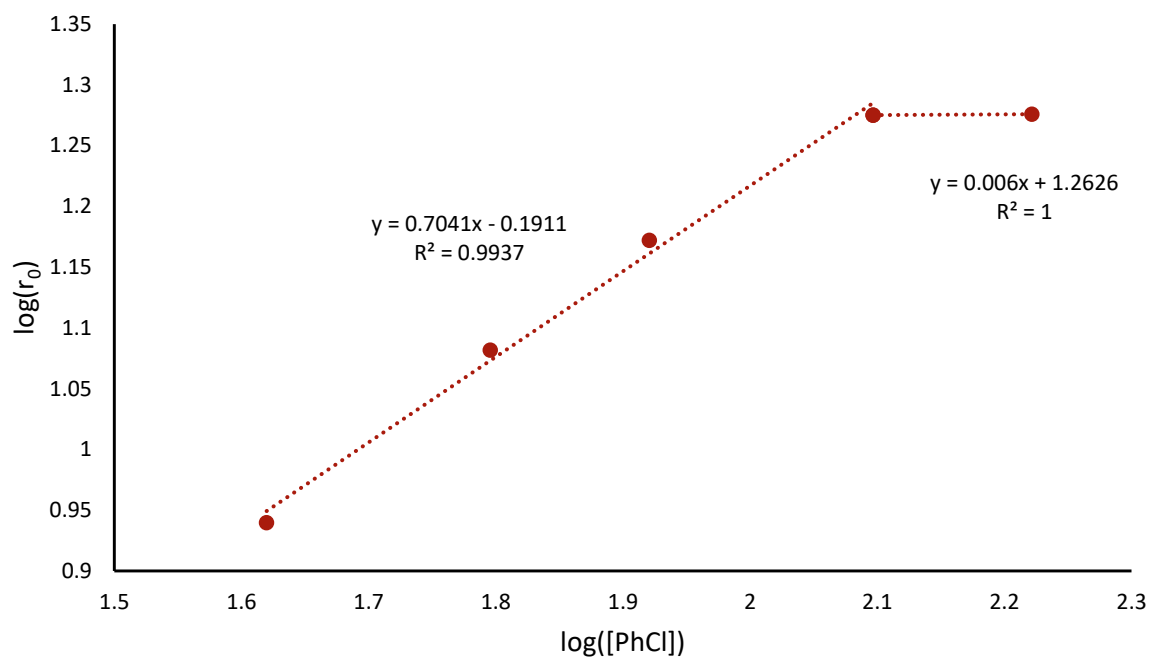
Figure 3.14 – Determination of the order of reaction in chlorobenzene by initial rates method.

3.5.1.3 Order in Nucleophile, 11

Following the determination of the order in electrophile on the cross-coupling reaction, the order in nucleophile, **11**, was determined. As the concentration of **11** was increased, the initial rate of formation of 4-methoxybiphenyl also increased (Figure 3.15).
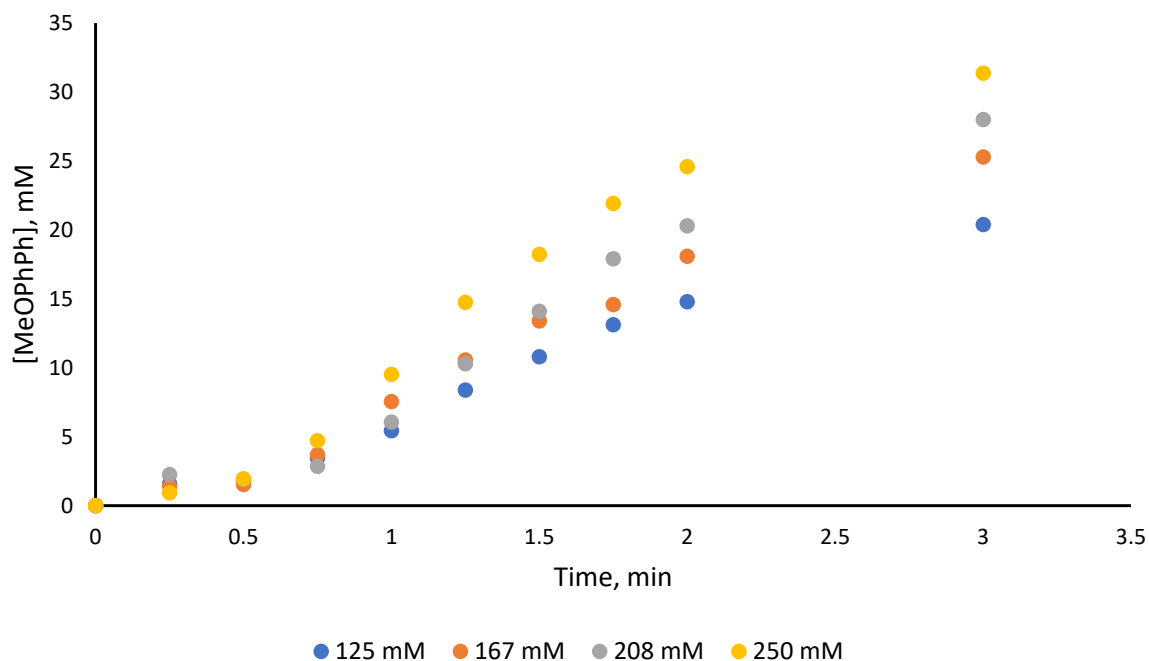
Figure 3.15 – Concentration-time plots for the formation of 4-methoxybiphenyl at varying concentrations of boronate, 11. Conditions: chlorobenzene (0.5 mmol), 11, FeBr₃ (0.05 mmol), IMes·HCl (0.05 mmol), MgBr₂·OEt₂ (0.1 mmol), MeMgBr (0.05 mmol), 2-MeTHF:1,4-dioxane (1:1) (6.0 mL), 100 °C, 3 h. Yield determined by GC using dodecane as an internal standard.

The observed gradient is 0.91, suggesting that the order in nucleophile is approximately 1 for the formation of 4-methoxybiphenyl; an excellent fit of data was observed (Figure 3.16). The positive dependence indicates that the nucleophile is involved in the rds of the reaction.
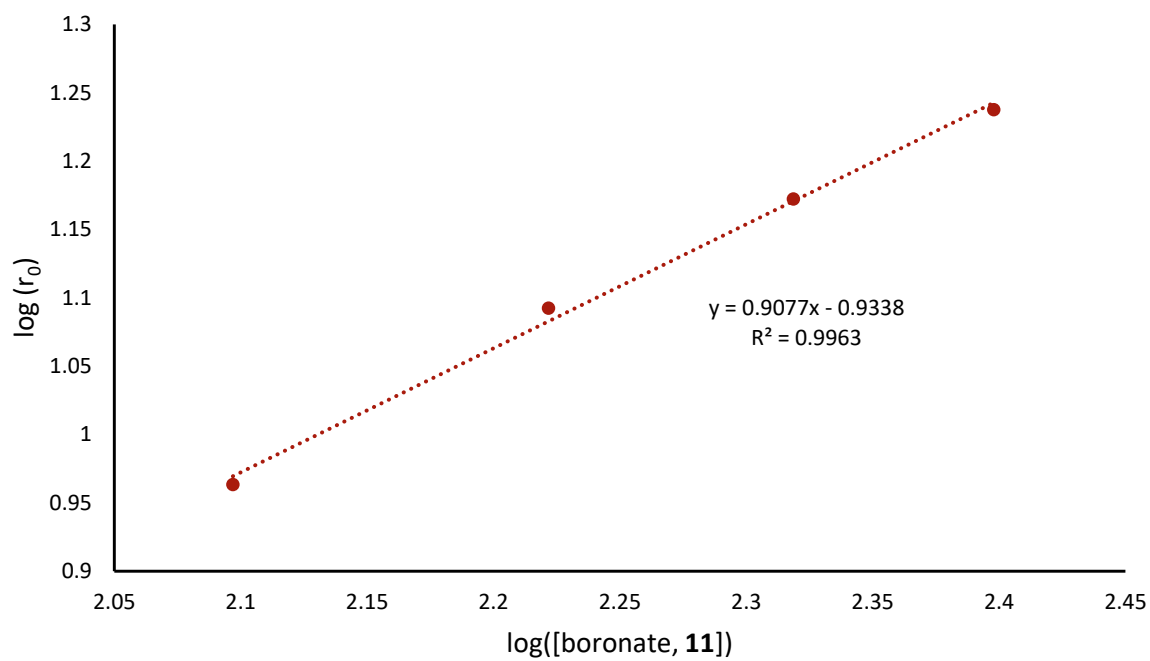
Figure 3.16 – Determination of the order of reaction in boronate by initial rates method.

3.5.1.4 Order in MeMgBr

In Section 3.2 it was suggested that the role of MeMgBr is to deprotonate the NHC salt to form the IMes carbene *in situ*. To further probe whether MeMgBr was involved elsewhere in the reaction mechanism, the initial rate of formation of 4-methoxybiphenyl was measured at different concentrations of MeMgBr (Figure 3.17). The results show very little change in the initial rate of formation of 4-methoxybiphenyl, with the 4 plots initially overlaying. However, there is a decrease in total formation of 4-methoxybiphenyl when the concentration of MeMgBr is 12.5 mM (15 mol%).
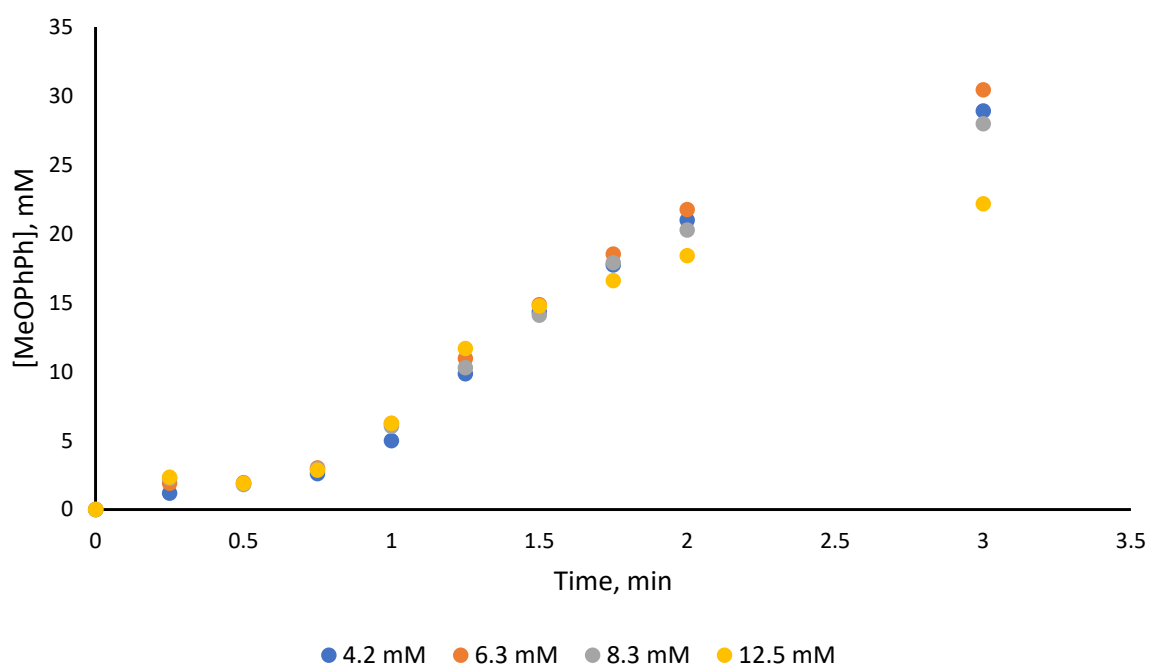
Figure 3.17 – Concentration-time plots for the formation of 4-methoxybiphenyl at varying concentrations of MeMgBr. Conditions: chlorobenzene (0.5 mmol), 11 (1.25 mmol), FeBr$_3$ (0.05 mmol), IMes·HCl (0.05 mmol), MgBr$_2$·OEt$_2$ (0.1 mmol), MeMgBr, 2-MeTHF:1,4-dioxane (1:1) (6.0 mL), 100 °C, 3 h. Yield determined by GC using dodecane as an internal standard.

When the logarithm of concentration of MeMgBr is plotted against the logarithm of the initial rate, a gradient of 0.035 is observed, indicative of the reaction being effectively 0 order with respect to MeMgBr (Figure 3.18). This suggests that MeMgBr is not involved in the rds of the reaction, which is in accordance with it deprotonating IMes·HCl.
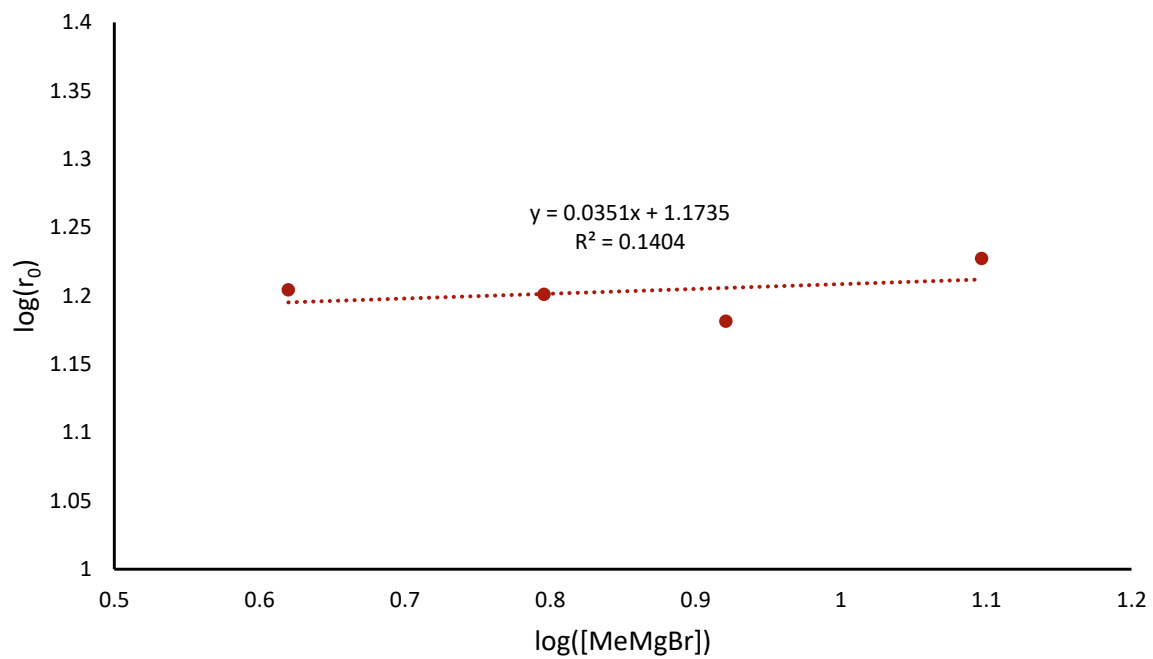
Figure 3.18 – Determination of the order of reaction in MeMgBr by initial rates method.

3.5.1.5 Order in MgBr$_2$

Finally, the effect of the concentration of MgBr$_2$ on the cross-coupling reaction was measured (Figure 3.19). To ensure the base level of Mg halide salt in the reaction was 0 and that the concentrations of added MgBr$_2$ were accurate, the reactions were carried out in the absence of MeMgBr, and IMes was used instead of IMes·HCl.
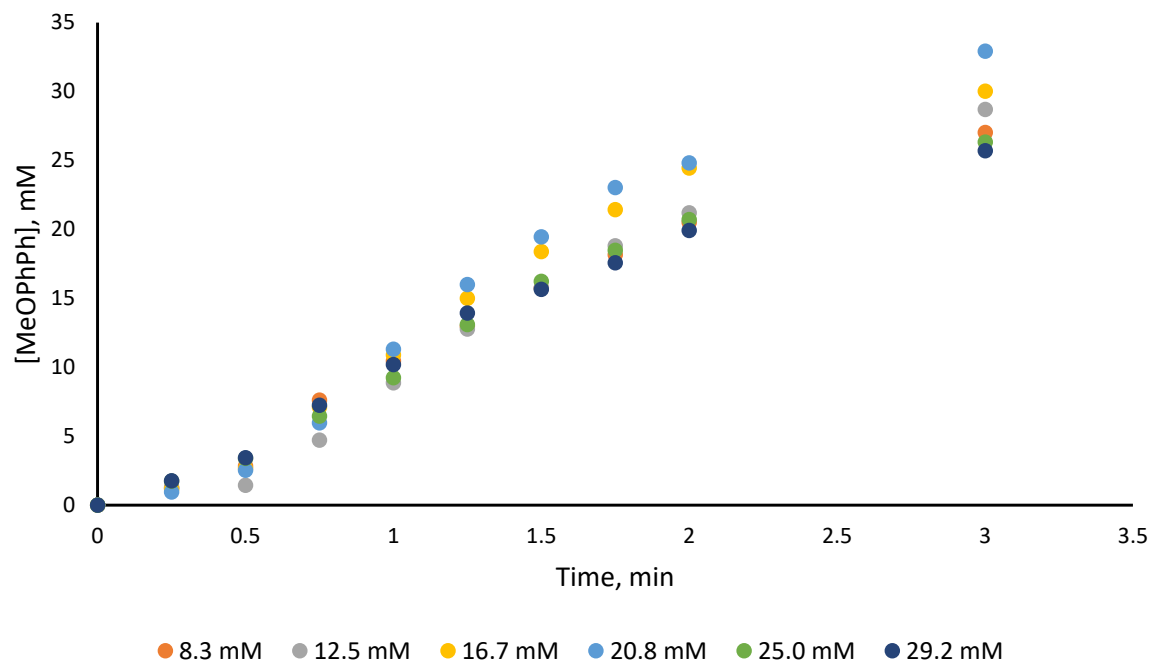
Figure 3.19 – Concentration-time plots for the formation of 4-methoxybiphenyl at varying concentrations of MgBr$_2$. Conditions: chlorobenzene (0.5 mmol), 11 (1.25 mmol), FeBr$_3$ (0.05 mmol), IMes (0.05 mmol), MgBr$_2$·OEt$_2$, 2-MeTHF:1,4-dioxane (1:1) (6.0 mL), 100 °C, 3 h. Yield determined by GC using dodecane as an internal standard.

When the logarithm of the concentration of MgBr$_2$ was plotted against the logarithm of the initial rate, there is an excellent fit of data between 8.3 and 20.8 mM (10 and 25 mol%), where a gradient of 0.3 is obtained (Figure 3.20). However, once the concentration of MgBr$_2$ is further increased to 25 and 29.2 mM (30 and 35 mol%), the initial rate of reaction decreases, and a negative dependency is observed. This correlation could suggest that MgBr$_2$ is involved in the rds, but more likely suggests that it is involved in a pre-equilibrium step with the rds; this could explain why there is a small positive non-integer order in MgBr$_2$. The reaction inhibition at higher concentrations of MgBr$_2$ might suggest that it is involved in two steps in the cycle, where first it must coordinate to an iron species but then later in the cycle it must dissociate for the cycle to complete. When concentrations of MgBr$_2$ are higher, the dissociation is inhibited and thus the catalysis is inhibited. This phenomenon is observed in the iron-catalysed substrate-directed Suzuki

biaryl cross-coupling reaction reported by Bedford.[87] It should be noted that they were unable to determine whether it was $MgBr_2$ or a bromide anion that coordinates to the iron centre.
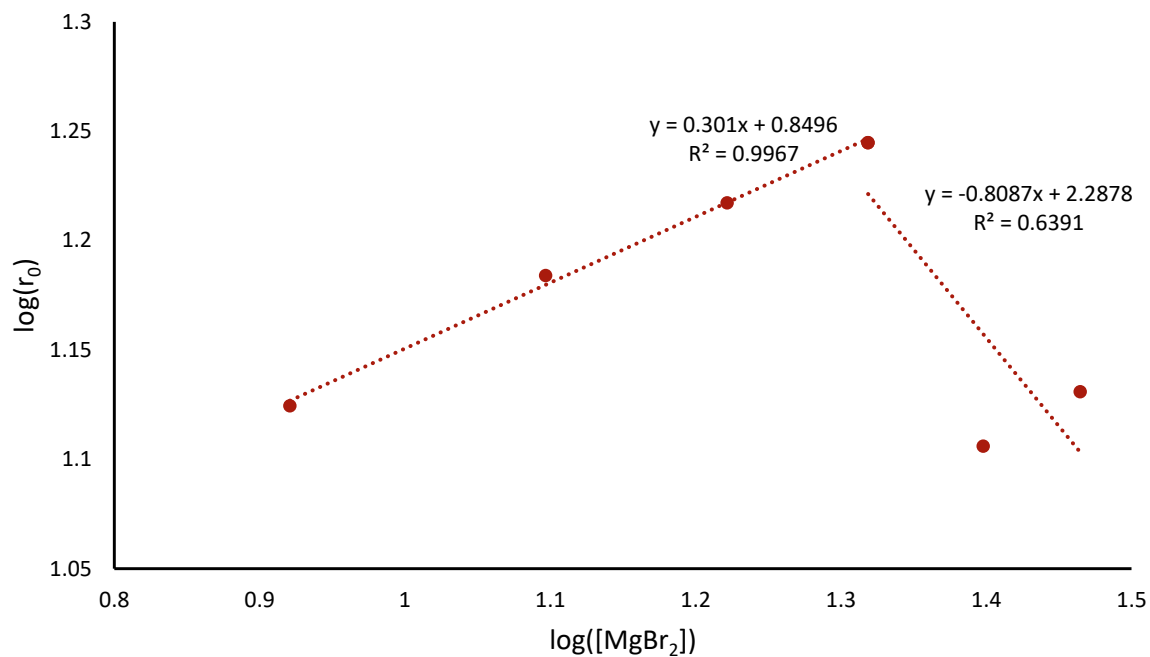

Figure 3.20 – Determination of the order of reaction in MgBr₂ by initial rates method.

3.5.2 Orders of Reaction for the Homo-Coupled Product, 14

After determining the orders in each reactant for the cross-coupling reaction, the attention was turned to experimentally determining the orders in reactants for the homo-coupling of the nucleophile. These were calculated predominantly by the initial rates method, but VTNA was also used to help calculate the order in pre-catalyst.

3.5.2.1 Order in FeBr$_3$-IMes·HCl Pre-Mix

The concentration in pre-catalyst, FeBr$_3$-IMes·HCl, was first investigated on the rate of formation of 4,4'-dimethoxybiphenyl. When the concentration of pre-catalyst is changed from 4.2 to 16.7 mM (5 to 20 mol%), there is a positive correlation with the initial rate of the reaction and overall product formation (Figure 3.21).
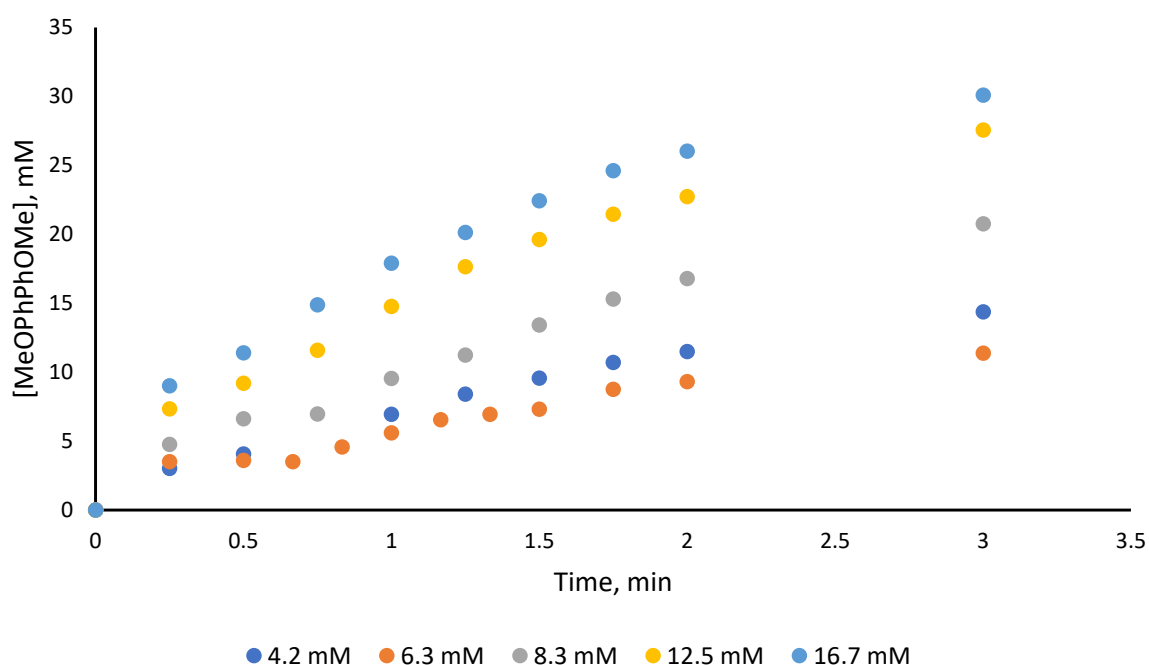
Figure 3.21 – Concentration-time plots for the formation of 4,4'-dimethoxybiphenyl at varying concentrations of FeBr$_3$-IMes·HCl. Conditions: chlorobenzene (0.5 mmol), 11 (1.25 mmol), FeBr$_3$, IMes·HCl, MgBr$_2$·OEt$_2$ (0.1 mmol), MeMgBr (0.05 mmol), 2-MeTHF:1,4-dioxane (1:1) (6.0 mL), 100 °C, 3 h. Yield determined by GC using dodecane as an internal standard.

Although a poor fit, there is approximately a 0.5 order dependence on the pre-catalyst for the homo-coupling of the nucleophile (Figure 3.22).
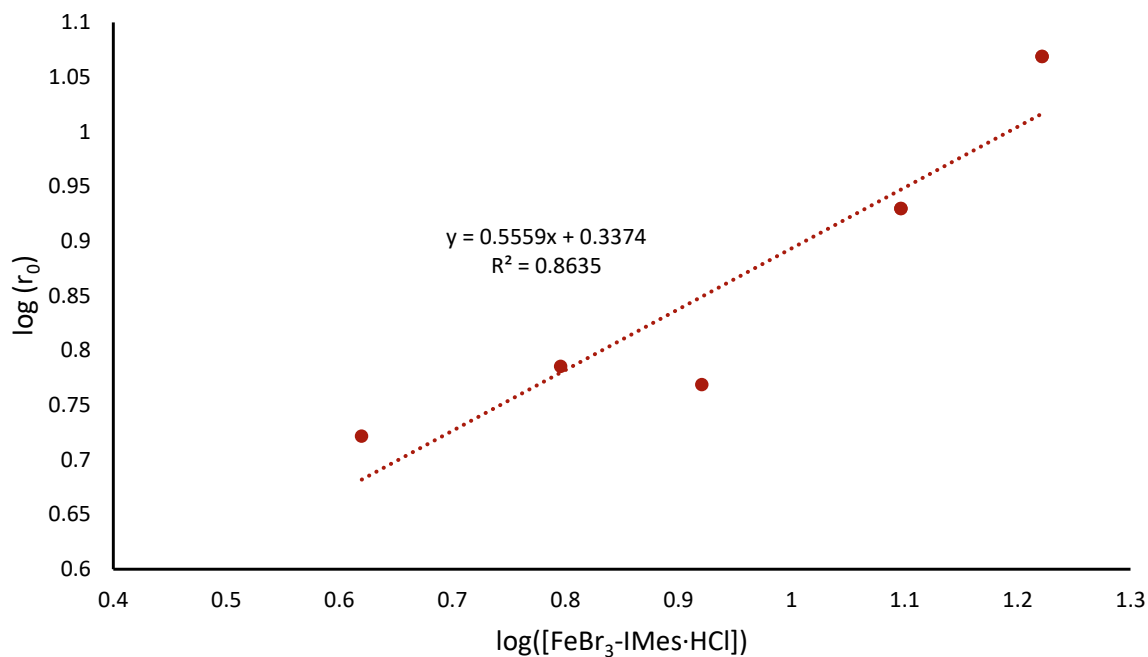
Figure 3.22 – Determination of the order of reaction in FeBr$_3$-IMes·HCl by initial rates method.

One way that this could be accounted for is by a catalytic intermediate being in equilibrium with an off-cycle, inactive species. Burés and co-workers have previously demonstrated that in a palladium-catalysed Heck reaction, that the fractional order was accounted for by an inactive palladium dimer being in equilibrium with an active monomeric palladium species.[230] A similar equilibrium with a bimolecular iron complex could explain the half order dependence observed here.
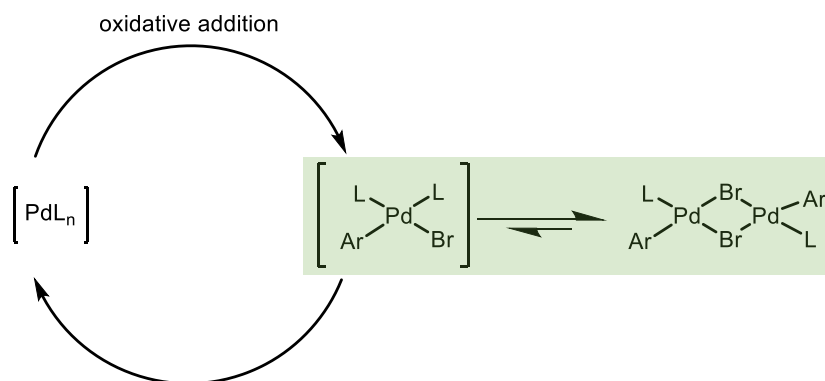
Scheme 3.11 – Pd dimer in equilibrium with catalytically active monomeric species that accounts for 0.5 order in Heck reaction investigated by Burés.[230]

The order determined in pre-catalyst by the initial rates method was approximately 0.5. However, when analysed by VTNA there is not an overlay of data when the order is set to 0.5 (Figure 3.23). In fact, there is no clear overlay of the plots when all the concentrations of pre-catalyst are used at any order. Although a better fit is obtained when the order is 1 and 6.3 mM (7.5 mol%) of pre-catalyst is omitted from the data. When two neighbouring data sets are used, a range of observed orders in pre-catalyst are determined (Table 3.5). One of the reasons for these observed non-sensical orders in pre-catalyst, could be due to the reaction using 6.3 mM of pre-catalyst having an induction period, whereas the other sets of data do not.

Table 3.5 – Summary of order in pre-catalyst at varying concentrations.

Entry	Concentration 1, mM	Concentration 2, mM	Observed order
1	4.2	6.3	-0.8
2	6.3	8.3	2.8
3	8.3	12.5	1.4
4	12.5	16.7	1
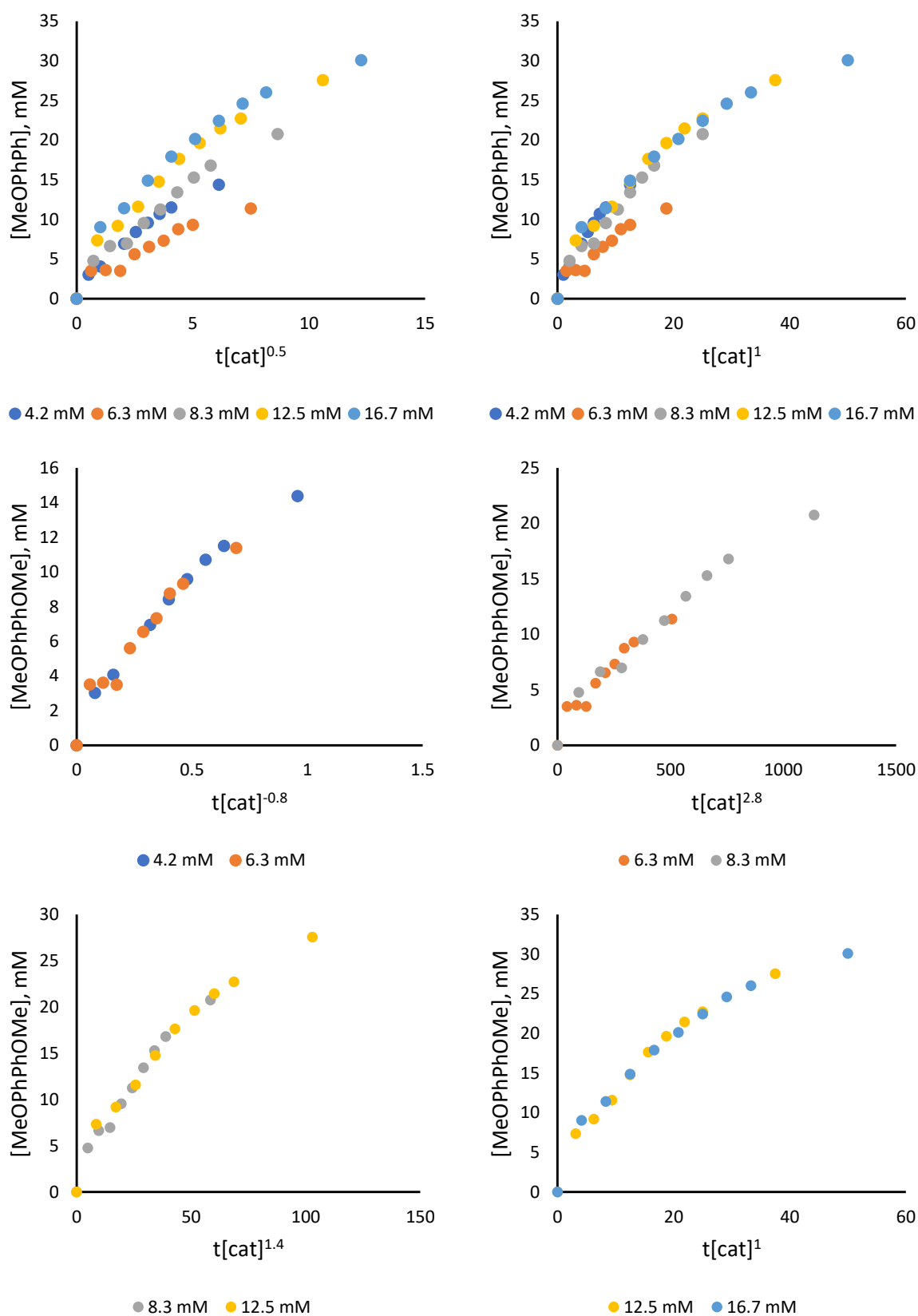
Figure 3.23 – VTNA for the formation of 14, with varying concentrations of pre-catalyst.

When the data is corrected for any induction period seen in the reaction profiles and then analysed by VTNA, a more reasonable set of orders in pre-catalyst is observed (Figure 3.24). As described previously, a better overlay of data is seen when the order is set to 1 rather than 0.5 (as determined by the initial rates method) but this still is not sufficient to say that the homo-coupling is 1ˢᵗ order in pre-catalyst. As seen previously, the order in pre-catalyst changes with concentration (Table 3.6). The range of orders observed when the concentration of pre-catalyst is changed strongly suggests that an order of 0.5 (as determined by the initial rates method) is unlikely.

Table 3.6 – Summary of order in pre-catalyst at varying concentrations.

Entry	Concentration 1, mM	Concentration 2, mM	Observed order
1	4.2	6.3	0.2
2	6.3	8.3	1
3	8.3	12.5	1.4
4	12.5	16.7	1
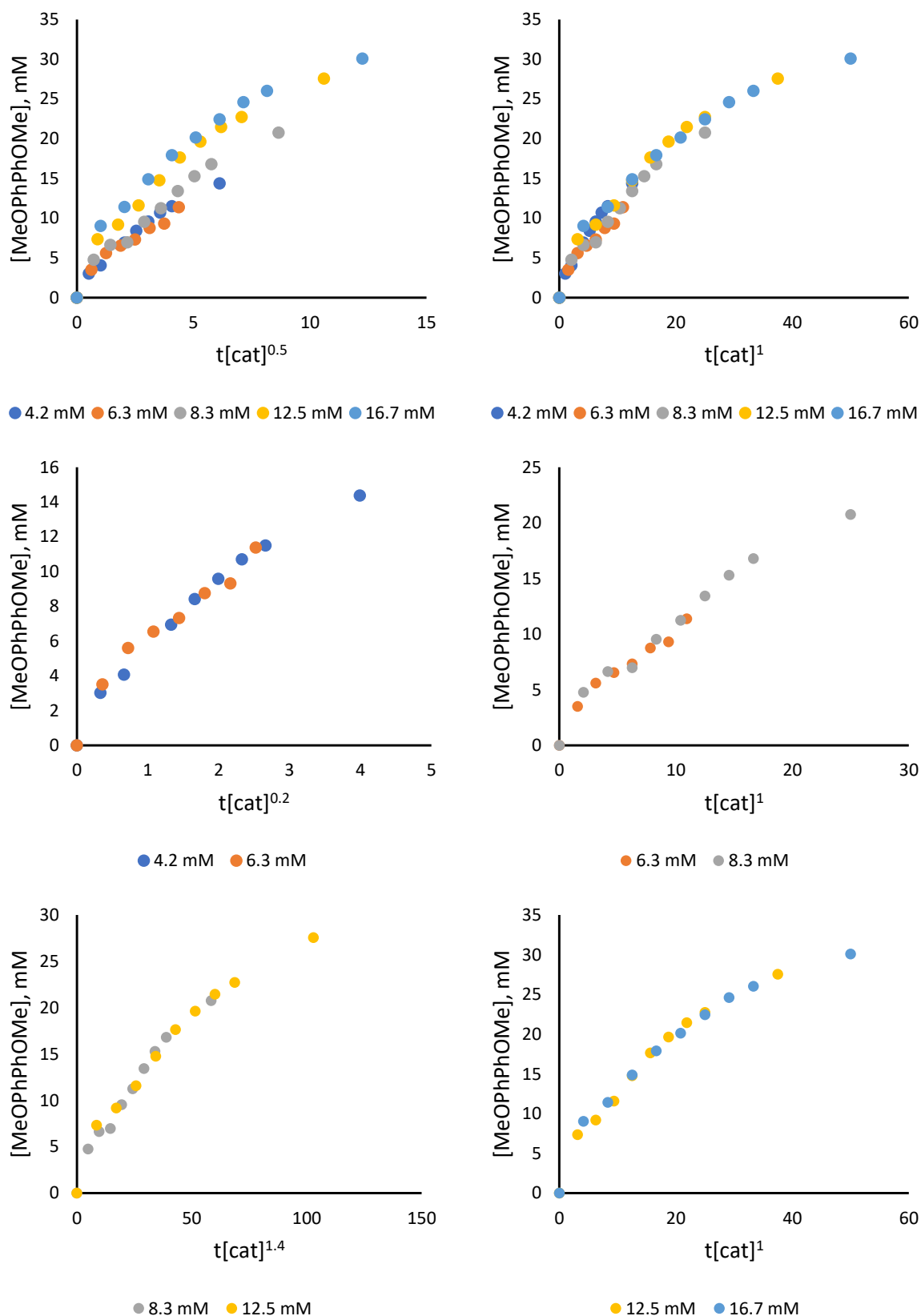
Figure 3.24 – VTNA (corrected for induction period) for the formation of 14, with varying concentrations of pre-catalyst.

As stated previously, VTNA might not be the best way to assess the data and a better way to interpret the data might be to use the initial rates method. Instead of taking all the data points, three continuous points are assessed to determine the order in these concentration ranges, and then the changes in order over the complete data set can be observed (Figure 3.25). When the data is analysed this way, we see an initial order in pre-catalyst of 0.17, that increases to 0.51 and then has an order of 0.99 at the highest concentrations.

Plot of $\log(r_0)$ versus $\log([FeBr_3/IMes \cdot HCl])$ with three linear fits:

$y = 0.1704x + 0.6261$, $R^2 = 0.6043$

$y = 0.5077x + 0.352$, $R^2 = 0.753$

$y = 0.991x - 0.1476$, $R^2 = 0.9969$
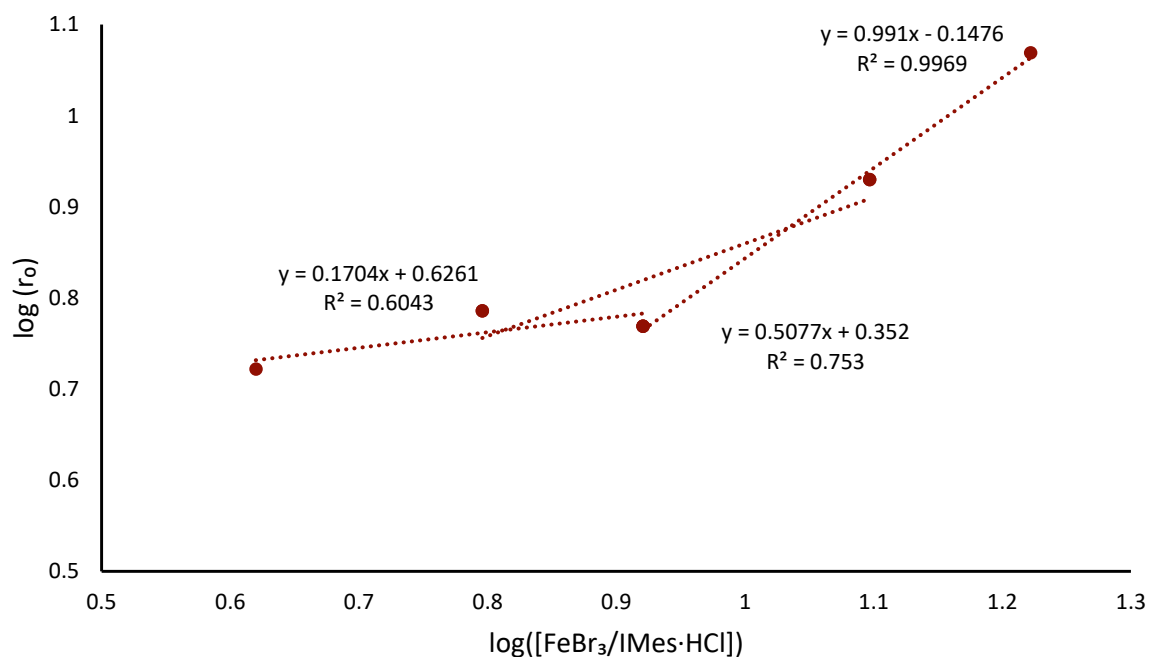
Figure 3.25 – Determination of the order of reaction in FeBr$_3$-IMes·HCl by initial rates method and using three continuous points at a time.

The change in orders observed when the data is assessed this way could suggest that there are two competing pathways (cross-coupling and homo-coupling), where different concentrations favour different pathways. When compared to the data obtained for the order in pre-catalyst of cross-coupling (Figure 3.12), this is the inverse. This suggests that perhaps lower concentrations of pre-catalyst promote cross-coupling, whereas at higher concentrations homo-coupling of the nucleophile is favoured.

3.5.2.2 Order in Electrophile, Chlorobenzene

Interestingly, a positive dependence of the concentration of the electrophile on the homo-coupling of the nucleophile was observed (Figure 3.26).
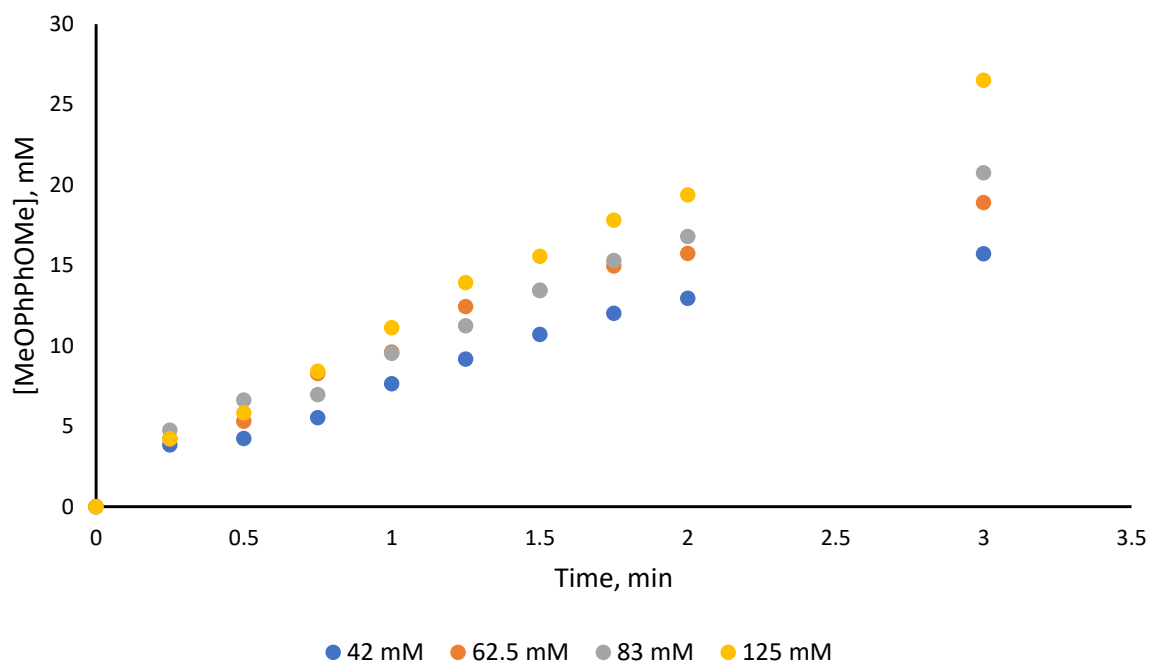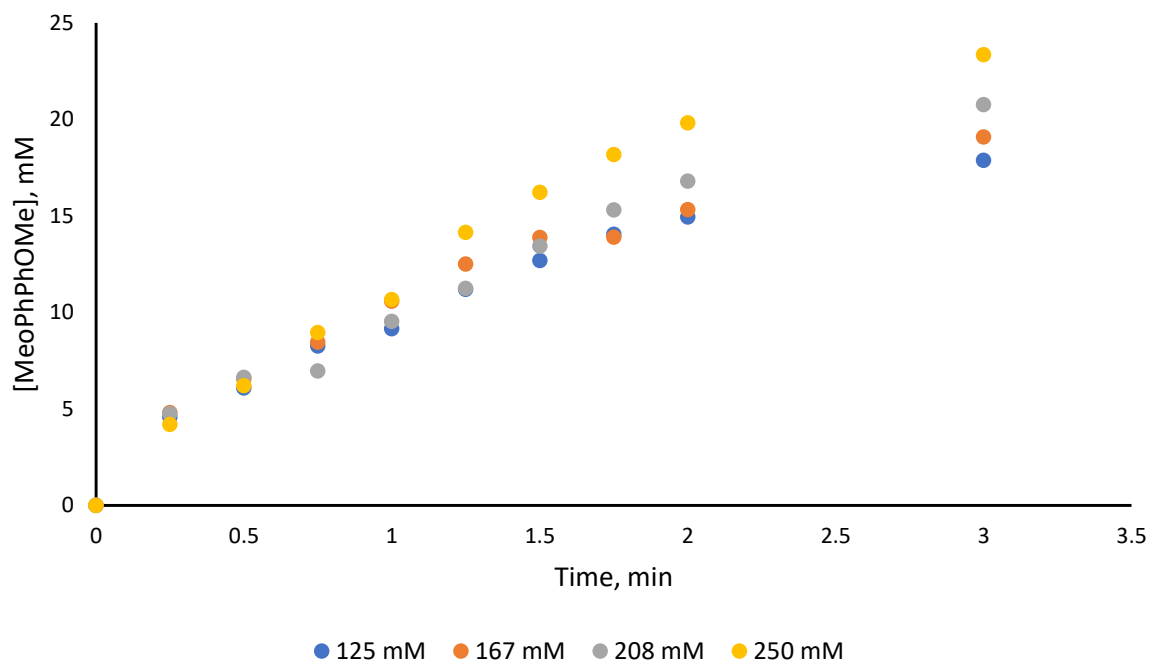

Figure 3.26 – Concentration-time plots for the formation of 4,4'-dimethoxybiphenyl at varying concentrations of chlorobenzene. Conditions: chlorobenzene, 11 (1.25 mmol), FeBr$_3$ (0.05 mmol), IMes·HCl (0.05 mmol), MgBr$_2$·OEt$_2$ (0.1 mmol), MeMgBr (0.05 mmol), 2-MeTHF:1,4-dioxane (1:1) (6.0 mL), 100 °C, 3 h. Yield determined by GC using dodecane as an internal standard.

The data shows that increasing the concentration of the electrophile has a positive effect on the homo-coupling of the nucleophile, with an experimentally determined order of 0.3 (Figure 3.27). This could suggest that there may be an equilibrium set up between several steps in the catalytic site and that oxidative addition of the electrophile promotes the subsequent transmetallation and reductive elimination steps in the homo-coupling reaction.
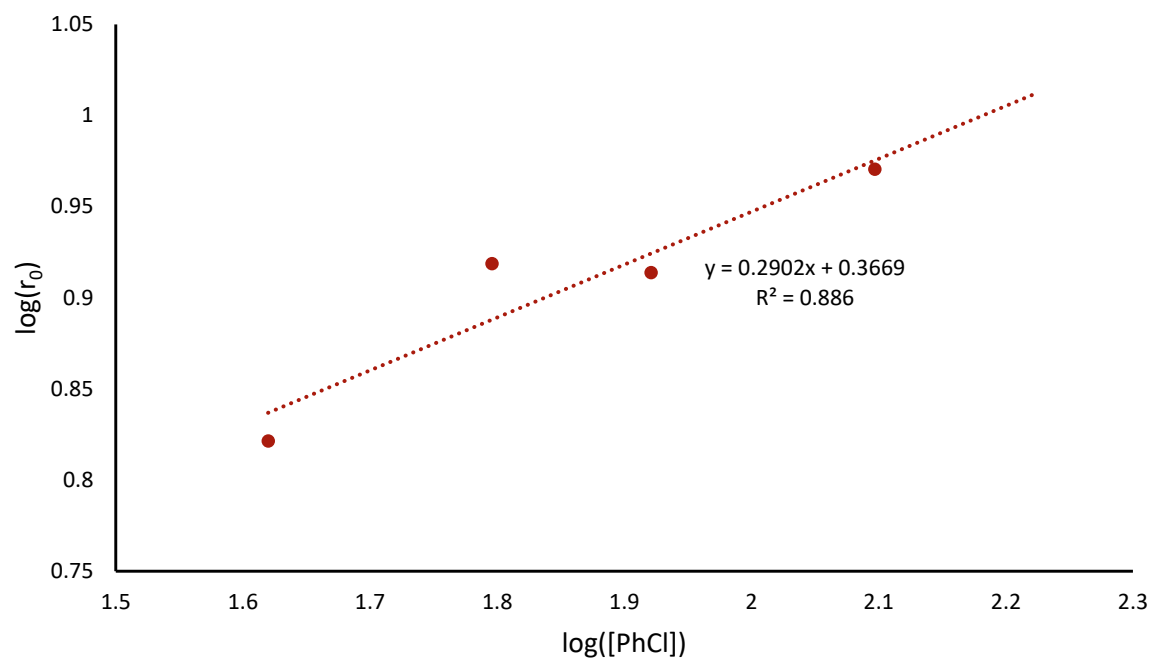
Figure 3.27 – Determination of the order of reaction in chlorobenzene by initial rates method.

3.5.2.3 Order in Nucleophile, 11

Next, the effect of changing the concentration of nucleophile on the initial rate of the homo-coupling reaction was investigated. This displays a positive dependence of initial rate of the concentration of the nucleophile (Figure 3.28).

Figure 3.28 – Concentration-time plots for the formation of 4,4'-dimethoxybiphenyl at varying concentrations of boronate, 11. Conditions: chlorobenzene (0.5 mmol), 11, FeBr$_3$ (0.05 mmol), IMes·HCl (0.05 mmol), MgBr$_2$·OEt$_2$ (0.1 mmol), MeMgBr (0.05 mmol), 2-MeTHF:1,4-dioxane (1:1) (6.0 mL), 100 °C, 3 h. Yield determined by GC using dodecane as an internal standard.

When the logarithm of the concentration of nucleophile is plotted against the logarithm of the initial rate, a good fit of data is observed (Figure 3.29). The gradient is 0.45, suggesting approximately a half order dependence on the nucleophile. The non-integer value obtained could be due to the effect of a series of equilibria present in the reaction mixture, as well as the nucleophile being involved in two processes: cross-coupling and homo-coupling of the nucleophile.
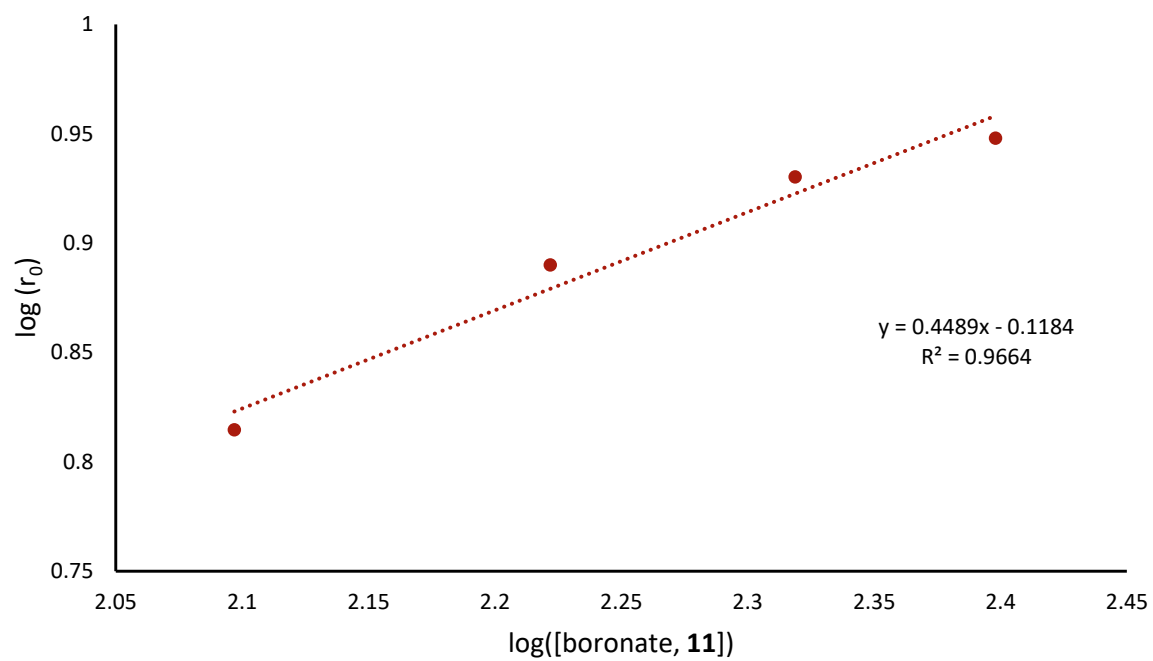
**Figure 3.29 – Determination of the order of reaction in boronate by initial rates method.**

3.5.2.4 Order in MeMgBr

The role of MeMgBr in the rds was next investigated. The concentration of MeMgBr was changed from 4.2 to 12.5 mM (5 to 15 mol%) and the initial rate of nucleophile homo-coupling was then measured (Figure 3.30).
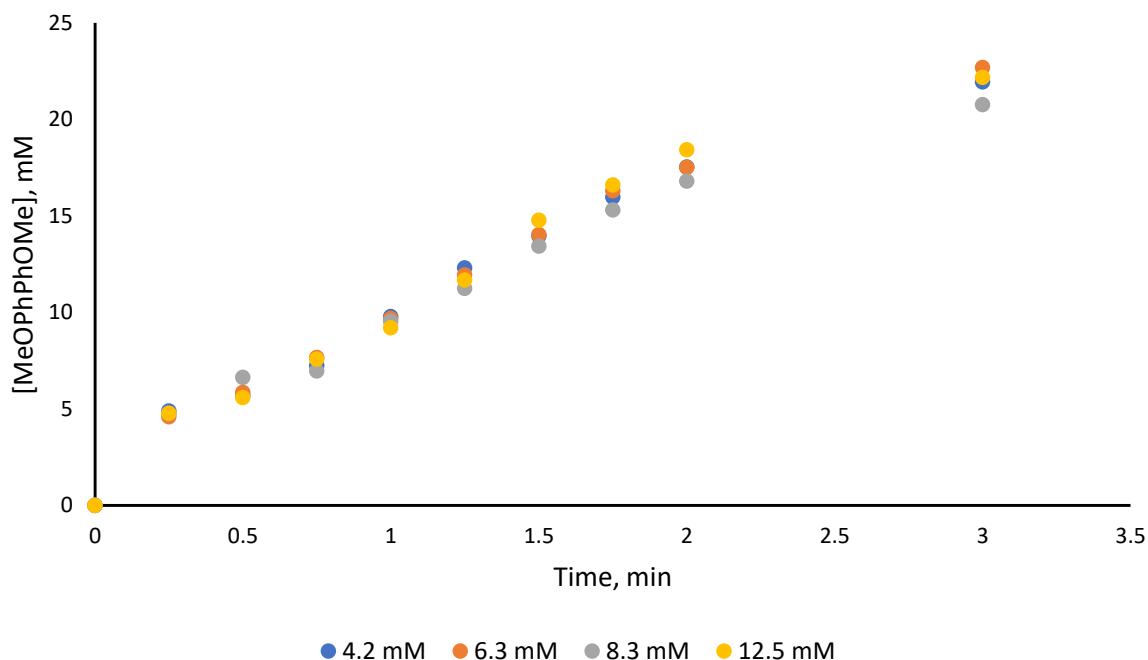
Figure 3.30 – Concentration-time plots for the formation of 4,4'-dimethoxybiphenyl at varying concentrations of MeMgBr. Conditions: chlorobenzene (0.5 mmol), 11 (1.25 mmol), FeBr$_3$ (0.05 mmol), IMes·HCl (0.05 mmol), MgBr$_2$·OEt$_2$ (0.1 mmol), MeMgBr, 2-MeTHF:1,4-dioxane (1:1) (6.0 mL), 100 °C, 3 h. Yield determined by GC using dodecane as an internal standard.

Increased loading of MeMgBr in the reaction mixture has a negative effect on the rate of formation of 4,4'-dimethoxybiphenyl (Figure 3.31). A good data fit is not obtained, but an order of -0.3 in MeMgBr was calculated, suggesting that it may perturb the rds of the reaction.
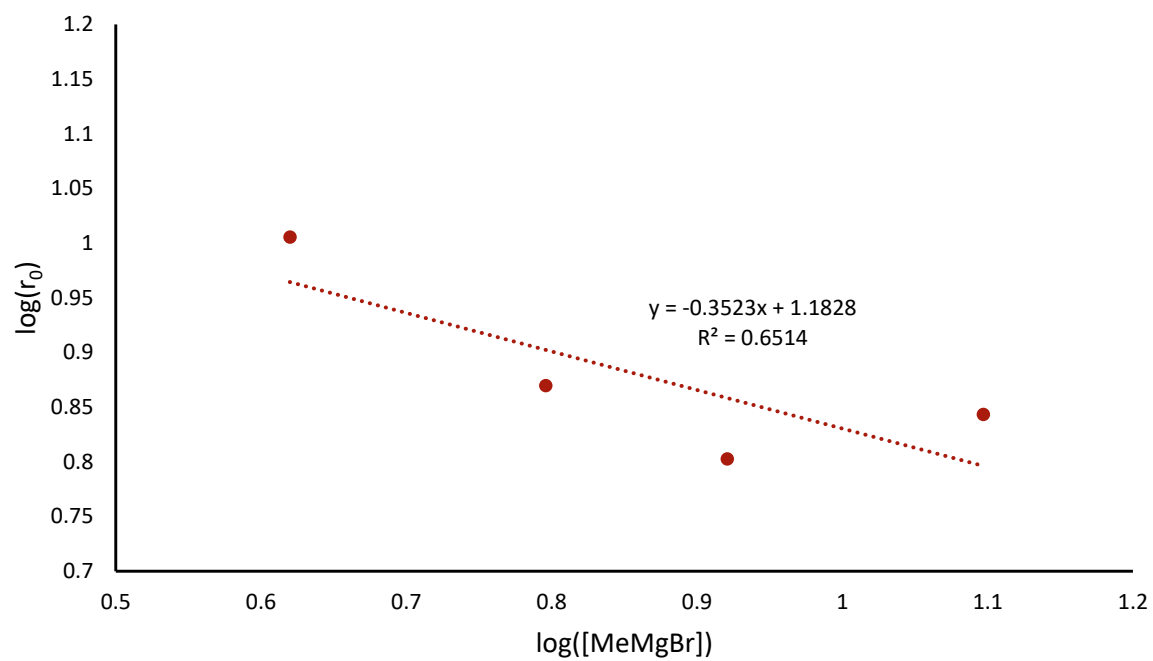
Figure 3.31 – Determination of the order of reaction in MeMgBr by initial rates method.

3.5.2.5 Order in MgBr$_2$

Finally, the effect of the concentration of MgBr$_2$ on the formation of 4,4'-dimethoxybiphenyl was investigated (Figure 3.32).
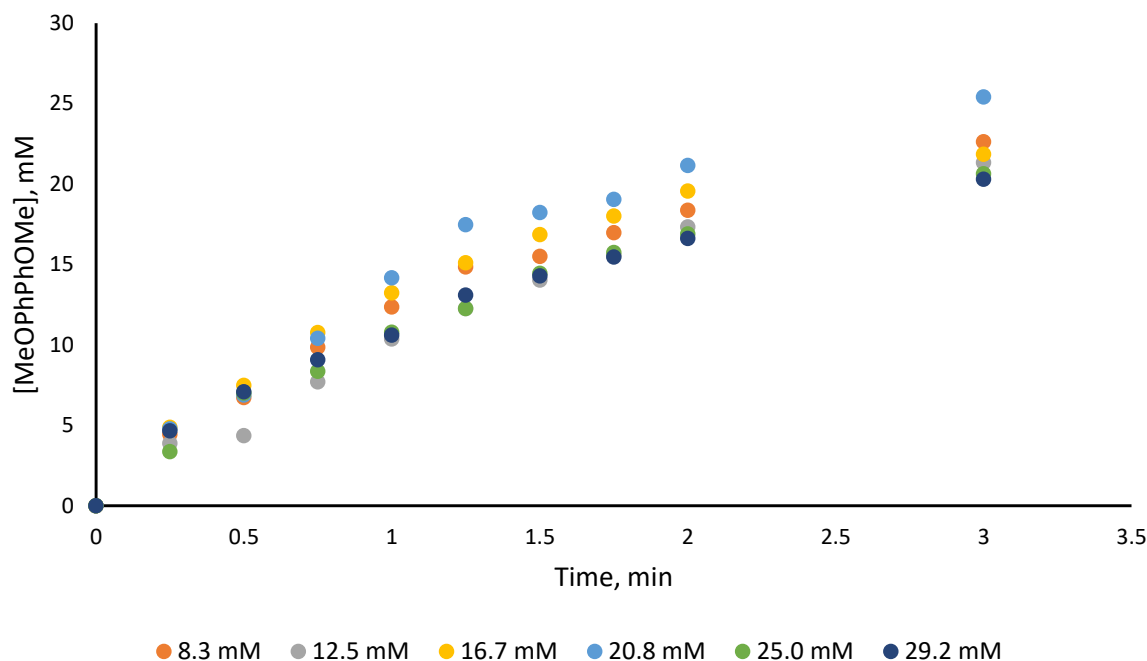
Figure 3.32 – Concentration-time plots for the formation of 4,4'-dimethoxybiphenyl at varying concentrations of MgBr$_2$. Conditions: chlorobenzene (0.5 mmol), 11 (1.25 mmol), FeBr$_3$ (0.05 mmol), IMes·HCl (0.05 mmol), MgBr$_2$·OEt$_2$, MeMgBr (0.05 mmol), 2-MeTHF:1,4-dioxane (1:1) (6.0 mL), 100 °C, 3 h. Yield determined by GC using dodecane as an internal standard.

Between concentrations of 8.3 and 20.8 mM (10 and 25 mol%) of MgBr$_2$, a positive dependence is observed. When the concentration of MgBr$_2$ is further increased to 25 and 29.2 mM (30 and 35 mol%), there is a negative dependence (Figure 3.33). The experimentally determined order between 8.3 and 20.8 mM is approximately 0.3, suggesting that MgBr$_2$ could be involved in the rds or that it could be involved in a step that is in equilibrium with the rds. The change in order from positive to negative further suggests that MgBr$_2$ is involved in two steps in the catalytic cycle, an initial associative step and then a dissociative step later in the cycle.
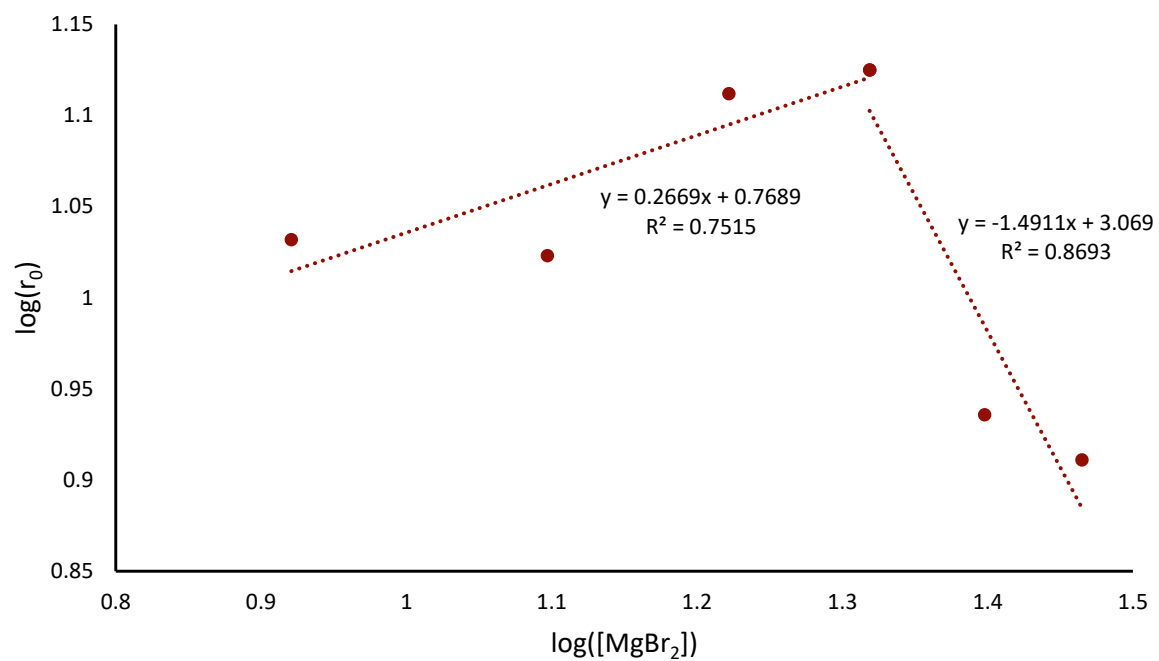
Figure 3.33 – Determination of the order of reaction in MgBr$_2$ by initial rates method.

3.5.2.6 Summary of Kinetic Data

To summarise the data collected, the fractional orders obtained from the initial rates data and VTNA clearly show that a complex and intricate mechanism is taking place (Table 3.7). The observation that there is a positive dependence on both the electrophile and nucleophile for both the cross- and homo-coupling indicates that there may be a series of steps in equilibria. The pre-catalyst being 1st order at lower concentrations and then tending towards 0 order at higher concentrations (initial rates method) in cross-coupling could suggest that there is only one iron centre involved in that reaction mechanism. Whereas for homo-coupling of the nucleophile, there is a zero order dependence on the pre-catalyst at low concentrations but then it becomes 1st order at higher concentrations (initial rates method). These combined effects could be explained by there being a common intermediate for both cross- and homo-coupling, where lower pre-catalyst loadings favour cross-coupling and higher pre-catalyst loadings favour homo-coupling. The low fractional order of $MgBr_2$ in both cross-coupling and homo-coupling suggests that it may be involved in a step that is in pre-equilibrium with the rds. The fact that there is only a positive dependence up to 25 mol%, and then the initial rate is hampered, suggests that the $MgBr_2$ is involved in two steps in the catalytic cycle. Perhaps it must associate to the iron centre first to aid reactivity but then later in the cycle it must dissociate, but at high concentrations the dissociation is impeded and therefore there is a decreased initial rate. This observation was previously reported by Bedford, but they were unable to deduce whether $MgBr_2$ or a bromide anion coordinates to the iron centre.[87]

Table 3.7 – Summary of order in reagents for cross- and homo-coupling reaction determined by the initial rates method.

Entry	Reaction Component	Order in Cross-Coupling	Order in Homo-Coupling of Nucleophile
1	$FeBr_3$-IMes·HCl	1 at low concentrations, 0 at high concentrations	0 at low concentrations, 1 at high concentrations
2	Chlorobenzene	0.7	0.3
3	Boronate, **11**	0.9	0.5
4	MeMgBr	0.0	-0.3
5	$MgBr_2$	0.3 (up to 25 mol%)	0.3 (up to 25 mol%)

3.5.3 Linear Free-Energy Relationship Experiments (LFER)

By changing the substituent in the para position of the phenyl groups, the steric effects are minimised and the effects on the electronic parameters can be measured in isolation.[231] Each para substituent has a corresponding σ value, originally developed by Hammett (Scheme 3.12).[232] This was originally created to see the electronic effect of substituents on the ionisation of benzoic acid derivatives, where the sigma value was based on electron donor ability. Following this, many other substituent scales have been developed, depending on the effect that has been measured, such as charge build up or radical stabilisation (Scheme 3.12).[233] However, it is not clear which σ scale is needed until the data are collected, and mixtures of parameters may also be necessary. In all cases the study is the same, with the initial rates being measured for a variety of substrates with a diverse range of σ values. The $\log\left(\frac{k_R}{k_H}\right)$ is then plotted against the σ_x values, with the gradient then measured giving ρ, from which information on the sensitivity of substituent effects on the reaction can be determined (Equation 3.2).

$$log\frac{k_R}{k_H} = \sigma\rho$$

Equation 3.2 – Hammett equation. Where k = rate of reaction, σ = substituent constant, ρ = reaction constant
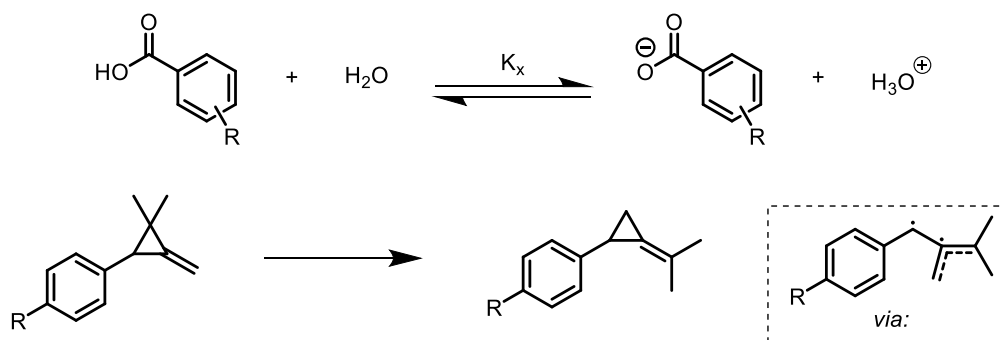
Scheme 3.12 – Reactions used to devise σ values by Hammett[232] (top) and Creary[234] (bottom).

As both the nucleophile and electrophile are shown to be present in the rds of both the cross-coupling and nucleophile homo-coupling, a study of the effect of the nucleophile and electrophile was undertaken on both the product formations.

3.5.3.1 Linear Free-Energy Relationship of Cross-Coupling on Changing Electrophile

The study was undertaken with a range of aryl chlorides and using the phenyl boronate (Figure 3.34). Due to the observed homo-coupling, chlorobenzene could not be used. This is because both the cross-coupled and homo-coupled products would be identical (biphenyl) and therefore deciphering what product was a result of cross-coupling and homo-coupling would be impossible. Thus, k_{Me} is used as the base rate and $\log\left(\frac{k_R}{k_{Me}}\right)$ is calculated and plotted in each case.
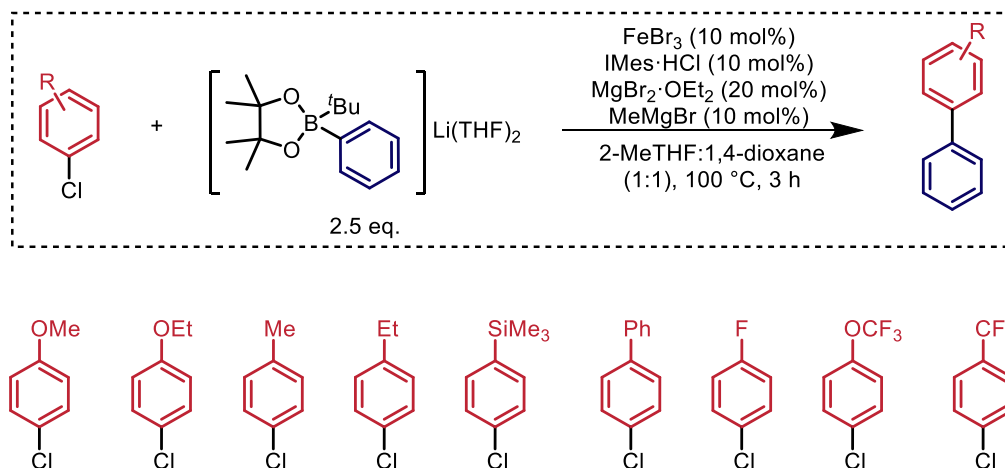
Figure 3.34 – Electrophiles used in LFER study.

The corresponding concentration-times plots were then measured for each substituent (Figure 3.35). As shown, there is a change in initial rate for each reaction.
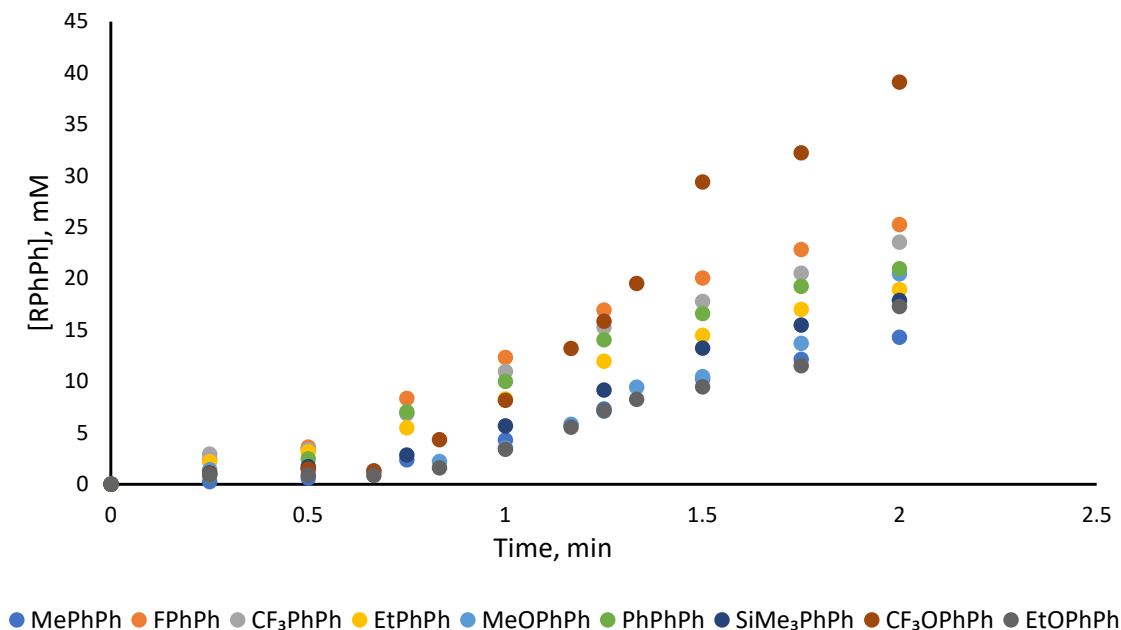
Figure 3.35 – Concentration-time plots for the formation of biaryls with varying the electrophile. Conditions: electrophile (0.5 mmol), phenyl boronate (1.25 mmol), FeBr₃ (0.05 mmol), IMes·HCl (0.05 mmol), MgBr₂·OEt₂ (0.1 mmol), MeMgBr (0.05 mmol), 2-MeTHF:1,4-dioxane (1:1) (6.0 mL), 100 °C, 3 h. Yield determined by GC using dodecane as an internal standard.

From using the initial rates data obtained, the ratio of $\log\left(\frac{k_R}{k_{Me}}\right)$ can be calculated against the σ scale of choice until a fit is observed. When the data was plotted against the Creary scale, developed σ values for the stabilisation of radical intermediates, there was no clear fit.[234] This indicates that the electrophile does not react in the cross-coupling reaction *via* a radical mechanism, unlike many other iron-catalysed cross-coupling reactions.[235] However, when plotted against the σ values devised by Hammett, to signify the build-up of charge in a transition state, there is a good fit (Figure 3.36).
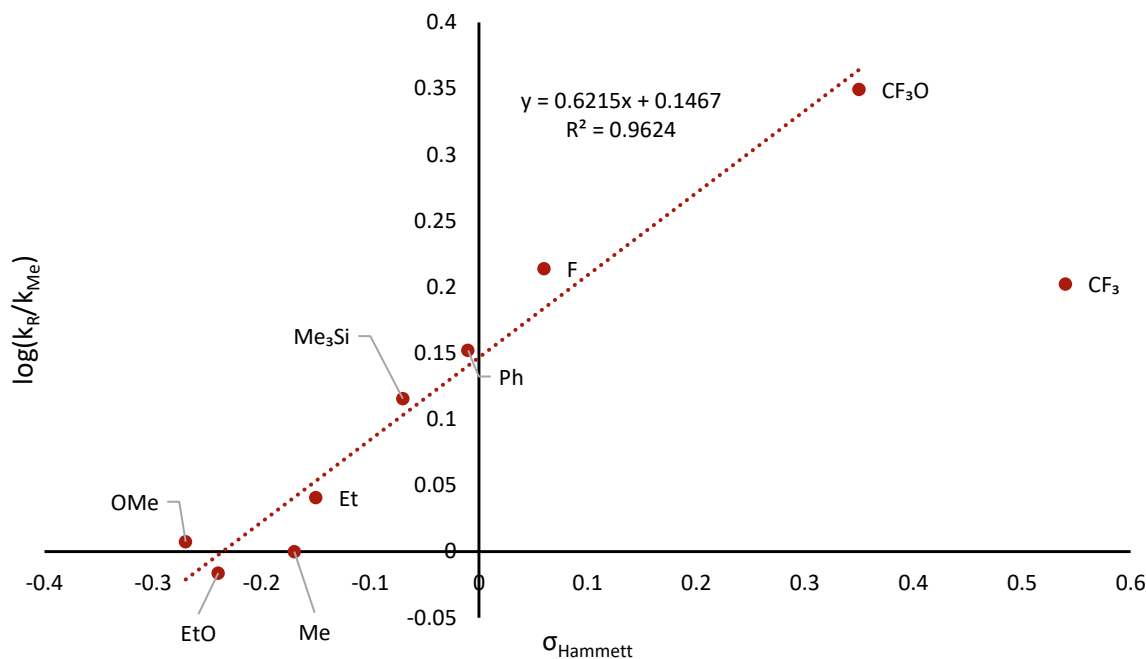
Figure 3.36 – LFER plot using σ$_{Hammett}$.

The data shows that there is a positive correlation between $\sigma_{Hammett}$ and $\log\left(\dfrac{k_R}{k_{Me}}\right)$, where the more electron-withdrawing the substituent the greater the initial rate, up to OCF$_3$. When the model is pushed to extreme electron-withdrawing properties, CF$_3$, the correlation is lost and the initial rate decreases. The correlation could show that the electrophile is involved in the rds of the reaction. Here, ρ = +0.6215 (when CF$_3$ is included ρ = 0.3733 and the R^2 = 0.6962), a positive ρ value indicates that there is a negative charge build up or loss of positive charge in the transition state of the rds. This result, and that the order of cross-coupling in electrophile was 0.7, is potentially consistent with oxidative addition being the rds of the cross-coupling reaction, where electron-withdrawing groups increase the initial rate of oxidative addition.[236–242] However, the low ρ value (ρ < 1) suggests that the electrophile is not involved in the rds but could be in a pre-equilibrium step with the rds. Therefore, an alternative assessment of the data would be to suggest that either transmetallation or reductive elimination is the rds in the reaction mechanism, not oxidative addition.

3.5.3.2 Linear Free-Energy Relationship of Cross-Coupling on Changing Nucleophile

Next, the substituent effects on the boronate were analysed to determine whether a LFER could be observed for the cross-coupling reaction. The study was undertaken with a range of boronates and using chlorobenzene as the electrophile (Figure 3.37). Due to the observed homo-coupling, the phenyl boronate could not be used and thus k_{Me} is used as the base rate and $\log\left(\frac{k_R}{k_{Me}}\right)$ is calculated and plotted in each case.
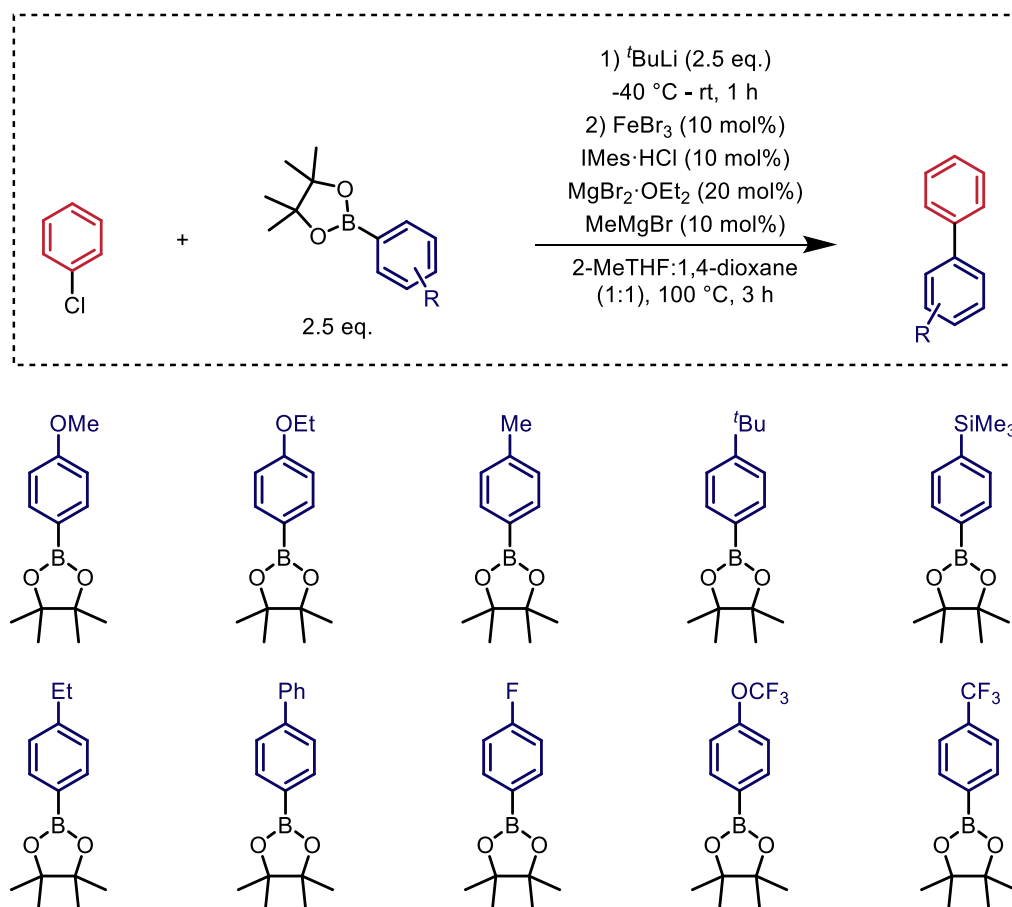
Figure 3.37 – Nucleophiles used in LFER study.

The corresponding concentration-time plots were then measured for each substituent (Figure 3.38). As shown, there is a change in initial rate for each reaction.

143
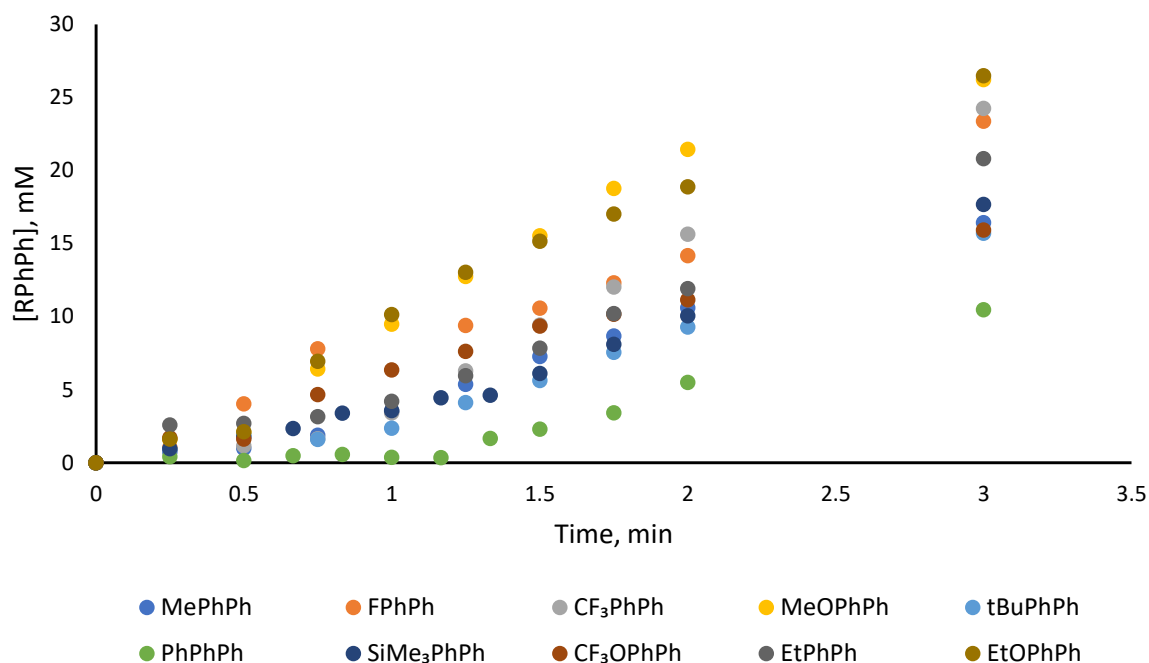
Figure 3.38 – Concentration-time plots for the formation of biaryls with varying the nucleophile. Conditions: chlorobenzene (0.5 mmol), nucleophile (1.25 mmol), FeBr₃ (0.05 mmol), IMes·HCl (0.05 mmol), MgBr₂·OEt₂ (0.1 mmol), MeMgBr (0.05 mmol), 2-MeTHF:1,4-dioxane (1:1) (6.0 mL), 100 °C, 3 h. Yield determined by GC using dodecane as an internal standard.

In this case when $\log\left(\frac{k_R}{k_{Me}}\right)$ is plotted against $\sigma_{Hammett}$ a V-shaped plot is observed (Figure 3.39). This is consistent with a change in either rds or mechanism depending on whether electron-withdrawing or donating groups are incorporated into the boronate. Where R is an electron-donating group, we see a large and negative ρ value (-2.493), showing either positive charge build-up or depletion of a negative charge. This is indicative of transmetallation being the rds and has been reported to be the case in palladium-catalysed cross-coupling.[243] However, when electron-withdrawing substituents are used on the boronate we see a weaker, positive correlation. A ρ of 0.4959 is indicative of a change in rds to reductive elimination.[244]

144
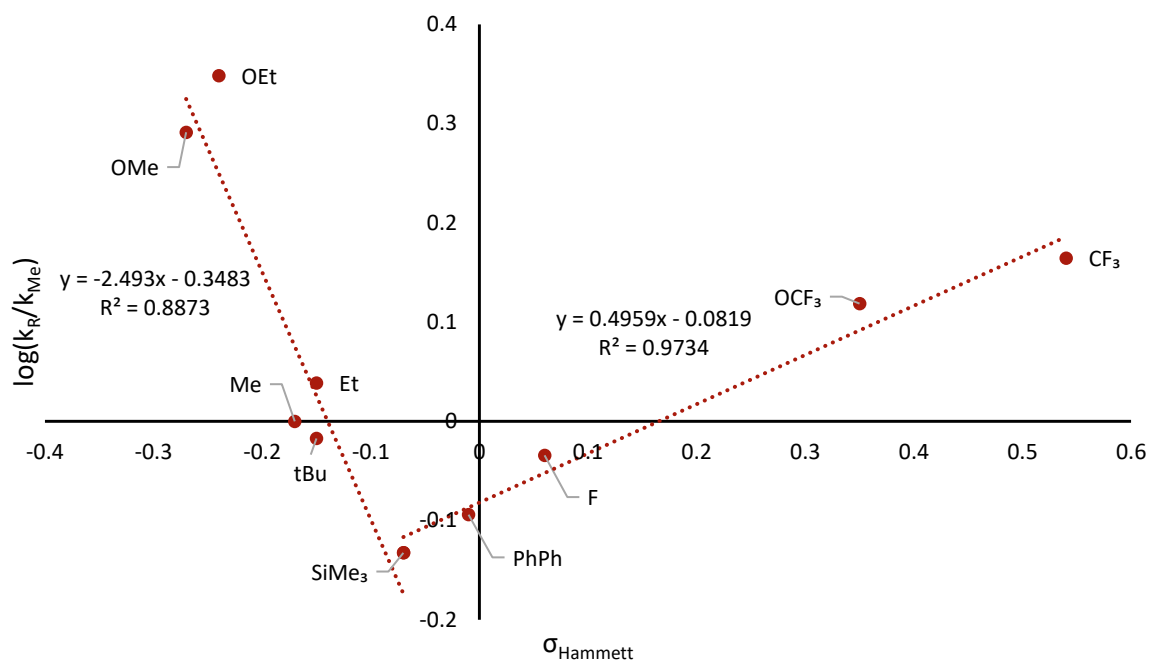
Figure 3.39 – LFER plot using σ_{Hammett}.

When plotted against the Creary σ scale, developed to show the stabilisation of radicals, no correlation is observed. This further suggests that the cross-coupling reaction does not proceed *via* a radical mechanism.

In conclusion, this data, combined with the experimentally determined orders of the cross-coupling reaction, could suggest that a series of delicately balanced equilibria could be set up in which slight changes to the reactants can change the rds of the mechanism. It is likely that either transmetallation or reductive elimination is the rds, depending on the nucleophile used.

3.5.3.3 Linear Free-Energy Relationship of Nucleophile Homo-Coupling on Changing Electrophile

The kinetic study shows that the homo-coupling of the nucleophile has a positive dependency on the electrophile concentration. To further investigate the role the electrophile was playing on the nucleophile homo-coupling, the rate of formation of biphenyl was monitored when various electrophiles were used (Figure 3.40). Again, k_R was measured against k_{Me} to determine the relationship rather than k_H.
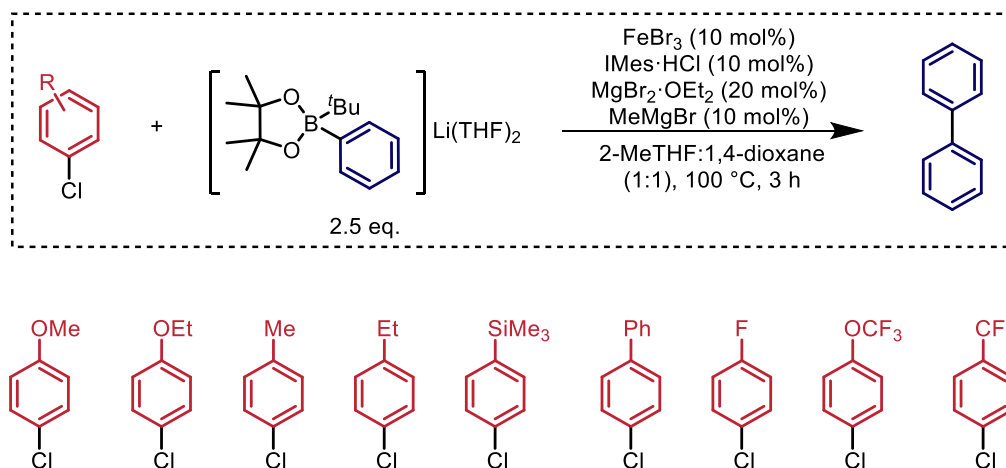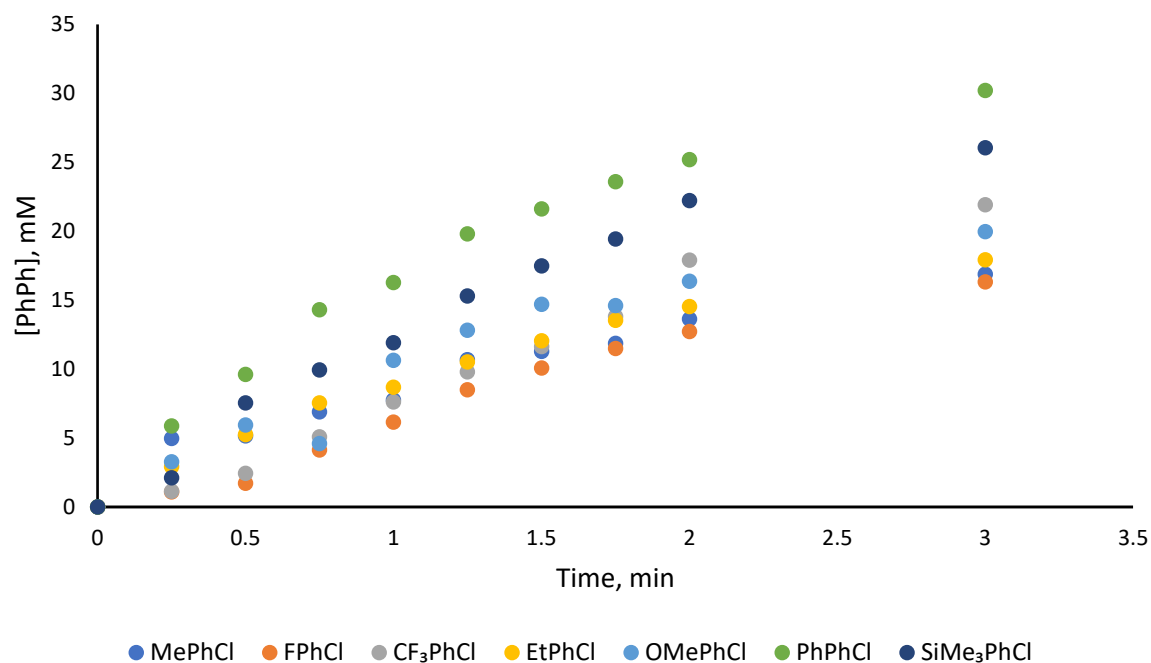

Figure 3.40 – Electrophiles used in LFER study.

In this case, quite a large range of initial rates of formation of biphenyl was observed when different electrophiles were employed in the reaction (Figure 3.41). This further demonstrates that the electrophile has a strong effect on the nucleophile homo-coupling.

Figure 3.41 – Concentration-time plots for the formation of biphenyl with varying the electrophile. Conditions: electrophile (0.5 mmol), phenyl boronate (1.25 mmol), FeBr₃ (0.05 mmol), IMes·HCl (0.05 mmol), MgBr₂·OEt₂ (0.1 mmol), MeMgBr (0.05 mmol), 2-MeTHF:1,4-dioxane (1:1) (6.0 mL), 100 °C, 3 h. Yield determined by GC using dodecane as an internal standard.

For this reaction, a reasonable data fit could not be obtained when $\sigma_{Hammett}$ values were used, or when σ^+ or σ^- scales (used in the case of positive or negative charge build up, respectively, stabilised *via* resonance delocalisation by the substituent) were used, suggesting that there is not a significant charge build up in this step of the reaction.[245] There was also not a good fit of the data when the σ_{Creary} scale was used, indicating that it does not proceed *via* a purely radical process. However, a modest correlation is obtained when the σ_{Creary} scale is mixed with the $\sigma_{Hammett}$ scale (Figure 3.42). This has previously been used by Norrby to account for any polar influences within the reaction, as the Creary scale is best applied to reactions with very low polar character.[245] σ_{Creary} values for OCF₃ and OEt have not been determined so these substituents could not be included in this study.
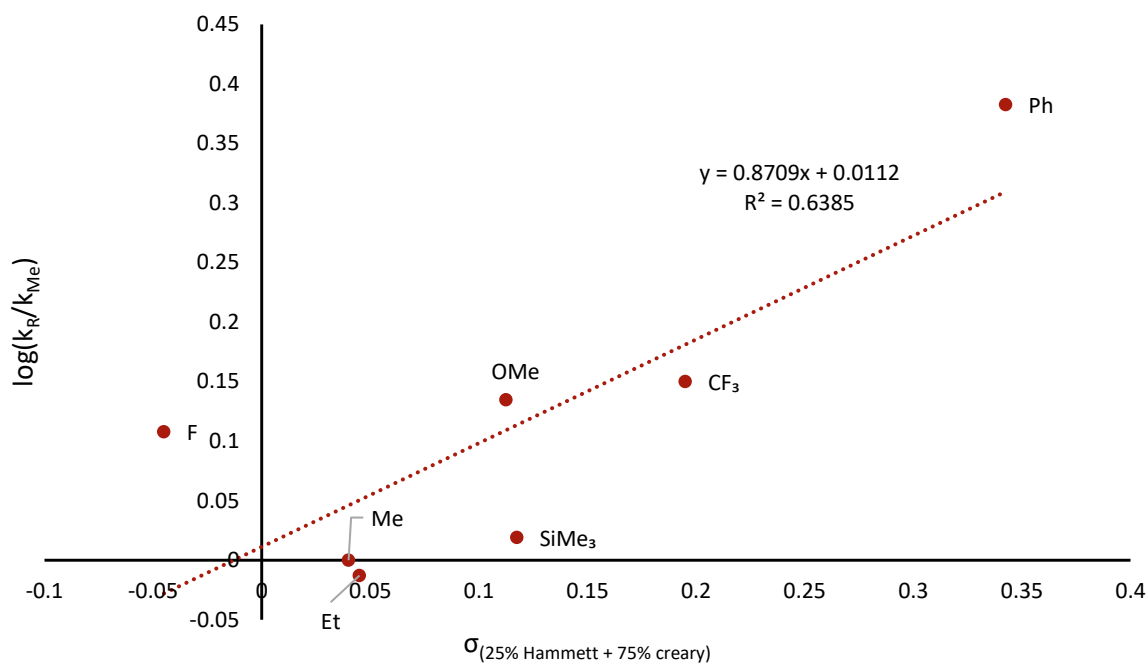
Figure 3.42 – LFER plot using a combination of $\sigma_{Hammett}$ and σ_{Creary} values.

The ρ value suggests that a phenyl based radical with some build-up of negative charge could be forming in the reaction. The relatively low ρ also suggests that a discrete radical species is unlikely to form and that a caged radical pair might be more likely to form, where the chloride has been extracted by an iron species (Scheme 3.13).[246] When 1-chloro-4-fluorobenzene is excluded from the data, ρ = 1.2667 and R^2 = 0.921. The low ρ value could also suggest that, rather than radical formation, the electrophile is not directly involved in the rds but is in a pre-equilibrium before the rds, indicating that either transmetallation or reductive elimination is the rds.
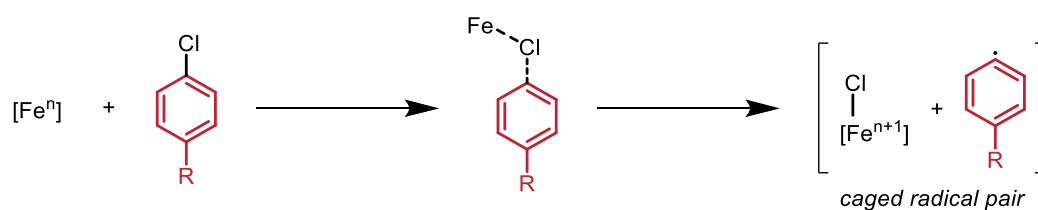
Scheme 3.13 – Potential formation of a caged radical pair.

A slightly better fit of data is obtained when the σ_{Creary} scale is mixed with the σ^- scale, ρ = 0.7738 and R^2 = 0.6579 (when 1-chloro-4-fluorobenzene is excluded from the data ρ = 1.1501 and R^2 = 0.9345) (Figure 3.43). This further suggests that there is some negative charge build-up in the transition state of the rds.[245]
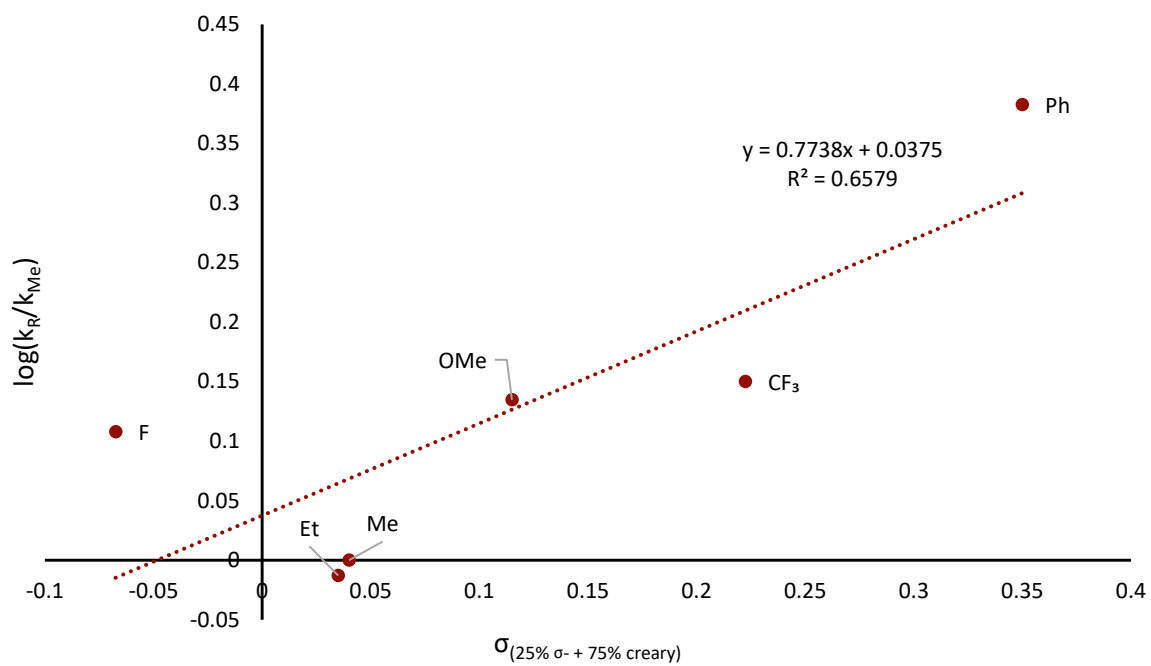
148

Figure 3.43 – LFER plot using a combination of σ- and σ_Creary values.

3.5.3.4 Linear Free-Energy Relationship of Nucleophile Homo-Coupling on Changing Nucleophile

As the formation of the nucleophile homo-coupled product showed a positive dependency on the boronate concentration in the initial rates study, the formation of homo-coupled product from the boronate was monitored with varying nucleophiles (Figure 3.44). k_R was measured against k_{Me} to determine the relationship rather than k_H.
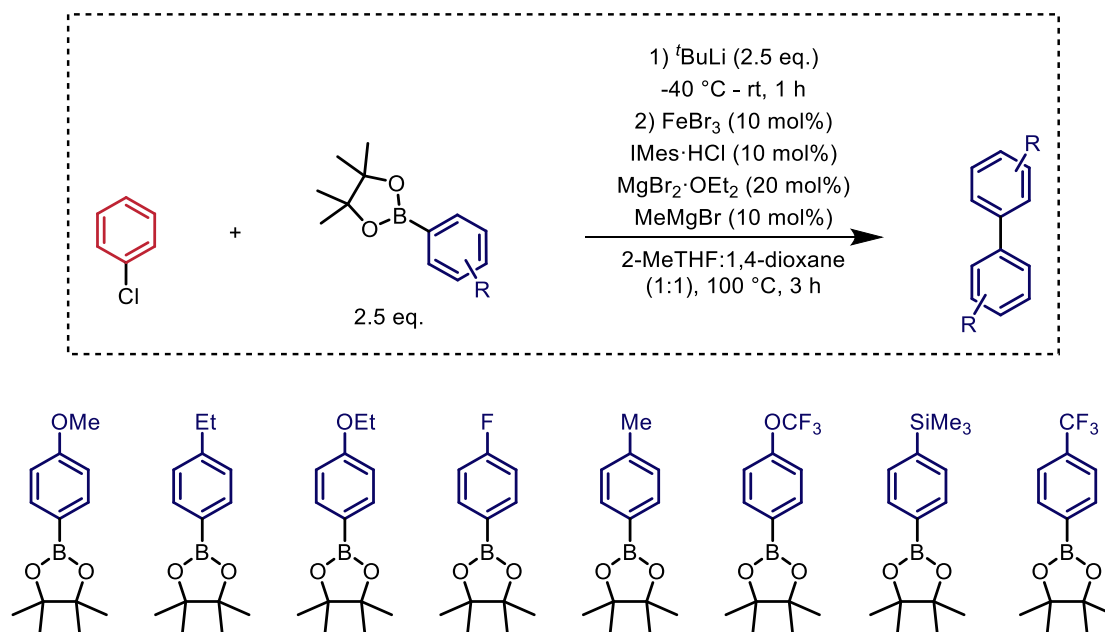
Figure 3.44 – Nucleophiles used in LFER study.

A range of initial rates of reaction were observed when the substituent in the 4-position of the phenyl group of the boronate was altered (Figure 3.45). Due to solubility issues, *p*-quaterphenyl formation could not be measured and due to the very high boiling point, 4,4'-di-*tert*-butylbiphenyl could not be observed by GC and therefore could not be included in this study.
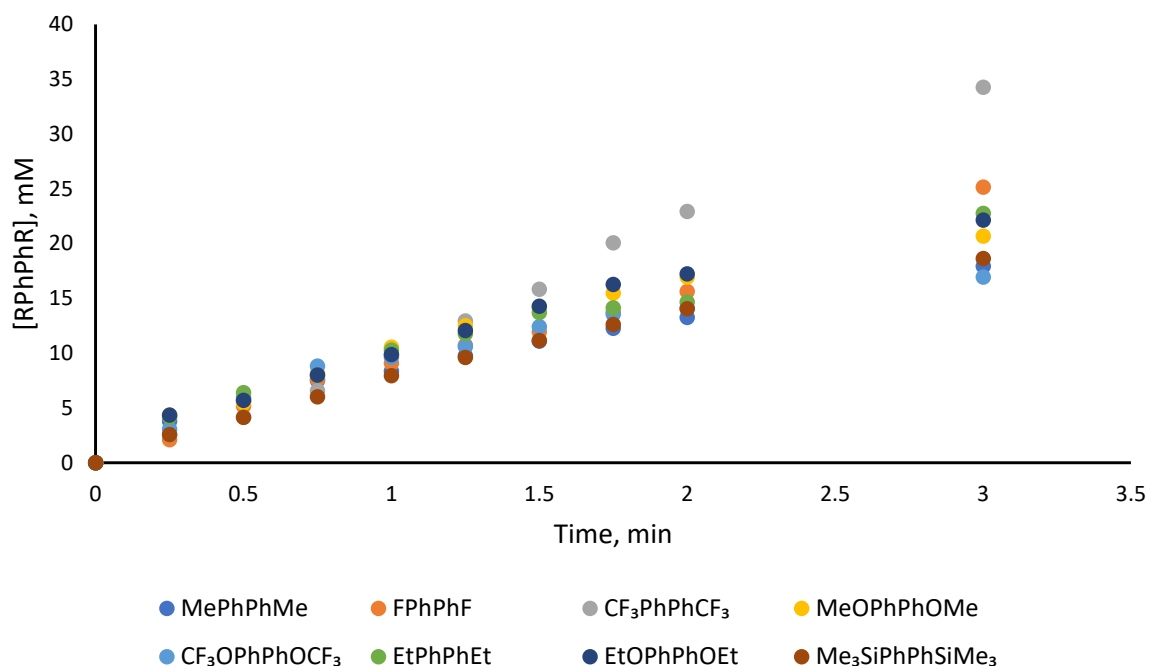
Figure 3.45 – Concentration-time plots for the formation of biaryls with varying the nucleophile. Conditions: chlorobenzene (0.5 mmol), nucleophile (1.25 mmol), FeBr$_3$ (0.05 mmol), IMes·HCl (0.05 mmol), MgBr$_2$·OEt$_2$ (0.1 mmol), MeMgBr (0.05 mmol), 2-MeTHF:1,4-dioxane (1:1) (6.0 mL), 100 °C, 3 h. Yield determined by GC using dodecane as an internal standard.

For the homo-coupling of the nucleophile, a V-shaped plot was observed when the substituent on the nucleophile was changed and plotted against $\sigma_{Hammett}$ (Figure 3.46). This is indicative of a change in mechanism or rds in the reaction. Electron-donating groups show a strong negative correlation to $\sigma_{Hammett}$, suggesting either a positive charge build-up or loss of negative charge, which is consistent with transmetallation being the rds, as seen in palladium-catalysed cross-coupling reactions.[243] When electron-withdrawing groups are placed on the boronate, $\rho = 0.6827$, this is in accordance with reductive elimination being the rds.[244]
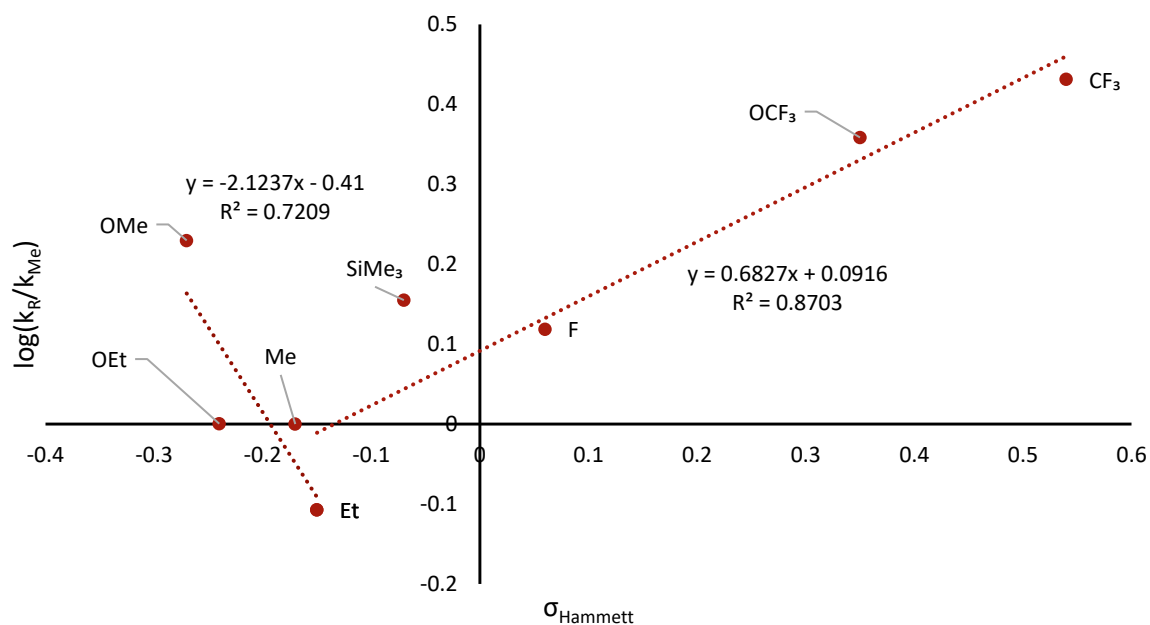
Figure 3.46 – LFER plot using σ$_{Hammett}$ values.

In conclusion, this data, combined with the experimentally determined orders of the homo-coupling reaction, could suggest that a series of finely balanced processes are set up for the formation of the nucleophile homo-coupled product. Where slight changes to the reactants can change the rds of the mechanism between transmetallation and reductive elimination.

3.5.4 Determination of the Activation Parameters

In order to gain further information regarding the transition state of the rds of both the cross-coupling and nucleophile homo-coupling reactions, their respective activation parameters were determined. The rate constant for both the production of the cross-coupled product and nucleophile homo-coupled product were determined at varying reaction temperatures (Figure 3.47).
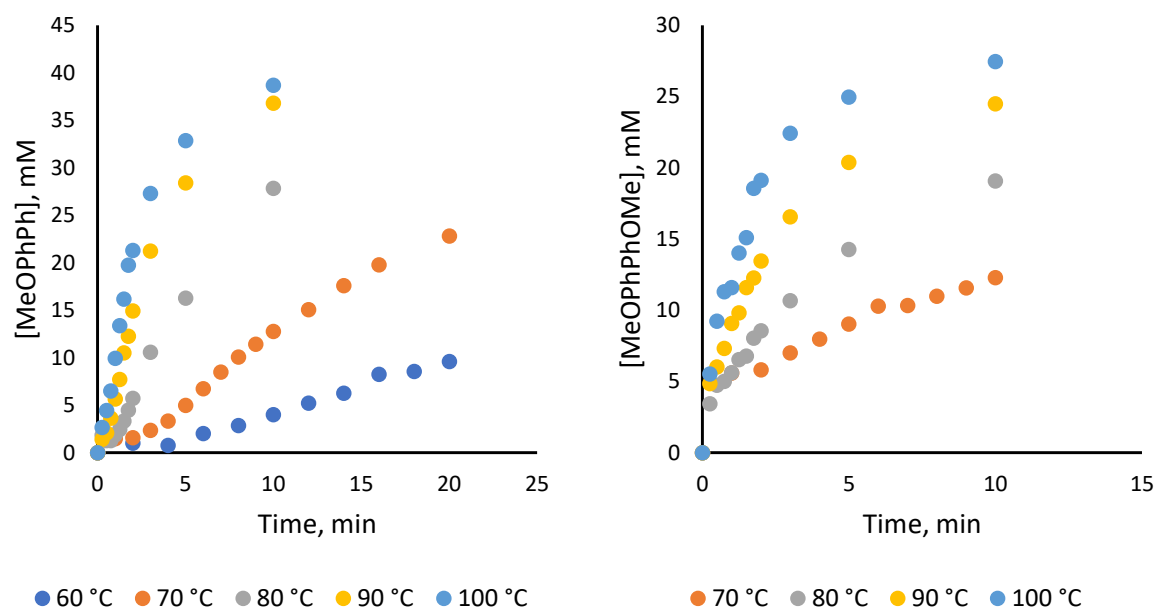

Figure 3.47 – Concentration-time plots for the formation of 4-methoxybiphenyl (left) and 4,4'-dimethoxybiphenyl (right) with varying temperatures. Conditions: chlorobenzene (0.5 mmol), 11 (1.25 mmol), FeBr₃ (0.05 mmol), IMes·HCl (0.05 mmol), MgBr₂·OEt₂ (0.1 mmol), MeMgBr (0.05 mmol), 2-MeTHF:1,4-dioxane (1:1) (6.0 mL), 3 h. Yield determined by GC using dodecane as an internal standard.

As expected, there is a significant change in the rate of product formation as the reaction temperature is varied. The initial rate was measure at each temperature using the initial rates method. Using this data and the linearised version of the Eyring equation (Equation 3.3), the $\Delta H^{\ddagger}$ and $\Delta S^{\ddagger}$ can be calculated by plotting $ln\frac{k}{T}$ against $\frac{1}{T}$, using the gradient and intercept respectively (Figure 3.48).

$$ln\frac{k}{T} = -\frac{\Delta H^{\ddagger}}{RT} + \frac{\Delta S^{\ddagger}}{R} + ln\frac{k_B}{h}$$

Equation 3.3 – Linearised version of the Eyring equation. Where k = rate constant, T = temperature, ΔH‡ = enthalpy of activation, R = gas constant, ΔS‡ = entropy of activation, k_B = Boltzmann constant, h = Planck's constant.
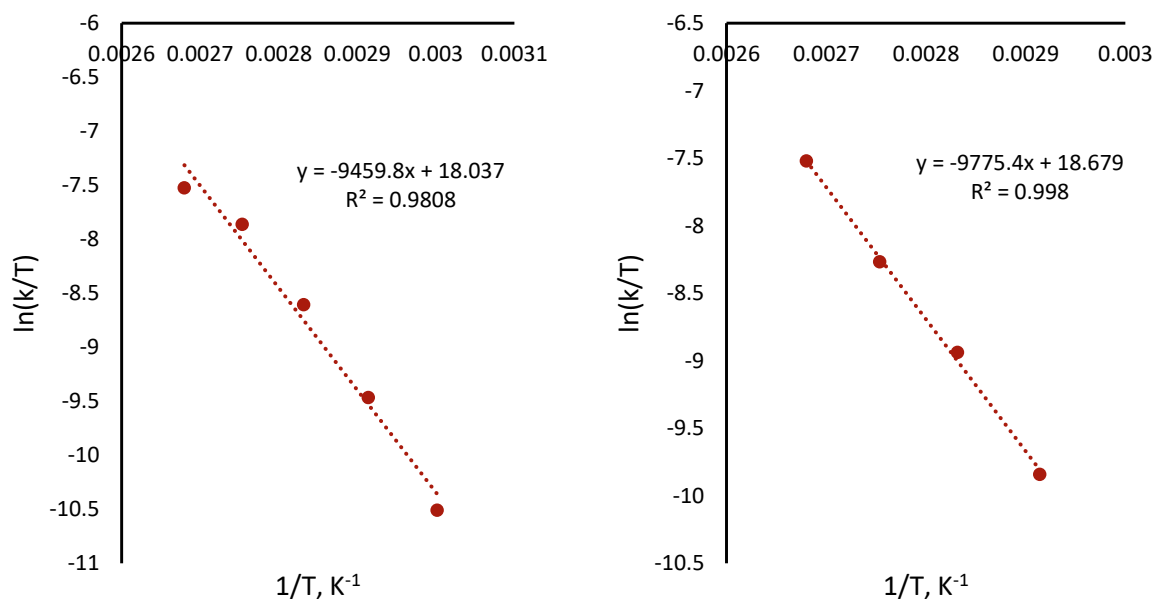

Figure 3.48 – Eyring plots for the formation of 4-methoxybiphenyl (left) and 4,4'-dimethoxybiphenyl (right).

In both cases an excellent fit of the data is observed. The experimentally calculated enthalpy of activation (ΔH‡) and Gibbs free energy of activation (ΔG‡) (Equation 3.4) are both positive, this is expected as the data corresponds to the rds of the reaction and therefore is likely to be high in energy (Table 3.8). The very similar values for both the cross- and homo-coupling show that the reactions are highly competitive, and this explains why the reaction is not very selective. In both cases, the entropy calculated is negative which reveals that the transition state of the rds involves a decrease in entropy, potentially suggestive of an associative mechanism. This could imply that oxidative addition is the rds, but as discussed in the LFER results (Section 3.5.3), this is unlikely. It could be that there are a series of equilibria in place and an associative step is occurring in an equilibrium before the rds. Alternatively, it could be explained by a 'challenging/slow' transmetallation process, which causes perturbation at the metal centre and could result in a negative entropic value. In this example, 4-methoxyphenyl boronate, **11**, is used, which aligns with

transmetallation being the rds in both cross-coupling (Figure 3.39) and homo-coupling of the nucleophile (Figure 3.46). Further complications of assessing the $\Delta S^{\ddagger}$ of the rds, are any solvent affects that may arise. If a significant amount of ordering of the solvent is required to make favourable enthalpic interactions with the transition state, the $\Delta S^{\ddagger}$ value can become more negative than may be expected.[227] However, the Eyring equation is best applied to elementary reactions, in this case it is likely the reaction is significantly more complex than this with many reaction steps, and therefore, the absolute values may not be accurate. However, comparisons between the $\Delta S^{\ddagger}$ values for each reaction can still be made.[227]

$$\Delta G^{\ddagger} = \Delta H^{\ddagger} - T\Delta S^{\ddagger}$$

Equation 3.4 – Determination $\Delta G^{\ddagger}$ of from $\Delta H^{\ddagger}$ and $T\Delta S^{\ddagger}$, where $\Delta G^{\ddagger}$ = Gibbs free energy of activation, $\Delta H^{\ddagger}$ = enthalpy of activation, and $\Delta S^{\ddagger}$ = entropy of activation.

Table 3.8 – Experimentally determined activation parameters for 4-methoxybiphenyl and 4,4'-dimethoxybiphenyl.

Entry	Activation Parameter	Cross-coupling	Nucleophile Homo-coupling
1	$\Delta H^{\ddagger}$ (kJ mol^{-1})	+78.6 ($\pm$6.4)	+81.3 ($\pm$2.6)
2	$\Delta S^{\ddagger}$ (J mol^{-1} K^{-1})	-47.6 ($\pm$5.7)	-42.2 ($\pm$2.0)
3	$\Delta G^{\ddagger}_{298}$ (kJ mol^{-1})	+92.8 ($\pm$4.7)	+93.8 ($\pm$2.0)

As well as the $\Delta H^{\ddagger}$, $\Delta S^{\ddagger}$, and $\Delta G^{\ddagger}$ of the reaction, the activation energy can also be calculated by using the same experimental data and the logarithm of the Arrhenius equation (Equation 3.5). By plotting lnk against $\frac{1}{T}$ the E_a can be calculated from the gradient of the data. In both cases an excellent fit is observed (Figure 3.49). The data shows that the activation barrier is slightly less for cross-coupling than it is for the homo-coupling of the nucleophile, and that could be why we see more cross-coupling than homo-coupling but also why the reaction is not very selective (Table 3.9).

$$lnk = -\frac{E_a}{RT} + lnA$$

Equation 3.5 – Natural logarithm of Arrhenius equation. Where k = rate constant, E_a = activation energy, R = gas constant, T = temperature, A = pre-exponential factor.
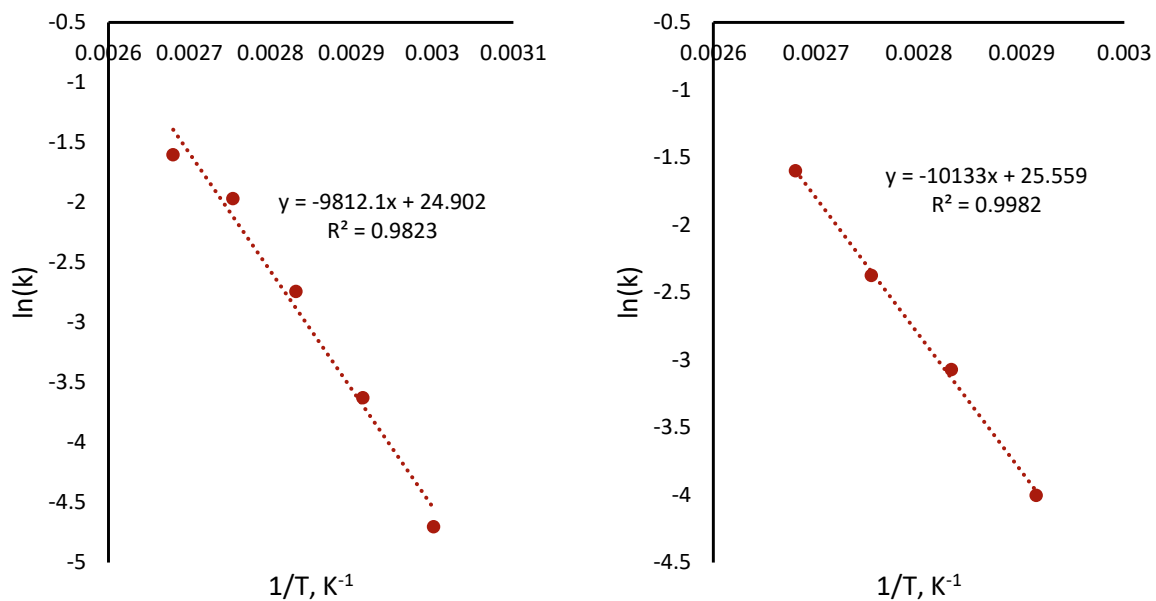
Figure 3.49 – Arrhenius plots for the formation of 4-methoxybiphenyl (left) and 4,4'-dimethoxybiphenyl (right).

Table 3.9 – Experimentally determined activation parameters for 4-methoxybiphenyl and 4,4'-dimethoxybiphenyl.

Entry	Activation Parameter	Cross-coupling	Nucleophile Homo-coupling
1	E_a (kJ mol^{-1})	81.6 (±6.3)	84.2 (±2.6)

3.6 Radical Probe Investigation

Iron has been shown to be able to undergo either single or two electron transfer processes in catalytic reactions.[48,52] From investigating the LFER of both the electrophile and nucleophile in both the cross-coupling and nucleophile homo-coupling, it was observed that the electrophile is potentially involved in a radical process in the formation of the nucleophile homo-coupled product. To further confirm whether this was the case in this reaction, radical probe experiments were undertaken using 1,4-cyclohexadiene,[247–250] butylated hydroxytoluene (BHT),[251–253] 1,1-diphenylethylene,[254–256] 2,2,6,6-tetramethylpiperidine-1-oxyl (TEMPO),[257–259] and trityl chloride (Table 3.10).[260]

Table 3.10 – Effect of adding radical probes to the reaction.

Entry	Radical Probe	12, % Yield	13, % Yield	14, % Yield
1	none	4	61	35
2	1,4-cyclohexadiene	5	56	39
3	1,1-diphenylethylene	7	59	40
4	BHT	3	27	25
5	TEMPO	0	2	54
6	Trityl chloride	1	12	70

Conditions: chlorobenzene (0.5 mmol), 11 (1.25 mmol), FeBr$_3$ (0.05 mmol), IMes·HCl (0.05 mmol), MgBr$_2$·OEt$_2$ (0.1 mmol), MeMgBr (0.05 mmol), radical probe (0.5 mmol), 2-MeTHF:1,4-dioxane (1:1) (6.0 mL), 100 °C, 3 h. Yield determined by GC using dodecane as an internal standard.

The results from the radical probes were varied. 1,4-cyclohexadiene and 1,1-diphenylethylene both showed very little change in the yield of cross-coupled product, along with reasonable yields of nucleophile homo-coupled product (Table 3.10, entries 1 & 2). Corroborating this, none of the potential products from the radical probes inhibiting the reaction were observed when analysed

by GCMS. This would support neither reaction proceeding *via* a radical mechanism. However, BHT, TEMPO and trityl chloride all showed a significant decrease in cross-coupling, and in the case of TEMPO and trityl chloride an increase in homo-coupling, implying that the reaction could in fact proceed *via* a radical process (Table 3.10, entries 4–6). Neither BHT, TEMPO or trityl chloride showed production of any products expected to be formed in a radical process from the radical probes and the reactants when analysed by GCMS. When looking at some of the radical probes chosen there are some potential issues; BHT contains a hydroxyl group which has the potential to react with the boronate and therefore reduces both the cross-coupling and nucleophile homo-coupling yields, as seen (4-chlorophenol was not tolerated in the reaction). TEMPO has been reported to act as a ligand and could have coordinated to iron to form a non-catalytically active species, causing a reduction in production of product.[261] Therefore, trityl chloride may be a more reliable source of information, in this case a significant increase in nucleophile homo-coupling is seen (70%) along with a reduction in cross-coupling (12%) and electrophile homo-coupling (1%). This could be explained by there being a common intermediate between the cross-coupling and homo-coupling processes, where this intermediate is in equilibrium with the two processes (Scheme 3.14). If an aryl radical is formed it can then react with the trityl chloride, preventing any formation of the electrophile homo-coupled product. This would then pull the equilibria to the right and lead to an increase in nucleophile homo-coupling but a decrease in cross-coupling and electrophile homo-coupling.
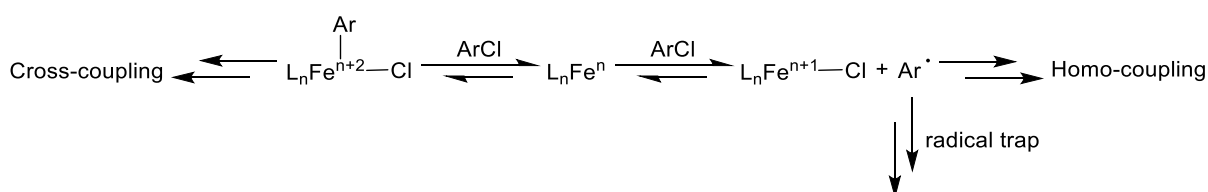

Scheme 3.14 – Radical formation in reaction and potential equilibria in place.

However, if this was the case then the same result would be expected to be seen for 1,4-cyclohexadiene and 1,1-diphenylethylene, as any free aryl radicals formed would react quickly with these alkenes. What is more likely in the case of trityl chloride, is a chloride extraction from trityl chloride to an Fe(n) centre to form an Fe(n+1)Cl species and the trityl radical (Scheme 3.15).[262] The trityl radical is then in equilibrium with a stable dimer, known as Gomberg's dimer, which upon exposure to oxygen, forms the peroxide.[263] If an Fe(n+1) species is responsible for homo-coupling of the nucleophile and an Fe(n+2) species responsible for cross-coupling, then addition

of trityl chloride would lead to competitive formation of an Fe(n+1) species. If this process is significantly quicker than oxidative addition, then the homo-coupled nucleophile would be preferentially formed over the cross-coupled product and homo-coupling of the electrophile would also be suppressed. Trityl chloride has been reported to react with Ni(n) complexes to form Ni(n+1)Cl complexes, so it is possible that iron could be reacting the same with it here.[264,265]
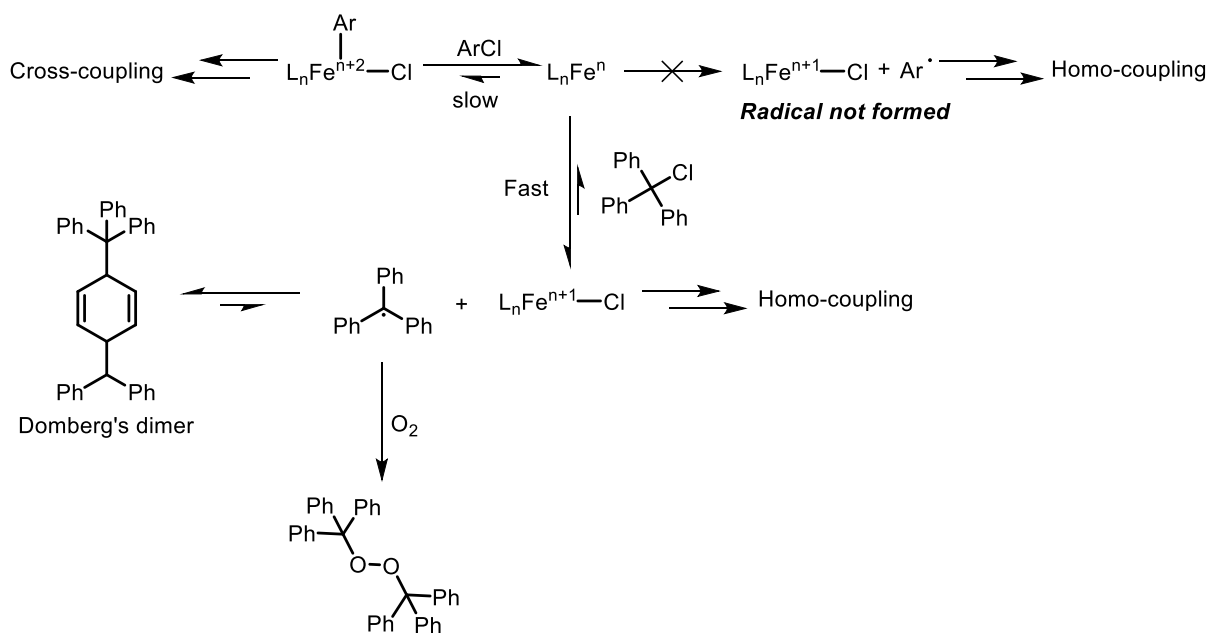
Scheme 3.15 – Potential reactivity of trityl chloride with Fe species.

In conclusion, the radical probe investigation suggests that radical species are not formed in the reaction. However, it does suggest that an Fe(n+1) species is responsible for the homo-coupling of the nucleophile, whereas an Fe(n)/Fe(n+2) manifold is responsible for cross-coupling.

3.7 Determining the Role of MgBr₂ in the Reaction

When assessing the effect that the concentration of $MgBr_2$ had on the reactions (Sections 3.5.1.5 and 3.5.2.5), a slight positive dependence is observed between 10 and 25 mol% but at greater concentrations (30 and 35 mol%) there is a negative dependence. It was hypothesised that $MgBr_2$ could be involved in two steps, an initial associative step followed by a dissociative step later in the cycle. At higher concentrations, dissociation is inhibited and therefore a slower rate of reaction is observed, but comparable yields are still be obtained.

To fully assess the effect of using a halide salt on the reaction a screen of additives was undertaken, IMes was used rather than IMes·HCl so MeMgBr could be removed from the reaction and the full effect of the halide salt could be observed (Table 3.11). The results show that $MgBr_2$ performs the best, followed by TEAB and TBAB. Both $ZnBr_2$ and $AlBr_3$ have been used as additives in iron-catalysed cross-coupling reactions, but when used here a significant decrease in yield was observed. The fact that the ammonium salts outperformed $ZnBr_2$ and $AlBr_3$ could suggest that the reaction is dependent on the halide rather than on the cation. When an additive was omitted from the reaction mixture, the reaction still proceeded in reasonable yields of cross-coupling (42%), showing that $MgBr_2$ is not vital for the reaction, but it does aid the catalytic turnover in some way.

**Table 3.11 – Effect of using different additives on the reaction mixture.**
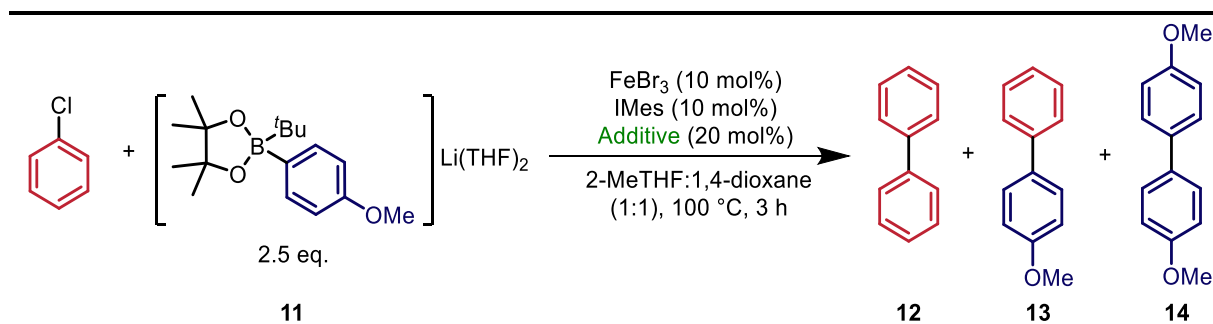
Entry	Additive	12, % Yield	13, % Yield	14, % Yield
1	LiBr	4	29	26
2	NaBr	2	20	39
3	KBr	3	35	37
4	MgBr₂	5	61	36
5	AlBr₃	2	23	34
6	ZnBr₂	1	4	29
7	TEAB	4	55	44
8	TBAB	7	52	35

9	MgCl$_2$	4	44	37
10	N/A	3	42	27

Conditions: chlorobenzene (0.5 mmol), 1 (1.25 mmol), FeBr$_3$ (0.05 mmol), IMes·HCl (0.05 mmol), additive (0.1 mmol), MeMgBr (0.05 mmol), 2-MeTHF:1,4-dioxane (1:1) (6.0 mL), 100 °C, 3 h. Yield determined by GC using dodecane as an internal standard.

It could be argued, in the case of MgBr$_2$, ZnBr$_2$, and AlBr$_3$, that there is formation of organo-main group metal intermediates where there is an aromatic species on these metal centres. This species could then react in a transmetallation process, transferring the aryl group to an iron centre, allowing the cross-coupling to occur. In fact, magnesium, zinc, and aluminium nucleophiles have all been used in iron-catalysed cross-couplings.[79] However, when these were used as nucleophiles in the reaction, in place of the boronate, the cross-coupling was severely hampered (Table 3.12). This shows that it is highly unlikely that the productive reaction proceeds *via* aryl transfer to Mg which then facilitates transmetallation, instead it is more likely that it acts as a halide source and aids oxidative addition as suggested by Bedford in the iron-catalysed substrate-directed biaryl cross-coupling reaction.[87]

Table 3.12 – Effect of using different nucleophiles in the reaction.
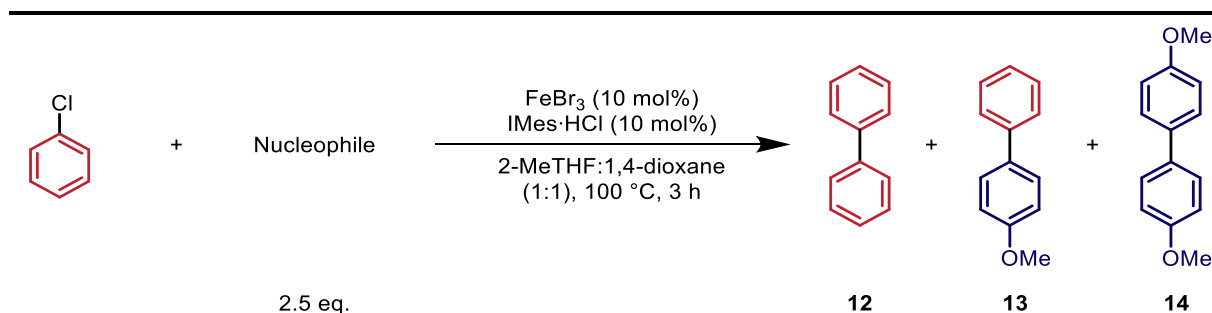
Entry	Nucleophile	12, % Yield	13, % Yield	14, % Yield
1	MeOC$_6$H$_4$MgBr	3	25	27
2	(MeOC$_6$H$_4$)$_2$Zn·2MgBr$_2$	0	2	13
3	[(MeOC$_6$H$_4$)$_4$Al]MgBr	2	13	20

Conditions: chlorobenzene (0.5 mmol), nucleophile (1.25 mmol), FeBr$_3$ (0.05 mmol), IMes·HCl (0.05 mmol), MgBr$_2$·OEt$_2$ (0.1 mmol), MeMgBr (0.05 mmol), 2-MeTHF:1,4-dioxane (1:1) (6.0 mL), 100 °C, 3 h. Yield determined by GC using dodecane as an internal standard.

The combined data suggests that a MgBr$_2$ might act as a bromide source, this initially, reversibly, coordinates to an iron species. This can then aid oxidative addition. Once oxidative addition is complete, the bromide source dissociates from the iron species. Then the coupling reaction can

be completed, and the catalyst regenerated (Figure 3.50). This is in accordance with the iron-catalysed substrate-directed Suzuki biaryl cross-coupling reaction.[87]
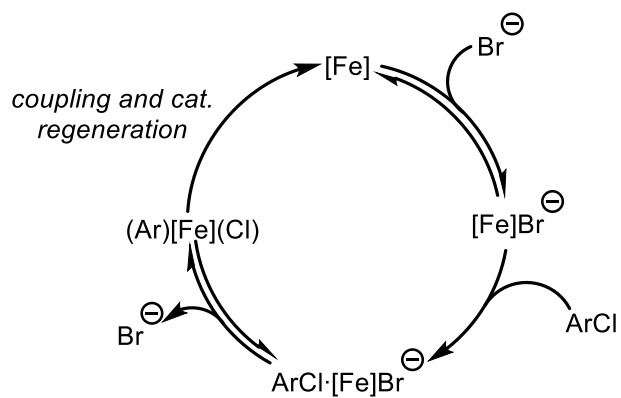

Figure 3.50 – Potential action of MgBr$_2$ in the catalytic cycle. It is not clear whether Br^- is a bromide species or a MgBr$_2$ species.

3.8 Accounting for the Nucleophile Homo-Coupling

In the standard reaction (0.5 mmol scale), the nucleophile homo-couples to give approximately 0.18 mmol of **14**. 0.06 mmol of this is due to the initial reduction of Fe(III) to an average bulk oxidation state of Fe(I). However, this still leaves 0.12 mmol of **14** unaccounted for. An oxidative process is required to oxidise the iron species back to a catalytically active species which can then lead to the formation of the additional 0.12 mmol of **14**. A complete picture of all the potential oxidative processes that could occur to promote the remaining homo-coupling of the nucleophile is required. However, due to the poor burning ability of chlorobenzene, its concentration cannot be determined accurately by GC-FID and therefore an accurate mass balance was not measured. A potential oxidative process is hydrodehalogenation, the product in this case is benzene. However, due to the boiling point of benzene, it is hard to accurately measure its concentration by GC-FID. Benzene also does not have any distinguishable features to observe by ^{1}H-NMR spectroscopy, compared to the other products. Therefore, to determine the mass balance of the reaction, based on the electrophile, a reaction was carried out with 1-fluoro-4-chlorobenzene as the electrophile. Using this electrophile meant that any fluorinated species could be observed by ^{19}F-NMR spectroscopy and a spectroscopic yield could be determined (Scheme 3.16). Analysis of this reaction mixture shows a good mass balance, with respect to 1-fluoro-4-chlorobenzene, was obtained. It also showed that 1-fluoro-4-chlorobenzene does not undergo hydrodehalogenation (fluorobenzene was not observed by ^{19}F-NMR spectroscopy) but whilst some homo-coupling of the electrophile is observed, there is also unreacted 1-fluoro-4-chlorobenzene in the reaction mixture. This result shows that the homo-coupling of the electrophile is involved in the oxidative process that is responsible for the homo-coupling of the nucleophile (not including the homo-coupled nucleophile product formed from the initial reduction of Fe).
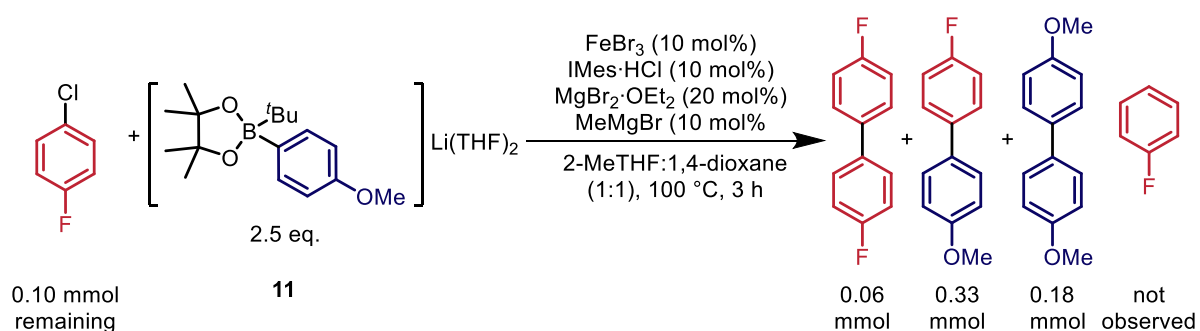
Scheme 3.16 – Reaction of 1-fluoro-4-chlorobenzene with 1. Conditions: 1-fluoro-4-chlorobenzene (0.5 mmol), 11 (1.25 mmol), FeBr₃ (0.05 mmol), IMes·HCl (0.05 mmol), MgBr₂·OEt₂ (0.1 mmol), MeMgBr (0.05 mmol), 2-MeTHF:1,4-dioxane (1:1) (6.0 mL), 100 °C, 3 h. Yield determined by GC using dodecane as an internal standard and 19F NMR spectroscopy using α,α,α-trifluorotoluene as an internal standard.

3.9 Proposed Catalytic Cycle

From the evidence discussed in the preceding sections, a simplified, tentative but plausible catalytic cycle is proposed (Figure 3.51). The evidence suggests that the reaction proceeds in the homogeneous phase with ligand(s) attached to the metal centre. As $MgBr_2$ is not vital for the reaction to proceed, it was omitted from the cycle for clarity. However, it is likely (as discussed in Section 3.7) that it has two roles, where it must first coordinate to the iron centre and then later in the cycle dissociate from an iron species (Figure 3.50). The determined order in pre-catalyst for both homo- and cross-coupling, and the radical probe study, could suggest the reactions proceed *via* a common intermediate.
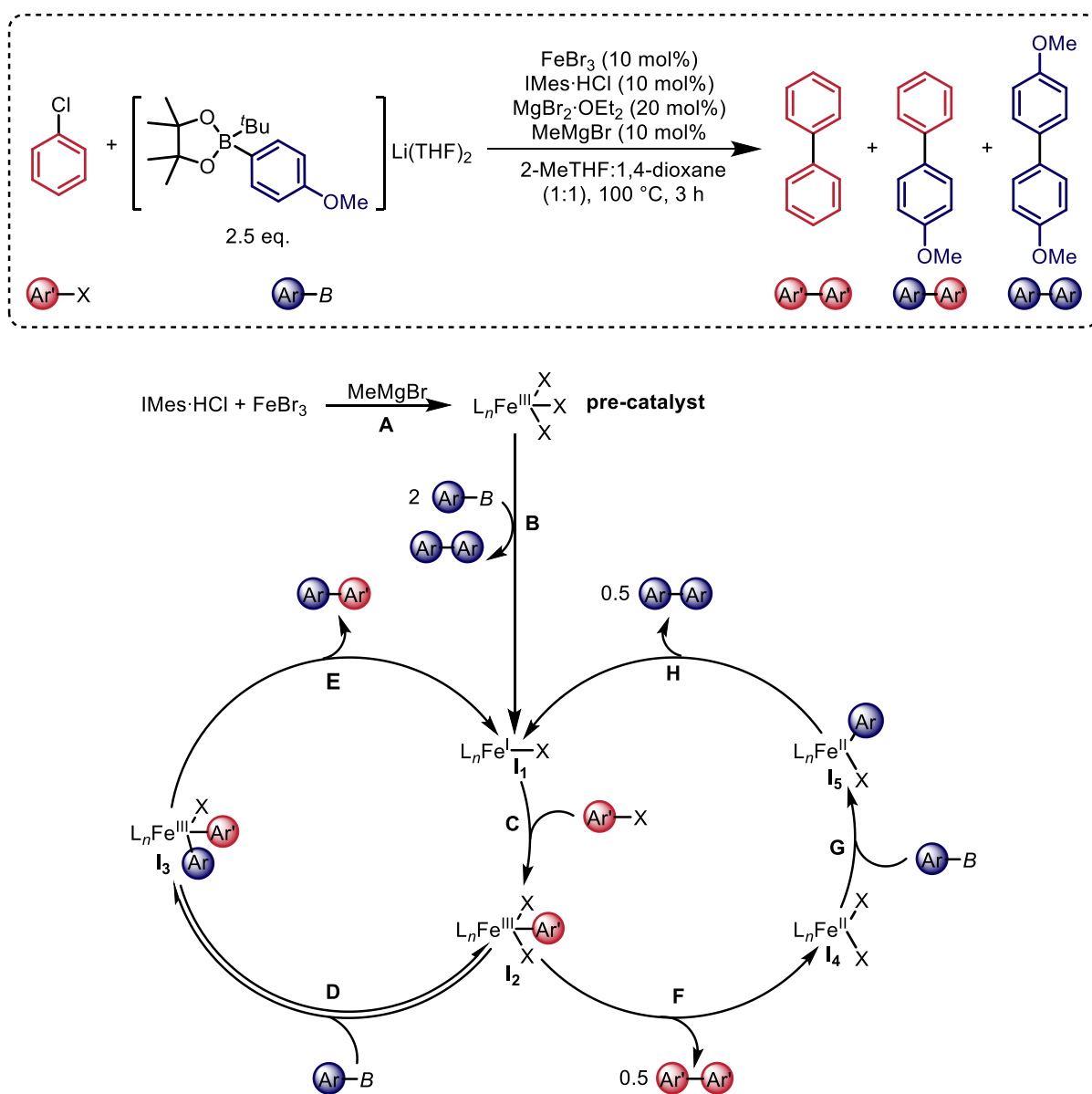
Figure 3.51 – Proposed catalytic cycle for the iron-catalysed Suzuki biaryl cross-coupling reaction.

A: MeMgBr acts a base to deprotonate the NHC salt, IMes·HCl, to form IMes which can then combine with $FeBr_3$ to form the pre-catalyst (evidence discussed in Section 3.2).

B: Upon addition of the boronate to the reaction mixture, the pre-catalyst is arylated. This species can then undergo reductive elimination, forming Ar-Ar and in turn reduces Fe(III) to Fe(I) forming **I₁** (evidence discussed in Section 3.3).

C: **I₁** reacts with Ar'X in an oxidative addition step forming **I₂**. While assessing the LFER of the cross-coupling reaction, the data fitted the $\sigma_{Hammett}$ values but did not fit σ_{Creary} values, suggesting a 2-electron transfer rather than a single electron transfer. Further investigations from the radical probe screen also suggests that radical processes are not observed.

The common intermediate, **I₂**, can then react *via* pathway **D** or **F**. For cross-coupling the reaction proceeds *via* step **D**.

D: **I₂** can then react with the boronate nucleophile, forming **I₃**, in a transmetallation process.

E: The final step of the catalytic cycle is reductive elimination. **I₃** releases the cross-coupled product Ar-Ar' and reforms **I₁**.

Alternatively, **I₂** can take part in homo-coupling rather than cross-coupling and react *via* pathway **F**.

F: **I₂** can undergo a bimolecular reductive elimination forming an Fe(II) species, **I₄**, and the homo-coupled electrophile product. The Fe(II) species was hypothesised to be the reason for the homo-coupling of the nucleophile when trityl chloride was investigated as a radical probe. Evidence for the bimolecular reductive elimination is potentially seen from the initial rates data for the pre-catalyst. At low concentrations of pre-catalyst, the order for cross-coupling was greater than for nucleophile homo-coupling. The inverse was seen at higher pre-catalyst concentrations. At higher pre-catalyst concentrations, there is a greater chance of bimolecular reductive elimination occurring and therefore there is a greater dependency on the pre-catalyst for nucleophile homo-coupling observed.

G: **I₄** can then react with the boronate in a transmetallation step to form **I₅**.

H: The final step of the cycle is for **I₅** to undergo a bimolecular reductive elimination, forming Ar-Ar, and reforming **I₁**.

3.10 Conclusions

In conclusion, a thorough mechanistic investigation has been undertaken to gain a greater understanding of the iron-catalysed Suzuki biaryl cross-coupling reaction described in Chapter 2. Through the investigation, it has been shown that the role of MeMgBr acts as a base to form the free carbene, IMes. It has also been shown that, although Fe(0) can also be accessed under the reaction conditions, the catalytically active species is likely to be Fe(I) and that the reaction takes place in the homogeneous phase. This reduction step is the initial activation step of the catalytic reaction where cross-coupling can only occur after this point.

Although $MgBr_2$ was not vital in catalysis, it did lead to greater yields being obtained. Its role is likely to be as a halide donor that aids oxidative addition rather than to aid transmetallation as seen in other iron-catalysed reactions. It was also shown that at greater concentrations of $MgBr_2$, the rate and yield were inhibited, this suggests that it may have two roles in the cycle (associative and dissociative processes).

The reaction kinetics were also investigated, and the results from this investigation suggested that a common intermediate was forming that could either take part in cross-coupling or homo-coupling. A range of non-integer values were also obtained for the orders in reactants for both cross- and homo-coupling. This suggests that the mechanism may take place with a series of equilibria. Investigating the linear free-energy relationship of the cross-coupling reaction showed that the reaction proceeds *via* two electron transfers and not a radical process. It also showed that there was a change in rds depending on the substituents on the aryl groups. When the homo-coupling of the nucleophile was inspected against σ values, it showed that the electrophile has a reasonable correlation with σ_{Creary} values, potentially suggesting that a radical process could be involved. This was further investigated by a radical probe investigation; the findings from this suggested that the reaction does not proceed *via* a radical mechanism.

Determination of the activation parameters of the reactions showed that there is not a strong thermodynamic preference between formation of the cross- and homo-coupled products, as activation energies were very similar. This is likely the cause of the relatively poor selectivity of the reaction.

3.11 Future Work

The mechanistic investigation discussed has shed light on the observed lack of selectivity, with homo-coupling of the nucleophile remaining competitive throughout. To aid routes to stop homo-coupling, the common intermediate, I_1, should be identified. Formation of I_1 is thought to occur from the reduction of the Fe(III) pre-catalyst to an Fe(I) species, after which cross-coupling can start and homo-coupling can continue. An Fe(I) species will have at least one unpaired electron and may therefore be potentially observed by EPR spectroscopy. At 100 °C, this process is very quick, occurring in the opening minute of the reaction, which could make observing it by EPR challenging. However, the reaction can still proceed at lower temperatures, and at 60 °C the induction period for cross-coupling is around 5 mins (Figure 3.47). This activation process and the formation of I_1 should therefore be much easier to observe by EPR spectroscopy. Fe(III) intermediates, I_2 and I_3, may also be detectable by EPR spectroscopy. Further efforts to identify catalytic intermediates could be focused on other techniques such as X-ray fluorescence spectroscopy (XFS) and ^{57}Fe Mössbauer spectroscopy. An alternative way to observe the intermediates might be to do stoichiometric reactions of iron with the substrates and see if any catalytically relevant species can be isolated, possibly at low temperatures.

Computational studies are also likely to aid the development and understanding of the reaction mechanism. By modelling the catalytic cycle using DFT studies, it will give insights into which processes are possible and which may be favoured. This will not only provide evidence for or against the proposed catalytic cycle but may suggest ways to prevent homo-coupling and promote cross-coupling.

Chapter 4 Iron-Catalysed Regioselective Carboboration of Styrene Derivatives

4.1 Introduction

Acknowledgements: Thanks to MSci student Jordan Garrard for her contribution to the substrate scope as part of the work described in this chapter. Her specific contribution is acknowledged accordingly.

Synthetic routes to boron-containing organic molecules are highly sought after due to their ability to be further functionalised. Examples include: Suzuki cross-coupling reactions, asymmetric reductions and the introduction of alcohols and amines, which themselves can be further functionalised.[31,266–268] As alkene substrates are widely available, routes to functionalise them to desired products are valuable, such as converting them to alkylboronates. Hydroboration was developed in the 1950's to achieve this, and this has since been advanced further (Scheme 4.1).[269–271]
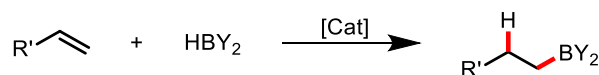
Scheme 4.1 – General scheme for metal-catalysed hydroboration

Since this discovery, more efforts have been made to increase molecular complexity whilst functionalising alkenes. A method that achieves this is the carboration of alkenes. As the name suggests, rather than forming a $C(sp^3)$–H bond, a $C(sp^3)$–$C(sp^3)$ bond is formed simultaneously alongside the $C(sp^3)$–$B(sp^2)$ bond.[272] There are three potential products: the 1,1-, 1,2- and 2,1-regioisomers (Scheme 4.2). This reaction offers access to organic compounds with a stereogenic centre if terminal alkenes are used, or two contiguous stereogenic centres if internal alkenes are functionalised. The reaction could also be rendered enantioselective, as well as regioselective, if the right conditions were employed.[273]
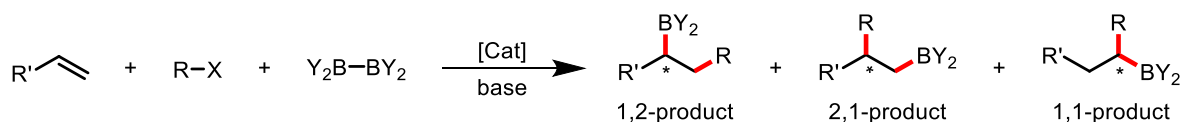
Scheme 4.2 – General scheme for metal-catalysed carboration of alkenes. * Denotes a stereogenic centre.

While typically catalysed by transition metals, metal free radical-mediated carboration reactions have been reported.[274–277] Although an exciting prospect, they are not at the same stage of development as metal-catalysed carboration reactions. Current protocols do not allow for

routine synthesis of desirable products, or they require heavily fluorinated radical precursors (Scheme 4.3).
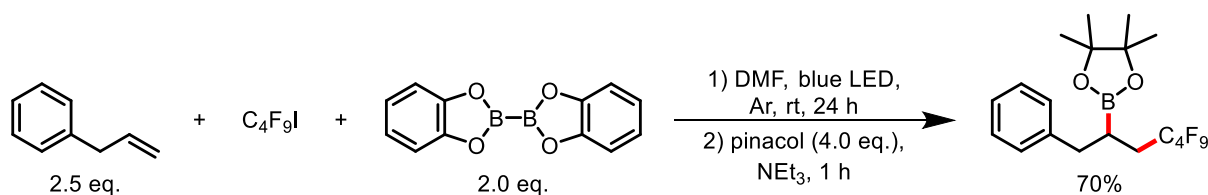
Scheme 4.3 – Transition Metal-free carboboration of alkenes.[277]

Palladium has been proven to be a competent catalyst in the carboboration of alkenes when using aryl or vinyl halides, but reactions using alkyl halides are severely hampered. One of the issues with palladium catalysed difunctionalisation of alkenes is β-hydride elimination, which can lead to undesired side-products and reduced product selectivity. To overcome this issue, the Engle group have developed protocols that require a strongly coordinating 8-aminoquinoline amide directing group (AQ). This is able to subsequently stabilise alkylPd(II) intermediates by forming conformationally rigid palladacycles.[278–282] This has since been exploited by Engle in a palladium(0)-catalysed carboboration reaction of aryl and alkenyl triflates (Scheme 4.4).[283] Engle was also able to use a palladium(II) catalyst in a carboboration initiated by a Wacker-type nucleopalladation, again this required the use of an 8-aminoquinoline amide directing group.[284]
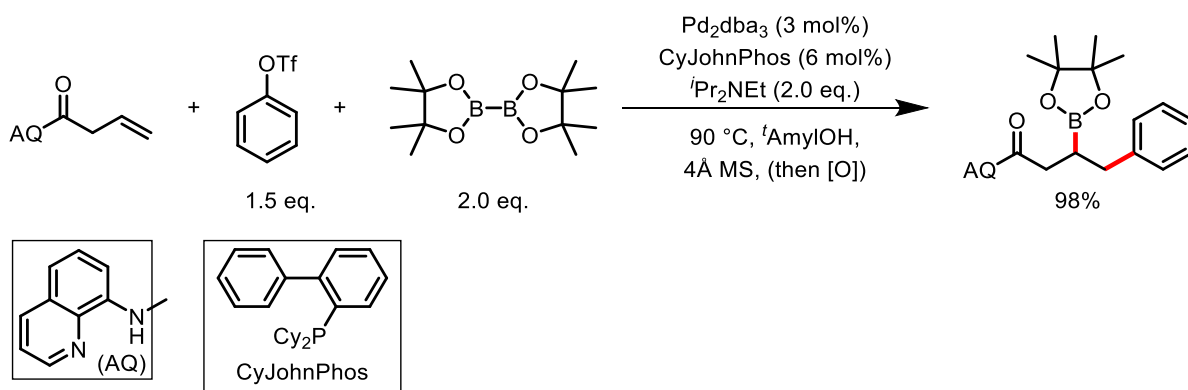
Scheme 4.4 – Palladium-catalysed carboboration of alkenes.[283]

Greater success with transition metal-catalysed carboboration of alkenes has been seen with copper and nickel catalysts.[285–288] However, nickel also is susceptible to β-hydride elimination and therefore, although it works well with aryl and alkenyl electrophiles, an example of a 2,1- or 1,2-carboboration of alkenes using alkyl electrophiles is yet to be published. β-hydride elimination is

not necessarily a disadvantage; Yin utilised it in a nickel-catalysed 1,1-alkylboration of terminal alkenes.[289]

The first reported nickel-catalysed 2,1-carboboration was reported by Brown in 2018 using aryl halides (Scheme 4.5).[290] Directing groups, such as those used by Engle, were not required in this transformation as the alkylnickel(I) intermediate is more resistant to β-hydride elimination when compared to alkylpalladium(II) intermediates.[291] Brown went on to further develop this reaction by incorporating DMA as an additive, which stabilised alkylnickel(I) intermediates to suppress β-hydride elimination and allow for the tolerance of tri-substituted alkenes.[292] Both Brown and Yin have advanced this methodology by developing protocols that can selectively form the regioisomer of choice by employing different substituents on the alkene.[293–295] Although alkyl electrophiles have not been reported in either a 1,2- or 2,1-carboboration, Brown has found a way to form these products by using alkenyl electrophiles followed by a hydrogenation to synthesise congested $C(sp^3)$–$C(sp^3)$ bonds.[296]

1.5 eq.   2.0 eq.   80%
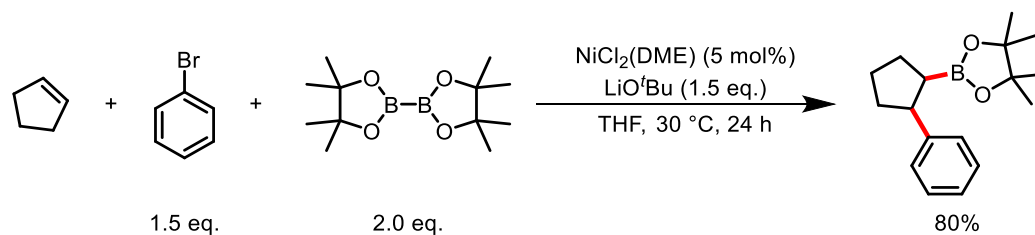
Scheme 4.5 – Nickel-catalysed carboboration of alkenes.[290]

Further success has been seen when copper-based catalysts have been employed.[297–300] The first three-component carboboration reaction was reported by Yoshida in 2013, although the scope of alkene was limited to styrene, a vinyl boronate and a vinyl silane.[301] This set the precedent for future work to be built on. The substrate scope was later expanded by Yoshida and reported in 2014.[302] Xiao and Fu were able to control the regioselectivity, giving either the 2,1- or 1,2-product, through the choice of ligand and alkyl halide, when reacting terminal alkenes with alkyl halides and diboron reagents.[303] By using Xantphos, formation of the 2,1-product (anti-Markovnikov addition) is favoured because of the better d(Cu)-π(alkene) back donation. Whereas, when the bulkier Cy-Xantphos was used, the 1,2-product (Markovnikov addition) was favoured due to steric effects (Scheme 4.6). Success has also been seen when using carbonyl-containing compounds as the electrophile.[304–307] A number of cooperative catalyst systems have been reported, mainly using

a copper/palladium system[308–315] but also a copper/nickel system.[316] This strategy activates multiple reaction components simultaneously using more than one catalyst to achieve transformations that would otherwise be kinetically prohibitive.[317,318]
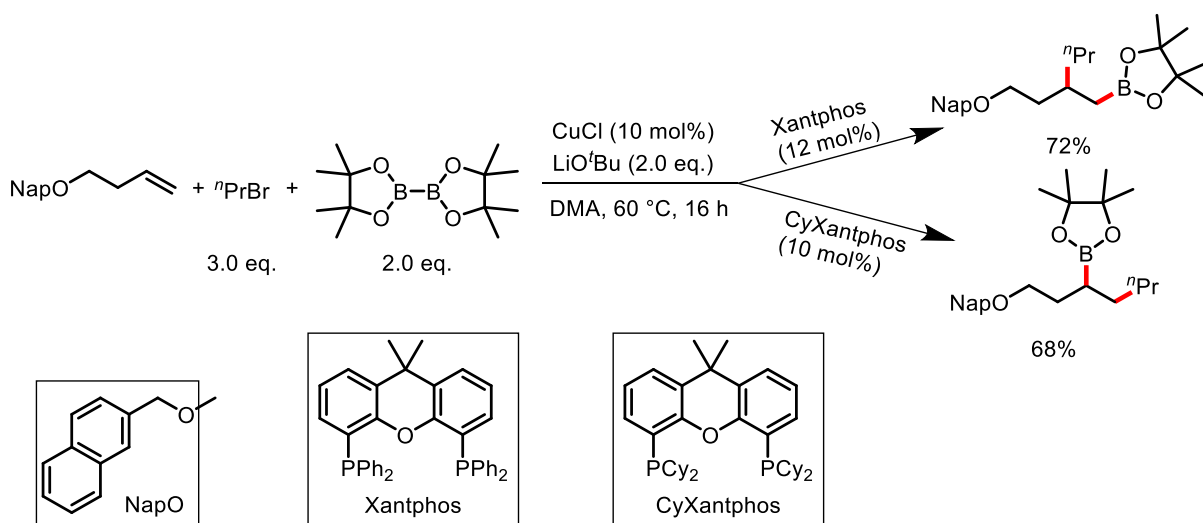
Scheme 4.6 – Copper-catalysed carboration of alkenes.[303]

In contrast to palladium, nickel, and copper, there have been limited breakthroughs with iron-catalysed carboration reactions. Iron is a highly desirable alternative target for catalysis in synthesis due to its low price and low toxicity. The first iron-catalysed carboration reaction was reported by Nakamura in 2015 and used alkynes rather than alkenes (Scheme 4.7).[319] Originally developing a diboration of alkynes, Nakamura found that alkenyliron intermediates could be trapped using carbon electrophiles such as alkyl halides. The reaction proceeded in good yields using FeBr$_2$, without requiring an additional ligand, and LiOMe as the base.
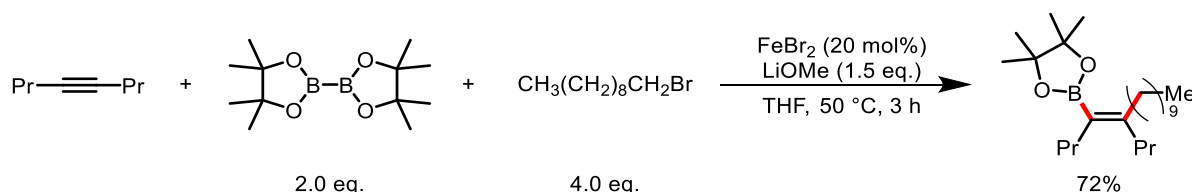
Scheme 4.7 – Iron-catalysed carboration of alkynes.[319]

Whilst the work discussed later in this chapter was underway, Koh reported the first iron-catalysed alkenylboration of alkenes (Scheme 4.8).[122] Koh was able to couple alkenyl halides with activated alkenes in good yields using FeBr$_2$ as the pre-catalyst. When unactivated alkenes were trialled, dppe, in conjunction with FeBr$_2$, was required. Mechanistic studies also showed that the reaction

proceeds through a carbometallation-elimination mechanism rather than previously reported oxidative cleavage pathways. Although the reaction worked well with alkenyl electrophiles, it was reportedly not possible to use either aryl or alkyl halides.

Scheme 4.8 – Iron-catalysed alkenylboration of alkenes.[122]

To build on the protocols currently published in the literature, we wanted to see if we could develop an alkylboration of alkenes catalysed by simple iron salts. To achieve this, we envisioned that activated alkenes would be required (such as styrene), as well as more activated alkyl halides such as benzyl chloride.

4.2 Reaction Optimisation

4.2.1 Initial Screening

We set out to see if we could functionalise styrene using bis(pinacolato)diboron (B_2Pin_2) and benzyl chloride (BnCl). Using similar conditions to Yoshida's copper-catalysed carboboration of alkenes,[302] we used $FeBr_3$, SIMes·HCl and potassium methoxide. This resulted in a yield of 5% and the single formation of the 2,1-isomer, **67** (Scheme 4.9). Although the yield was low, the selectivity was good and therefore an optimisation was undertaken to improve the yield of the reaction.
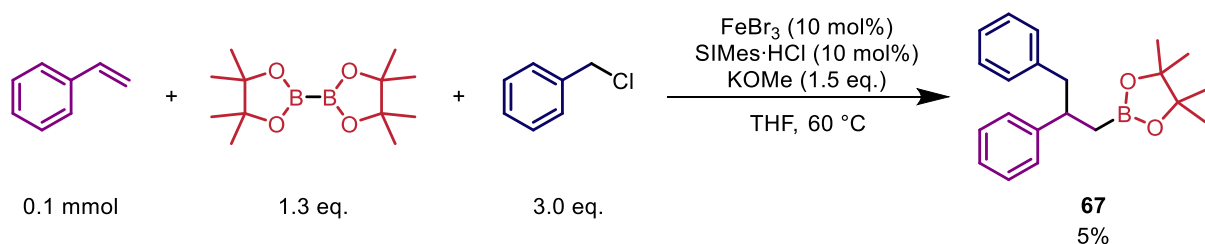
Scheme 4.9 – Iron-catalysed carboboration of styrene. Yield determined by GC using dodecane as an internal standard.

With the preliminary result in hand, the first thing that was investigated was the iron salt that was used as the pre-catalyst (Table 4.1). It was found that moving to iron(II) salts gave greater conversions compared to iron(III) salts. The greatest yield was achieved using $FeBr_2$ (13%), which is almost 3 times greater than when $FeBr_3$ was used (Table 4.1, entries 4 & 10). This result was also seen with Koh's alkenylboration of alkenes and Nakamura's carboboration of alkynes.[122,319]

Table 4.1 – Effect of changing iron source on the reaction.
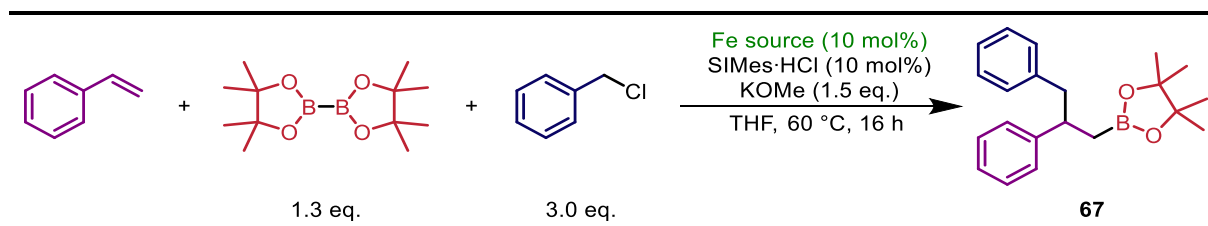
Entry	Fe Source	Yield, %
1	N/A	0
2	FeF₂	8
3	FeCl₂	8

4	$FeBr_2$	13
5	FeI_2	11
6	$Fe(CH_3CO_2)_2$	5
7	$Fe(CF_3SO_3)_2$	10
8	FeF_3	11
9	$FeCl_3$	5
10	$FeBr_3$	5

Conditions: styrene (0.1 mmol), B_2Pin_2 (0.13 mmol), benzyl chloride (0.3 mmol), KOMe (0.15 mmol), Fe source (0.01 mmol), SIMes·HCl (0.01 mmol), THF (3.0 mL), 60 °C, 16 h. Yield determined by GC using dodecane as an internal standard.

The attention was then turned to see if a change in ligand could lead to a greater yield; a range of NHC-, diphosphine-, and nitrogen-containing ligands were trialled in the reaction (Figure 4.1). IMes·HCl gave a very similar result to SIMes·HCl, whereas moving to the much bulkier IPr·HCl and SIPr·HCl led to a decrease in yield. Moving to nitrogen-based ligands led to an increase in yield to 19–20%. The chelate effect of using these multidentate ligands could be the reason for increased activity or the weaker σ-donation from the ligand resulting in a more labile ligand and therefore allowing other catalytic species to form. With the success of multidentate *N*-containing ligands, it was thought that moving to bidentate phosphine ligands, which are stronger σ-donors than nitrogen-based ligands, could be beneficial. Using diphosphine ligands had mixed results, the lowest yield (9%) was obtained when using dpbz, but a greater yield (24%) was obtained when using Xantphos.
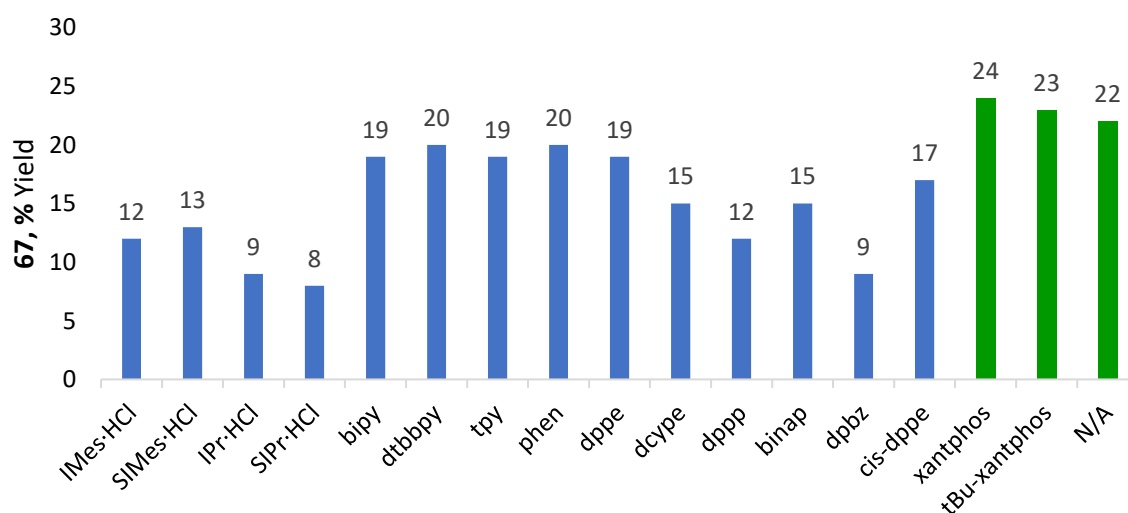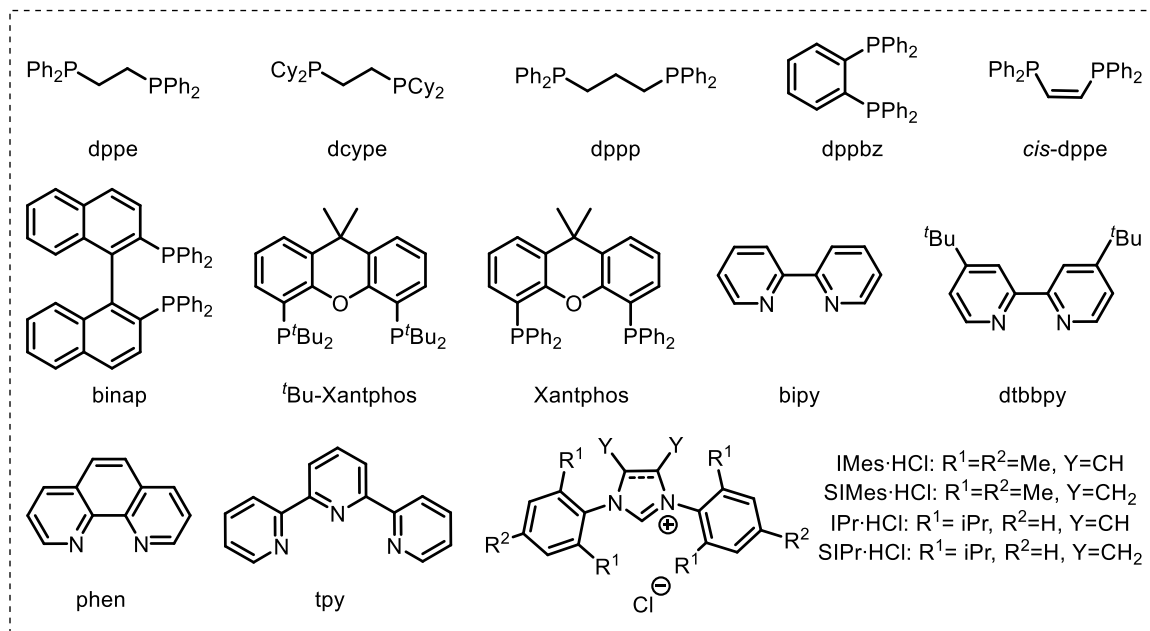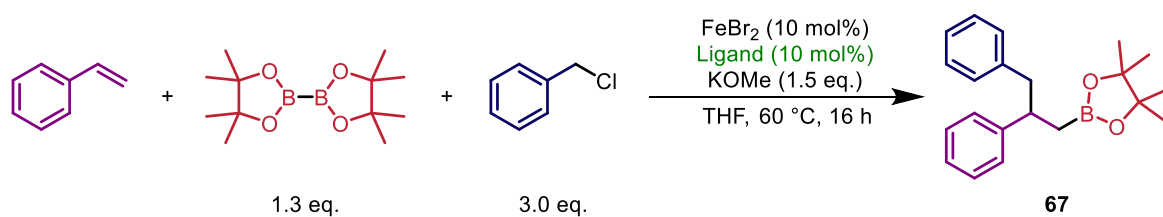
Figure 4.1 – Effect of changing ligand on the reaction. Conditions: styrene (0.1 mmol), B₂Pin₂ (0.13 mmol), benzyl chloride (0.3 mmol), KOMe (0.15 mmol), FeBr₂ (0.01 mmol), ligand (0.01 mmol), THF (3.0 mL), 60 °C, 16 h. Yield determined by GC using dodecane as an internal standard.

Although not a clear trend, when comparing the steric bulk and calculated electronic parameters of the phosphine ligands, the larger bite angle and calculated Tolman parameter both led to the greatest yield (Table 4.2).[320,321] With the weaker σ-donor ligands performing the best, it was thought that perhaps the ligand was dissociating from the iron to allow the catalysis to take place.
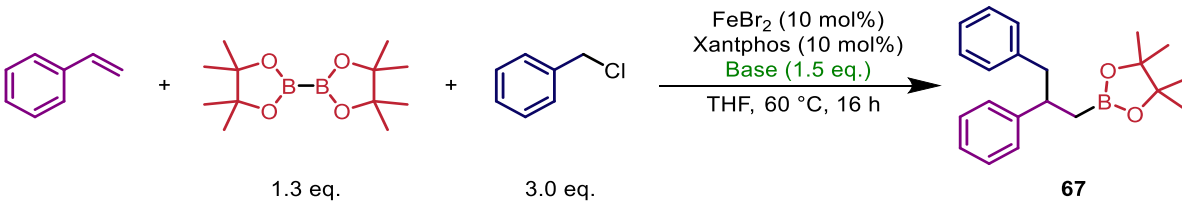
Therefore, the reaction was also trialled without an additional ligand and gave a yield of 22%, comparable to Xantphos (Figure 4.1). Xantphos was used in the optimisation as it gave slight improvements in yield and its full effect on the reaction could be uncovered in a DoE optimisation (Section 4.2.2).

Table 4.2 – Calculated Tolman Parameters (CEP) and bite angles (θ) of selected bidentate phosphine ligands of NiL$_2$CO$_2$ complexes.[321]

Entry	Ligand	CEP$_{NiL_2(CO_2)}$	θ_{PNiP}
1	dppe	2068	90.8
2	dcype	2062	91.8
3	dppp	2067	102.1
4	Xantphos	2070	116.4
5	binap	2070	102.0

The use of potassium methoxide as the base gave limited reactivity, therefore other mild bases were screened for use in this reaction (Table 4.3). Use of KOEt and KO^{t}Bu led to a decrease in activity, but LiOMe gave a slight increase in yield (26%) (Table 4.3, entries 2, 3 & 5). As Li seemed to be the more effective counterion, other Li bases were explored. Lithium amine bases, LiHMDS and LiNMe$_2$ both resulted in a loss of reactivity, but LiO^{i}Pr gave a slight increase in yield (29%) (Table 4.3, entries 6, 7 & 11). Use of milder bases gave limited catalytic turnover, so it was proposed that harsher bases might give greater yields. Use of EtMgCl and ^{n}BuLi resulted in a complete loss of activity, but use of the more reactive ^{t}BuLi led to a significant yield increase to 40% (Table 4.3, entries 10, 9 & 8). Although other carboboration reactions have been successful whilst employing alkoxide bases, the results here show that in iron-catalysed alkylborations a harsher base is required. Previously reported iron-catalysed borylation and Suzuki cross-coupling reactions also required ^{t}BuLi to be used as a base.[87,322] The ^{t}BuLi activated bis(pinacolato)diboron (**68**) species could be made *in situ* and used immediately, or made in batch on multi gram scale and stored under an inert atmosphere.

Table 4.3 – Effect of changing base on the reaction.

Entry	Base	Yield, %
1	KOMe	24
2	KOEt	12
3	KO^{t}Bu	16
4	KOTMS	12
5	LiOMe	26
6	LiHMDS	0
7	LiNMe$_2$	17
8	^{t}BuLi*	40
9	^{n}BuLi*	2
10	EtMgCl	2
11	LiO^{i}Pr	29

Conditions: styrene (0.1 mmol), B$_2$Pin$_2$ (0.13 mmol), benzyl chloride (0.3 mmol), base (0.15 mmol, *0.13 mmol), FeBr$_2$ (0.01 mmol), Xantphos (0.01 mmol), THF (3.0 mL), 60 °C, 16 h. Yield determined by GC using dodecane as an internal standard.

A range of solvents have shown success when employed in metal-catalysed carboboration of alkenes, for example Brown used DMA in a nickel-catalysed carboboration to suppress β-hydride elimination and promote the reaction.[292] The effect of changing solvent was investigated (Figure 4.2). Cyclic ethers outperformed the other solvents, with 2-MeTHF giving the best result; an increase in yield to 50% was observed. 2-MeTHF is considered as a green solvent as it is generated from biomass rather than being derived from non-renewable sources like THF. Switching from THF to 2-MeTHF is therefore advantageous from a 'green' perspective.[323,324] Linear ethers (DME, CPME, diglyme, and MTBE) performed less well but still resulted in reasonable amounts of product formation. Although there is not a clear correlation between dielectric constant[325–327] and yield, moving to considerably more polar solvents led to a significant decrease in yield. Although

DMA and DMF were found to be the best solvent in Koh's iron-catalysed alkenylboration, they performed poorly under these conditions (13 and 15%, respectively).[122]
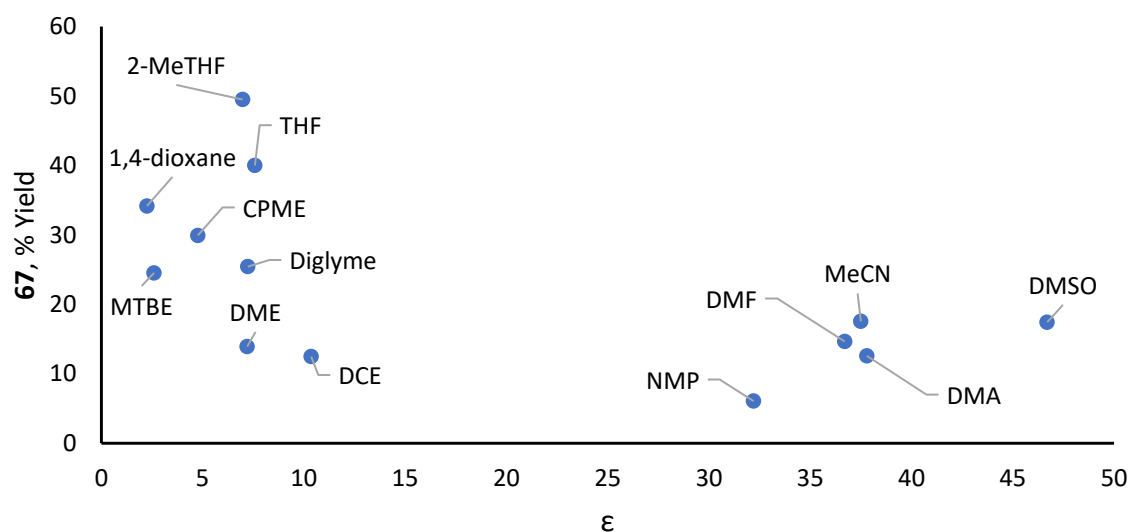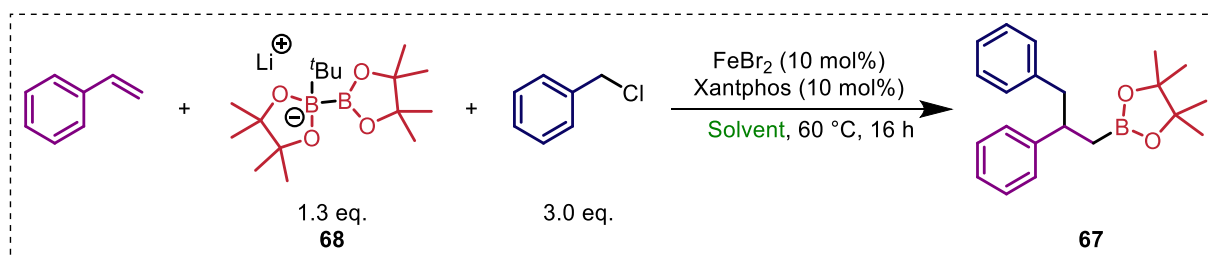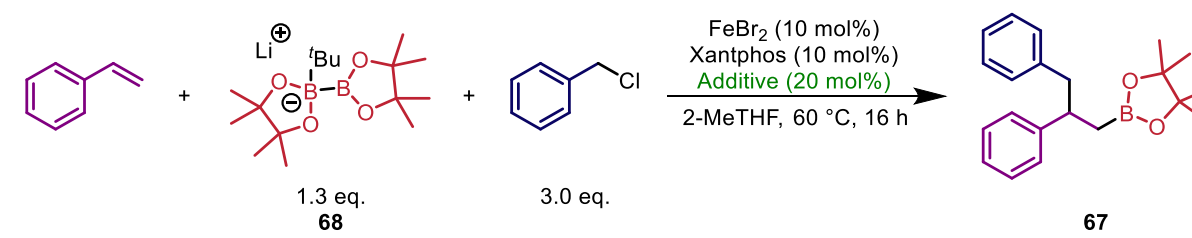
Figure 4.2 – Effect of changing solvent on the reaction. Conditions: styrene (0.1 mmol), 68 (0.13 mmol), benzyl chloride (0.3 mmol), FeBr₂ (0.01 mmol), Xantphos (0.01 mmol), solvent (3.0 mL), 60 °C, 16 h. Yield determined by GC using dodecane as an internal standard.

The effect of using salt additives on the yield of the reaction was then investigated (Table 4.4). The use of metal salt additives was shown to be vital in the iron-catalysed substrate-directed Suzuki biaryl cross-coupling reaction and it was also found to promote an iron-catalysed borylation reported by Bedford.[87,322] As the carboboration of alkenes involves many of the same catalytic steps as those seen in Suzuki cross-coupling and borylation reactions, it was thought that addition of a metal salt could aid this reaction; several were screened. The addition of MgBr₂ led to a slight reduction in yield, which was also observed with addition of MgCl₂ (40 and 41% respectively) (Table 4.4, entries 5 & 7). When other metal salts were used the yield dropped further, and addition of AlCl₃ resulted in almost complete shutdown of reactivity (Table 4.4, entry 8). It was reported in the iron-catalysed substrate-directed Suzuki biaryl cross-coupling that the bromide in MgBr₂ coordinated to the iron centre and facilitates oxidative addition.[87] However, the loss in

reactivity in this case could be due to this effect, where the $MgBr_2$ perturbs the system by coordinating to an iron species and rendering it catalytically inactive. When ammonium salts were trialled in the reaction, they gave very similar reactivity to when no additive was used (Table 4.4, entries 9–11). Tetraethylammonium bromide (TEAB) was carried through as an additive in the optimisation as it gave slight improvements in yield and its full effect on the reaction could be uncovered in a DoE optimisation (Section 4.2.2).

Table 4.4 – Effect of the introduction of additives to the reaction.
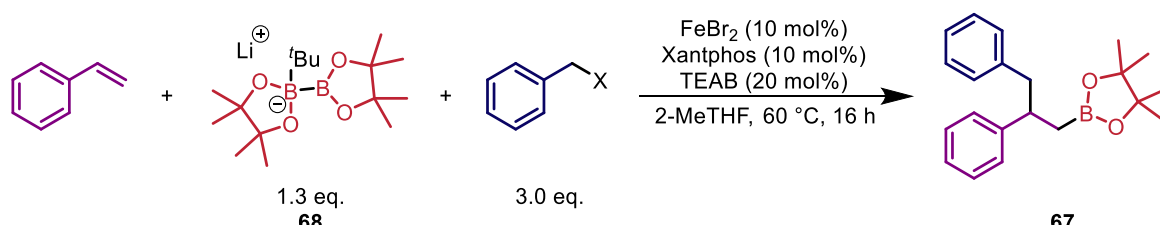
Entry	Additive	Yield, %
1	No additive	50
2	LiBr	41
3	NaBr	44
4	KBr	39
5	$MgBr_2$	40
6	$ZnBr_2$	31
7	$MgCl_2$	41
8	$AlCl_3$	2
9	$[NMe_4]Br$	47
10	$[NEt_4]Br$	52
11	$[NBu_4]Br$	50

Conditions: styrene (0.1 mmol), 68 (0.13 mmol), benzyl chloride (0.3 mmol), FeBr₂ (0.01 mmol), Xantphos (0.01 mmol), additive (0.02 mmol), 2-MeTHF (3.0 mL), 60 °C, 16 h. Yield determined by GC using dodecane as an internal standard.

Throughout the optimisation, only benzyl chloride had been considered as the electrophile. To probe the effect of the halide leaving group, benzyl iodide and benzyl bromide were subjected to the reaction conditions (Table 4.5). The use of benzyl iodide gave a complete loss of reactivity,

and no desired product was observed. Analysis of the reaction mixture by GCMS showed presence of starting material. Use of benzyl bromide resulted in a 45% yield of **67**, which is only slightly lower than that observed with benzyl chloride. Previously reported nickel-catalysed carboration of alkenes all required organobromide electrophiles,[285,286,288–290,292–296], whereas copper-catalysed carboration reactions could work with either organochlorides or bromides.[299,300,303] Both Koh and Nakamura found that organobromides only worked well under their conditions.[122,319] The fact that benzyl chlorides outperform benzyl bromides and iodides in this reaction provides an alternative choice when deciding on synthetic strategies.

Table 4.5 – Effect of varying halide leaving group on the reaction.

Entry	X	Yield, %
1	Cl	51
2	Br	45
3	I	0

Conditions: styrene (0.1 mmol), 68 (0.13 mmol), benzyl halide (0.3 mmol), FeBr₂ (0.01 mmol), Xantphos (0.01 mmol), TEAB (0.02 mmol), 2-MeTHF (3.0 mL), 60 °C, 16 h. Yield determined by GC using dodecane as an internal standard.

During the previous optimisation steps, the alkene was used as the limiting reagent. However, several metal-catalysed carboration reactions have shown that use of an excess of the alkene can lead to greater product formation.[122,298,300,313] For example, Koh's iron-catalysed alkenylboration of alkenes used 2.5 eq. of alkene, 1.0 eq. of alkenyl bromide and 2.0 eq. of B₂Pin₂.[122] To study the effect that an excess of styrene had on the reaction, both benzyl chloride and **68** were independently used as the limiting reagent (Table 4.6). A loss of reactivity was observed with benzyl chloride as the limiting reagent with an excess of styrene and **68**; the yield of **67** was reduced to 22% (Table 4.6, entry 1). When **68** was used as the limiting reagent and benzyl chloride and styrene were used in excess, the yield was further reduced to 16% (Table 4.6, entry 2). This shows that the organohalide and the diboron species are required in excess. Further probing of the extent of excess they are required in was investigated in the DoE optimisation (Section 4.2.2).

Table 4.6 – Effect of using styrene in excess.

Entry	Styrene loading, eq.	BnCl loading, eq.	68 loading, eq.	Yield, %
1	3.0	1.0	3.0	22
2	3.0	3.0	1.0	16
3	1.0	3.0	3.0	55

Conditions: limiting reagent 0.1 mmol, styrene, 68, benzyl chloride, FeBr₂ (0.01 mmol), Xantphos (0.01 mmol), TEAB (0.02 mmol), 2-MeTHF (3.0 mL), 60 °C, 16 h. Yield determined by GC using dodecane as an internal standard.

4.2.2 Design of Experiments (DoE) Optimisation

So far, the reaction was optimised by changing one variable at a time (OVAT). All variables are held constant except one that is varied, and the effect of this change is recorded and used as the optimum condition for subsequent variable optimisations. This is then repeated for the other variables until all the variables have been exhausted. The issue with the OVAT method is that it assumes all variables are independent of each other, which is often not the case and thus only a limited chemical space is explored in the reaction optimisation and a false optimum is found (Figure 4.3). The true potential of the system is very unlikely to be uncovered in this way. This process also generally requires a large investment of time and resources, especially when there are many components to the reaction mixture.
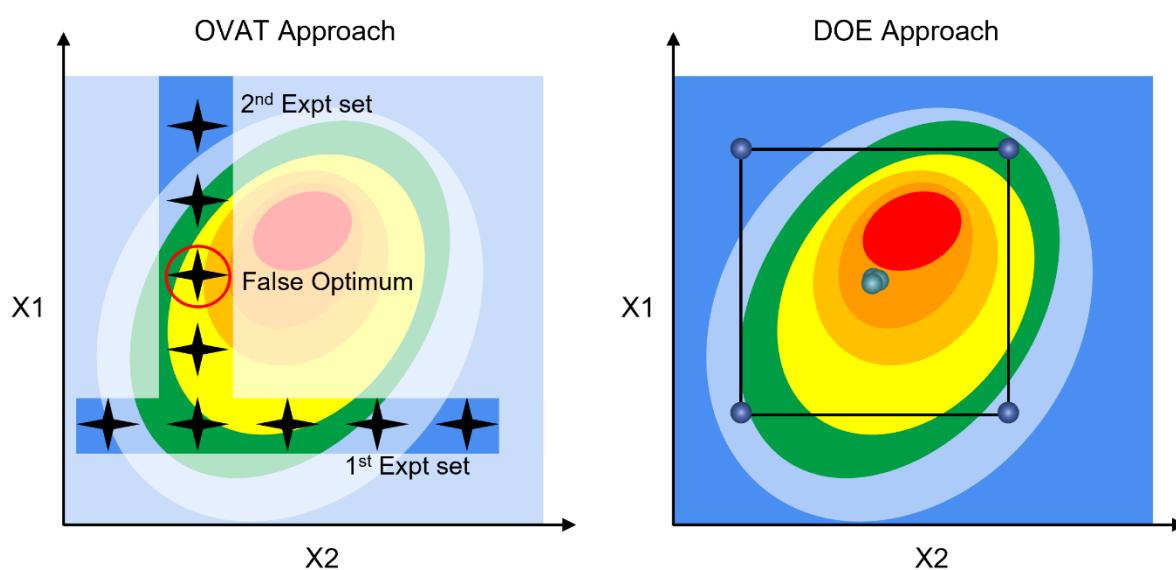
Figure 4.3 – How reaction space is uncovered through OVAT and DoE approaches. X = variable.

An alternative to the OVAT approach is the Design of Experiments (DoE) approach (also known as statistical or factorial experimental design).[328] It is a systematic and statistical approach to process optimisation that is widely used by chemical engineers and industrial chemists but has seen limited use in academic chemistry.[329] DoE involves planning, conducting, and interpreting a set of controlled experiments, where multiple factors are varied simultaneously to get a full picture of the 'reaction space'. This allows the user to evaluate a large number of reaction parameters in a relatively small number of experiments and also to examine the effects of individual variables as well as the combined effects of variables.[330,331] By setting limits for each variable and then investigating the extremes of each variable as well as the midpoint of all variables, the software is able to predict and map the full multi-dimensional chemical space in the optimisation and suggest

the optimum conditions. The midpoint is also repeated three times to allow the experimental error of the reaction to be calculated (Figure 4.3).

The selection of factors and ranges in the study need to be carefully considered, as poor choices can limit the efficacy of the model. A wide-enough range of each variable must be selected to enable the design to explore a sufficiently large reaction space. However, the extremes of the ranges must still give a non-zero result (*i.e.*, a positive yield). The 'continuous' variables used in this case were Xantphos (0.0–0.2 eq.), TEAB (0.0–0.3 eq.), BnCl (1.0–5.0 eq.) and **68** (1.0–5.0 eq.) loadings, temperature (30–75 °C), and reaction solvent volume (2.0–5.0 mL). Although the needs of Xantphos and TEAB were questionable, they were included anyway to see the full effect of their presence and to see if there were any combined effects with other variables. The minimum temperature was set at 30 °C, as this could be kept constant; temperatures below 30 °C were variable with the temperature of the lab. The study was carried out using Umetrics MODDE experimental design software. For the 6 variables, the software suggested 32 experiments, in addition to the 3 centre points, to determine the effect of each factor and combined factors. 7 experiments were carried out each day for 5 days, with the three midpoints completed on separate days to ensure reproducibility and that human error is limited (Table 4.7). Stock solutions were made for each reactant and reagent (except for **68** due to poor solubility) to minimise error and increase accuracy; the minimisation of experimental error is vital to construct an accurate DoE model.

Table 4.7 – Experiments for the DoE study of the iron-catalysed carboboration of styrene.

Entry	Ligand Loading, eq.	BnCl Loading, eq.	68 Loading, eq.	TEAB Loading, eq.	Temp., °C	Reaction Solvent Volume, mL	Yield, %
1	0.0	1.0	1.0	0.0	30	5.0	11
2	0.2	1.0	1.0	0.0	30	2.0	25
3	0.0	5.0	1.0	0.0	30	2.0	37
4	0.2	5.0	1.0	0.0	30	5.0	34

5	0.0	1.0	5.0	0.0	30	2.0	30
6	0.2	1.0	5.0	0.0	30	5.0	31
7	0.0	5.0	5.0	0.0	30	5.0	56
8	0.2	5.0	5.0	0.0	30	2.0	61
9	0.0	1.0	1.0	0.3	30	5.0	12
10	0.2	1.0	1.0	0.3	30	2.0	20
11	0.0	5.0	1.0	0.3	30	2.0	22
12	0.2	5.0	1.0	0.3	30	5.0	35
13	0.0	1.0	5.0	0.3	30	2.0	28
14	0.2	1.0	5.0	0.3	30	5.0	32
15	0.0	5.0	5.0	0.3	30	5.0	67
16	0.2	5.0	5.0	0.3	30	2.0	53
17	0.0	1.0	1.0	0.0	75	2.0	8
18	0.2	1.0	1.0	0.0	75	5.0	17
19	0.0	5.0	1.0	0.0	75	5.0	31
20	0.2	5.0	1.0	0.0	75	2.0	41
21	0.0	1.0	5.0	0.0	75	5.0	17
22	0.2	1.0	5.0	0.0	75	2.0	28
23	0.0	5.0	5.0	0.0	75	2.0	47
24	0.2	5.0	5.0	0.0	75	5.0	49
25	0.0	1.0	1.0	0.3	75	2.0	15
26	0.2	1.0	1.0	0.3	75	5.0	17
27	0.0	5.0	1.0	0.3	75	5.0	38
28	0.2	5.0	1.0	0.3	75	2.0	43
29	0.0	1.0	5.0	0.3	75	5.0	16
30	0.2	1.0	5.0	0.3	75	2.0	23
31	0.0	5.0	5.0	0.3	75	5.0	63
32	0.2	5.0	5.0	0.3	75	5.0	46
33	0.1	3.0	3.0	0.15	52.5	3.5	61
34	0.1	3.0	3.0	0.15	52.5	3.5	45
35	0.1	3.0	3.0	0.15	52.5	3.5	46

Conditions: styrene (0.1 mmol), 68, benzyl chloride, FeBr$_2$ (0.01 mmol), Xantphos, TEAB, 2-MeTHF, 16 h. Yield determined by GC using dodecane as an internal standard.

Two out of the three centre points gave very consistent results, with the third resulting in a greater yield; there is still a relatively small variation when compared to the scatter of other reactions in terms of yield of product formation (Figure 4.4).
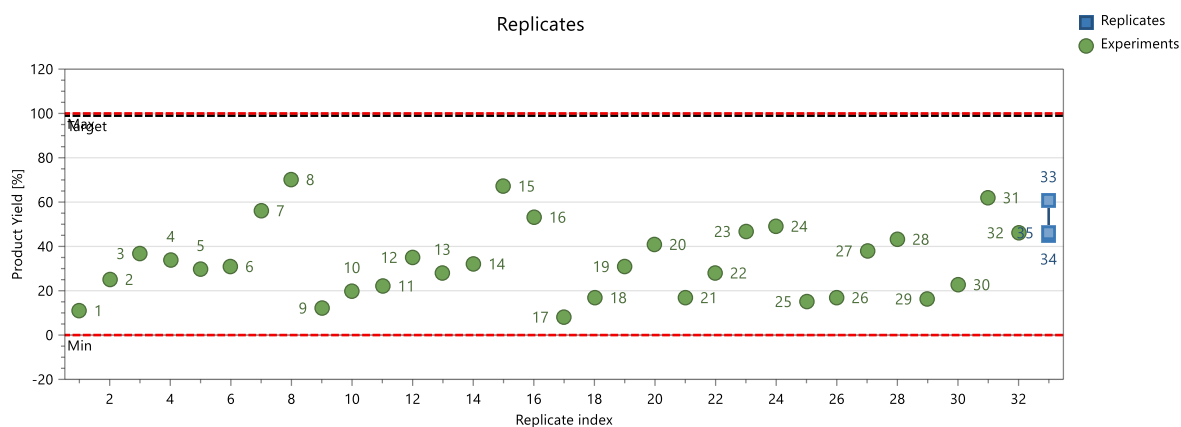
Figure 4.4 – Variation in yield of 67 across the 35 DoE experiments.

The model statistics are important in providing confidence in the designed model, data collection, and subsequently, the conclusions that are drawn from it. The summary of the fit of the DoE model indicates the reliability of the results (Figure 4.5). The R^2 shows the model fit, with a lower limit of 0.5 to show a significance of findings, in this case it is 0.822 which means that this model has a good fit. The Q^2 shows an estimate of future prediction precision. This must be greater than 0.1 to be significant and greater than 0.5 to be a good model. In this case we have a Q^2 of 0.741 showing that we can have a strong confidence in the prediction of optimised conditions suggested by the model. The model validity is a test of diverse model problems. A value of less than 0.25 indicates statistically significant model problems, such as anomalies, an incorrect model, or a transformation problem. Here the model validity is very high (0.912) showing that we can trust our model. The reproducibility of the reaction is also given, here it is 0.725. A value greater than 0.5 shows that the data can be trusted.

Summary of Fit

Product Yield
N=35, R2=0.822, RSD=8.101, DF=26, Q2=0.741
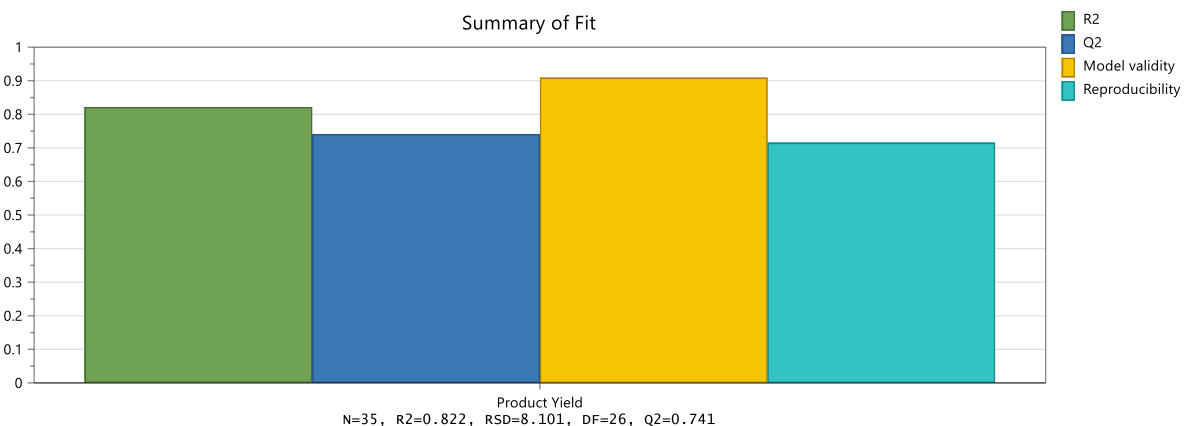
Figure 4.5 – Fit of the model obtained for the DoE for the yield of 67.

An observed vs predicted plot demonstrates the ability of the model to explain the results by showing the observed value vs the model's predicted value of each experiment. The closer the points are to the diagonal dotted line the more accurate the model. In this case most of the points are close to the line which shows that the model gives a good prediction of the data (Figure 4.6)

Observed vs. Predicted

N=34, R2=0.888, RSD=6.299, DF=25, Q2=0.811
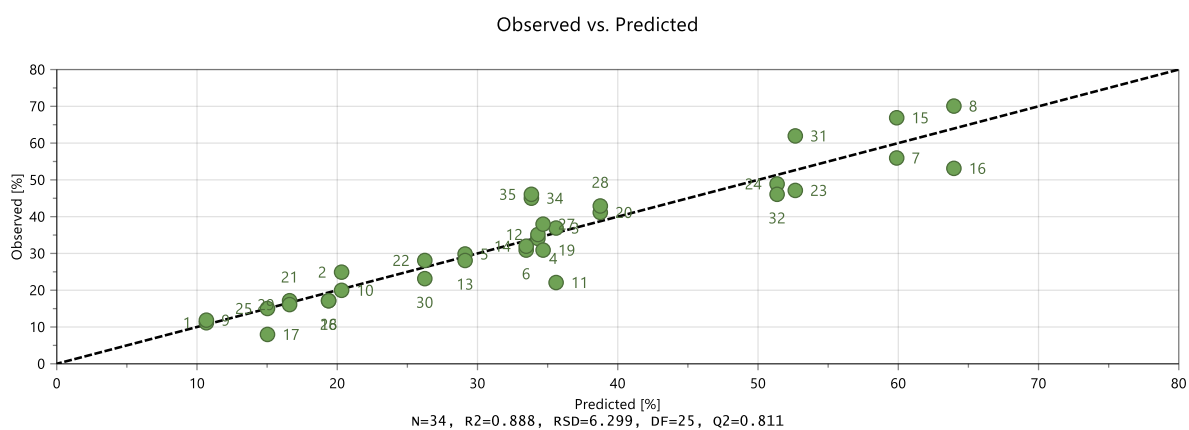
Figure 4.6 – How the observed experimental results align with the predicted results.

Analysis of the results provides insights into which of the continuous variables affect the product formation. These are illustrated in the form of a coefficient plot (Figure 4.7). Each bar represents a significant factor in the reaction and illustrates the effect on the product formation of increasing each factor from the mid-point in the design to the highest point in the design. The error bar is also shown for each coefficient, if this is greater than the size of the bar then it is considered to not be an important factor (*e.g.*, ligand loading (LL)). In this case, benzyl chloride loading has the largest effect, increasing the yield by 12.5% from the midpoint to the maximum. The only other significant positive factor is increasing the loading of **68**, which raises the yield by 8%. An increase

in the reaction temperature and solvent volume from the midpoint did not positively influence the reaction yield, but in fact slightly decreased it, although, the error is high in these examples. Xantphos and TEAB loading had a very minimal effect on product formation, proving that their impact on the reaction is limited.
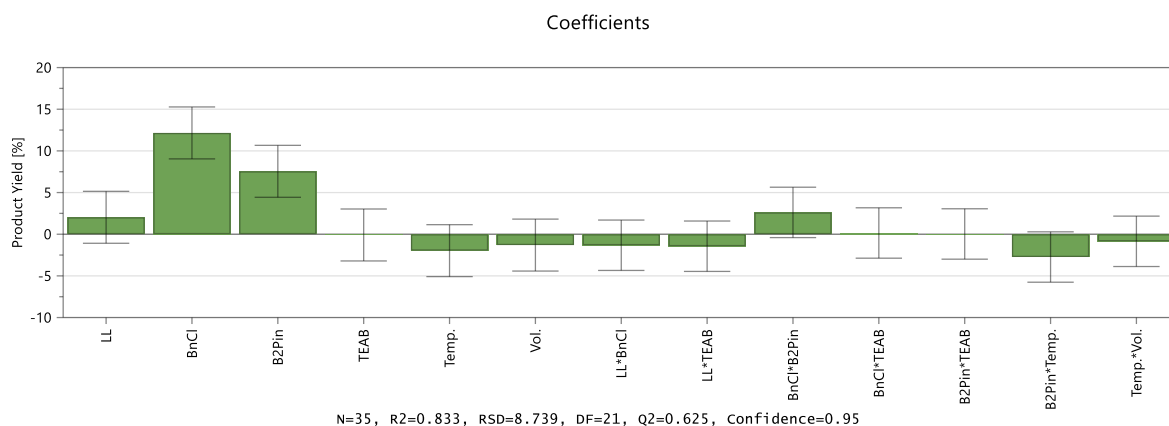
Figure 4.7 – Factors effecting the yield of 67.

A contour plot displays the predicted response values spanned by the factors incorporated in the model. This is an easy way to visualise how the variables affect the outcome, in this case how the loading of reactants and reagents effects the yield of the reaction (Figure 4.8). The reaction hotspots are highlighted in red and indicate that a higher yield can be obtained under these conditions. In this case, it is clear that high loadings of benzyl chloride and **68** are needed to reach higher yields. It shows that Xantphos can be removed from the reaction and maximum yields can still be obtained. It also predicts that lower temperatures may favour higher yields.
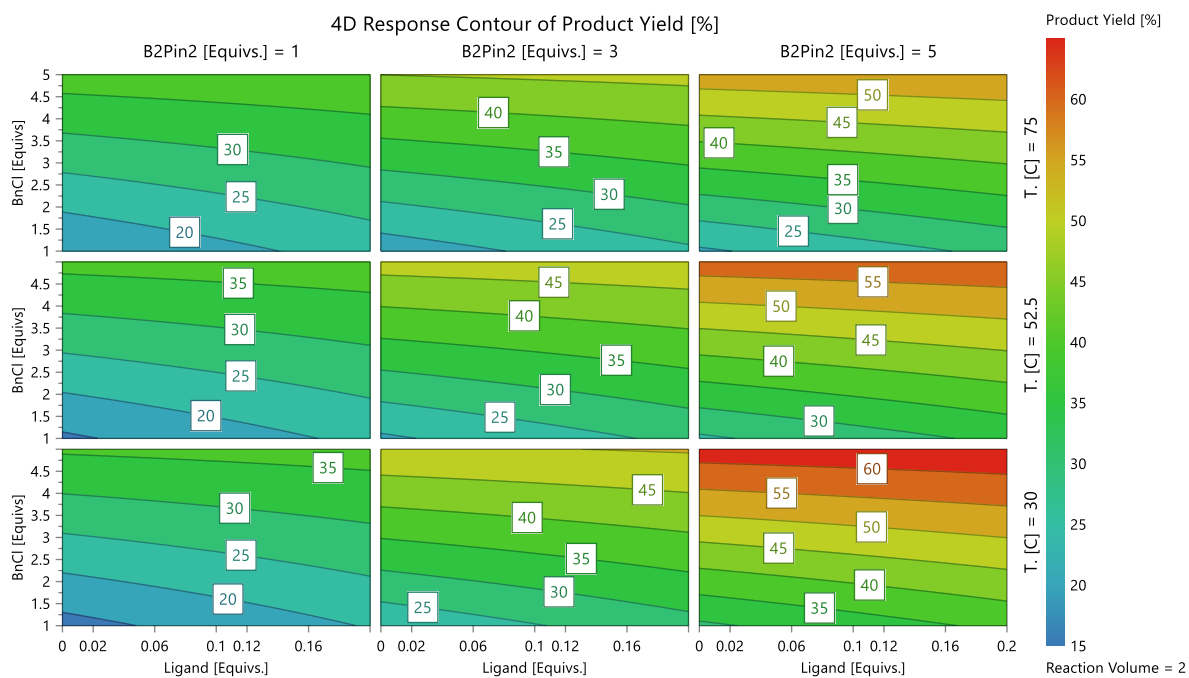
Figure 4.8 – 4D response contour plot indicating conditions where the greatest yield of 67 can be obtained.

The model predicted that the optimised conditions are: 5.0 eq. of benzyl chloride and **68**, 0.0 eq. of Xantphos and TEAB, a reaction volume of 2.0 mL and a reaction temperature of 30 °C and this will result in a yield of 64%. However, when these conditions were trialled three times, they resulted in yields of 42, 44, and 45% (Table 4.8, entries 1–3). It was observed that there was an issue with the solubility of **68** at this temperature and concentration. By increasing the temperature to 60 °C, with the reaction repeated three times, the yield increased to 62%, 65%, and 63% (Table 4.8, entries 4–6). Increasing the temperature further to 75 °C led to a decrease in yield to 46% (Table 4.8, 7–8).

Table 4.8 – Confirmation of DoE results.

Entry	Temp., °C	Yield, %
1	30	42
2	30	44
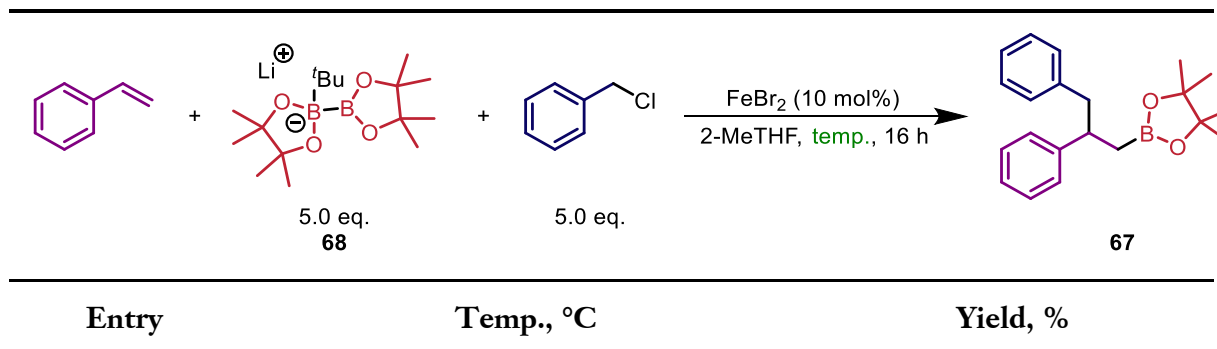
3	30	45
4	60	62
5	60	65
6	60	63
7	75	46
8	75	45

Conditions: styrene (0.1 mmol), 68 (0.5 mmol), benzyl chloride (0.5 mmol), FeBr$_2$ (0.01 mmol), 2-MeTHF (2.0 mL), 16 h. Yield determined by GC using dodecane as an internal standard.

The loading of benzyl chloride and **68** were very high, both 5.0 eq., and this was the upper limit of the variable set in the DoE study. As the maximum limit was 5.0 eq., additional increases of this were not modelled and therefore could not be predicted in the suggested optimised conditions. The effect of changing these loadings was studied to determine whether similar or greater yields could be obtained with reduced loadings, or to see whether greater amounts of either reactant (that had not been modelled) would further increase the yield (Table 4.9). Whilst holding **68** at 5.0 eq., the eq. of benzyl chloride were altered from 1.0 to 6.0 in increments of 1.0 (Table 4.9, entries 1–6). The result of this showed that there was a small gradual increase in yield as the eq. were increased to 5.0 but no further improvement when the eq. were increased to 6.0. Next, the eq. of benzyl chloride were held constant at 5.0 and the eq. of **68** were varied from 1.0 to 6.0 with increments of 1.0 (Table 4.9, entries 7–12). This resulted in an increase in yield up to 4.0 eq. but then a slight reduction in yield when the eq. were increased further. To confirm these as the optimum eq. and to see whether there was a combined effect of both benzyl chloride and **68**, the eq. of **68** was held at 4.0 eq. and the amount of benzyl chloride was changed from 1.0 to 6.0 eq. with increments of 1.0 (Table 4.9, 13–18). In this case, we again saw an optimum of 5.0 eq. of benzyl chloride.

Table 4.9 – Effect of changing the loading of benzyl chloride and 68.

Entry	68 Loading, eq.	BnCl Loading, eq.	Yield, %
1	5.0	1.0	24
2	5.0	2.0	33
3	5.0	3.0	49
4	5.0	4.0	58
5	5.0	5.0	65
6	5.0	6.0	63
7	1.0	5.0	28
8	2.0	5.0	46
9	3.0	5.0	55
10	4.0	5.0	72
11	5.0	5.0	63
12	6.0	5.0	58
13	4.0	1.0	26
14	4.0	2.0	39
15	4.0	3.0	58
16	4.0	4.0	64
17	4.0	5.0	72
18	4.0	6.0	68

Conditions: styrene (0.1 mmol), 68, benzyl chloride, FeBr$_2$ (0.01 mmol), 2-MeTHF (2.0 mL), 60 °C, 16 h. Yield determined by GC using dodecane as an internal standard.

One thing that had not been explored so far in the optimisation was the loading of FeBr$_2$. Thus, the loading was changed to 5 and 20 mol% (Table 4.10). The result of lowering the loading from

10 to 5 mol% resulted in a significant drop in yield to 41%. The loss of product formation is likely to be due to having less catalyst in the reaction mixture. Increasing the loading to 20 mol% led to a decrease in yield to 37%. This significantly lower yield could be due to over saturation of the system or aggregation of iron species leading to a decrease in catalytic activity.

Table 4.10 – Effect of changing the loading of FeBr₂.

Entry	FeBr$_2$ Loading, mol%	Yield, %
1	5.0	41
2	10	72
3	20	37

Conditions: styrene (0.1 mmol), 68 (0.4 mmol), benzyl chloride (0.5 mmol), FeBr₂, 2-MeTHF (2.0 mL), 60 °C, 16 h. Yield determined by GC using dodecane as an internal standard.

Throughout the optimisation, the 2,1-regioisomer (**67**) was formed exclusively, with no observation of the 1,2- and 1,1-regioisomers. However, along with **67**, two side products were seen in very low amounts. These were bibenzyl, formed from the homocoupling of benzyl chloride, and benzylboronic acid pinacol ester, formed from the borylation of benzyl chloride (Figure 4.9). Removal of these side products could be achieved by column chromatography.

bibenzyl benzylboronic acid pinacol ester
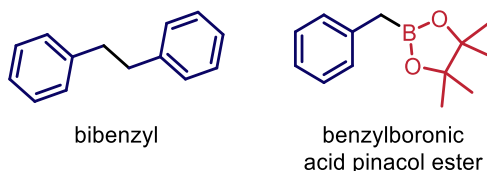
Figure 4.9 – Side products observed in small amounts in the reaction.

The final optimised conditions developed from a mixture of OVAT and DoE techniques are: FeBr$_2$ (10 mol%), styrene (1.0 eq.), benzyl chloride (5.0 eq.), **68** (4.0 eq.), 2-MeTHF (50 mM, based on styrene) at 60 °C (Scheme 4.10).
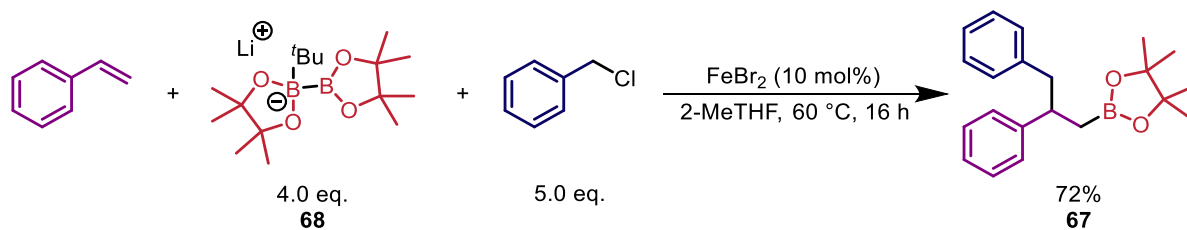
Scheme 4.10 – Optimised conditions of the iron-catalysed carboboration of styrene.

4.3 Determining Whether Iron is Responsible for the Catalytic Behaviour

Before ascertaining the functional group tolerance of the reaction, control experiments were undertaken to show that the reaction was indeed iron-catalysed (Table 4.11). When an iron source was omitted from the reaction, there was no product formation observed. This indicates that the iron source is responsible for the observed reactivity, and not an impurity in the other reactants. To further probe whether the activity was due to an impurity in the iron source, iron sources from a range of different suppliers were trialled alongside higher purity $FeBr_2$. Switching to different suppliers did not affect the overall product formation and the use of higher purity $FeBr_2$ (99.995%) also had no effect.

Table 4.11 – Control experiments to show iron is the catalyst.
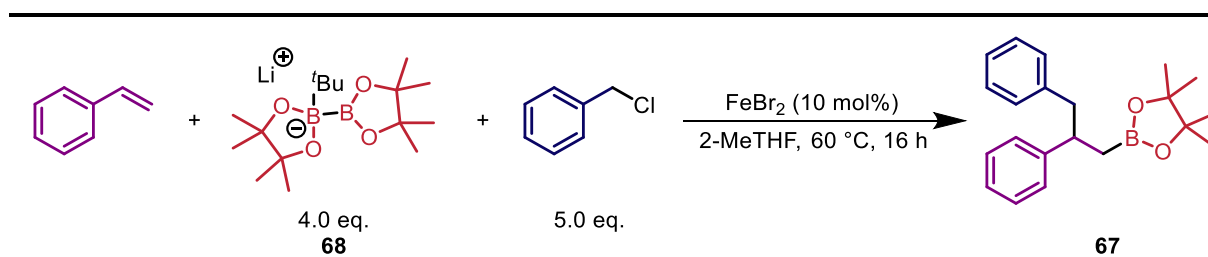
Entry	Fe salt, purity, supplier	Yield, %
1	N/A	0
2	$FeBr_2$, Acros, 98%	72
3	$FeBr_2$, Aldrich, 98%	72
4	$FeBr_2$, Alfa Aesar, 98%	71
5	$FeBr_2$, Alfa Aesar, 99.995%	73
6	$FeCl_3$, Aldrich, 98%	46
7	$FeCl_3$, Aldrich, 99.99%	45

Conditions: styrene (0.1 mmol), 68 (0.4 mmol), benzyl chloride (0.5 mmol), $FeBr_2$ (0.01 mmol), 2-MeTHF (2.0 mL), 60 °C, 16 h. Yield determined by GC using dodecane as an internal standard.

ICP-MS, conducted by Johannes Krieger of Merck Healthcare, of three 100 mg samples of each 98% and 99.995% purity $FeBr_2$ showed palladium loadings of 23–200 and 76–281 ppb respectively. As the reaction does not proceed in the absence of an iron source, it is highly unlikely that the reaction is catalysed by anything other than iron.

4.4 Functional Group Tolerance

4.4.1 Robustness Screen

When a new methodology is created, or an improvement of a previous methodology is reported, the aim is for this process to be taken on by others in the scientific community. In particular, it is desirable for the new process to be adopted by industrial chemists, where the technique can have a greater impact. However, this is often not the case and there are long delays between a methodology being created and it being incorporated into the chemists' toolkit. One of the reasons for this delay is a lack of information regarding a new methodology's application beyond the idealised conditions in the original report. One of these pieces of desired information is the functional group tolerance of the reaction *i.e.*, the stability of specific chemical moieties under the reaction constraints.

Sometimes, examples of a methodology's use in the synthesis of a specific drug molecule or an intermediate of a drug molecule are shown. However, this process often requires several steps to synthesise the substrates that are subsequently reacted in the new methodology, which can be time-consuming. The most common way to show the functional group tolerance of a reaction is through a substrate scope, often changing one substituent on a substrate and seeing the effect, this can also be very time-consuming. A substrate scope has its limitations when assessing functional groups tolerance in a wider synthesis. Often the functional group is placed close to the reactive centre, which then strongly effects the sterics and electronic limitations of this position. However, in a late-stage synthesis of a drug target, this functional group may be much further away from the reactive centre and have a significantly weakened steric and electronic influence on it. Therefore, when transferring a methodology created in an academic group to mass use in industrial processes, the true effect of having a substituent in your substrate can not be fully understood from a substrate scope. A substrate scope can also suffer from the author's bias, often unintentional. Specific substrates that are thought likely to be successful are included, whereas more challenging examples may not be attempted.[332] Substrates that are unsuccessful are not always reported, leading to a lack of transparency and a limited understanding of the reaction.

To overcome the issues outlined above, a technique has been developed by Glorius over the last ten years, named a 'robustness screen'.[203] The technique involves adding a stoichiometric amount of an additive to the standard reaction under optimised conditions. The product yield, remaining additive, and any remaining starting materials are then measured by GC.[204] Each additive has a

different functional group in its makeup, and when added to the standardised reaction both the additive survival and the effect of the formation of the product can quickly be evaluated. When compared to a standard substrate scope, the use of a standardised group of additives means that substrates do not have to be bought or synthesised and which therefore saves time and money. Further to this, it removes any bias from the scientist; the same additives are used by the whole community, making direct comparisons between methodologies straightforward. Originally Glorius used 41 additives; he subsequently showed that this can be reduced to 15 with the same benefits being observed (Figure 4.10).[205] This makes the technique highly accessible to chemists, enabling it to be adopted worldwide.
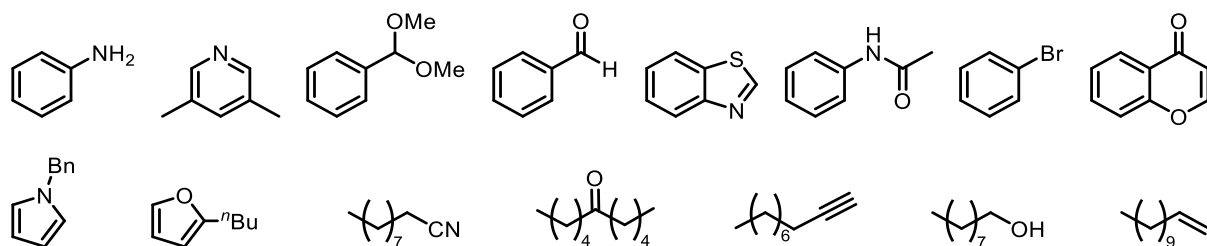
Figure 4.10 – The 15 additives used in a robustness screen developed by Glorius.

For these reasons, we wanted to incorporate a robustness screen into the development of this reaction. The 15 additives were subjected to the standardised optimised reaction conditions and the amount of product, additive, and starting materials were measured by GC (Table 4.12). A simplified way to analyse the success of the reaction, rather than just yield, is to look at the percentage yield compared to the standard yield (%oS).

Table 4.12 – Effect of the introduction of an additive on the reaction yield.

Entry	Additive	Yield, %	%oS	Additive Recovered, %	Styrene Recovered, %
1	No additive	71	n/a	n/a	0
2	aniline	57	80	68	0
3	3,5-dimethylpyridine	52	73	54	0

4	decanenitrile	63	89	12	0
5	benzothiazole	53	75	30	0
6	1-decyne	1	1	14	81
7	1-nonanol	3	4	0	44
8	1-dodecene	63	90	53	0
9	2-butylfuran	70	99	98	0
10	1-benzyl-1H-pyrrole	66	93	0	0
11	(dimethoxymethyl)benzene	63	89	96	0
12	benzaldehyde	36	51	0	0
13	5-decanone	61	86	18	0
14	N-phenylacetamide	5	7	28	0
15	bromobenzene	61	86	95	0
16	4-chromanone	30	42	27	0

Conditions: styrene (0.1 mmol), 68 (0.4 mmol), benzyl chloride (0.5 mmol), additive (0.1 mmol) FeBr$_2$ (0.01 mmol), 2-MeTHF (2.0 mL), 60 °C, 16 h. Yield determined by GC using dodecane as an internal standard.

The additive survival in general was quite poor, with 8 out of the 15 additives being recovered between 0 and 33% (Figure 4.11).
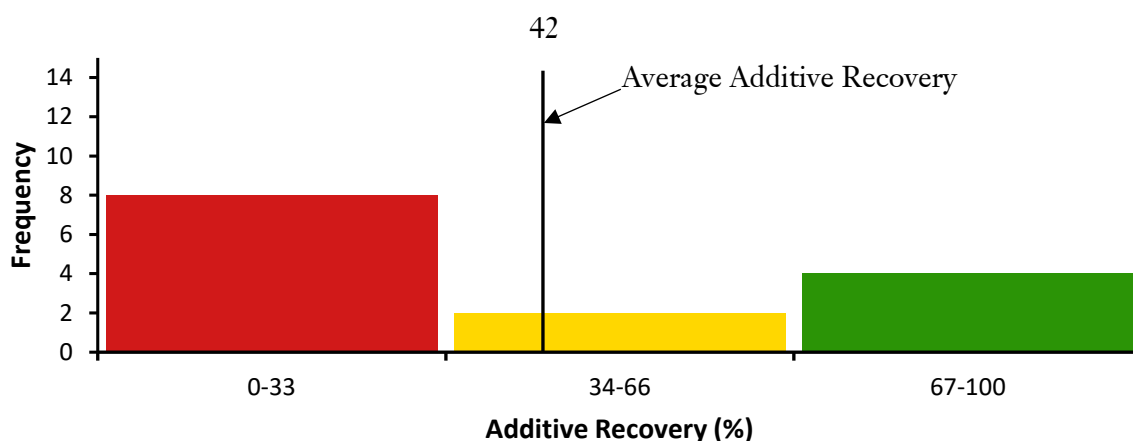
Figure 4.11 – Additive recovery after being subjected to the reaction conditions.

Aniline, 2-butylfuran, (dimethoxymethyl)benzene, and bromobenzene were recovered in good amounts and show promise that they can be used as substituents in at least one of the coupling partners in the reaction. The survival of bromobenzene shows promise, as it is an electrophile that could react in the carboboration reaction itself and, therefore, if included in the any of the substrates could lead to side reactions. Although bromobenzene was recovered in good yields, it was also able to act as the electrophile in the reaction, as the product, **69**, was observed in low amounts in the reaction mixture when analysed by GCMS (Figure 4.12). This indicates that the reaction might work with aryl halides as well benzyl halides. If chlorobenzene was used instead, we might expect to see greater formation of **69**, as greater activity was observed when benzyl chloride was used compared to benzyl bromide (Table 4.5). Amines have had limited success in iron-catalysed Suzuki cross-couplings when ^{t}BuLi activated boronates are used,[87] and the good recovery of aniline shows promise that an amine could be incorporated into either substrate here, which would then allow for further functionalisation of the product. 2-Butylfuran was also recovered in good amounts, which gives insights into the potential incorporation of oxygen based heteroaryls, which are important in active pharmaceutical products.[333]

Only 14% of 1-decyne was recovered after it was added to the reaction mixture. Analysis of the reaction mixture by GCMS showed that **70** was formed in small amounts (Figure 4.12). This suggests that under these reaction conditions, the carboboration of alkynes can also be achieved. Along with **70**, large amounts of the addition of a BPin unit to the alkyne were also observed, giving **71**. Decanenitrile was also recovered in low amounts. In the GCMS trace of this reaction, **72** was observed, formed from the benzyl chloride and the aqueous work up. Whilst 53% of 1-dodecene was recovered after the reaction, approximately half of it was not recovered. Observed in the GCMS trace of its reaction mixture was the carboboration product of itself, **73**. This is a good indicator that unactivated alkenes could be used in the reaction, although when there is a more activated alkene present this reacts preferentially. The lack of compatibility of ^{t}BuLi activated boron reagents with substrates containing alcohol groups has been previously reported,[82] so it is no surprise here that the 1-nonanol did not survive the reaction conditions. In the GCMS trace of this reaction, **74** was observed. It is likely that for alcohol groups to be incorporated in the final product, they must first be protected. *N*-phenylacetamide was not particularly tolerated in the reaction, and **75** was observed in the reaction mixture. The formation of **75** is particularly exciting as it could lead to the development of an iron-catalysed amination reaction. 1-Benzyl-1*H*-pyrrole is light-, air-, and moisture-sensitive and therefore it cannot be determined whether the

moiety is stable under the reaction conditions or not, as the subsequent work-up and analysis by GC could lead to degradation. Carbonyl groups such as aldehydes and ketones have also shown poor tolerability in iron-catalysed reactions and therefore the poor recovery of benzaldehyde and 5-decanone are not surprising here. Carbonyls are susceptible to nucleophilic attack and substitution, although these products were not observed in either reaction mixtures when analysed by GCMS.
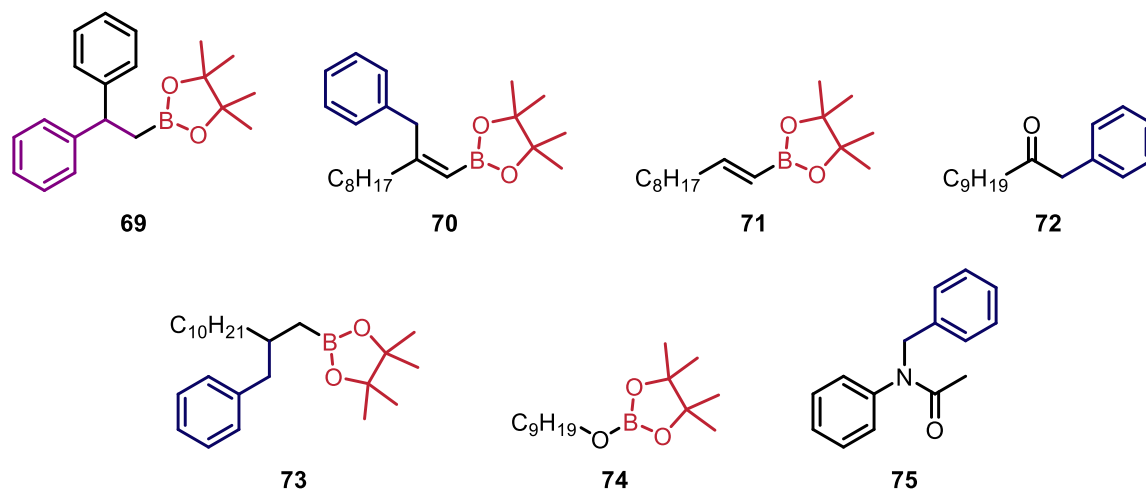
Figure 4.12 – Side-products observed in the reaction mixture by GCMS.

The effect of additives on the percentage yields compared to the standard yield (%oS) was studied (Figure 4.13). In general, the yield has not changed much with the use of additives: 7 out of 15 have a %oS greater than 86% and a further 3 have a %oS greater than 66%. *N*-phenylacetamide, 1-decyne and 1-nonanol were not tolerated in the reaction at all. One would expect there to be some correlation between additive recovery and the yield of **67**, with high additive recoveries being observed with high yields. However, this is not always seen here. For example, when decanenitrile is the additive, a %oS of 89% was observed but an additive recovery of only 12% was obtained. The lack of correlation is likely to be due to the high equivalents of benzyl chloride and **68** used. This could result in some of the reactants reacting with the additives and leading to poor recovery, but there still being a sufficient amount of the reactants remaining to form the desired product.
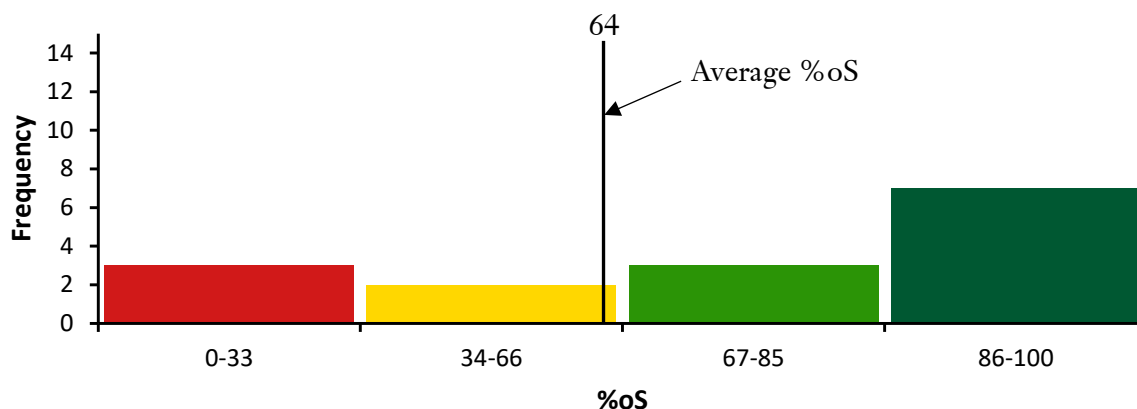
Figure 4.13 – %oS after the introduction of additives on the reaction.

The additives can be grouped into bases, nucleophiles, and electrophiles, and then generalisations about the subsets can be made (Figure 4.14). The highest tolerance (when based on %oS) was seen when bases were used as the additive, whereas the lowest was with electrophiles. When tolerance is based on additive recovery none of the subsets stand out, but the highest tolerance was seen with nucleophiles and the lowest seen with electrophiles. However, grouping these substrates might not be the best way to assess the data. For example, hydroxyl groups are not tolerated but this may not be based on their nucleophilicity but rather its acidic proton that can react with **68**. Therefore, not all generalisations can be taken as certain that other functional groups in the same subset won't be tolerated in the reaction.

Figure 4.14 – Effect of the use of groups of additives on the additive recovery and %oS.

In summary, a rapid assessment of the functional group tolerance under the reaction conditions was carried out by performing a robustness screen. Compared to a normal substrate scope this was significantly quicker and more information could be gained from the additive recovery to see if a

functional group is tolerated. In this example, a robustness screen may not provide a complete picture of the functional group tolerance of this reaction. Due to the large excess of benzyl chloride and **68** a correlation between yield and additive recovery was not always seen, with some high yielding reactions having low additive recoveries. In these examples, the substrates would need to be trialled to see how they fared under the reaction conditions.

4.4.2 Scope and Limitations

To further assess the functional group tolerance and the scope and limitations of the reaction, a series of alkenes were subjected to the optimised reaction conditions and the yields recorded (Figure 4.15). When 4-methylstyrene was trialled in the reaction, there was a reduction in yield to 54% (**76**). From the robustness screen we expected that ethers would be tolerated in the reaction, as when (dimethoxymethyl)benzene was used as an additive the %oS was 88% and 96% of the additive was recovered. Trial of 4-methoxystyerene in the reaction confirmed this, as only a slight reduction in yield, to 61%, was observed (**77**). Fluoro substituents were not investigated in the robustness screen, so their tolerance in the reaction was unknown. Pleasingly, both 4-fluorostyrene (**78**, 68%) and 4-trifluoromethylstyrene (**79**, 65%) worked very well in the reaction with only slight drops in yield compared to when styrene was used. Fluorine groups are widely seen in pharmacologically active products and therefore their tolerance here is highly desired.[334] Anilines are not commonly tolerated in iron-catalysed cross-couplings, but the robustness screen showed that a primary amine might be tolerated in this reaction; 4-vinylaniline was subsequently trialled in the reaction and the desired product was formed in 52% yield (**81**). Not only are anilines widely seen in commercial products, but they also offer a way to further diversify the product and add molecular complexity.[335]

Two heteroaromatic styrene derivatives were trialled in the reaction, 4-vinylpyridine and 2-vinylthiophene. 3,5-Dimethylpyridine was used as an additive in the robustness screen with a %oS of 80% and an additive recovery of 54%. Based on this data, it might be predicted that 4-vinylpyridine would be tolerated but with reduced yields of desired product. However, 4-vinylpyridine was not tolerated at all in the reaction, with trace product not observed in either ^{1}H-NMR or GCMS spectra. 2-Vinylthiophene was tolerated and gave a yield of 46% (**81**). Switching to a biaryl with 2-vinylnaphthalene gave slightly improved yields of 73% (**82**).

The robustness screen incorporates 3 different carbonyls as part of the 15 additives. In all three cases additive recovery was less than 30%, and the highest %oS recorded was 50%. When 4-vinylbenzoic acid was trialled in the reaction no product was observed. However, when methyl-4-vinylbenzoate was trialled activity was seen and a yield of 45% was recorded (**83**). This shows that although perhaps the carbonyl groups do lead to a reduction in yield, when there is an acidic proton there is a significant deleterious effect on the reaction. It is likely that the acid reacted with **68**. In general, both electron donating and electron withdrawing groups were tolerated similarly.

Increasing the steric bulk at the α position of the styrene led to decreases in yield. When a methyl group was employed in this position the yield dropped to 38% (**85**), this dropped further to 32% when exchanged for a phenyl group (**84**). This shows the limits of using more sterically encumbered alkenes, as the yield has dropped significantly with only a small addition to the steric bulk of the reaction centre.
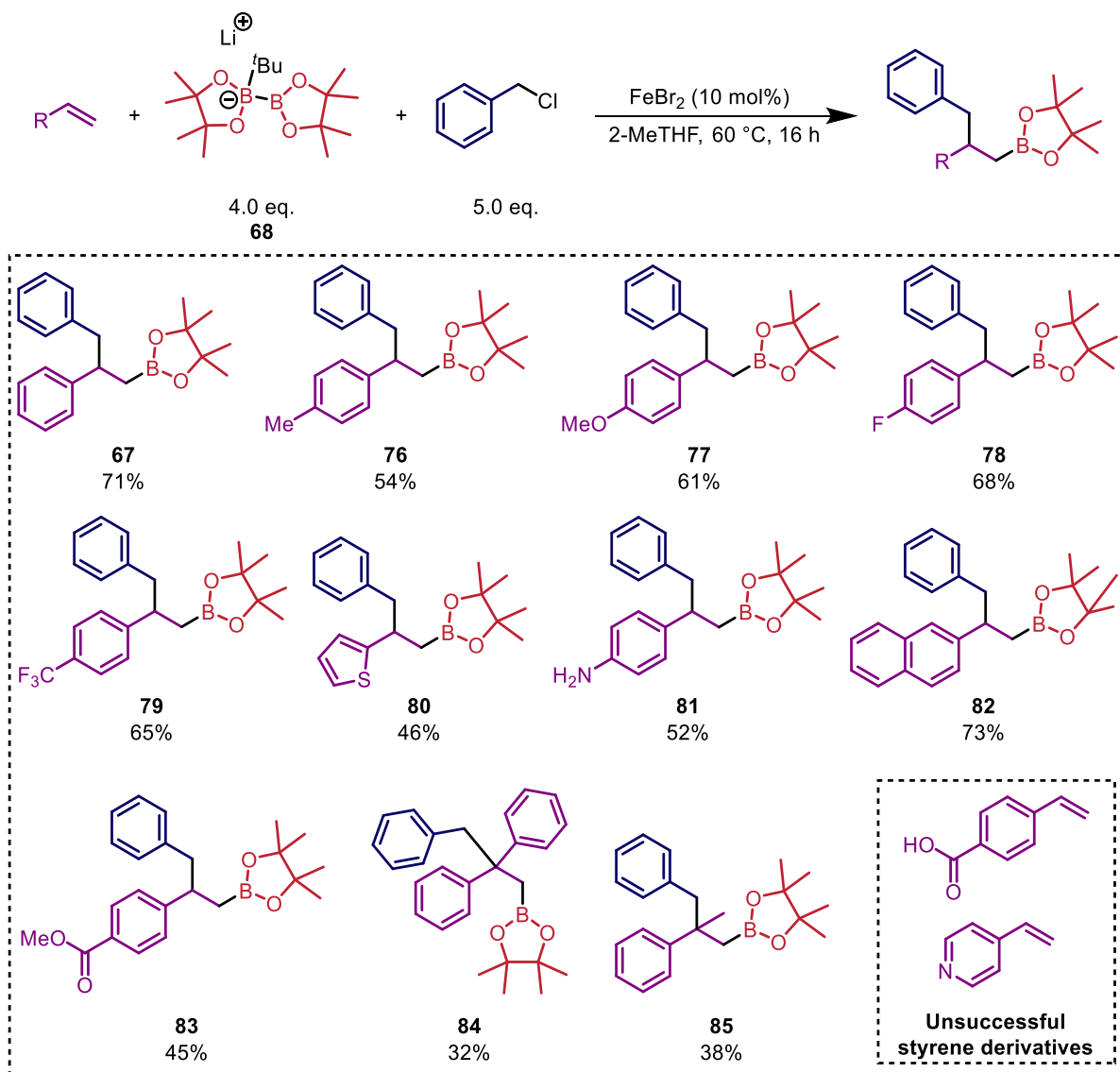
Figure 4.15 – Scope of styrene derivatives in iron-catalysed carboration of alkenes. Conditions: alkene (0.5 mmol), 68 (2.0 mmol), benzyl chloride (2.5 mmol), FeBr₂ (0.05 mmol), 2-MeTHF (10 mL), 60 °C, 16 h. Isolated yields shown.

Moving away from styrene derivatives, attempts using other mono-substituted alkenes proved unsuccessful (Figure 4.16). The products formed from vinylboronic acid pinacol ester (**86**), vinyltrimethylsilane (**87**), 1-octene (**88**), vinylcyclochexane (**89**), and methyl acrylate (**93**) could

only be seen in small amounts in ^{1}H NMR and GCMS spectra. This was disappointing as these alkenes had proven to be successful in copper-catalysed carboboration reactions.[302] In the robustness screen when 1-dodecene was used as an additive, the product of the carboboration of this was also observed in the reaction mixture (**72**). However, here when 1-octene was trialled very little product formation was observed (**88**). In these cases, it might be that harsher conditions or the use of a ligand are required to get significant product formation. Koh's iron-catalysed alkenylboration of alkenes required the use of dppe with unactivated alkenes.[122] Using 1,2-disubstituted internal alkenes also gave very limited product formation (**90–92**). This was not unexpected after previous results show that increased steric bulk reduces product formation significantly.
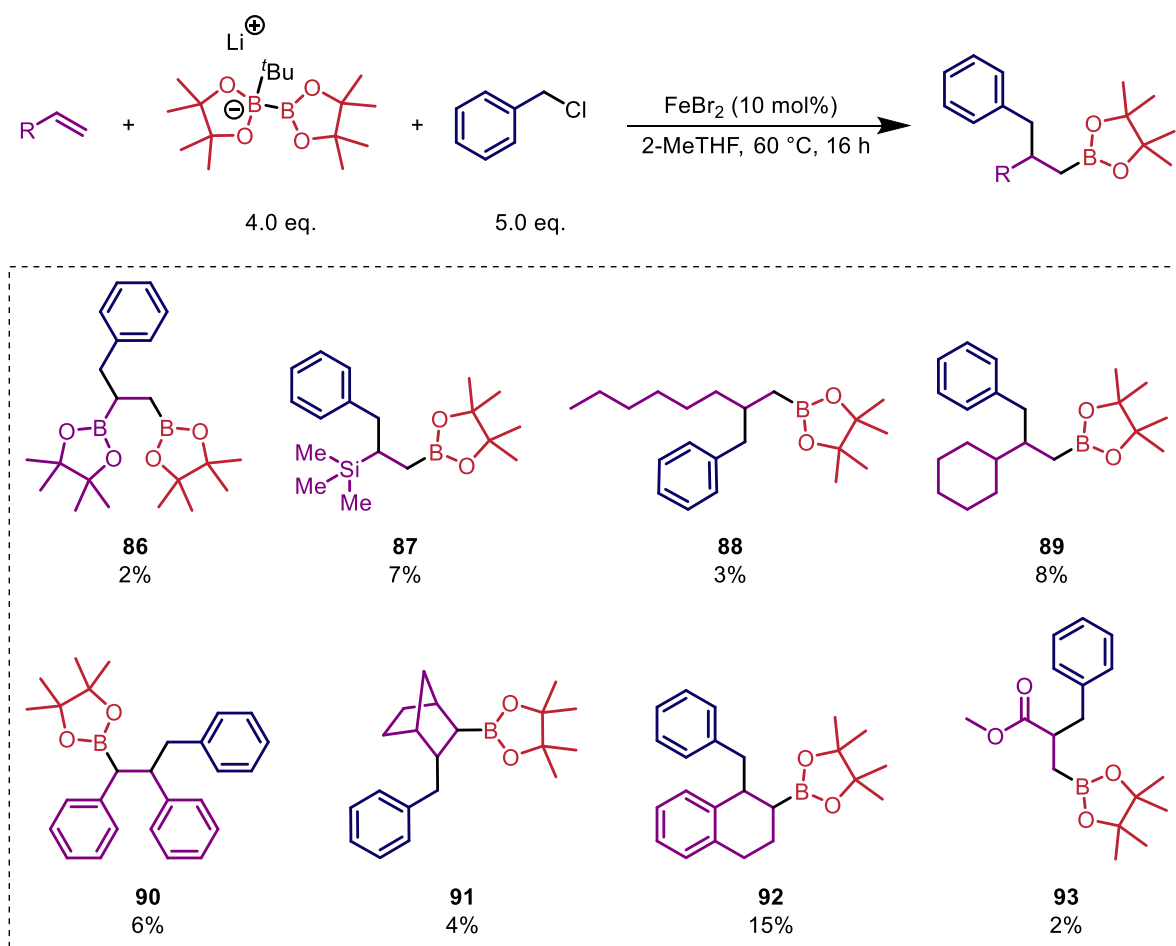
Figure 4.16 – Scope of alkenes in iron-catalysed carboboration of alkenes. Conditions: alkene (0.5 mmol), 68 (2.0 mmol), benzyl chloride (2.5 mmol), FeBr₂ (0.05 mmol), 2-MeTHF (10 mL), 60 °C, 16 h. Yields determined by ^{1}H NMR spectroscopy using 1,3,5-trimethoxybenzene as an internal standard.

The scope of electrophiles that could be used in the reaction was next investigated (Figure 4.17). Incorporating a methyl group into the reaction, by using 4-methylbenzyl chloride, led to a

decrease in yield to 57% (**94**). Fluoro substituents worked well when incorporated into the alkene. However, when 4-fluorobenzyl chloride, 4-trifluoromethylbenzyl chloride, and 4-(trifluoromethoxy)benzyl chloride were used, the yields decreased to 30 (**95**), 39 (**97**), and 45% (**98**), respectively. Suggesting that to incorporate fluoro groups into the product most efficiently, they must be added *via* the alkene rather than the electrophile. Although using a methyl ester worked reasonably well in the alkene screen, using methyl-4-(chloromethyl)benzoate proved deleterious to product formation, with a low yield of 19% being recorded (**100**). Using the much bulkier 1-(chloromethyl)naphthalene, only formed the desired product in 31% yield (**99**). Suggesting that increased steric bulk reduces product formation. Incorporating an electron-donating group into the electrophile, by using, 4-methoxybenzylchloride gave a reasonable yield of the desired product (**96**, 50%). In general, it seems that electron-donating groups outperform electron-withdrawing groups. When benzaldehyde was used as an additive in the robustness screen, the %oS was 50% and none of the benzaldehyde was recovered. So, it was not surprising to see that 4-(chloromethyl)benzaldehyde was not tolerated in the reaction. As seen in the alkene screen, carboxylic acids were also not tolerated in the reaction when incorporated into the electrophile. A nitro group was not tested in either the robustness screen or the screen of suitable alkenes, so its tolerance in the reaction was unknown. Thus, 4-nitrobenzyl chloride was trialled in the reaction. However, no product formation was observed by either ^{1}H-NMR spectroscopy or GCMS. This is in line with previously reported iron-catalysed cross-coupling reactions.[336] This could be due to intolerance of extremely electron-withdrawing groups or due to the ability of the nitro substituent to form or combine with radical species. As seen in the alkene screen, pyridines were not tolerated in the reaction; when 4-(chloromethyl)pyridine was trialled in the reaction, the resulting product was not observed in either the ^{1}H-NMR or GCMS spectrum. The robustness screen showed that aryl halides might be able to be used as the electrophilic partner in the reaction. However, when chlorobenzene was used in the reaction only trace amounts of product were observed in the GCMS spectrum. Attempts to use unactivated alkyl chlorides were also unsuccessful in the reaction. Use of 1-chloropropane did not lead to any product formation showing that more activated alkyl halides are currently needed for the reaction to proceed.
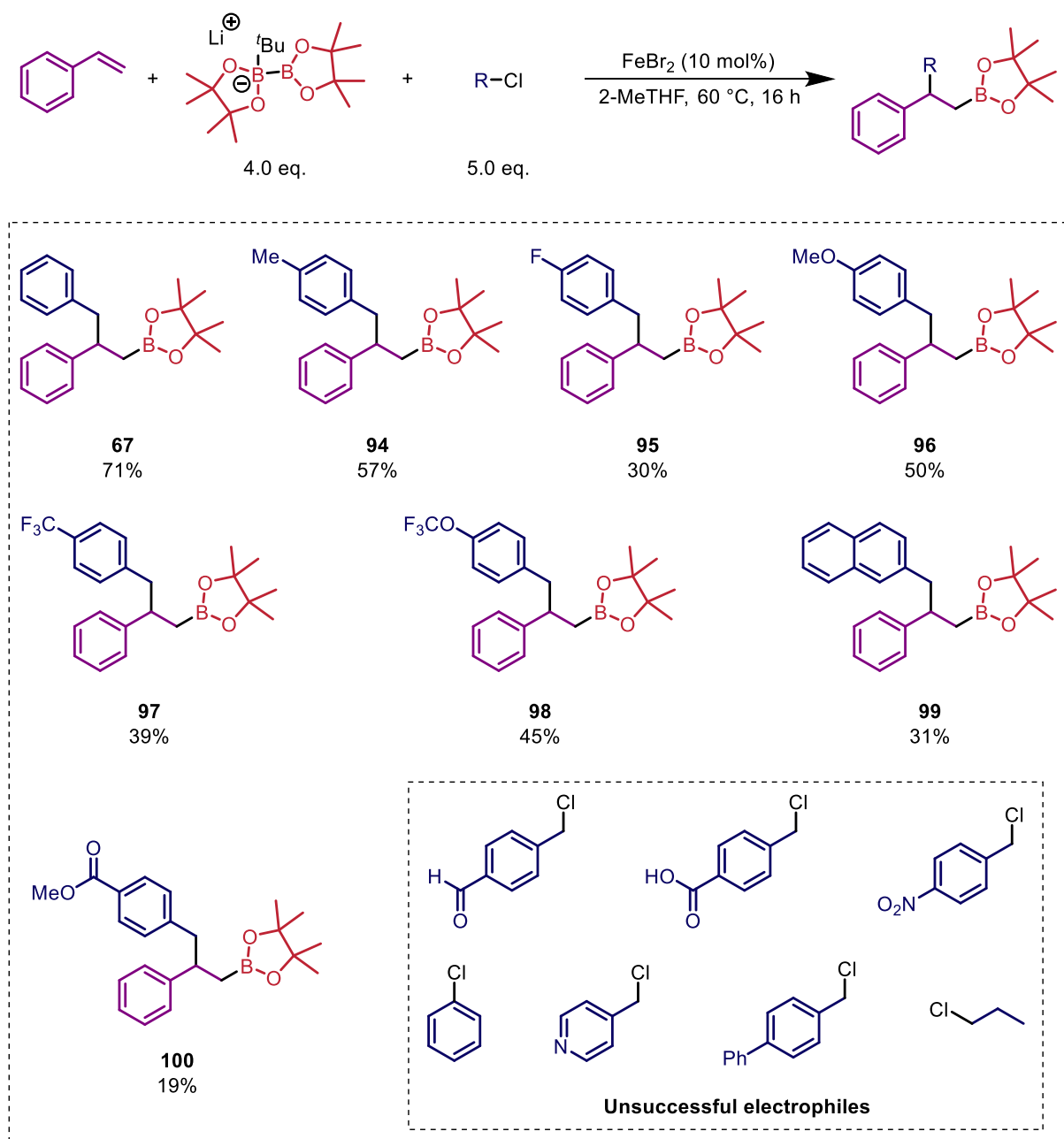
Figure 4.17 – Scope of electrophiles in iron-catalysed carboboration of alkenes. Conditions: styrene (0.5 mmol), **68** (2.0 mmol), electrophile (2.5 mmol), FeBr$_2$ (0.05 mmol), 2-MeTHF (10 mL), 60 °C, 16 h. Yields determined by ^{1}H-NMR spectroscopy using 1,3,5-trimethoxybenzene as an internal standard. Data collected by MSci student Jordan Garrard under the supervision of the author.

Although pinacol derived boronic esters are one of the most used in synthesis, other boronic esters have shown improved results when employed instead. Neopentyl glycol derived boronic esters have been utilised in cobalt-[42,337] and palladium-catalysed[338] Suzuki cross-couplings and a nickel catalysed carboxylation of organoboronates.[339] Catechol derived boronic esters have been utilised in a ruthenium-catalysed Suzuki cross-coupling.[340] Due to this, we wanted to see if other diboron reagents could be used in this reaction (Figure 4.18). When bis(neopentylglycolato)diboron was

used, the yield dropped to 45% (**101**), and when bis(catecholato)diboron was used there was no product observed (**102**). This shows that bis(pinacolato)diboron is the optimum diboron reagent to use under these conditions, but if required a neopentyl glycol derived boronic ester can also be installed.
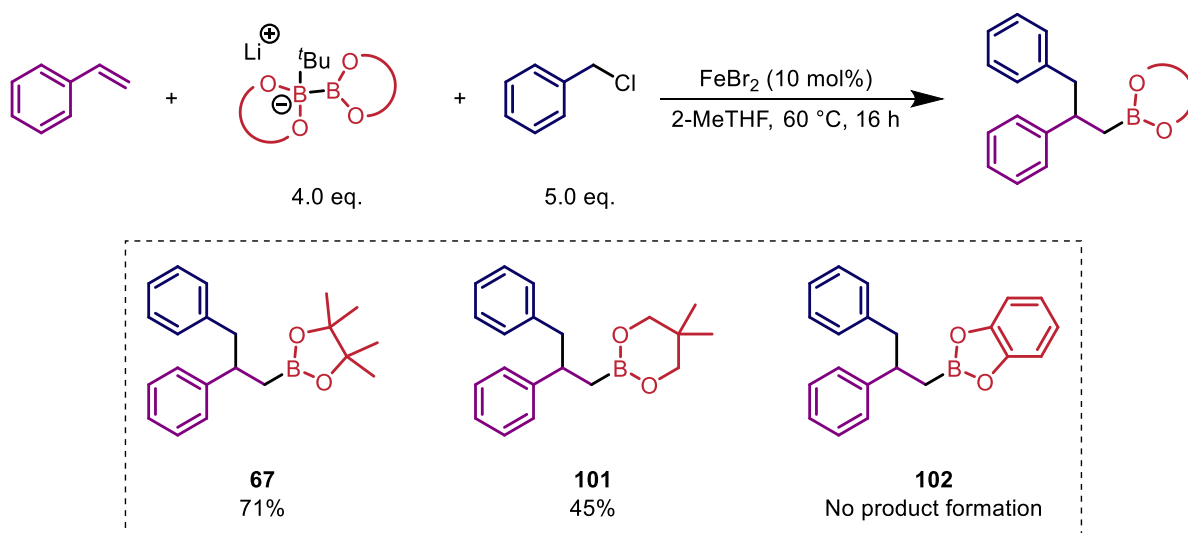
Figure 4.18 – Scope of diboron reactants in iron-catalysed carboboration of alkenes. Conditions: styrene (0.5 mmol), B₂OR₂[ᵗBuLi] (2.0 mmol), benzyl chloride (2.5 mmol), FeBr₂ (0.05 mmol), 2-MeTHF (10 mL), 60 °C, 16 h. Isolated yields shown.

In all products, the regioisomer was confirmed by DEPT-135 ^{13}C-NMR experiments. Due to the quadrupolar relaxation of the boron nucleus present in the products, the carbon bonded to it is not observed in the ^{13}C-NMR spectra (highlighted in yellow in Figure 4.19). This missing peak allows for a difference in the expected number of **C**H₂ vs **C**H₃ + **C**H peaks between the three isomers. For example, with **76** we would expect the 2,1-regioisomer to have 9 **C**H + **C**H₃ peaks and only 1 **C**H₂ peak (the R**C**H₂B peak is absent) but the 1,2- and 1,1-regioisomers would have 8 **C**H + **C**H₃ peaks and 2 **C**H₂ peaks (the R₂**C**HB peak is absent). The DEPT-135 ^{13}C-NMR spectrum of **76** shows only 1 **C**H₂ peak and therefore can be assigned as the 2,1-regioisomer (Figure 4.19). As well as this assignment method, ^{1}H-, ^{13}C-, ^{11}B- and ^{19}F-NMR spectra of products were also compared to literature assignments where possible.
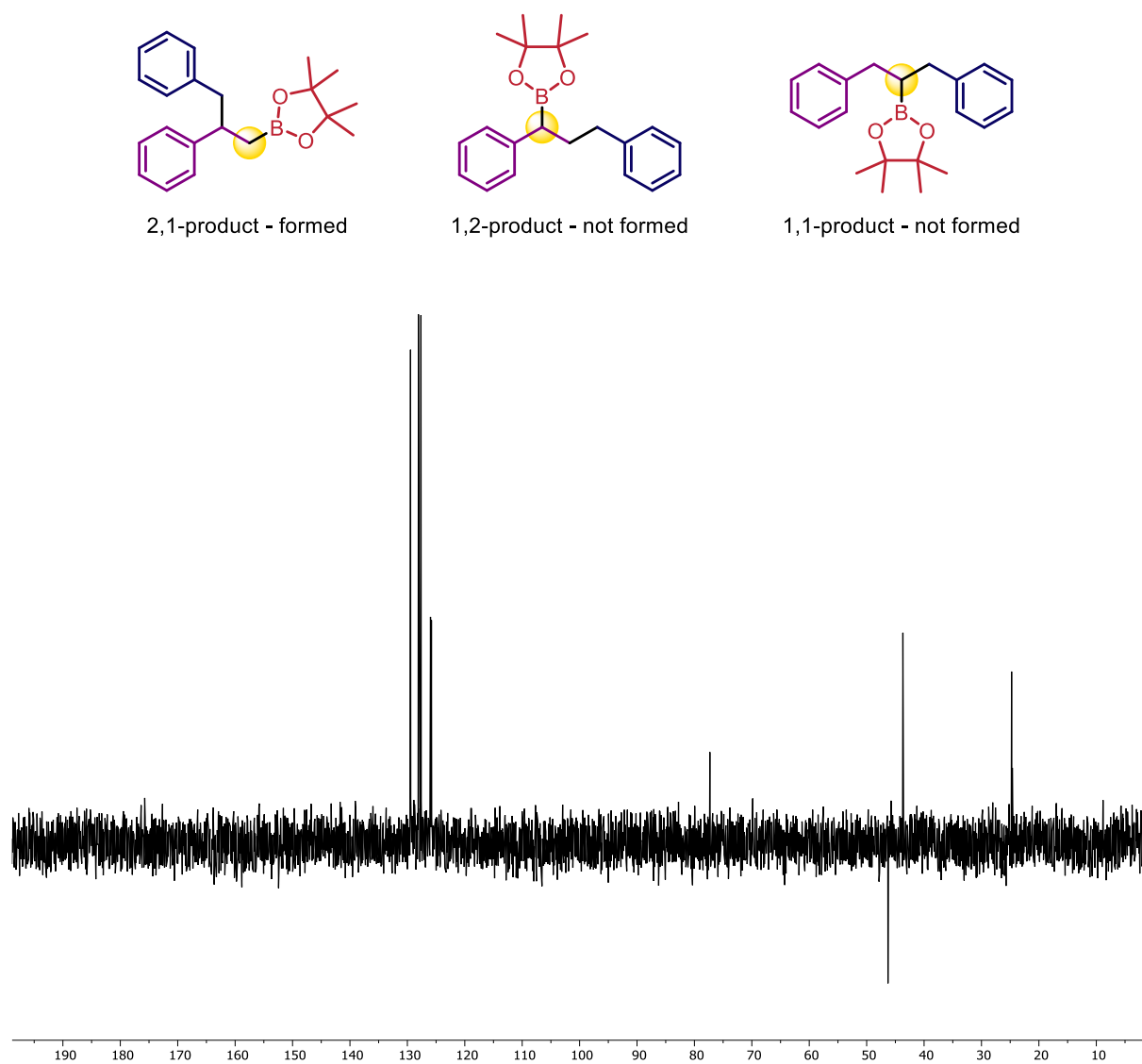
Figure 4.19 – Potential regioisomers and the DEPT-135 ^{13}C- NMR spectrum for 76.

4.5 Conclusions

In conclusion, a combined OVAT and DoE approach has been utilised to optimise an iron-catalysed carboration of styrene derivatives using benzyl halides. The transformation has been achieved under mild conditions and without the need of an additional ligand, whilst also being regioselective, forming exclusively the 2,1-regioisomer (Scheme 4.11). The product of this reaction is highly desirable in synthesis as it has a boronic ester moiety which can be further functionalised. A robustness screen was carried out to provide insights into the functional group tolerance of the reaction. This was followed by a screen of reactants to further deduce the functional group tolerance of the reaction. It was found that, even though the reaction worked well with styrene derivatives, other alkenes could not be used in the transformation. The reaction worked well with benzyl chlorides, but alternative electrophiles such as aryl chlorides and unactivated alkyl halides were not tolerated. Moving from bis(pinacolato)diboron to other diboron sources did not prove fruitful, and bis(pinacolato)diboron was by far the best boron source. In total, 19 examples were synthesised using a range of electrophiles, nucleophiles, and alkenes.
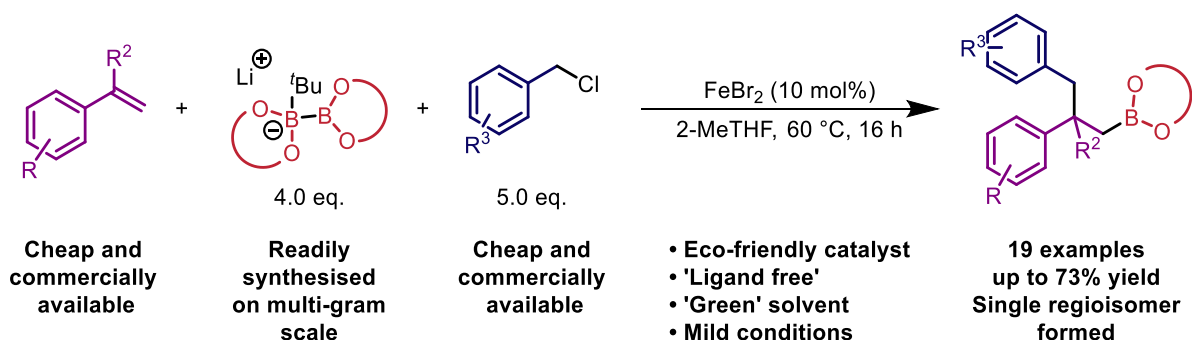
Scheme 4.11 – Summary of iron-catalysed carboration of styrene derivatives

4.6 Future Work

The reaction worked well for styrene derivatives but did not tolerate any other alkene that was trialled under the reaction conditions. Conditions that would allow for the carboboration of other alkenes are highly desirable. Therefore, one of the first things that should be investigated is a way to overcome this barrier. Koh found with activated alkenes that the reaction could proceed 'ligand free' but for less activated alkenes, dppe, a change in solvent and an increased excess of alkene were required to achieve the transformation.[122] Further investigation of this was not carried out, and further probing of these reaction conditions, *e.g.* varying the ligand and reactant loading, could prove beneficial with alkenes other than styrene. Fu found that less activated alkenes could be used in a copper-catalysed alkylboration by introducing a heteroatom into the alkene.[303] This class of alkene was not explored in the reaction scope, and could provide a route to functionalise alkenes that are not styrene derivatives.

So far, the only reported iron-catalysed carboboration of alkynes was reported by Nakamura in 2015, but only three examples were synthesised.[319] The robustness screen showed that alkynes could possibly be used in this iron-catalysed carboboration reaction. Therefore, to build on this existing methodology it would be beneficial to explore the tolerance of alkynes in the reaction.

The process currently relies on diboron species that have been activated by ^{t}BuLi. However, this is not appealing for industrial chemists as ^{t}BuLi has several safety issues, such as its pyrophoric nature. Therefore, to further improve on the methodology developed in this chapter, the focus should shift towards using less hazardous alkoxide bases that have routinely been used in copper- and nickel-catalysed carboboration reactions. In the base screen, LiO^{i}Pr showed promise that it could be used in the reaction. Further reaction development should focus on the use of this base.

The enantioselectivity of this reaction was not explored at all, but as there was nothing to promote the enantioselectivity, *e.g.*, a chiral ligand, the product will have been formed as a racemic mixture. However, the product has a stereogenic centre where the C(sp^3)–C(sp^3) bond is formed and therefore the reaction has the potential to be rendered enantioselective. The ability to control the enantioselectivity is highly sought after, particularly in the pharmaceutical industry[341] where one enantiomer might have beneficial properties whereas the other has detrimental effects to the drug user *e.g.* thalidomide.[342] Routes to single enantiomers are commonly achieved through the use of chiral catalysts where chiral ligands are employed.[343–345] Indeed, there have been various reports of

enantioselective transition metal-catalysed carboboration of alkenes.[304,311,312,314,346] However, this reaction is 'ligand free' and therefore the introduction of chiral ligands might reduce product formation.

The reaction was completely selective in the formation of the 2,1-regioisimer over the 1,1- and 1,2-regioisomers. However, routes to these other regioisomers are also desirable. Fu and co-workers found that through choice of ligand they were able to selectively form either the 1,2- or 2,1-regioisomer.[303] This would be very interesting to explore in this reaction, but with the reaction proceeding without an additional ligand, alternative routes might need to be investigated; for example using directing groups in the substrates.

Chapter 5 Summary and Future Outlook

The work described in this thesis has explored the reactivity and development of two novel protocols for iron-catalysed cross-coupling reactions using organoboron reagents, with significant progress made in both reactions. However, there are still advancements required to take iron-catalysis further into the realm of synthetic use and to further understand the reaction mechanisms of iron-catalysed transformations.

The aim of the work described in Chapter 2 was to remove the directing group dependency of the electrophile in an iron-catalysed Suzuki biaryl cross-coupling reaction. This aim was met, with the development of reaction conditions where a simple iron catalyst could be used to catalyse the cross-coupling of aryl chlorides without a directing group (such as chlorobenzene) with boronate species'; 47 biaryls were synthesised with isolated yields up to 87%. Whilst reaction conditions for this highly desirable transformation have now been reported, the reaction also led to the formation of the homo-coupled nucleophile in relatively large amounts (although this is not uncommon in iron-catalysed cross-coupling reactions). Therefore, future efforts should focus on improving the selectivity of the catalyst. Research should also focus on moving away from the use of ^{t}BuLi to activate the boronic ester to form boronates, which is currently required to achieve the transformation. Byers's has shown that lithium amide bases can be used in iron-catalysed Suzuki alkyl-aryl C–C bond formation, and variations of these bases may be applicable in biaryl synthesis.

The aim of the work described in Chapter 3 was to investigate the mechanism of the iron-catalysed Suzuki biaryl cross-coupling reaction described in Chapter 2. Whilst the mechanism was extensively studied using a range of techniques and many aspects of the mechanism uncovered (with a plausible though tentative mechanism suggested), a way to improve the selectivity was not found. Further information about the speciation of catalytically active iron complexes also needs to be obtained. It is likely that by working with experts in other fields, such as X-ray- and EPR-spectroscopy, that further information regarding the mechanism can be discovered. By understanding the mechanism of this reaction further, the reactivity of iron-catalysts can be unlocked, and catalyst design can be improved in future reactions.

Previous work:

This work:
Removal of directing group dependence

Cheap and commercially available

Readily synthesised on multi-gram scale

47 examples
up to 87% yield

Future work:

- **Increased catalyst selectivity**
- **Milder bases**
- **Air and moisture stable catalyst**
- **Increased catalyst activity**
- **Increased mechanistic understanding**
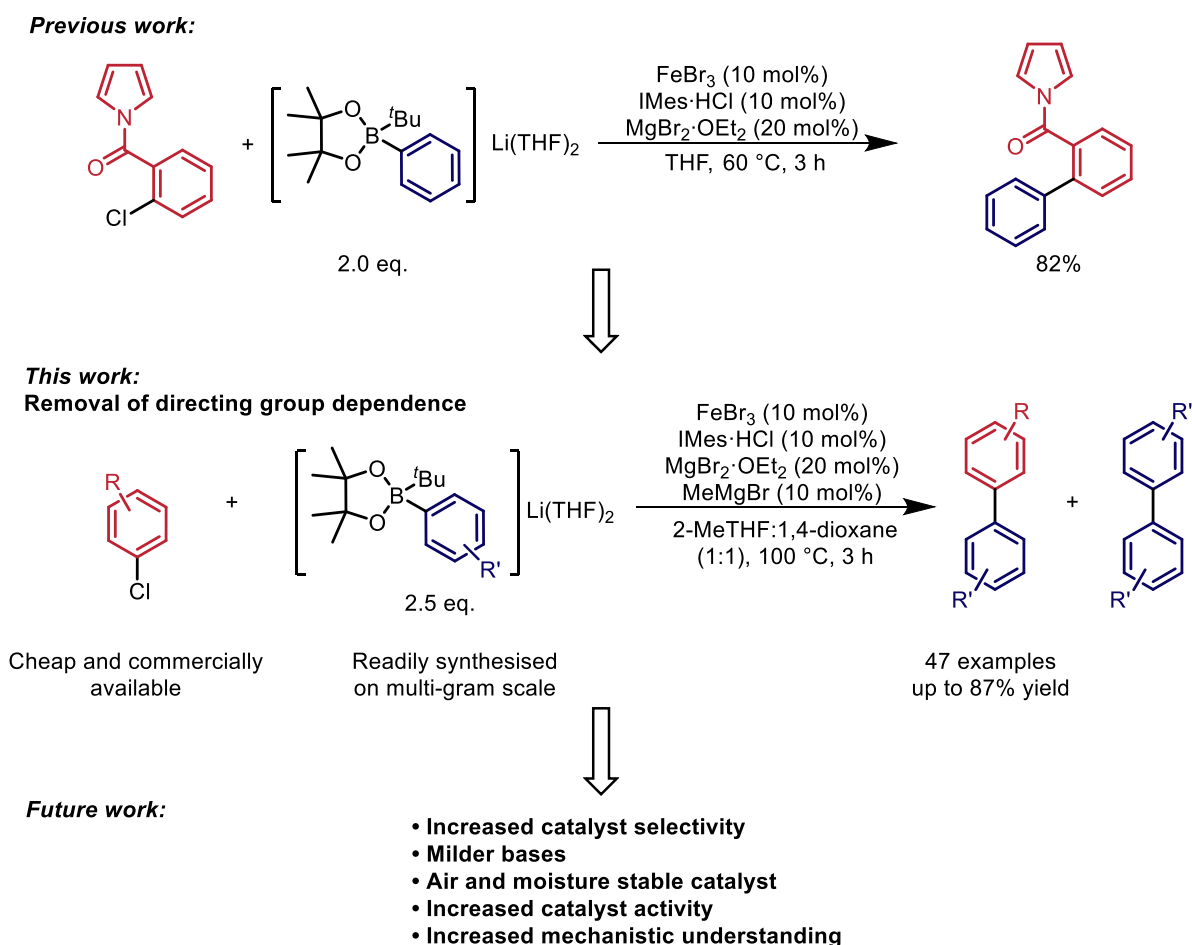
Figure 5.1 – Current perspective of iron-catalysed Suzuki biaryl cross-coupling and future aims.

The work described in Chapter 4 was carried out with the aim of creating the first reported iron-catalysed alkylboration of alkenes. This aim was met, and 19 examples were recorded with yields up to 73%. This work used a mixture of OVAT and DoE methods to optimise the reaction and both a robustness screen and a substrate scope to assess the functional group tolerance of the reaction. Although this reaction provides a great starting point for iron-catalysed alkylborations of alkenes, there are a number of ways in which it could be improved. Firstly, a large excess of electrophile and nucleophile are required to achieve the transformation in reasonable yield. Therefore, one of the first improvements to be made is to reduce the excess of these reagents. As with the iron-catalysed Suzuki reaction, this reaction also required ^{t}BuLi to activate the diboron reagent. However, the use of ^{t}BuLi is not desirable due to its pyrophoric nature, therefore, other activating agents should be investigated. The reaction also only worked for styrene derivatives and not for other alkenes and therefore conditions that allow other alkenes would be highly beneficial.

Figure 5.2 – Current perspective of iron-catalysed carboboration of alkenes and future aims.

216

Chapter 6 Experimental

6.1 General Considerations

Unless otherwise specified, all reactions were carried out in an inert atmosphere of nitrogen or argon using standard Schlenk-line or glovebox techniques. All reagents purchased from commercial suppliers were used as received without further purification. THF, CH_2Cl_2 and hexane and were dried using an Anhydrous Engineering alumina column drying system and all other solvents were dried over 3 or 4 Å molecular sieves. TLC was performed on Silica Gel 60 F^{254} (Merck) and visualised using UV light (254 nm). Flash column chromatography was performed using technical grade silica gel, pore size 60 Å, 230-400 mesh particle size. Aryl halides, boronic esters, additives, dodecane and the radical traps were either dried under vacuum, stored over molecular sieves (3 Å or 4 Å), or azeotroped with toluene before being used. The following were prepared according to literature procedure: INap·HCl,[159] IMe·HCl,[347] IMes^{Me}·HCl,[348] IXyl(2,6)·HCl,[154] SIXyl(3,5)·HCl,[349] 6Mes,[161] 7Mes,[161] 8Mes,[161] 6Pr,[161] IMesFeCl$_2$ dimer (**15**),[350] monoanionic bis(NHC)borate ligands (**16**) and (**17**),[172] [(IMes)Fe(dvtms)] (**66**).[212] All other reagents were purchased from commercial suppliers and used without further purification.

NMR spectra were measured at 400 MHz and recorded on Bruker Nano 400, Varian 400-MR, JEOL ECS 400 or JEOL ECZ 400 spectrometers. The corresponding ^{13}C, ^{19}F and ^{11}B frequencies are 101, 377 and 128 MHz respectively. NMR samples were analysed as solutions with solvents specified below at 298 K. ^1H and ^{13}C NMR spectra were referenced to residual solvent peaks (CDCl$_3$ δ_H 7.26 and δ_C 77.2 and ^{d8}THF δ_H 1.73 and 3.58, δ_C 25.5 ppm); chemical shifts are reported in parts per million (ppm) relative to tetramethylsilane standard. Coupling constants (*J*) are reported to the nearest 0.1 Hz and were calculated using *MestreNova 11.0*. Multiplicities are abbreviated as: a (apparent), br (broad), s (singlet), d (doublet), t (triplet), q (quartet), p (pentet), m (multiplet) or combinations thereof. Mass spectrometry was performed by the University of Bristol mass spectrometry service by electrospray ionisation (ESI) using a micrOTOF II spectrometer or using GC-FID/MS. GC-FID/MS analysis was conducted using an Agilent 7820A GC system and 5977B MSD. Infrared spectra were recorded using a Perkin Elmer Spectrum Two FT-IR spectrometer. GC-FID analysis was performed using an Agilent Technologies 7820A, with quantification implemented using calibration curves obtained from a minimum of five different concentrations of the samples being investigated with dodecane used as an internal standard.

6.2 Experimental Details for Chapter 2

6.2.1 General Procedure 1: Synthesis of boronic esters
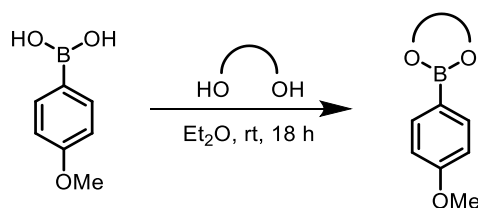
4-methoxyphenylboronic acid (1.0 eq.) was added a solution of diol (1.0 eq., 0.44 M) dissolved in Et$_2$O. After 30 mins, MgSO$_4$ was added, and the reaction mixture was left to stir at rt for 16 h. After, the reaction mixture was filtered, and the solvent was removed *in vacuo* affording the desired product. If necessary, the product was purified by flash column chromatography (25% EtOAc in hexane).

2-(4-methoxyphenyl)-4,4,5-trimethyl-1,3,2-dioxaborolane
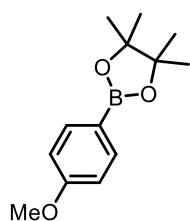
Isolated as a white solid, quantitative yield. **^{1}H NMR** (400 MHz, Chloroform-*d*) δ 7.76 (d, *J* = 8.7 Hz, 2H), 6.90 (d, *J* = 8.7 Hz, 2H), 3.83 (s, 3H), 1.34 (s, 12H); **^{13}C NMR** (101 MHz, Chloroform-*d*) δ 162.3, 136.6, 113.4, 83.6, 55.3, 25.0; **^{11}B NMR** (128 MHz, Chloroform-*d*) δ 30.87; **MS (*m/z*)**: (EI) calculated for [C$_{13}$H$_{19}$BO$_3$]$^+$: 234.14, found 234.1. Spectroscopic data in accordance with literature.[351]

2-(4-methoxyphenyl)-5,5-dimethyl-1,3,2-dioxaborinane
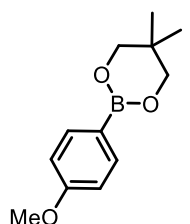
Isolated as a white solid, quantitative yield. **^{1}H NMR** (400 MHz, Chloroform-*d*) δ 7.77 (d, *J* = 8.9 Hz, 2H), 6.91 (d, *J* = 8.9 Hz, 2H), 3.83 (s, 3H), 3.77 (s, 4H), 1.03 (s, 6H); **^{13}C NMR** (101 MHz, Chloroform-*d*) δ 161.9, 135.6, 113.4, 72.4, 55.2, 32.0, 22.0; **^{11}B NMR** (128 MHz, Chloroform-*d*) δ 26.72; **MS (*m/z*)**: (EI) calculated for [C$_{12}$H$_{17}$BO$_3$]$^+$: 220.13, found 220.1. Spectroscopic data in accordance with literature.[352]

2-(4-methoxyphenyl)-1,3,2-dioxaborinane
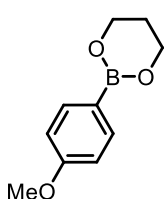
Isolated as a colourless oil, quantitative yield. **^{1}H NMR** (400 MHz, Chloroform-*d*) δ 7.74 (d, *J* = 8.7 Hz, 2H), 6.90 (d, *J* = 8.7 Hz, 2H), 4.15 (q, *J* = 5.5 Hz, 4H), 3.82 (s, 3H), 2.03 (p, *J* = 5.5 Hz, 2H); **^{13}C NMR** (101 MHz, Chloroform-*d*) δ 161.8, 135.4, 113.2, 61.9, 55.1, 27.5; **^{11}B NMR** (128 MHz, Chloroform-*d*) δ 27.02; **MS**

(***m/z***): (EI) calculated for $[C_{10}H_{13}BO_3]^+$: 192.10, found 192.1. Spectroscopic data in accordance with literature.[353]

2-(4-methoxyphenyl)-4,6-dimethyl-1,3,2-dioxaborinane
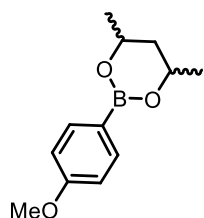
Isolated as a colourless oil, quantitative yield. **¹H NMR** (400 MHz, Chloroform-*d*) δ 7.79 – 7.74 (m, 2H), 6.88 (d, *J* = 8.6 Hz, 2H), 4.43 – 4.36 (m, 1H), 4.29 – 4.21 (m, 1H), 3.82 (s, 3H), 1.96 (dt, *J* = 13.8, 2.7 Hz, 1H), 1.82 (t, *J* = 5.3 Hz, 1H), 1.38 (d, *J* = 6.3 Hz, 3H), 1.36 (d, *J* = 6.3 Hz, 3H); **¹³C NMR** (101 MHz, Chloroform-*d*) δ 161.7, 161.7, 135.6, 135.5, 113.2, 113.1, 68.2, 64.7, 55.1, 42.7, 39.4, 23.4, 22.9; **¹¹B NMR** (128 MHz, Chloroform-*d*) δ 26.94; **HRMS (m/z)**: (ESI+) calculated for $C_{12}H_{17}BNaO_3$ [M+Na]⁺ : 243.1168. Found: 243.1170; **IR (neat) ν**$_{max}$: 2971, 2932, 1571, 1543, 1397,1341, 1146,1029, 832, 647 cm⁻¹.

2-(4-methoxyphenyl)-4,4,6,6-tetramethyl-1,3,2-dioxaborinane
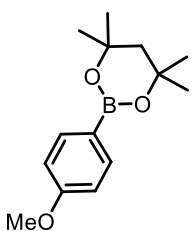
Isolated as a colourless oil, quantitative yield. **¹H NMR** (400 MHz, Chloroform-*d*) δ 7.79 (d, *J* = 8.2 Hz, 2H), 6.88 (d, *J* = 8.2 Hz, 2H), 3.83 (s, 3H), 1.90 (s, 2H), 1.42 (s, 12H); **¹³C NMR** (101 MHz, Chloroform-*d*) δ 161.6, 135.6, 113.1, 70.8, 55.2, 49.2, 32.0; **¹¹B NMR** (128 MHz, Chloroform-*d*) δ 26.41; **MS (m/z)**: (EI) calculated for $C_{14}H_{21}BO_3$ [M]⁺: 271.14. Found: 271.1; **IR (neat) ν**$_{max}$: 2973, 2934, 1602, 1351, 1301, 1243, 1170, 1029, 832, 647 cm⁻¹.

2-(4-methoxyphenyl)hexahydrobenzo[d][1,3,2]dioxaborole
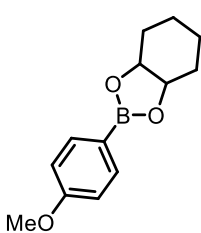
Isolated as a yellow oil, quantitative yield. **¹H NMR** (400 MHz, Chloroform-*d*) δ 7.78 (d, *J* = 8.8 Hz, 2H), 6.91 (d, *J* = 8.8 Hz, 2H), 4.49 (t, *J* = 3.6 Hz, 2H), 3.83 (s, 3H), 1.94 – 1.77 (m, 4H), 1.62 – 1.54 (m, 2H), 1.43 – 1.35 (m, 2H); **¹³C NMR** (101 MHz, Chloroform-*d*) δ 162.4, 136.7, 113.5, 75.6, 55.2, 28.8, 19.5; **¹¹B NMR** (128 MHz, Chloroform-*d*) δ 31.73; **HRMS (m/z)**: (ESI+) calculated for $C_{13}H_{17}BNaO_3$ [M+Na]⁺ : 255.1168. Found: 255.1169; **IR (neat) ν**$_{max}$: 2936, 2863, 1602, 1559, 1356, 1333, 1304, 1173, 1170, 1028, 976, 832, 614 cm⁻¹.

2-(4-methoxyphenyl)tetrahydro-4H-cyclopenta[d][1,3,2]dioxaborole
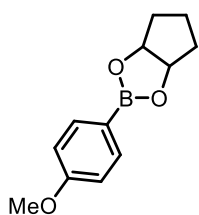
Isolated as a yellow oil, quantitative yield. **¹H NMR** (400 MHz, Chloroform-*d*) δ 7.75 (d, *J* = 8.9 Hz, 2H), 6.91 (d, *J* = 8.9 Hz, 2H), 4.97 (t, *J* = 4.4 Hz, 2H), 3.82 (s, 3H), 2.04 – 1.99 (m, 2H), 1.72 – 1.60 (m, 4H); **¹³C NMR** (101 MHz, Chloroform-*d*) δ 162.3, 136.7, 113.5, 82.7, 55.1, 34.8, 21.7; **¹¹B NMR** (128 MHz, Chloroform-*d*) δ 30.82; **HRMS (m/z)**: (ESI+) calculated for $C_{12}H_{15}BNaO_3$ [M+Na]⁺ : 241.1012. Found: 241.1019; **IR (neat) ν$_{max}$**: 2969, 1603, 1440, 1400, 1366, 1333, 1247, 1174, 648 cm⁻¹.

6.2.2 Synthesis of boronates
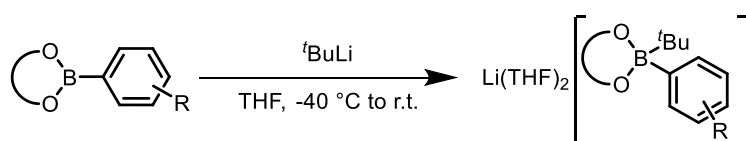
General Procedure 2: Synthesis of activated boronic esters generated *in situ*.

In a Schlenk-flask, the appropriate arylboronic ester (1.0 eq., 0.62 M) was dissolved in THF or 2-MeTHF. The solution was cooled to -40 °C (acetonitrile/liq. N₂ bath) and tert-butyllithium (1.0 eq., 1.7 M in pentane) was added dropwise. The solution was stirred for 30 min and then warmed to room temperature and stirred for a further 45 min. This resulting solution was used immediately after preparation.

General Procedure 3: Synthesis of isolated activated boronic esters in THF
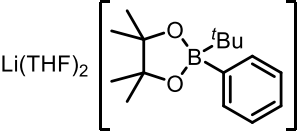
In a Schlenk-flask, the appropriate arylboronic ester (1.0 eq., 0.62 M) was dissolved in THF. The solution was cooled to -40 °C (acetonitrile/liq. N₂ bath) and tert-butyllithium (1.0 eq., 1.7 M in pentane) was added dropwise. The solution was stirred for 30 min and then warmed to room temperature and stirred for a further 45 min before the volatiles were removed in vacuo affording a viscous gum. Hexane was added and the mixture stirred rapidly for 1 h resulting in the formation of a white precipitate. The solvent was removed *via* cannula filtration. This was purified further by washing with hexane (3x) and then the solid dried *in vacuo* overnight affording the desired product.

General Procedure 4: Synthesis of isolated activated boronic esters in hexane
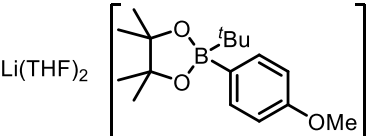
In a Schlenk-flask, the appropriate arylboronic ester (1.0 eq., 0.62 M) was dissolved in hexane. The solution was cooled to -40 °C (acetonitrile/liq. N₂ bath) and tert-butyllithium (1.0 eq., 1.7 M in

pentane) was added dropwise. The solution was stirred for 30 min and then warmed to room temperature and stirred for a further 45 min. The resulting precipitate was then filtered before being washed with hexane (3x) and then the solid dried *in vacuo* overnight affording the desired product.

Phenyl activated boronic ester

Isolated as an air- and moisture-sensitive white solid, 90% yield. **¹H NMR** (400 MHz, THF-d_8) δ 7.33 (d, J = 6.7 Hz, 2H), 6.91 (t, J = 7.3 Hz, 2H), 6.78 – 6.74 (m, 1H), 3.64 – 3.60 (m, 4H), 1.79 – 1.76 (m, 4H), 1.09 (s, 6H), 0.79 (s, 6H), 0.59 (s, 9H); **¹³C NMR** (101 MHz, THF-d_8) δ 133.4, 125.9, 123.2, 78.5, 68.4, 30.9, 28.6, 28.2, 26.5; **¹¹B NMR** (128 MHz, THF-d_8) δ 8.10.

4-methoxyphenyl activated boronic ester, 11

Isolated as an air- and moisture-sensitive white solid, 88% yield. **¹H NMR** (400 MHz, THF-d_8) δ 7.27 (d, J = 8.4 Hz, 2H), 6.56 (d, J = 8.4 Hz, 2H), 3.65 (s, 3H), 1.13 (s, 6H), 0.84 (s, 6H), 0.63 (s, 9H); **¹³C NMR** (101 MHz, THF-d_8) δ 157.4, 133.9, 111.7, 78.5, 54.9, 30.9, 28.7, 28.2; **¹¹B NMR** (128 MHz, THF-d_8) δ 8.13.

6.2.3 Optimisation

General Procedure 5: Screening of aryl halide, iron source and ligand
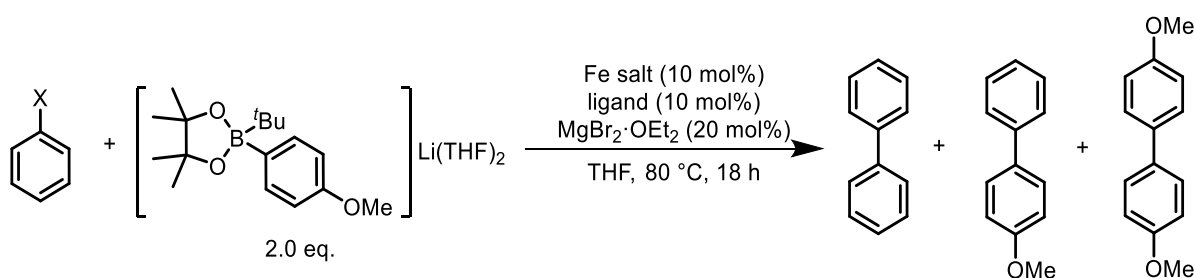
In an argon-filled glovebox, an oven dried 7.5 mL vial was charged with the appropriate iron salt (0.5 mL, 0.02 M in THF, 0.01 mmol) and ligand (0.01 mmol), the resulting mixture was allowed to stir at rt for 30 min. MgBr₂·OEt₂ (0.2 mL, 0.1 M in THF, 0.02 mmol), aryl halide (0.1 mmol) and boronate **11** (0.5 mL, 0.4 M in THF, 0.2 mmol) were then added to the vial sequentially. The reaction mixture was then heated to 80 °C and stirred for 16 h. The resulting mixture was cooled to room temperature and quenched with 1.0 M HCl (1.0 mL) before dodecane (22.7 µL, 0.1 mmol)

was added and extracted into CH_2Cl_2 (5.0 mL). After being thoroughly stirred, an aliquot was then taken and filtered through Celite (eluting with CH_2Cl_2) and was then analysed by GC.

General Procedure 6: Screening of boronic acids
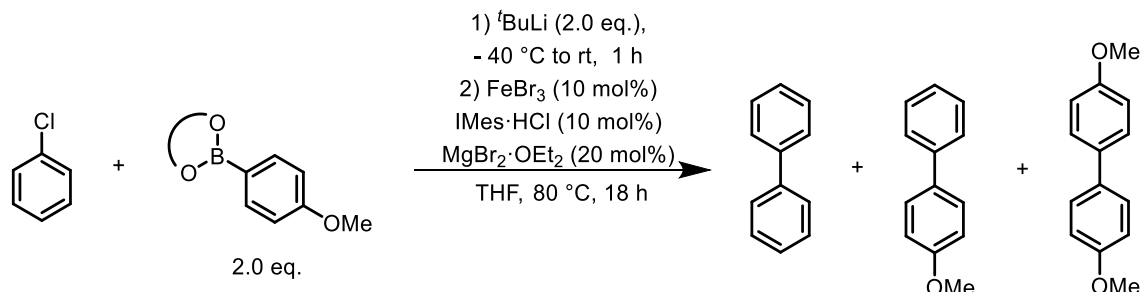
Under an N_2 atmosphere, an oven dried Schlenk tube was charged with the appropriate boronic ester (0.5 mmol) and was dissolved in THF (3.0 mL) and cooled to -40 °C. ^tBuLi (0.29 mL, 1.7 M in hexane, 0.5 mmol) was then added dropwise and allowed to stir for 30 mins at -40 °C. The reaction mixture was slowly brought to rt and stirred for a further 45 mins.

Meanwhile, in an argon-filled glovebox, IMes·HCl (8.6 mg, 0.025 mmol) and $FeBr_3$ (7.4 mg, 0.025 mmol) were added to a dried Schleck tube, containing a stirrer bar, followed by THF (1.5 mL), and allowed to stir for 30 min at rt. $MgBr_2·OEt_2$ (12.9 mg, 0.05 mmol) and chlorobenzene (25.5 µL, 0.25 mmol) were then added. The Schlenk tube was sealed and taken out of the glovebox and attached to a Schlenk line and heated to an external temperature of 80 °C. The boronate formed *in situ*, assumed quantitative conversion, was then added in one go to the Fe Schlenk, sealed, and reacted at 80 °C for 16 h. The resulting mixture was cooled to room temperature and quenched with 1.0 M HCl (2.5 mL) and dodecane (56.8 µL, 0.25 mmol) was added to the reaction mixture. The organics were extracted into CH_2Cl_2 (10 mL), and an aliquot was taken to be analysed by GC.

General Procedure 7: Screening of temperature and solvents
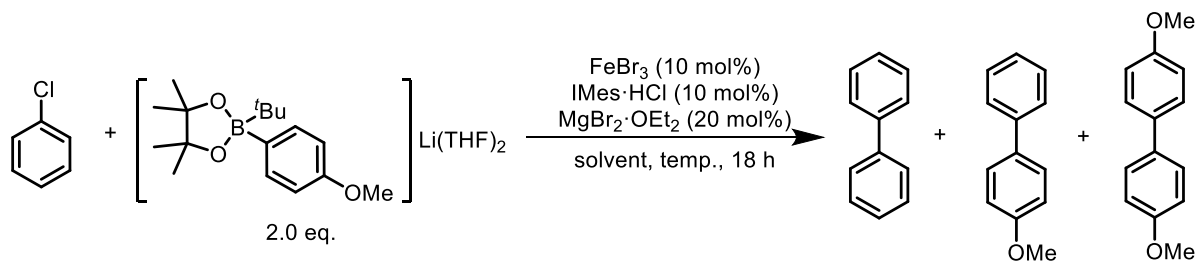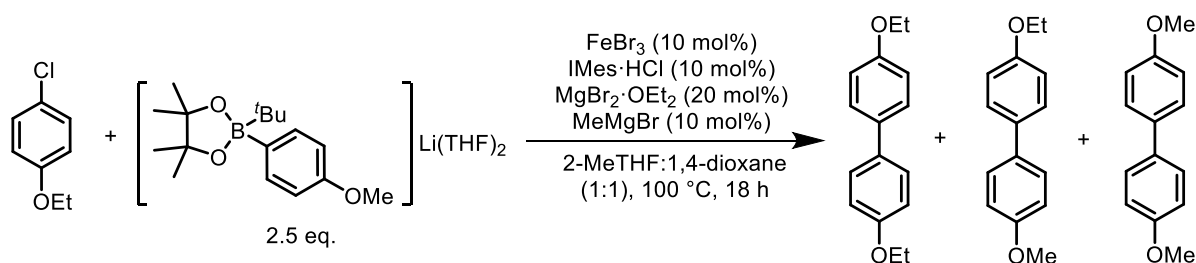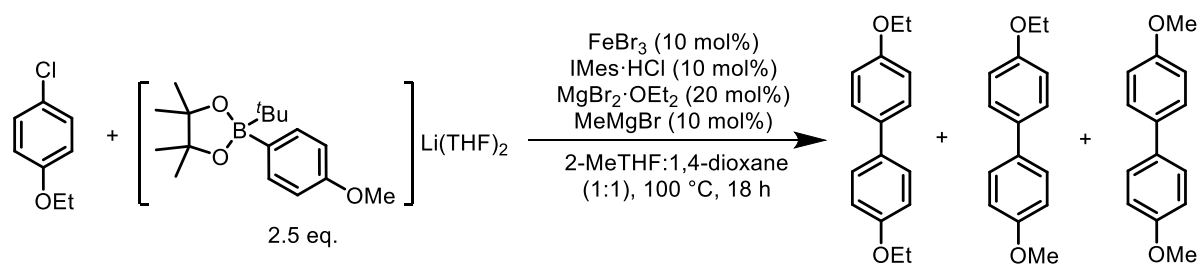

In an argon-filled glovebox, IMes·HCl (8.6 mg, 0.025 mmol) and $FeBr_3$ (7.4 mg, 0.025 mmol) were added to a dried Schleck tube, containing a stirrer bar, followed by the appropriate solvent

(1.5 mL), and allowed to stir for 30 min at rt. MgBr$_2$·OEt$_2$ (12.9 mg, 0.05 mmol) and chlorobenzene (25.5 µL, 0.25 mmol) were then added. In a separate Schlenk tube the boronate **11** (221.1 mg, 0.5 mmol) was dissolved in the appropriate solvent (1.5 mL). Both Schlenk's were sealed and taken out of the glove box and attached to a Schlenk line and heated to the appropriate temperature whilst being stirred. The boronate solution was then added quickly to the Fe Schlenk, sealed, and left to react for 16 h. The resulting mixture was cooled to room temperature and quenched with 1.0 M HCl (2.5 mL) and dodecane (56.8 µL, 0.25 mmol) was added to the reaction mixture. The organics were extracted into CH$_2$Cl$_2$ (10 mL), and an aliquot was taken to be analysed by GC.

General Procedure 8: Screening of 'reducing agents'
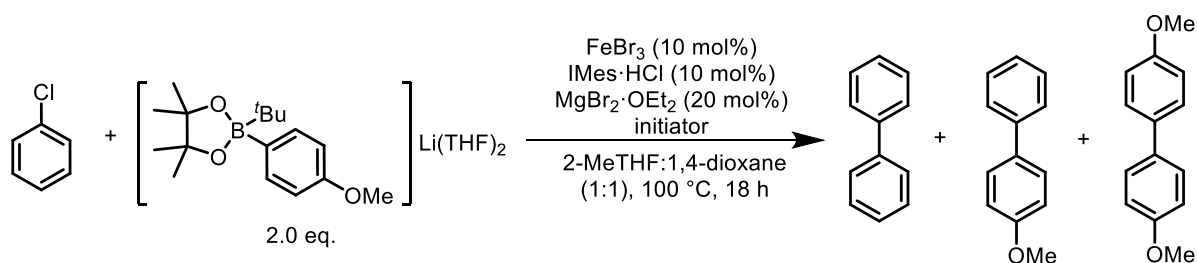
In an argon-filled glovebox, IMes·HCl (34.4 mg, 0.1 mmol) and FeBr$_3$ (29.6 mg, 0.1 mmol) were added to a dried Schleck tube, containing a stirrer bar, followed by 1,4-dioxane (6.0 mL), and allowed to stir for 30 min at rt (suspension forms). MgBr$_2$·OEt$_2$ (51.6 mg, 0.2 mmol) and chlorobenzene (102 µL, 1.0 mmol) were then added. In a separate Schlenk tube the boronate **11** (884.7 mg, 2.0 mmol) was dissolved in 2-MeTHF (6.0 mL). Both Schlenk's were sealed and taken out of the glove box and attached to a Schlenk line and heated 100 °C, whilst being stirred. The 'reducing agent' was then added to the Fe Schlenk tube and was allowed to stir for 5 mins. The boronate solution was then added quickly to the Fe Schlenk, sealed, and left to react for 16 h. The resulting mixture was cooled to room temperature and quenched with 1.0 M HCl (5.0 mL) and dodecane (227.1 µL, 0.1 mmol) was added to the reaction mixture. The organics were extracted into CH$_2$Cl$_2$ (20 mL), and an aliquot was taken to be analysed by GC.

General Procedure 9: Screening of additives
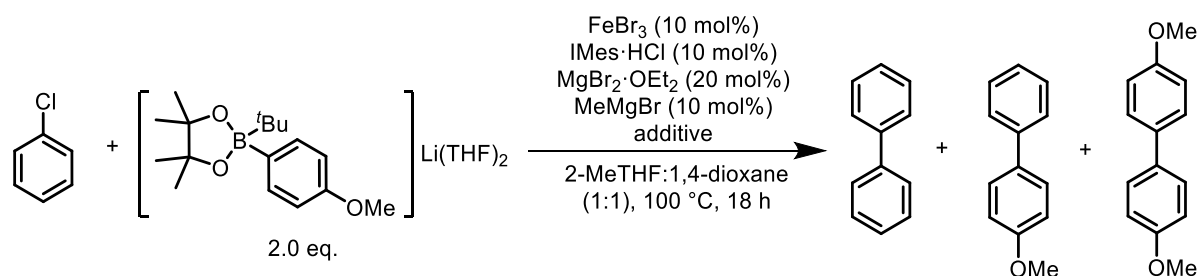
In an argon-filled glovebox, IMes·HCl (34.4 mg, 0.1 mmol) and FeBr₃ (29.6 mg, 0.1 mmol) were added to a dried Schleck tube, containing a stirrer bar, followed by 1,4-dioxane (6.0 mL), and allowed to stir for 30 min at rt (suspension forms). MgBr₂·OEt₂ (51.6 mg, 0.2 mmol) and chlorobenzene (102 µL, 1.0 mmol) were then added. In a separate Schlenk tube the boronate **11** (884.7 mg, 2.0 mmol) was dissolved in 2-MeTHF (6.0 mL). Both Schlenk tubes were sealed and taken out of the glove box and attached to a Schlenk line and heated to 100 °C whilst being stirred. MeMgBr (0.1 mL, 1.0 M in Et₂O, 0.1 mmol), if using, was then added to the Fe Schlenk tube, and was allowed to stir for 5 mins, this was followed by the additive and allowed to stir for 30 mins. The boronate solution was then added quickly to the Fe Schlenk, sealed, and left to react for 16 h. The resulting mixture was cooled to room temperature and quenched with 1.0 M HCl (5.0 mL) and dodecane (227.1 µL, 0.1 mmol) was added to the reaction mixture. The organics were extracted into CH₂Cl₂ (20 mL), and an aliquot was taken to be analysed by GC.

General Procedure 10: Halide salt screen
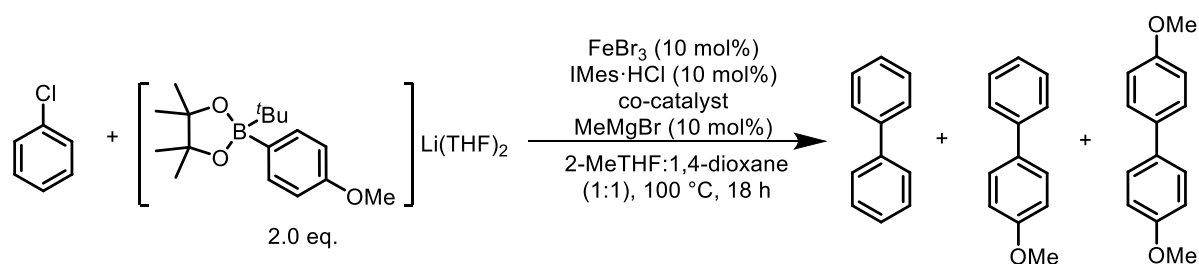
In an argon-filled glovebox, IMes·HCl (8.6 mg, 0.025 mmol) and FeBr₃ (7.4 mg, 0.025 mmol) were added to an oven dried 7.5 mL vial, containing a stirrer bar, followed by 1,4-dioxane (1.5 mL), and allowed to stir for 30 min at rt. The appropriate additive (0.05 mmol) and chlorobenzene (25.5 µL, 0.25 mmol) were then added and heated to 100 °C. MeMgBr (0.025 mL, 1.0 M in Et₂O, 0.025 mmol) then added to the Fe Schlenk tube and was allowed to stir for 5 mins, this was followed by boronate **11** (1.5 mL, 0.33 M in 2-MeTHF, 0.5 mmol). The reaction mixture was left to react for 16 h at 100 °C. The resulting mixture was cooled to room temperature and quenched with 1.0 M HCl (2.5 mL) and dodecane (56.8 µL, 0.25 mmol) was added to the reaction mixture. The organics were extracted into CH₂Cl₂ (10 mL), and an aliquot was taken to be analysed by GC.

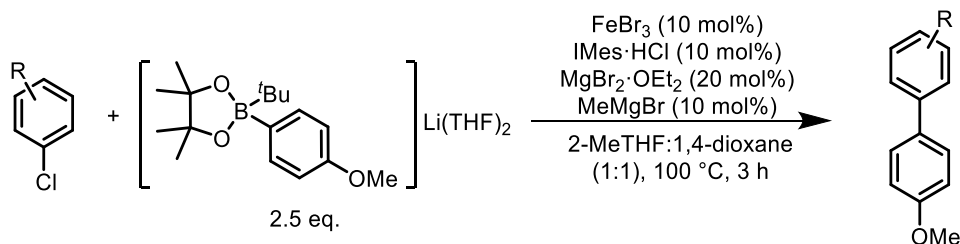## General Procedure 11: Reaction profiling

In an argon-filled glovebox, IMes·HCl and FeBr₃ were added to a dried Schleck tube, containing a stirrer bar, followed by 1,4-dioxane (6.0 mL), and allowed to stir for 30 min at rt (suspension forms). MgBr₂·OEt₂, chlorobenzene, and dodecane were then added. In a separate Schlenk tube the boronate **11** was dissolved in 2-MeTHF. Both Schlenk's were sealed and taken out of the glove box and attached to a Schlenk line and heated to 100 °C whilst being stirred. MeMgBr (1.0 M in Et₂O) was then added to the Fe Schlenk tube and was allowed to stir for 5 mins. The boronate solution was then added quickly to the Fe Schlenk, and aliquots were taken at the times given. Each aliquot was quenched with 1.0 M HCl and extracted into CH₂Cl₂ and then analysed by GC.

Slow addition of electrophile

In an argon-filled glovebox, IMes·HCl (17.1 mg, 0.05 mmol), FeBr₃ (14.8 mg, 0.05 mmol), MgBr₂·OEt₂ (25.8 mg, 0.1 mmol), and dodecane (113.6 µL, 0.5 mmol) were added to a dried Schleck tube, containing a stirrer bar, followed by 1,4-dioxane (3.0 mL) and 2-MeTHF (1.5 mL), forming a suspension. In a second Schlenk tube the boronate **11** (552.9 mg, 1.25 mmol) was dissolved in 2-MeTHF (1.5 mL). A third Schlenk tube was charged with 4-ethoxy-1-chlorobenzene (78.3 mg, 0.5 mmol) and 2-MeTHF (1.5 mL). The Schlenk tubes were sealed and taken out of the glove box and attached to a Schlenk line and the Fe Schlenk tube was heated to 100 °C, whilst being stirred. MeMgBr (0.05 mL, 1.0 M in Et₂O, 0.05 mmol) was then added to the Fe Schlenk tube and was allowed to stir for 5 mins. The boronate solution was then added quickly to the Fe Schlenk. The electrophile solution was then added dropwise over an hour using a syringe pump, and aliquots (0.05 mL) were taken at the times given. Each aliquot was quenched with 1.0 M HCl (0.5 mL) and extracted into CH₂Cl₂ (2.0 mL) and then analysed by GC.
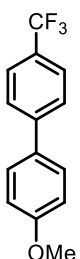
Slow Addition of nucleophile

In an argon-filled glovebox, IMes·HCl (17.1 mg, 0.05 mmol), FeBr₃ (14.8 mg, 0.05 mmol), MgBr₂·OEt₂ (25.8 mg, 0.1 mmol), 4-ethoxy-1-chlorobenzene (78.3 mg, 0.5 mmol), and dodecane (113.6 µL, 0.5 mmol) were added to a dried Schleck tube, containing a stirrer bar, followed by 1,4-dioxane (3.0 mL) and 2-MeTHF (3.0 mL). In a second Schlenk tube the boronate **11** (552.9 mg, 1.25 mmol) was dissolved in 2-MeTHF (1.5 mL). The Schlenk tubes were sealed and taken out of the glove box and attached to a Schlenk line and the Fe Schlenk tube was heated to 100 °C, whilst being stirred. MeMgBr (0.05 mL, 1.0 M in Et₂O, 0.05 mmol) was then added to the Fe Schlenk tube and was allowed to stir for 5 mins. The boronate solution was then added dropwise over an hour using a syringe pump, and aliquots (0.05 mL) were taken at the times given. Each aliquot was quenched with 1.0 M HCl (0.5 mL) and extracted into CH₂Cl₂ (2.0 mL) and then analysed by GC.

Cross-coupling reaction using blue LED light
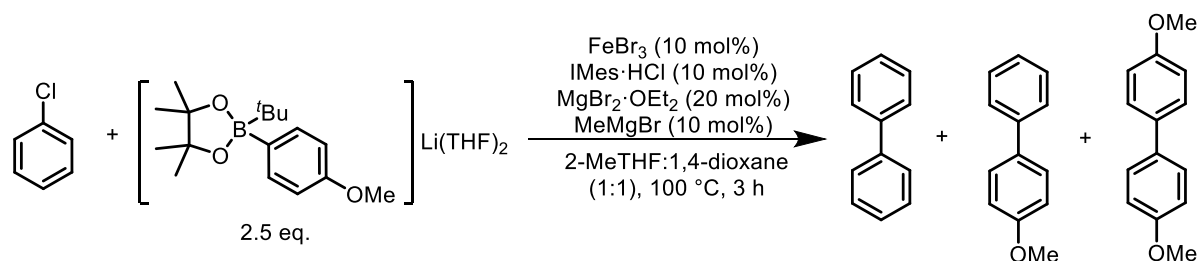
In an argon-filled glovebox, IMes·HCl (17.1 mg, 0.05 mmol), FeBr₃ (14.8 mg, 0.05 mmol), MgBr₂·OEt₂ (25.8 mg, 0.1 mmol) and chlorobenzene (50.9 µL, 0.5 mmol) were added to a dried Schleck tube, containing a stirrer bar, followed by 1,4-dioxane (3.0 mL), forming a suspension. In a separate dried Schlenk tube the boronate **11** (552.9 mg, 1.25 mmol) was dissolved in the 2-MeTHF (3.0 mL). Both Schlenk tubes were sealed and taken out of the glove box and attached to a Schlenk line and heated to the appropriate external temperature, whilst stirred. Blue LED lights were placed to surround the Fe reaction mixture and aluminium foil was used to enclose the reaction mixture and lights, with only the top of the Sub-Seal septa exposed. MeMgBr (0.05 mL, 1.0 M, 0.05 mmol) was added to the Fe Schlenk tube and left to stir for 5 mins. The boronate solution was then added quickly to the Fe Schlenk tube, aluminium foil was used to cover the exposed Sub-Seal septa and it was left to react at 100 °C (external temp.) for 3 hrs. The resulting

mixture was cooled to room temperature and quenched with 1.0 M HCl (5.0 mL) and dodecane (113.6 µL, 0.5 mmol) was added to the reaction mixture. The organics were extracted into CH_2Cl_2 (10 mL), and an aliquot was taken to be analysed by GC.

Cross-coupling reaction in the absence of light
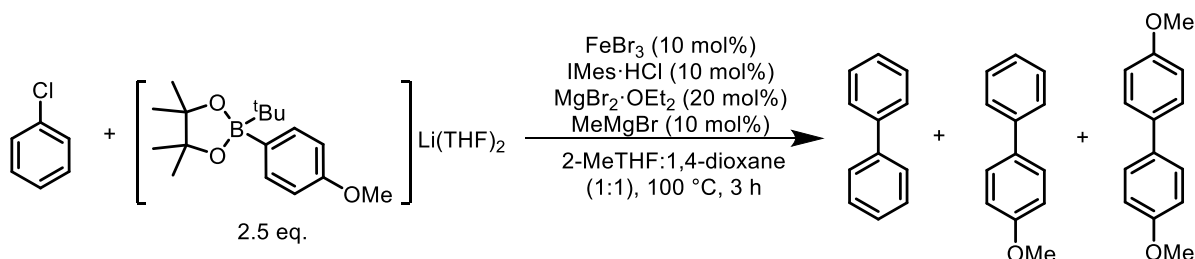
In an argon-filled glovebox, IMes·HCl (17.1 mg, 0.05 mmol), FeBr₃ (14.8 mg, 0.05 mmol), MgBr₂·OEt₂ (25.8 mg, 0.1 mmol) and chlorobenzene (50.9 µL, 0.5 mmol) were added to a dried Schleck tube, containing a stirrer bar, followed by 1,4-dioxane (3.0 mL), forming a suspension. In a separate dried Schlenk tube the boronate **11** (552.9 mg, 1.25 mmol) was dissolved in the 2-MeTHF (3.0 mL). Both Schlenk tubes were sealed and taken out of the glove box and attached to a Schlenk line and heated to the appropriate external temperature, whilst stirred. Aluminium foil was used to enclose the Fe reaction mixture, with only the top of the Sub-Seal septa exposed. MeMgBr (0.05 mL, 1.0 M, 0.05 mmol) was added to the Fe Schlenk tube and left to stir for 5 mins. The boronate solution was then added quickly to the Fe Schlenk tube, aluminium foil was used to cover the exposed Sub-Seal septa and it was left to react at 100 °C (external temp.) for 3 hrs. The resulting mixture was cooled to room temperature and quenched with 1.0 M HCl (5.0 mL) and dodecane (113.6 µL, 0.5 mmol) was added to the reaction mixture. The organics were extracted into CH_2Cl_2 (10 mL), and an aliquot was taken to be analysed by GC.

6.2.4 Substrate Scope

General Procedure 12: Electrophile screen

In an argon-filled glovebox, IMes·HCl (17.1 mg, 0.05 mmol), FeBr₃ (14.8 mg, 0.05 mmol), MgBr₂·OEt₂ (25.8 mg, 0.1 mmol) and aryl chloride (0.5 mmol) were added to a dried Schleck tube, containing a stirrer bar, followed by 1,4-dioxane (3.0 mL), forming a suspension. In a separate dried Schlenk tube the boronate **11** (552.9 mg, 1.25 mmol) was dissolved in the 2-MeTHF (3.0 mL). Both Schlenk tubes were sealed and taken out of the glove box and attached to a Schlenk line and heated to the appropriate external temperature, whilst stirred. MeMgBr (0.05 mL, 1.0 M, 0.05 mmol) was added to the Fe Schlenk tube and left to stir for 5 mins. The boronate solution was then added quickly to the Fe Schlenk tube and reacted at 100 °C (external temp.) for 3 hrs. The resulting mixture was cooled to room temperature and quenched with 1.0 M HCl (5.0 mL). The organics were extracted with CH_2Cl_2 (3 x 10 mL), the combined organics layers dried over $MgSO_4$ and filtered. 1,3,5-Trimethoxybenzene (84.1 mg, 0.5 mmol) was added, and an aliquot taken for analysis by ^{1}H NMR spectroscopy. The volatiles were then removed under vacuum. The crude mixture was purified by flash column chromatography (gradient elution: 100% hexanes to 25% ethyl acetate in hexanes) to yield the desired biaryl cross-coupled product.

4-methoxy-1,1'-biphenyl, 13
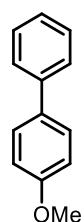
Isolated as a white solid (55 mg, 60%). ^{1}**H NMR** (400 MHz, Chloroform-*d*) δ 7.60 – 7.54 (m, 4H), 7.46 (t, *J* = 7.2 Hz, 2H), 7.33 (t, *J* = 7.0 Hz, 1H), 7.01 (d, *J* = 9.9 Hz, 2H), 3.87 (s, 3H); ^{13}**C NMR** (101 MHz, Chloroform-*d*) δ 159.3, 141.0, 133.9, 128.9, 128.3, 126.9, 126.8, 114.3, 55.5; **MS (*m/z*)**: (EI) calculated for $[C_{13}H_{12}O]^+$: 184.09. Found: 184.1. Spectroscopic data in accordance with literature.[354]
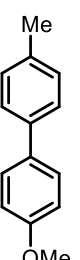
4-methoxy-4'-(trifluoromethyl)-1,1'-biphenyl, 19

Isolated as a white solid (91 mg, 72%). **^{1}H NMR** (400 MHz, Chloroform-*d*) δ 7.68 – 7.62 (m, 4H), 7.55 (d, *J* = 10.0 Hz, 2H), 7.00 (d, *J* = 8.8 Hz, 2H), 3.87 (s, 3H); **^{13}C NMR** (101 MHz, Chloroform-*d*) δ 160.0, 144.4, 132.3, 129.0, 128.5 127.0, 125.8 (q, *J* = 3.8 Hz), 123.2, 114.6, 55.5; **^{19}F NMR** (377 MHz, Chloroform-*d*) δ -62.21; **MS (*m/z*)**: (EI) calculated for $[C_{14}H_{11}F_3O]^+$: 252.08. Found: 252.1. Spectroscopic data in accordance with literature.[355]
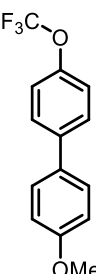
4'-methoxy-*N,N*-dimethyl-[1,1'-biphenyl]-4-carboxamide, 20

Isolated as a white solid (94 mg, 74%). **^{1}H NMR** (400 MHz, Chloroform-*d*) δ 7.56 (d, *J* = 8.3 Hz, 2H), 7.51 (d, *J* = 8.8 Hz, 2H), 7.45 (d, *J* = 8.4 Hz, 2H), 6.97 (d, *J* = 9.0 Hz, 2H), 3.84 (s, 3H), 3.12 (s, 3H), 3.03 (s, 3H); **^{13}C NMR** (101 MHz, Chloroform-*d*) δ 171.6, 159.6, 142.1, 134.5, 132.9, 128.3, 127.7, 126.6, 114.3, 55.4, 39.7, 35.5; **MS (*m/z*)**: (EI) calculated for $[C_{16}H_{17}NO_2]^+$: 255.13. Found: 255.1. Spectroscopic data in accordance with literature.[356]

4-methoxy-4'-methyl-1,1'-biphenyl, 21

Isolated as a white solid (70 mg, 71%). **^{1}H NMR** (400 MHz, Chloroform-*d*) δ 7.52 – 7.49 (m, 2H), 7.47-7.44 (m, 2H) 7.23 (d, *J* = 9.3 Hz, 2H), 6.86 (dd, *J* = 9.3, 8.3 Hz, 2H), 3.85 (s, 3H), 2.39 (s, 3H); **^{13}C NMR** (101 MHz, Chloroform-*d*) δ 159.1, 138.0, 138.1, 136.9, 133.9, 129.6, 128.1, 126.7, 114.3, 55.5, 21.2; **MS (*m/z*)**: (EI) calculated for $[C_{14}H_{14}O]^+$: 198.10. Found: 198.1. Spectroscopic data in accordance with literature.[357]

4-methoxy-4'-(trifluoromethoxy)-1,1'-biphenyl, 22

Isolated as a white solid (90 mg, 67%). **^{1}H NMR** (400 MHz, Chloroform-*d*) δ 7.55 (d, *J* = 8.8 Hz, 2H), 7.50 (d, *J* = 8.8 Hz, 2H), 7.25 (d, *J* = 8.4 Hz, 2H), 7.00 (d, *J* = 8.4 Hz, 2H), 3.86 (s, 3H); **^{13}C NMR** (101 MHz, Chloroform-*d*) δ 159.6, 148.3, 139.8, 132.5, 128.3, 127.9, 122.0, 120.6 (d, *J* = 255 Hz, 1C), 114.5, 55.5; **^{19}F NMR** (377 MHz, Chloroform-*d*) δ 4.95; MS: **MS (*m/z*)**: (EI) calculated for $[C_{14}H_{11}F_3O_2]^+$: 268.07. Found: 268.1. Spectroscopic data in accordance with literature.[358]

4-fluoro-4'-methoxy-1,1'-biphenyl, 23
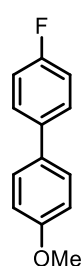
Isolated as a white solid (65 mg, 64%). **^{1}H NMR** (400 MHz, Chloroform-*d*) δ 7.52 – 7.45 (m, 4H), 7.11 (q, *J* = 8.5 Hz, 2H), 6.97 (d, *J* = 8.5 Hz, 2H), 3.85 (s, 3H); **^{13}C NMR** (101 MHz, Chloroform-*d*) δ 162.1 (d, *J* = 244 Hz), 159.3, 137.1 (d, *J* = 3.4 Hz), 133.0, 128.4 (d, *J* = 7.9 Hz), 128.2, 115.7 (d, *J* = 21.2 Hz), 114.4, 55.5; **^{19}F NMR** (377 MHz, Chloroform-*d*) δ -116.63 (tt, *J* = 9.3, 5.4 Hz); **MS (*m/z*)**: (EI) calculated for $[C_{13}H_{11}FO]^+$: 202.08. Found: 202.1. Spectroscopic data in accordance with literature.[357]

4'-methoxy-N-methyl-[1,1'-biphenyl]-4-amine, 24
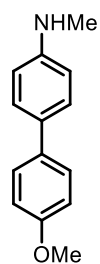
Isolated as a colourless oil (70 mg, 66%). **^{1}H NMR** (400 MHz, Chloroform-*d*) δ 7.46 (d, *J* = 8.7 Hz, 2H), 7.40 (d, *J* = 8.7 Hz, 2H), 6.94 (d, *J* = 8.7 Hz, 2H), 6.67 (d, *J* = 8.7 Hz, 2H), 3.84 (s, 3H), 2.88 (s, 3H), 1.57 (br, 1H); **^{13}C NMR** (101 MHz, Chloroform-*d*) δ 158.4, 148.4, 134.2, 130.1, 127.7, 127.4, 114.2, 112.8, 55.5, 31.0; **MS (*m/z*)**: (EI) calculated for $[C_{14}H_{15}NO]^+$: 213.12. Found: 213.1; **IR (neat) ν$_{max}$**: 3440, 2997, 1275, 1258, 749, 712 cm^{-1}.

4-(tert-butoxy)-4'-methoxy-1,1'-biphenyl, 25
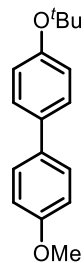
Isolated as a white solid (82 mg, 64%). **^{1}H NMR** (400 MHz, Chloroform-*d*) δ 7.50 (d, *J* = 8.6 Hz, 2H), 7.45 (d, *J* = 8.6 Hz, 2H), 7.04 (d, *J* = 8.7 Hz, 2H), 6.97 (d, *J* = 8.7 Hz, 2H), 3.85 (s, 3H), 1.38 (s, 9H); **^{13}C NMR** (101 MHz, Chloroform-*d*) δ 159.0, 154.6, 136.0, 133.6, 128.0, 127.2, 124.5, 114.3, 78.7, 55.5, 29.0; **MS (*m/z*)**: (EI) calculated for $[C_{17}H_{20}O_2]^+$: 256.1456. Found: 256.1458; **IR (neat) ν$_{max}$**: 2986, 1274, 1264, 1102, 764, 731, 703 cm^{-1}.

4'-methoxy-*N,N*-dimethyl-[1,1'-biphenyl]-4-amine, 26
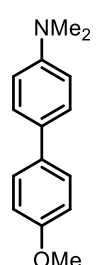
Isolated as a white solid (68 mg, 60%). **^{1}H NMR** (400 MHz, Chloroform-*d*) δ 7.51 – 7.45 (m, 4H), 6.96 (d, *J* = 12.4 Hz, 2H), 6.81 (d, *J* = 8.8 Hz, 2H), 3.85 (s, 3H), 2.99 (s, 6H); **^{13}C NMR** (101 MHz, Chloroform-*d*) δ 158.4, 149.8, 136.8, 134.1, 129.3, 127.5, 114.3, 113.1, 55.4, 40.8; **MS (*m/z*)**: (EI) calculated for $[C_{15}H_{17}NO]^+$: 227.13. Found: 227.1. Spectroscopic data in accordance with literature.[84]

N-(4'-methoxy-[1,1'-biphenyl]-4-yl)acetamide, 27
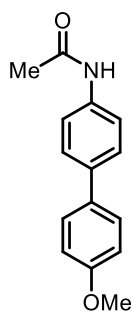
Isolated as a yellow solid (59 mg, 49%). **^{1}H NMR** (400 MHz, Chloroform-*d*) δ 7.56 – 7.50 (m, 6H), 7.10 (t, *J* = 9.1 Hz, 1H), 6.97 (d, *J* = 8.7 Hz, 2H), 3.85 (s, 3H), 2.20 (s, 3H); **^{13}C NMR** (101 MHz, Chloroform-*d*) δ 168.4, 136.6, 129.1, 128.0, 127.3, 121.2, 120.4, 120.0, 114.4, 54.5, 24.7; **MS (*m/z*)**: (EI) calculated for [C$_{15}$H$_{15}$NO$_2$]$^+$: 241.11. Found: 241.1. Spectroscopic data in accordance with literature.[359]

3,4'-dimethoxy-1,1'-biphenyl, 28
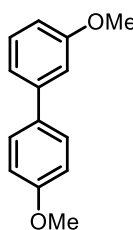
Unable to isolate (NMR yield 87%), white solid. Observed in **^{1}H NMR** (400 MHz, Chloroform-*d*) δ 7.57 – 7.52 (m), 7.40 – 7.32 (m), 7.18 – 7.18 (m), 7.01 – 6.95 (m), 3.89 (s, 3H), 3.86 (s, 3H); Observed in GCM: **MS (*m/z*)**: (EI) calculated for [C$_{14}$H$_{14}$O$_2$]$^+$: 214.10. Found: 214.1. Spectroscopic data in accordance with literature.[360]

4'-methoxy-3-(trifluoromethyl)-1,1'-biphenyl, 29
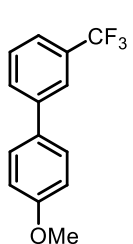
Isolated as a white solid (98 mg, 78%). **^{1}H NMR** (400 MHz, Chloroform-*d*) δ 7.79 (s, 1H), 7.72 (d, *J* = 7.1 Hz, 1H), 7.58 – 7.51 (m, 4H), 7.00 (d, *J* = 9.1 Hz, 2H), 3.87 (s, 3H); **^{13}C NMR** (101 MHz, Chloroform-*d*) δ 159.9, 141.7, 132.4, 131.0 (q, *J* = 31.6 Hz), 130.1, 129.3, 128.4, 127.8 (q, *J* = 272.6 Hz), 123.5 (q, *J* = 3.9 Hz), 123.3 (q, *J* = 3.9 Hz), 114.6, 55.5; **^{19}F NMR** (377 MHz, Chloroform-*d*) δ -62.49; **MS (*m/z*)**: (EI) calculated for [C$_{14}$H$_{11}$F$_3$O]$^+$: 252.08. Found: 252.1. Spectroscopic data in accordance with literature.[361]

4'-methoxy-*N,N*-dimethyl-[1,1'-biphenyl]-3-amine, 30
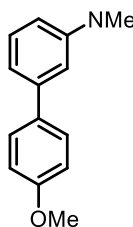
Isolated as a white solid (85 mg, 75%). **^{1}H NMR** (400 MHz, Chloroform-*d*) δ 7.55 (d, *J* = 8.0 Hz, 2H), 7.30 (t, *J* = 7.8 Hz, 1H), 6.98 (d, *J* = 8.0 Hz, 2H), 6.95 – 6.88 (m, 2H), 6.77 – 6.71 (m, 1H), 3.86 (s, 3H), 3.01 (s, 6H); **^{13}C NMR** (101 MHz, Chloroform-*d*) δ 159.2, 151.1, 142.0, 134.9, 129.5, 128.4, 115.7, 114.2, 111.4, 111.3, 55.5, 40.9; **MS (*m/z*)**: (EI) calculated for [C$_{15}$H$_{17}$NO]$^+$: 227.13. Found: 227.1. Spectroscopic data in accordance with literature.[362]

4'-methoxy-3-methyl-1,1'-biphenyl, 31
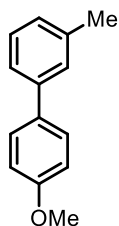
Isolated as a white solid (75 mg, 76%). **^{1}H NMR** (400 MHz, Chloroform-*d*) δ 7.54 (d, *J* = 8.9 Hz, 2H), 7.41 – 7.35 (m, 2H), 7.32 (t, *J* = 7.5 Hz, 1H), 7.14 (d, *J* = 7.5 Hz, 1H), 6.98 (d, *J* = 8.9 Hz, 2H), 3.86 (s, 3H), 2.43 (s, 3H); **^{13}C NMR** (101 MHz, Chloroform-*d*) δ 159.2, 141.0, 138.4, 134.0, 128.8, 128.3, 127.7, 127.6, 124.0, 114.3, 55.5, 21.7; **MS (*m/z*)**: (EI) calculated for $[C_{14}H_{14}O]^+$: 198.10. Found: 198.1. Spectroscopic data in accordance with literature.[363]

methyl 4'-methoxy-[1,1'-biphenyl]-3-carboxylate, 32
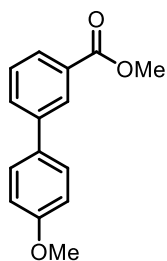
Unable to Isolate (NMR yield 71%), white solid. Observed in **^{1}H NMR** (400 MHz, Chloroform-*d*) δ 8.24 (s, 1H), 7.97 (d, *J* = 7.61, 1H), 7.74 (d, *J* = 8.33, 1H), 7.57 (m, 2H), 7.48 (m, 1H), 7.00 (d, *J* = 8.80, 2H), 3.9 (s, 3H), 3.86 (s, 3H); observed in GCMS: **MS (*m/z*)**: (EI) calculated for $[C_{15}H_{14}O_3]^+$: 242.09. Found: 242.1. Spectroscopic data in accordance with literature.[364]

2-fluoro-4'-methoxy-1,1'-biphenyl, 33
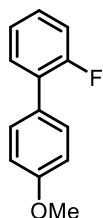
Isolated as a white solid (78 mg, 77%). **^{1}H NMR** (400 MHz, Chloroform-*d*) δ 7.57 – 7.47 (m, 2H), 7.42 (td, *J* = 7.8, 2.1 Hz, 1H), 7.31 – 7.26 (m, 1H), 7.19 (dd, *J* = 7.5, 1.4 Hz, 1H), 7.17 – 7.10 (m, 1 H), 6.99 (d, *J* = 6.9 Hz, 2H), 3.85 (s, 3H); **^{13}C NMR** (101 MHz, Chloroform-*d*) δ 159.4 (d, *J* = 245.5 Hz), 159.3, 130.6 (d, *J* = 3.7 Hz), 130.2 (d, *J* = 2.8 Hz), 128.5 (d, *J* = 13.0 Hz), 128.4 (d, *J* = 8.1 Hz), 128.3, 124.5 (d, *J* = 3.6 Hz), 116.2 (d, *J* = 23.0 Hz), 114.1, 55.5; **^{19}F NMR** (377 MHz, Chloroform-*d*) δ -118.16; **MS (*m/z*)**: (EI) calculated for $[C_{13}H_{11}FO]^+$: 202.08. Found: 202.1. Spectroscopic data in accordance with literature.[365]

2,4'-dimethoxy-1,1'-biphenyl, 34
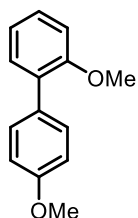
Unable to Isolate (73% NMR yield), white solid. Observed in **^{1}H NMR** (400 MHz, Chloroform-*d*) δ 7.48 – 7.42 (m), 7.34 – 7.21 (m), 7.09 - 6.86(m), 3.82 (s, 3H), 3.78 (s, 3H); Observed in GCM: **MS (*m/z*)**: (EI) calculated for $[C_{14}H_{14}O_2]^+$: 214.10. Found: 214.1. Spectroscopic data in accordance with literature.[366]

4'-methoxy-2-methyl-1,1'-biphenyl, 35
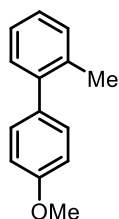
Isolated as a white solid (59 mg, 60%). **^{1}H NMR** (400 MHz, Chloroform-*d*) δ 7.25 – 7.20 (m, 6H), 6.94 (d, *J* = 7.8 Hz, 2H), 3.84 (s, 3H), 2.27 (s, 3H); **^{13}C NMR** (101 MHz, Chloroform-*d*) δ 158.6, 141.7, 135.6, 134.5, 130.4, 130.4, 130.0, 127.1, 125.9, 113.6, 55.4, 20.7; **MS (*m/z*)**: (EI) calculated for [C$_{14}$H$_{14}$O]$^+$: 198.10. Found: 198.1. Spectroscopic data in accordance with literature.[367]

4'-methoxy-2,6-dimethyl-1,1'-biphenyl, 36
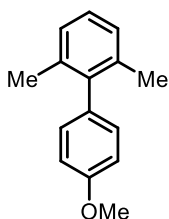
Isolated as a white solid (32 mg, 30%). **^{1}H NMR** (400 MHz, Chloroform-*d*) δ 7.17 – 7.13 (m, 1H), 7.11 – 7.08 (m, 2H), 7.08 – 7.04 (m, 2H), 6.98 – 6.95 (m, 2H), 3.86 (s, 3H), 2.04 (s, 6H); **^{13}C NMR** (101 MHz, Chloroform-*d*) δ 158.4, 141.7, 136.7, 133.5, 130.2, 127.4, 127.0, 114.0, 55.4, 21.0; **MS (*m/z*)**: (EI) calculated for [C$_{15}$H$_{16}$O]$^+$: 212.12. Found: 212.1. Spectroscopic data in accordance with literature.[365]

1-(4-methoxyphenyl)naphthalene, 37
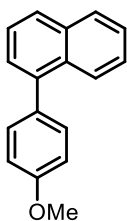
Isolated as a white solid (88 mg, 75%). **^{1}H NMR** (400 MHz, Chloroform-*d*) δ 7.94 – 7.94 (m, 2H), 7.84 (d, *J* = 8.2 Hz, 1H), 7.54 – 7.37 (m, 6H), 7.04 (d, *J* = 8.6 Hz, 2H), 3.90 (s, 3H); **^{13}C NMR** (101 MHz, Chloroform-*d*) δ 159.1, 140.1, 134.0, 133.3, 132.0, 131.3, 128.4, 127.5, 127.1, 126.2, 126.1, 125.8, 125.5, 113.9, 55.5; **MS (*m/z*)**: (EI) calculated for [C$_{17}$H$_{14}$O]$^+$: 234.10. Found: 234.1. Spectroscopic data in accordance with literature.[356]

### 2-(4-methoxyphenyl)naphthalene, 38
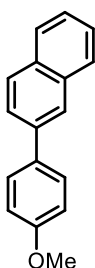
Isolated as a white solid (71 mg, 61%). **^{1}H NMR** (400 MHz, Chloroform-*d*) δ 7.99 (s, 1H), 7.93 – 7.81 (m, 3H), 7.72 (d, *J* = 8.6 Hz, 1H), 7.71 – 7.62 (m, 2H), 7.54 – 7.41 (m, 2H), 7.02 (d, *J* = 9.2 Hz, 2H), 3.88 (s, 3H); **^{13}C NMR** (101 MHz, Chloroform-*d*) δ 159.1, 140.1, 134.0, 133.3, 132.0, 131.3, 128.4, 127.5, 127.1, 126.2, 126.1, 125.8, 125.5, 113.9, 55.5; **MS (*m/z*)**: (EI) calculated for [C$_{17}$H$_{14}$O]$^+$: 234.10. Found: 234.1. Spectroscopic data in accordance with literature.[358]

2-(4-methoxyphenyl)benzo[d]thiazole, 39
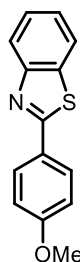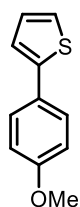
Isolated as a white solid (96 mg, 80%). **^{1}H NMR** (400 MHz, Chloroform-*d*) δ 8.02 (d, *J* = 8.5 Hz, 3H), 7.86 (d, *J* = 8.5 Hz, 1H), 7.47 (t, *J* = 7.5 Hz, 1H), 7.35 (t, *J* = 8.3 Hz, 1H), 6.99 (d, *J* = 9.0 Hz, 2H), 3.87 (s, 3H); **^{13}C NMR** (101 MHz, Chloroform-*d*) δ 168.0, 162.1, 154.4, 135.0, 129.2, 126.6, 126.3, 124.9, 122.9, 121.6, 114.4, 55.5; **MS (*m/z*)**: (EI) calculated for $[C_{14}H_{11}NOS]^+$: 241.06. Found: 241.1. Spectroscopic data in accordance with literature.[368]

2-(4-methoxyphenyl)thiazole, 40
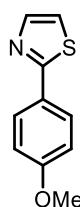
Isolated as a yellow solid (76 mg, 80%). **^{1}H NMR** (400 MHz, Chloroform-*d*) δ 7.91 (d, *J* = 9.0 Hz, 2H), 7.80 (d, *J* = 3.3 Hz, 1H), 7.25 (d, *J* = 3.3 Hz, 1H), 6.96 (d, *J* = 9.0 Hz, 2H), 3.86 (s, 3H); **^{13}C NMR** (101 MHz, Chloroform-*d*) δ 168.5, 161.3, 143.5, 128.2, 126.8, 118.0, 114.5, 55.6; **MS (*m/z*)**: (EI) calculated for $[C_{10}H_9NOS]^+$: 191.04. Found: 191.0. Spectroscopic data in accordance with literature.[369]

5-(4-methoxyphenyl)benzo[d][1,3]dioxole, 41
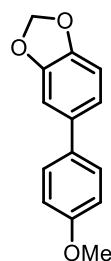
Isolated as a white solid (89 mg, 78%). **^{1}H NMR** (400 MHz, Chloroform-*d*) δ 7.51 – 7.44 (m, 2H), 7.06 – 6.99 (m, 1H), 7.02 – 6.95 (m, 2H), 6.95 (td, *J* = 4.8, 2.4 Hz, 3H), 6.86 (dd, *J* = 8.0, 5.3 Hz, 1H), 5.99 (s, 2H), 3.85 (s, 3H); **^{13}C NMR** (101 MHz, Chloroform-*d*) δ 159.0, 148.2, 146.7, 135.4, 133.6, 127.8, 120.2, 114.3, 108.6, 107.5, 101.2, 55.4; **MS (*m/z*)**: (EI) calculated for $[C_{14}H_{12}O_3]^+$: 228.08. Found: 228.1. Spectroscopic data in accordance with literature.[358]

2-(4-methoxyphenyl)thiophene, 42
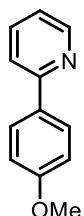
Isolated as a white solid (71 mg, 75%). **^{1}H NMR** (400 MHz, Chloroform-*d*) δ 7.54 (d, *J* = 8.1 Hz, 2H), 7.23 – 7.16 (m, 2H), 7.07 – 7.01 (m, 1H), 6.91 (d, *J* = 8.1 Hz, 2H), 3.84 (s, 3H); **^{13}C NMR** (101 MHz, Chloroform-*d*) ^{13}C NMR (101 MHz, Chloroform-*d*) δ 159.3, 144.5, 128.1, 127.9, 127.4, 124.0, 122.2, 114.3, 55.5; **MS (*m/z*)**: (EI) calculated for $[C_{11}H_{10}OS]^+$: 190.05. Found: 190.0. Spectroscopic data in accordance with literature.[369]

5-(4-methoxyphenyl)-1H-indole, 43
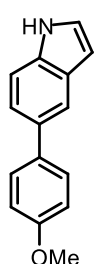
Isolated as a white solid (80 mg, 72%). **^{1}H NMR** (400 MHz, Chloroform-*d*) δ 8.17 (br s, 1H), 7.69-7.67 (m, 1H), 7.60-7.54 (m, 2H), 7.41-7.36 (m, 2H), 7.22 (t, *J* = 2.7 Hz, 1H), 6.99 (d, *J* = 8.8 Hz, 2H), 6.57 (t, *J* = 2.4 Hz, 1H), 3.86 (s, 3H); **^{13}C NMR** (101 MHz, Chloroform-*d*) δ 158.6, 135.3, 135.1, 133.2, 128.5, 128.5, 124.9, 121.9, 118.9, 114.2, 111.3, 103.1, 55.5; MS: **MS (*m/z*)**: (EI) calculated for $[C_{15}H_{13}NO]^+$: 223.10. Found: 223.1. Spectroscopic data in accordance with literature.[370]

3-(4-methoxyphenyl)quinoline, 44
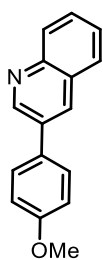
Isolated as a pale yellow solid (82 mg, 70%). **^{1}H NMR** (400 MHz, Chloroform-*d*) δ 9.16 (d, *J* = 2.3 Hz, 1H), 8.21 (d, *J* = 2.3 Hz, 1H), 8.11 (d, *J* = 8.0 Hz, 1H), 7.83 (d, *J* = 8.1 Hz, 1H), 7.68 (ddd, *J* = 8.4, 6.9, 1.5 Hz, 1H), 7.63 (d, *J* = 8.5 Hz, 3H), 7.55 (ddd, *J* = 8.1, 6.9, 1.2 Hz, 1H), 7.04 (d, *J* = 8.8 Hz, 2H), 3.87 (s, 3H); **^{13}C NMR** (101 MHz, Chloroform-*d*) δ 159.6, 149.6, 146.8, 133.2, 132.1, 130.0, 129.0, 128.8, 128.3, 127.9, 127.7, 126.7, 114.4, 55.2; **MS (*m/z*)**: (EI) calculated for $[C_{16}H_{13}NO]^+$: 235.10. Found: 235.1. Spectroscopic data in accordance with literature.[371]

2-(4-methoxyphenyl)pyridine, 45

Isolated as a white solid (60 mg, 65%). **^{1}H NMR** (400 MHz, Chloroform-*d*) δ 8.66 (d, *J* = 5.0 Hz, 1H), 7.97 (d, *J* = 8.4 Hz, 2H), 7.76 – 7.67 (m, 2H), 7.21 – 7.17 (m, 1H), 7.00 (d, *J* = 8.4 Hz, 2H), 3.86 (s, 3H); **^{13}C NMR** (101 MHz, Chloroform-*d*) δ 160.9, 156.9, 149.1, 143.7, 137.4, 128.5, 122.7, 120.2, 114.4, 55.5; **MS (*m/z*)**: (EI) calculated for $[C_{12}H_{11}NO]^+$: 185.08. Found: 185.1. Spectroscopic data in accordance with literature.[369]

6-(4-methoxyphenyl)-1H-indole, 46
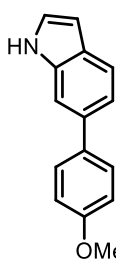
Isolated as an off-white solid (73 mg, 65%). **^{1}H NMR** (400 MHz, Chloroform-*d*) δ 8.17 (s, 1H), 7.68 (d, *J* = 8.2 Hz, 1H), 7.63–7.54 (m, 3H), 7.36 (dd, *J* = 8.2, 1.6 Hz, 1H), 7.24 (dd, *J* = 3.2, 2.4 Hz, 1H), 7.04-6.90 (m, 2H), 6.58 (ddd, *J* = 3.1, 2.0, 1.0 Hz, 1H), 3.87 (s, 3H); **^{13}C NMR** (101 MHz, Chloroform-*d*) δ 158.8, 136.6, 135.4, 135.1, 128.5, 126.9, 124.7, 121.0, 119.7, 114.3, 109.2, 102.7, 55.5; **MS (*m/z*)**: (EI) calculated for $[C_{15}H_{13}NO]^+$: 223.10. Found: 223.1. Spectroscopic data in accordance with literature.[372]

6-(4-methoxyphenyl)-2-methylquinoline, 47
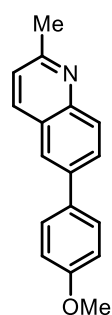
Isolated as a yellow oil (75 mg, 60%). **¹H NMR** (400 MHz, Chloroform-*d*) δ 8.06 (d, *J* = 3.1 Hz, 2H), 7.90 – 7.81 (m, 2H), 7.59 (d, *J* = 8.8 Hz, 2H), 7.28 (d, *J* = 8.4 Hz, 1H), 7.03 (d, *J* = 8.8 Hz, 2H), 3.87 (s, 3H), 2.76 (s, 3H); **¹³C NMR** (101 MHz, Chloroform-*d*) δ 159.5, 158.8, 147.0, 138.2, 136.4, 133.0, 129.1, 129.0 128.5, 126.8, 124.6, 122.5, 114.5, 55.5, 25.5; **MS (*m/z*)**: (EI) calculated for $[C_{17}H_{15}NO+H]^+$: 250.1221. Found: 250.1226; **IR (neat) ν$_{max}$**: 2925, 1607, 1519, 1493, 1284, 1247, 1180, 1040, 1022, 827 cm^{-1}.

2-(4-methoxyphenyl)pyrimidine, 48
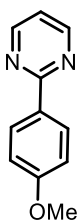
Isolated as a white solid (56 mg, 60%). **¹H NMR** (400 MHz, Chloroform-*d*) δ 8.75 (d, *J* = 4.8 Hz, 2H), 8.39 (d, *J* = 8.8 Hz, 2H), 7.12 (t, *J* = 4.8 Hz, 1H), 7.00 (d, *J* = 8.8 Hz, 2H), 3.89 (s, 3H); **¹³C NMR** (101 MHz, Chloroform-*d*) δ 164.7, 162.1, 157.3, 130.5, 129.9, 118.5, 114.1, 55.5; **MS (*m/z*)**: (EI) calculated for $[C_{11}H_{10}N_2O]^+$: 186.08. Found: 186.1. Spectroscopic data in accordance with literature.[373]

4-(4-methoxyphenyl)pyridine, 49
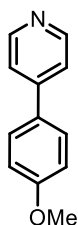
Isolated as a white solid (55 mg, 59%). **¹H NMR** (400 MHz, Chloroform-*d*) δ 8.60 (d, *J* = 6.7 Hz, 2H), 7.59 (d, *J* = 8.4 Hz, 2H), 7.47 (d, *J* = 6.7 Hz, 2H), 7.00 (d, *J* = 8.4 Hz, 2H), 3.87 (s, 3H); **¹³C NMR** (101 MHz, Chloroform-*d*) δ 160.7, 150.0, 148.2, 130.4, 128.3, 121.3, 114.7, 55.5; **MS (*m/z*)**: (EI) calculated for $[C_{12}H_{11}NO]^+$: 185.08. Found: 185.1. Spectroscopic data in accordance with literature.[366]

2-(4-methoxyphenyl)quinoline, 50
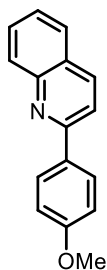
Isolated as a yellow oil (68 mg, 58%). **¹H NMR** (400 MHz, Chloroform-*d*) δ 8.20 – 8.09 (m, 4H), 7.92 – 7.76 (m, 2H), 7.70 (t, *J* = 8.4 Hz, 1H), 7.50 (t, *J* = 8.1 Hz, 1H), 7.03 (d, *J* = 8.9 Hz, 2H), 3.89 (s, 3H); **¹³C NMR** (101 MHz, Chloroform-*d*) δ 161.0, 157.1, 148.2, 136.8, 132.8, 129.7, 129.6, 129.1, 127.6, 127.1, 126.1, 118.7, 114.4, 55.5; **MS (*m/z*)**: (EI) calculated for $[C_{16}H_{13}NO]^+$: 235.10. Found: 235.1. Spectroscopic data in accordance with literature.[374]

3-(4-methoxyphenyl)thiophene, 51
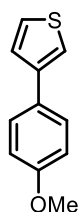
Isolated as a white solid (55 mg, 58%). **¹H NMR** (400 MHz, Chloroform-*d*) δ 7.52 (d, *J* = 8.8 Hz, 2H), 7.38 – 7.34 (m, 3H), 6.94 (d, *J* = 8.8 Hz, 2H), 3.84 (s, 3H); **¹³C NMR** (101 MHz, Chloroform-*d*) δ 159.0, 142.2, 128.9, 127.7, 126.4, 126.2, 119.1, 114.3, 55.5; **MS (*m/z*)**: (EI) calculated for [$C_{11}H_{10}OS$]⁺: 190.05. Found: 190.0. Spectroscopic data in accordance with literature.[375]

5-(4-methoxyphenyl)pyrimidine, 52
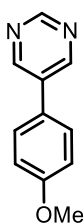
Isolated as a colourless oil (47 mg, 51%). **¹H NMR** (400 MHz, Chloroform-*d*) δ 9.19 (s, 1H), 8.68 (d, *J* = 5.5 Hz, 1H), 8.06 (d, *J* = 8.3 Hz, 2H), 7.63 (d, *J* = 5.5, 1H), 7.00 (d, *J* = 8.3 Hz, 2H), 3.86 (s, 3H); **¹³C NMR** (101 MHz, Chloroform-*d*) δ 163.5, 162.3, 159.1, 157.3, 128.9, 128.8, 116.2, 114.5, 55.5; **MS (*m/z*)**: (EI) calculated for [$C_{11}H_{10}N_2O$]⁺: 186.08. Found: 186.1. Spectroscopic data in accordance with literature.[376]

2-(4-methoxyphenyl)-1-methyl-1H-imidazole, 53
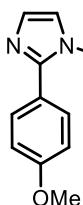
Isolated as a yellow oil (45 mg, 48%). **¹H NMR** (400 MHz, Chloroform-*d*) δ 7.56 (d, *J* = 9.4 Hz, 2H), 7.09 (d, *J* = 1.3 Hz, 1H), 6.97 (d, *J* = 9.4 Hz, 2H), 6.94 (d, *J* = 1.3 Hz, 1H), 3.85 (s, 3H), 3.72 (s, 3H); **¹³C NMR** (101 MHz, Chloroform-*d*) δ ¹³C NMR (101 MHz, CDCl₃) δ 160.1, 148.0, 130.2, 128.3, 123.3, 121.2, 114.2, 55.5, 34.5; **MS (*m/z*)**: (EI) calculated for [$C_{11}H_{12}N_2O$]⁺: 188.09. Found: 188.1. Spectroscopic data in accordance with literature.[374]

3-(4-methoxyphenyl)pyridine, 54
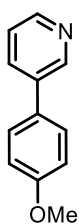
Isolated as a white solid (37 mg, 40%). **¹H NMR** (400 MHz, Chloroform-*d*) δ 8.83 (s, 1H), 8.56 (s, 1H), 7.85 – 7.82 (m, 1H), 7.53 (d, *J* = 9.0 Hz, 2H), 7.34 (dd, *J* = 7.8, 4.6 Hz, 1H), 7.00 (d, *J* = 9.0 Hz, 2H), 3.86 (s, 3H); **¹³C NMR** (101 MHz, Chloroform-*d*) δ 159.9, 148.1, 148.0, 141.1, 134.0, 130.4, 128.4, 124.1, 114.7, 55.5; MS: **MS (*m/z*)**: (EI) calculated for [$C_{12}H_{11}NO$]⁺: 185.08. Found: 185.1. Spectroscopic data in accordance with literature.[357]

2-(4-methoxyphenyl)pyrazine, 55
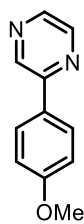
Isolated as a white solid (17 mg, 18%). **^{1}H NMR** (400 MHz, Chloroform-*d*) δ 8.98 (d, *J* = 1.6 Hz, 1H), 8.60 – 8.59 (m, 1H), 8.44 (d, *J* = 2.5 Hz, 1H), 7.98 (d, *J* = 9.2 Hz, 2H), 7.03 (d, *J* = 9.2 Hz, 2H), 3.88 (s, 3H); **^{13}C NMR** (101 MHz, Chloroform-*d*) δ 161.4, 152.8, 142.2, 142.0, 141.6, 128.9, 128.5, 114.7, 55.6; **MS (*m/z*)**: (EI) calculated for $[C_{11}H_{10}N_2O]^+$: 186.08. Found: 186.1. Spectroscopic data in accordance with literature.[374]

General Procedure 13: Nucleophile screen


Under an N_2 atmosphere, an oven dried Schlenk tube was charged with the appropriate boronic ester (1.25 mmol) and was dissolved in 2-MeTHF (3.0 mL) and cooled to -40 °C. ^{t}BuLi (1.7 M in hexane, 0.74 mL 1.25 mmol) was then added dropwise and allowed to stir for 30 mins at -40 °C. The reaction mixture was slowly brought to rt and stirred for a further 45 mins.

Meanwhile, in an argon-filled glovebox, IMes·HCl (17.1 mg, 0.05 mmol), FeBr₃ (14.8 mg, 0.05 mmol), MgBr₂·OEt₂ (25.8 mg, 0.1 mmol) and chlorobenzene (50.9 µL, 0.5 mmol) were added to a dried Schleck tube, containing a stirrer bar, followed by 1,4-dioxane (3.0 mL), forming a suspension. The Schlenk tube was sealed and taken out of the glovebox and attached to a Schlenk line and heated to an external temperature of 100 °C. MeMgBr (0.05 mL, 1.0 M, 0.05 mmol) was added to the Fe Schlenk and left to stir for 5 mins. The boronate formed *in situ*, assumed quantitative conversion, was then added in one go to the Fe Schlenk, sealed, and reacted at 100 °C for 3 hrs. The resulting mixture was cooled to room temperature and quenched with 1.0 M HCl (5.0 mL). The organics were extracted with CH_2Cl_2 (3 x 10 mL), the combined organics layers dried over MgSO₄ and filtered. 1,3,5-Trimethoxybenzene (84.1 mg, 0.5 mmol) was added, and an aliquot taken for analysis by ^{1}H NMR spectroscopy. The volatiles were then removed under vacuum. The crude mixture was purified by flash column chromatography (gradient elution: 100% hexanes to 25% ethyl acetate in hexanes) to yield the desired biaryl cross-coupled product.

4-methyl-1,1'-biphenyl, 56
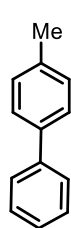
Isolated as a white solid (43 mg, 51%). **^{1}H NMR** (400 MHz, Chloroform-*d*) δ 7.51 – 7.45 (m, 2H), 7.41 (d, J = 8.2 Hz, 2H), 7.33 (t, J = 7.5 Hz, 2H), 7.27 – 7.19 (m, 1H), 7.15 (d, J = 8.2 Hz, 2H), 2.31 (s, 3H); **^{13}C NMR** (101 MHz, Chloroform-*d*) δ 141.3, 138.5, 137.1, 129.6, 128.8, 127.1, 127.1, 21.2; **MS (*m/z*)**: (EI) calculated for $[C_{13}H_{12}]^+$: 168.09. Found: 168.1. Spectroscopic data in accordance with literature.[377]

2-(p-tolyl)naphthalene, 57
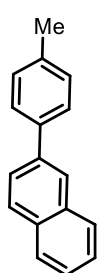
Isolated as an off-white solid (88 mg, 81%). **¹H NMR** (400 MHz, Chloroform-*d*) δ 8.03 (s, 1H), 7.94 – 7.81 (m, 3H), 7.75 (dd, *J* = 8.6, 1.8 Hz, 1H), 7.63 (d, *J* = 8.4 Hz, 2H), 7.55 – 7.41 (m, 2H), 7.30 (d, *J* = 7.9 Hz, 2H), 2.43 (s, 3H); **¹³C NMR** (101 MHz, Chloroform-*d*) δ 138.6, 138.4, 137.3, 133.9, 132.6, 129.7, 128.5, 128.3, 127.8, 127.4, 126.3, 125.9, 125.7, 125.6, 21.3; **MS (*m/z*)**: (EI) calculated for $[C_{17}H_{14}]^+$: 218.11. Found: 218.1. Spectroscopic data in accordance with literature.[378]

4-methoxy-4'-methyl-1,1'-biphenyl, 21
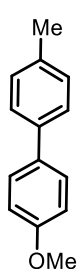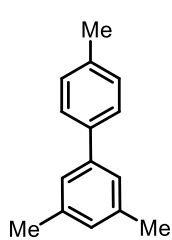
Isolated as a white solid (70 mg, 71%). **¹H NMR** (400 MHz, Chloroform-*d*) δ 7.53 – 7.49 (m, 2H), 7.45 (d, *J* = 9.3 Hz, 2H), 7.22 (d, *J* = 7.9 Hz, 2H), 6.96 (dd, *J* = 8.8, 8.3 Hz, 2H), 3.85 (s, 3H), 2.39 (s, 3H); **¹³C NMR** (101 MHz, Chloroform-*d*) δ 159.1, 138.1, 136.5, 133.9, 129.6, 128.1, 126.7, 114.3, 55.5, 21.2; **MS (*m/z*)**: (EI) calculated for $[C_{14}H_{14}O]^+$: 198.10. Found: 198.1. Spectroscopic data in accordance with literature.[379]

3,4',5-trimethyl-1,1'-biphenyl, 58

Isolated as a colourless oil (69 mg, 70%). **¹H NMR** (400 MHz, Chloroform-*d*) δ 7.52 (d, *J* = 8.2 Hz, 2H), 7.28 (d, *J* = 7.5 Hz, 2H), 7.25 (s, 2H), 7.02 (s, 1H), 2.44 (s, 3H), 2.42 (s, 6H); **¹³C NMR** (101 MHz, Chloroform-*d*) δ 141.6, 138.2, 136.9, 129.5, 128.9, 127.2, 126.9, 125.3, 21.5, 21.2; **MS (*m/z*)**: (EI) calculated for $[C_{15}H_{16}]^+$: 196.13. Found: 196.1. Spectroscopic data in accordance with literature.[380]

4-fluoro-4'-methyl-1,1'-biphenyl, 59
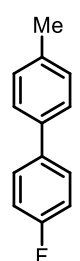
Isolated as a white solid (68 mg, 62%). **¹H NMR** (400 MHz, Chloroform-*d*) δ 7.55 – 7.47 (m, 2H), 7.43 (d, *J* = 8.5 Hz, 2H), 7.23 (d, *J* = 9.2 Hz, 2H), 7.12 – 7.08 (m, 2H), 2.40 (s, 3H); **¹³C NMR** (101 MHz, Chloroform-*d*) δ 163.5 (d, *J* = 247 Hz), 137.4, 137.3 (d, *J* = 4 Hz), 137.0, 129.5, 128.4 (d, *J* = 8 Hz), 126.8, 115.6 (d, *J* = 21 Hz), 21.2; **¹⁹F NMR** (377 MHz, Chloroform-*d*) δ -116.20 (ddd, *J* = 14.1, 8.8, 5.4 Hz); **MS (*m/z*)**: (EI) calculated for $[C_{13}H_{11}F]^+$: 186.08. Found: 186.1. Spectroscopic data in accordance with literature.[381]

N,N-4'-trimethyl-[1,1'-biphenyl]-4-amine, 60
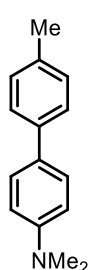
Isolated as an off-white solid (63 mg, 60%.) **¹H NMR** (400 MHz, Chloroform-*d*) δ 7.48 (d, *J* = 8.7 Hz, 2H), 7.45 (d, *J* = 7.8 Hz, 2H), 7.21 (d, *J* = 8.3 Hz, 2H), 6.81 (d, *J* = 8.7 Hz, 2H), 2.99 (s, 6H), 2.38 (s, 3H); **¹³C NMR** (101 MHz, Chloroform-*d*) δ 150.0, 138.5, 135.8, 129.5, 127.7, 126.3, 113.0, 40.8, 21.2; **MS (*m/z*)**: (EI) calculated for $[C_{15}H_{17}N]^+$: 211.14. Found: 211.1. Spectroscopic data in accordance with literature.[382]

2,4'-dimethyl-1,1'-biphenyl, 61
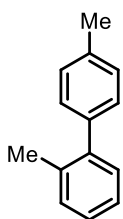
Unable to Isolate (NMR yield 60%), white solid. Observed in **¹H NMR** (400 MHz, Chloroform-*d*) δ 7.30 - 7.26 (m), 2.44 (s, 3H), 2.30 (s, 3H); observed in GCMS: **MS (*m/z*)**: (EI) calculated for $[C_{14}H_{14}]^+$: 182.11. Found: 182.1. Spectroscopic data in accordance with literature.[383]

4-methyl-4'-(trifluoromethyl)-1,1'-biphenyl, 62
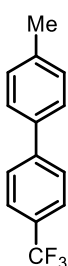
Isolated as a white solid, (55 mg, 47%). **¹H NMR** (400 MHz, Chloroform-*d*) δ 7.73 – 7.65 (m, 4H), 7.51 (d, *J* = 7.7 Hz, 2H), 7.28 (d, *J* = 8.6 Hz, 2H), 2.42 (s, 3H); **¹³C NMR** (101 MHz, Chloroform-*d*) δ 144.8, 138.3, 137.0, 129.9, 129.8 (q, *J* = 32.3 Hz), 127.3, 127.3, 126.0 (q, *J* = 3.8 Hz), 125.9 (q, *J* = 271.8 Hz), 21.3; **¹⁹F NMR** (377 MHz, Chloroform-*d*) δ; -62.24 **MS (*m/z*)**: (EI) calculated for $[C_{14}H_{11}F_3]^+$: 236.08. Found: 236.1. Spectroscopic data in accordance with literature.[384]

### 2-methoxy-4'-methyl-1,1'-biphenyl, 63
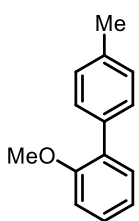
Isolated as a white solid (44 mg, 45%). **¹H NMR** (400 MHz, Chloroform-*d*) δ 7.43 (d, *J* = 7.5 Hz, 2H), 7.30 (td, *J* = 7.8, 6.5, 1.9 Hz, 2H), 7.21 (d, *J* = 8.1 Hz, 2H), 7.04 – 6.97 (m, 2H), 3.82 (s, 3H), 2.40 (s, 3H); **¹³C NMR** (101 MHz, Chloroform-*d*) δ 156.7, 136.7, 135.7, 130.9, 130.9, 129.5, 128.9, 128.5, 120.9, 111.3, 55.7, 21.3; **MS (*m/z*)**: (EI) calculated for $[C_{14}H_{14}O]^+$: 198.10. Found: 198.1. Spectroscopic data in accordance with literature.[385]

6.3 Experimental Details for Chapter 3

Electrophile omitted from reaction

In an argon-filled glovebox, IMes·HCl (17.1 mg, 0.05 mmol), FeBr$_3$ (14.8 mg, 0.05 mmol), and MgBr$_2$·OEt$_2$ (25.8 mg, 0.1 mmol) were added to a dried Schleck tube, containing a stirrer bar, followed by 1,4-dioxane (3.0 mL), forming a suspension. In a separate dried Schlenk tube the boronate **11** (552.9 mg, 1.25 mmol) was dissolved in the 2-MeTHF (3.0 mL). Both Schlenk tubes were sealed and taken out of the glove box and attached to a Schlenk line and heated to the appropriate external temperature, whilst stirred. MeMgBr (0.05 mL, 1.0 M, 0.05 mmol) was added to the Fe Schlenk tube and left to stir for 5 mins. The boronate solution was then added quickly to the Fe Schlenk tube and reacted at 100 °C (external temp.), and aliquots (~0.05 mL) were taken at the times given. Each aliquot was quenched with 1.0 M HCl (0.1 mL) and extracted into CH$_2$Cl$_2$ (2.0 mL) and then analysed by GC.

Late addition of electrophile
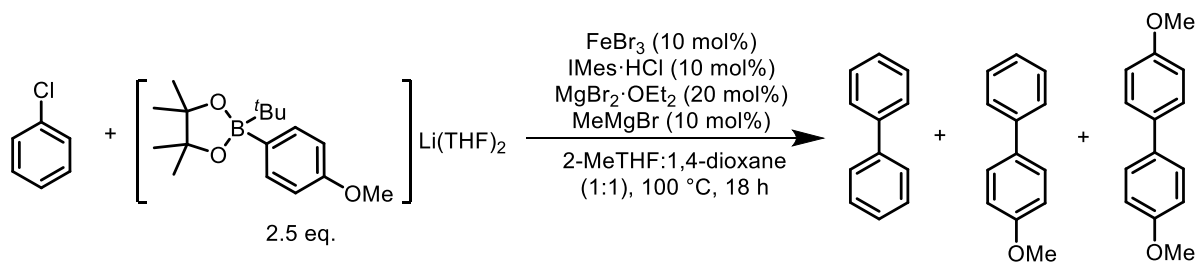
In an argon-filled glovebox, IMes·HCl (17.1 mg, 0.05 mmol), FeBr$_3$ (14.8 mg, 0.05 mmol), and MgBr$_2$·OEt$_2$ (25.8 mg, 0.1 mmol) were added to a dried Schleck tube, containing a stirrer bar, followed by 1,4-dioxane (3.0 mL), forming a suspension. In a separate dried Schlenk tube the boronate **11** (552.9 mg, 1.25 mmol) was dissolved in the 2-MeTHF (2.5 mL). A third Schlenk tube was charged with chlorobenzene (50.9 µL, 0.5 mmol) and 2-MeTHF (0.5 mL). All Schlenk tubes were sealed and taken out of the glove box and attached to a Schlenk line and heated to the appropriate external temperature, whilst stirred. MeMgBr (0.05 mL, 1.0 M, 0.05 mmol) was added to the Fe Schlenk tube and left to stir for 5 mins. The boronate solution was then added quickly to the Fe Schlenk tube and reacted at 100 °C (external temp.), and aliquots (~0.05 mL) were taken

at the times given. Each aliquot was quenched with 1.0 M HCl (0.1 mL) and extracted into CH_2Cl_2 (2.0 mL) and then analysed by GC. After 1 min 50 secs, the electrophile solution was added to the reaction mixture and aliquots were continued to be taken as described above.

Observing IMesFe(dvtms) (66) using 66 as a reducing agent
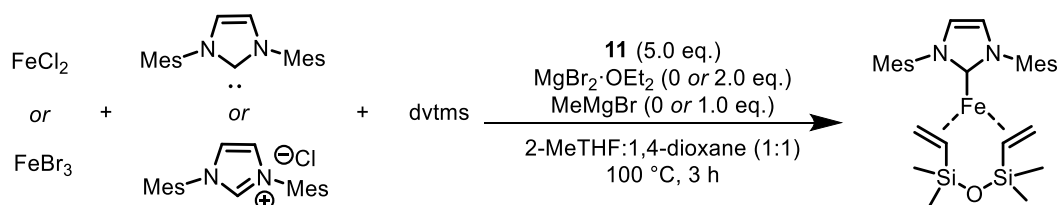
In an argon-filled glovebox, a Schlenk-tube was charged with either IMes (38 mg, 0.125 mmol) or IMes·HCl (42.6 mg, 0.125 mmol), either $FeCl_2$ (16.0 mg, 0.125 mmol) or $FeBr_3$ (37 mg, 0.125 mmol), 1,3- divinyltetramethyldisiloxane (29 µL, 0.125 mmol), and 1,4-dioxane (2.0 mL) and the resulting mixture was stirred for 1 h at room temperature. $MgBr_2 \cdot OEt_2$ (64 .5 mg, 0.25 mmol or 0 mmol) was added followed by boronate **11** (2.0 mL, 0.31 M in 2-MeTHF, 0.625 mmol or 0 mmol) and the mixture heated to 100 °C for 3 h. An aliquot was taken, the solvent removed in vacuo and the residue dissolved in C_6D_6 for ^{1}H NMR analysis.

Addition of PEG
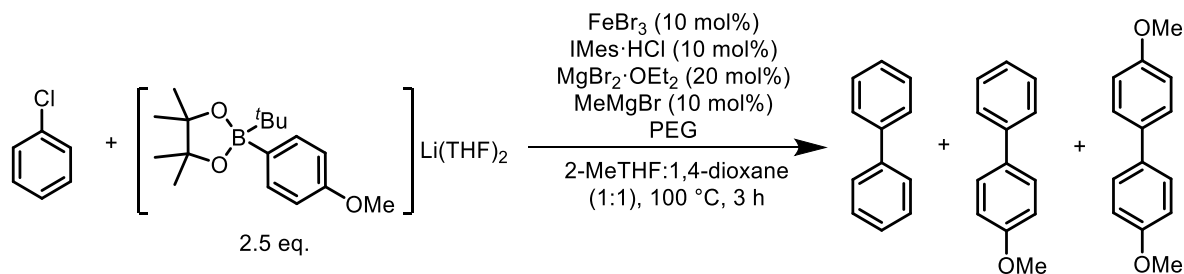
See General Procedure 9

Hg Drop Experiment

In an argon-filled glovebox, IMes·HCl (17.1 mg, 0.05 mmol), $FeBr_3$ (14.8 mg, 0.05 mmol), $MgBr_2 \cdot OEt_2$ (25.8 mg, 0.1 mmol), and chlorobenzene (50.9 µL, 0.5 mmol) were added to a dried Schleck tube, containing a stirrer bar, followed by 1,4-dioxane (3.0 mL), forming a suspension. In

a separate dried Schlenk tube the boronate **11** (552.9 mg, 1.25 mmol) was dissolved in the 2-MeTHF (3.0 mL). Both Schlenk tubes were sealed and taken out of the glove box and attached to a Schlenk line and heated to the appropriate external temperature, whilst stirred. MeMgBr (0.05 mL, 1.0 M, 0.05 mmol) was added to the Fe Schlenk tube and left to stir for 5 mins. The boronate solution was then added quickly to the Fe Schlenk tube and reacted at 100 °C (external temp.), and aliquots (~0.05 mL) were taken at the times given. Each aliquot was quenched with 1.0 M HCl (0.1 mL) and extracted into CH_2Cl_2 (2.0 mL) and then analysed by GC. One drop from a Pasteur pipette was added to the reaction mixture 1 min and 50 secs after the addition of the boronate. Aliquots were continued to be taken as described above.

Pre-formed Fe NPs
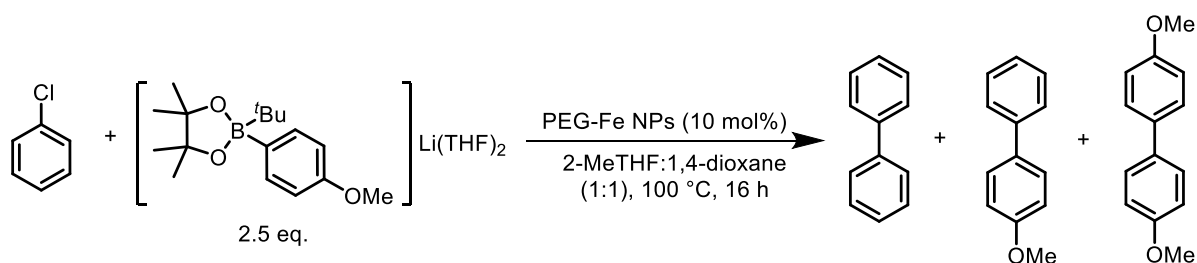
A suspension of iron nanoparticles was prepared according to a literature method.[98] In a glovebox, a Schlenk-tube was charged with $FeCl_3$ (8.1 mg, 0.05 mmol) and polyethylene glycol (pre-dried by toluene azeotrope, Mw = 10,000, 3.0 mg, 0.05 mmol). The tube was sealed, taken out of the glovebox and CH_2Cl_2 (2.0 mL) was added. The mixture was stirred for 2 min before the volatiles were removed in vacuo. Et_2O (2.0 mL) was added before 4-tolylmagnesium bromide (0.5 M in Et_2O, 0.3 mL, 0.15 mmol) and the resulting mixture stirred for 1 h at room temperature. To a separate Schlenk-tube was added chlorobenzene (50.9 µL, 0.5 mmol) and boronate **11** (3.0 mL 0.416 M in 2-MeTHF, 1.25 mmol) and the resulting mixture was added to the first Schlenk-tube which was then sealed. The reaction was stirred at 100 °C for 16 h and then quenched by the addition of 1.0 M HCl (10 mL). The organics were extracted from the aqueous layer with CH_2Cl_2 (3 x 10 mL), the combined layers dried over $MgSO_4$ and filtered. Dodecane (113.6 µL, 0.5 mmol) was added and an aliquot taken for analysis by gas chromatography.

General Procedure 14: Kinetic experiments

Unless otherwise stated, the amounts used are shown in the general procedure below.

In an argon-filled glovebox, IMes·HCl (17.1 mg, 0.05 mmol), FeBr₃ (14.8 mg, 0.05 mmol), MgBr₂·OEt₂ (25.8 mg, 0.1 mmol) and chlorobenzene (50.9 µL, 0.5 mmol) were added to a dried Schleck tube, containing a stirrer bar, followed by 1,4-dioxane (3.0 mL), forming a suspension. In a separate dried Schlenk tube the boronate **11** (552.9 mg, 1.25 mmol) was dissolved in the 2-MeTHF (3.0 mL). Both Schlenk tubes were sealed and taken out of the glove box and attached to a Schlenk line and heated to the appropriate external temperature, whilst stirred. MeMgBr (0.05 mL, 1.0 M, 0.05 mmol) was added to the Fe Schlenk tube and left to stir for 5 mins. The boronate solution was then added quickly to the Fe Schlenk tube and reacted at 100 °C (external temp.) and aliquots (~0.05 mL) were taken at the times given. Each aliquot was quenched with 1.0 M HCl (0.1 mL) and extracted into CH₂Cl₂ (2.0 mL) and then analysed by GC.

General Procedure 15: LFER Electrophile

In an argon-filled glovebox, IMes·HCl (17.1 mg, 0.05 mmol), FeBr₃ (14.8 mg, 0.05 mmol), MgBr₂·OEt₂ (25.8 mg, 0.1 mmol) and aryl chloride (0.5 mmol) were added to a dried Schleck tube, containing a stirrer bar,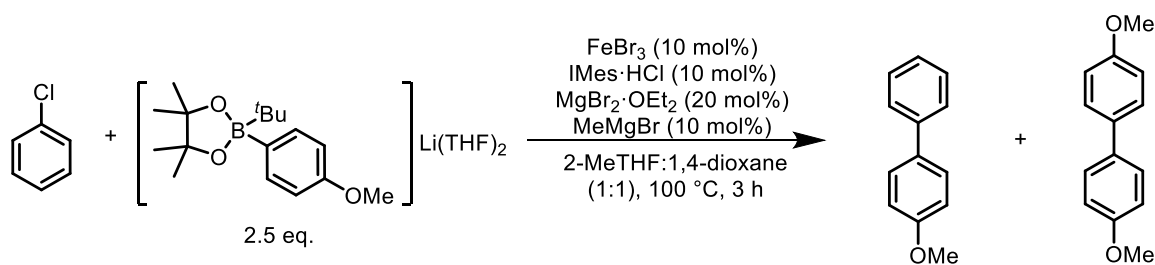 followed by 1,4-dioxane (3.0 mL), forming a suspension. In a separate dried Schlenk tube the boronate **11** (552.9 mg, 1.25 mmol) was dissolved in the 2-MeTHF (3.0 mL). Both Schlenk tubes were sealed and taken out of the glove box and attached to a Schlenk line and heated to the appropriate external temperature, whilst stirred. MeMgBr (0.05 mL, 1.0 M, 0.05 mmol) was added to the Fe Schlenk tube and left to stir for 5 mins. The boronate solution was then added quickly to the Fe Schlenk tube and reacted at 100 °C (external temp.) and aliquots

(~0.05 mL) were taken at the times given. Each aliquot was quenched with 1.0 M HCl (0.1 mL) and extracted into CH_2Cl_2 (2.0 mL) and then analysed by GC.

General Procedure 16: LFER Nucleophile

Under an N_2 atmosphere, an oven dried Schlenk tube was charged with the appropriate boronic ester (1.25 mmol) and was dissolved in 2-MeTHF (3.0 mL) and cooled to -40 °C. ^tBuLi (1.7 M in hexane, 0.74 mL 1.25 mmol) was then added dropwise and allowed to stir for 30 mins at -40 °C. The reaction mixture was slowly brought to rt and stirred for a further 45 mins.

Meanwhile, in an argon-filled glovebox, IMes·HCl (17.1 mg, 0.05 mmol), FeBr₃ (14.8 mg, 0.05 mmol), MgBr₂·OEt₂ (25.8 mg, 0.1 mmol) and chlorobenzene (50.9 µL, 0.5 mmol) were added to a dried Schleck tube, containing a stirrer bar, followed by 1,4-dioxane (3.0 mL), forming a suspension. The Schlenk tube was sealed and taken out of the glovebox and attached to a Schlenk line and heated to an external temperature of 100 °C. MeMgBr (0.05 mL, 1.0 M, 0.05 mmol) was added to the Fe Schlenk and left to stir for 5 mins. The boronate formed *in situ*, assumed quantitative conversion, was then added in one go to the Fe Schlenk, sealed, and reacted at 100 °C and aliquots (~0.05 mL) were taken at the times given. Each aliquot was quenched with 1.0 M HCl (0.1 mL) and extracted into CH_2Cl_2 (2.0 mL) and then analysed by GC.

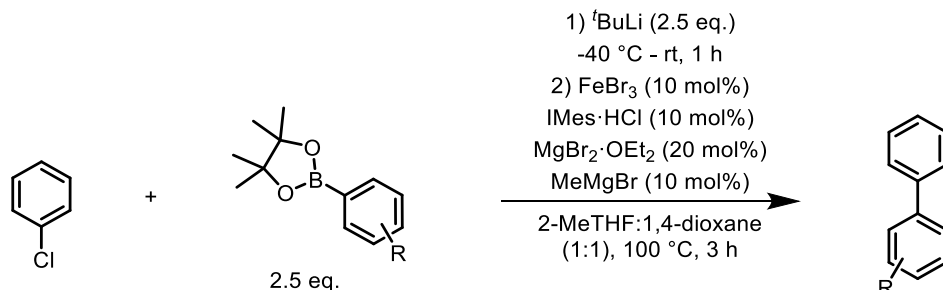## General Procedure 17: Determination of activation parameters
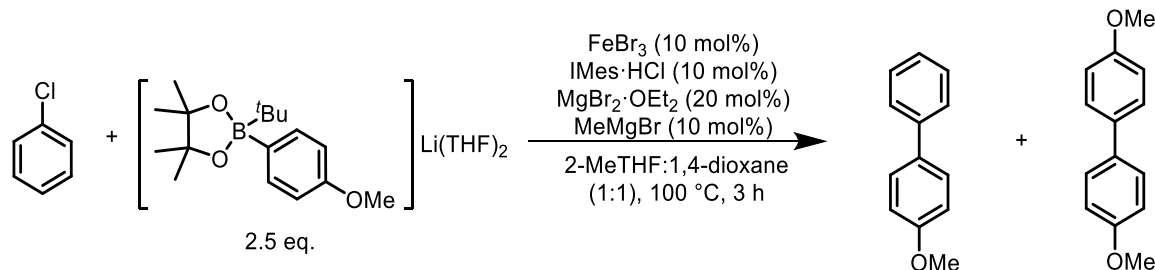
See General Procedure 14 – Reactions are done at the following temperatures: 60, 70, 80, 90 and 100 °C.

General Procedure 18: Radical probe experiment
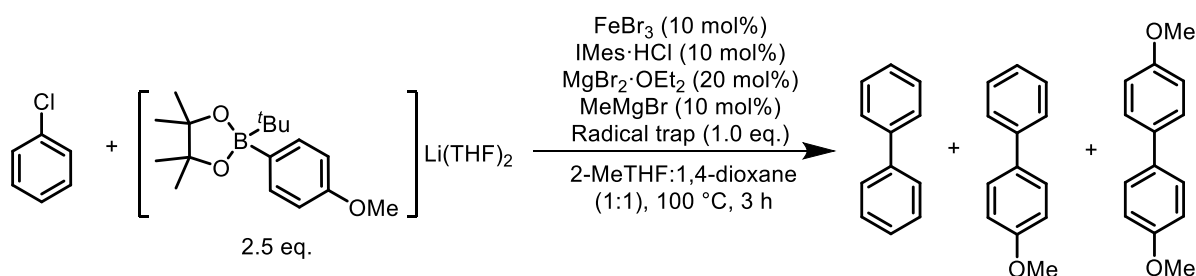
See General Procedure 9. Radical probes used were: 1,4-cyclohexadiene, BHT, 1,1-dipehnylethylene, TEMPO and trityl chloride

Cross-coupling of chlorobenzene with 4-methoxyphenylmagnesium bromide
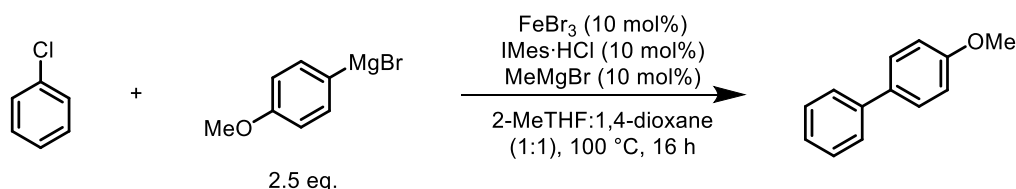
In an argon-filled glovebox, a Schlenk-tube was charged with IMes·HCl (17.1 mg, 0.05 mmol), FeBr$_3$ (14.8 mg, 0.05 mmol) and 1,4-dioxane (3.0 mL). The mixture was stirred at room temperature for 1 h before chlorobenzene (50.9 µL, 0.5 mmol) and 2-MeTHF (2.75 mL) were added. The Schlenk tube was sealed, taken out of the glovebox, and heated to 100 °C. MeMgBr (0.05 mL, 0.1 M, 0.05 mmol) was then added to the reaction mixture and left to stir for 5 mins. 4-methoxyphenylmagnesium bromide (1.25 mL,1.0 M in THF, 1.25 mmol) was then added, the Schlenk-tube was sealed, and the reaction stirred for 16 h at 100 °C. The reaction was then quenched by the addition of 1.0 M HCl (5.0 mL). The organics were extracted from the aqueous layer with CH$_2$Cl$_2$ (3 x 5.0 mL), the combined layers dried over MgSO$_4$ and filtered. Dodecane (113.6 µL, 0.5 mmol) was added and an aliquot taken for analysis by GC.

Cross-coupling of chlorobenzene with bis(4-methoxyphenyl)zinc
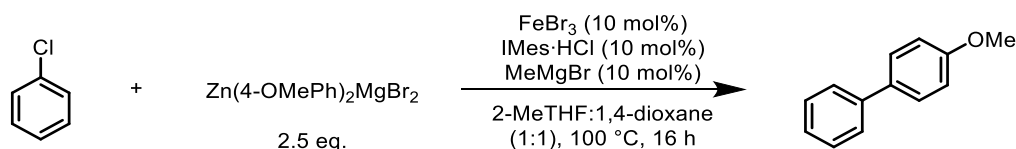
In a glovebox, a Schlenk-tube was charged with ZnBr$_2$ (281 mg, 1.25 mmol) and 2-MeTHF (3.0 mL). The tube was sealed, taken out of the glovebox. 4-methoxyphenylmagnesium bromide (2.5 mL, 1.0 M in THF, 2.5 mmol) was added and the resulting mixture stirred for 1 h. A separate Schlenk-tube was charged with IMes·HCl (17.1 mg, 0.05 mmol), FeBr$_3$ (14.8 mg, 0.05 mmol) and

1,4-dioxane (3.0 mL). The mixture was stirred at room temperature for 1 h before the addition of chlorobenzene (50.9 µL, 0.5 mmol), the reaction mixture was then heated to 100 °C and MeMgBr (0.05 mL, 0.1 M, 0.05 mmol) was then added to the reaction mixture and left to stir for 5 mins. The freshly prepared Zn(4-OMePh)$_2$/MgBr$_2$ was then added to the reaction mixture, the Schlenk-tube was sealed, and the reaction stirred for 16 h at 100 °C. The reaction was then quenched by the addition of 1.0 M HCl (5.0 mL). The organics were extracted from the aqueous layer with CH$_2$Cl$_2$ (3 x 5.0 mL), the combined layers dried over MgSO$_4$ and filtered. Dodecane (113.6 µL, 0.5 mmol) was added and an aliquot taken for analysis by GC.

Cross-coupling of chlorobenzene with MgBr[Al(4-MeOPh)$_4$]
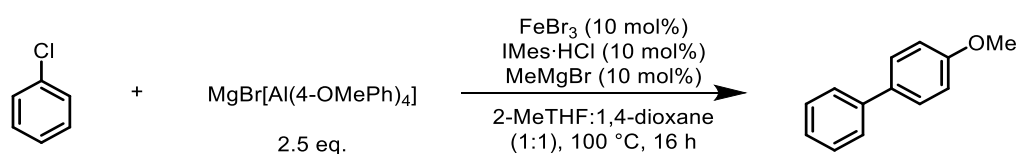
In a glovebox, a Schlenk-tube was charged with AlBr$_3$ (333 mg, 1.25 mmol) and 2-MeTHF (3.0 mL). The tube was sealed, taken out of the glovebox. The solution was cooled to 0 °C and 4-methoxyphenylmagnesium bromide (5.0 mL, 1.0 M in THF, 5.0 mmol) was added and the resulting mixture then warmed to room temperature and stirred for 30 min. A separate Schlenk-tube was charged with IMes·HCl (17.1 mg, 0.05 mmol), FeBr$_3$ (14.8 mg, 0.05 mmol). The mixture was stirred at room temperature for 1 h before the addition of chlorobenzene (50.9 µL, 0.5 mmol), the reaction mixture was then heated to 100 °C and MeMgBr (0.05 mL, 0.1 M, 0.05 mmol) was then added to the reaction mixture and left to stir for 5 mins. The freshly prepared [Al(4-OMePh)$_4$]MgBr was then added to the reaction mixture, the Schlenk-tube was sealed, and the reaction stirred for 16 h at 100 °C. The reaction was then quenched by the addition of 1.0 M HCl (5.0 mL). The organics were extracted from the aqueous layer with CH$_2$Cl$_2$ (3 x 5.0 mL), the combined layers dried over MgSO$_4$ and filtered. Dodecane (113.6 µL, 0.5 mmol) was added and an aliquot taken for analysis by GC.

6.4 Experimental Details for Chapter 4

6.4.1 Synthesis of [B₂Pin₂][ᵗBuLi]
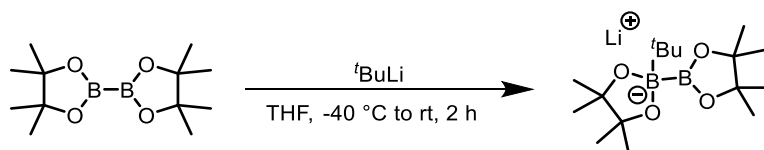
A Schlenk tube was charged with bis(pinacolato)diboron (10.92 g, 43 mmol) and THF (150 mL) and was then cooled to -40 °C and stirred. ᵗBuLi (25 mL, 1.7 M in hexane, 42.5 mmol) was then added dropwise to the solution. The reaction mixture was left to stir for 30 mins, before being brought slowly to rt and left to stir for a further 1 hr, a white precipitate formed. The reaction mixture was then filtered and washed with THF (3 x 100 mL) and dried under vacuum for 2 h. This formed the product as a white solid in quantitative yield and was able to be stored under an inert atmosphere. **¹H NMR** (400 MHz, Chloroform-*d*) δ 1.19 (s, 12 H), 1.01 (s, 6 H), 0.98 (s, 6 H), 0.63 (s, 9 H) ; **¹³C NMR** (101 MHz, Chloroform-*d*) δ 81.9, 77.1, 30.6, 26.6, 26.0, 25.8, 25.6; **¹¹B NMR** (128 MHz, Chloroform-*d*) δ 38.8, 5.9.

6.4.2 Optimisation

General Procedure 19: Fe salt, ligand, and base screen
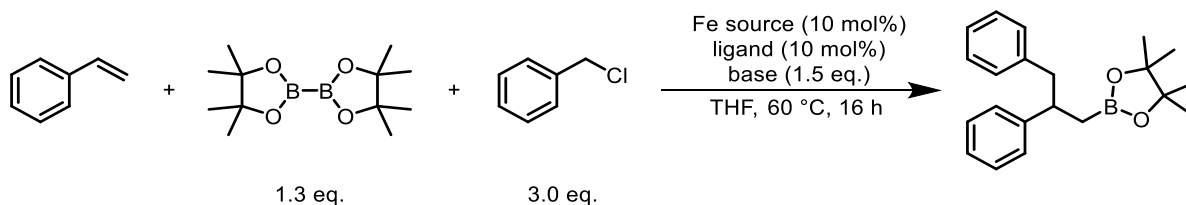
In a glovebox, an oven dried vial was charged with the ligand (0.01 mmol) and Fe salt (500 μL, 0.02 M in THF, 0.01 mmol) and was stirred at rt for 15 mins. In the following order: styrene (11.5 μL, 0.1 mmol), benzyl chloride (34.5 μL, 0.3 mmol), bis(pinacolato)diboron (325 μL, 0.4 M in THF, 0.13 mmol) and base (500 μL, 0.3 M in THF, 0.15 mmol) were then added to the vial. The vial was sealed, heated to 60 °C and allowed to stir for 16 h. The reaction was quenched with sat. NH₄Cl (1.0 mL) and 1,3,5-trimethoxybenzene (8.4 mg, 0.05 mmol) was added. The organics were then extracted into CH₂Cl₂ (5.0 mL). The volatiles were then removed, and the reaction mixture was analysed by ¹H NMR and GCMS to observe the components of the reaction mixture.

General Procedure 20: B$_2$Pin$_2$ activator screen

1.3 eq.   3.0 eq.
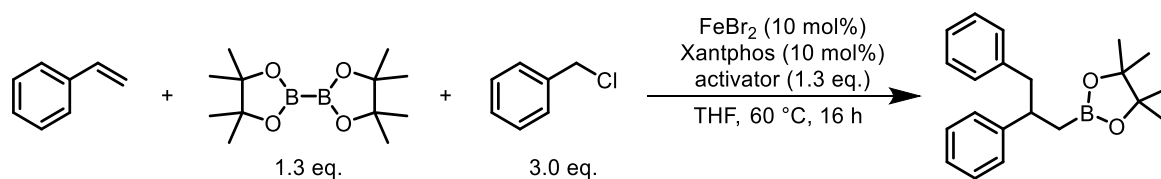
In a glovebox, an oven dried Schlenk tube was charged with Xantphos (5.8 mg, 0.01 mmol) and FeBr$_2$ (500 µL, 0.02 M in THF, 0.01 mmol) and was stirred at rt for 15 mins. In a separate Schlenk tube, bis(pinacolato)diboron (38.1 mg, 0.15 mmol) was dissolved in THF (1.0 mL). Styrene (11.5 µL, 0.1 mmol), benzyl chloride (34.5 µL, 0.3 mmol) and THF (0.5 mL) were then added to the Fe Schlenk tube. Both Schlenk tubes were sealed and taken out of the glovebox. The iron Schlenk tube was heated to 60 °C and stirred. The Schlenk tube containing B$_2$Pin$_2$ solution was cooled to -40 °C and stirred, the B$_2$Pin$_2$ activator (0.15 mmol) was then added dropwise to the solution. The reaction mixture was left to stir for 30 mins, before being brought slowly to RT and left to stir for a further 30 mins. This solution was then added in one portion to the Fe Schlenk tube and left to stir for 16 h at 60 °C. The reaction was quenched with sat. NH$_4$Cl (1.0 mL) and 1,3,5-trimethoxybenzene (8.4 mg, 0.05 mmol) was added. The organics were then extracted into CH$_2$Cl$_2$ (5.0 mL). The volatiles were then removed, and the reaction mixture was analysed by ^{1}H NMR and GCMS to observe the components of the reaction mixture.

General Procedure 21: Solvent screen

1.3 eq.   3.0 eq.
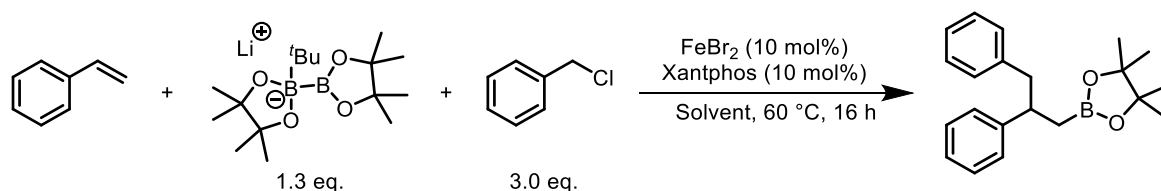
In a glovebox, an oven dried vial was charged with Xantphos (5.8 mg, 0.01 mmol), FeBr$_2$ (2.2 mg, 0.01 mmol) and solvent (0.5 mL) and was stirred at rt for 15 mins. In the following order: styrene (11.5 µL, 0.1 mmol), benzyl chloride (34.5 µL, 0.3 mmol), [B$_2$Pin$_2$][^{t}BuLi] (47.7 mg, 0.15 mmol) and solvent (2.5 mL) were then added to the vial. The vial was sealed, heated to 60 °C and allowed to stir for 16 h. The reaction was quenched with sat. NH$_4$Cl (1.0 mL) and 1,3,5-trimethoxybenzene (8.4 mg, 0.05 mmol) was added. The organics were then extracted into CH$_2$Cl$_2$ (5.0 mL). The volatiles were then removed, and the reaction mixture was analysed by ^{1}H NMR and GCMS to observe the components of the reaction mixture.

General Procedure 22: Additive screen

1.3 eq.   3.0 eq.
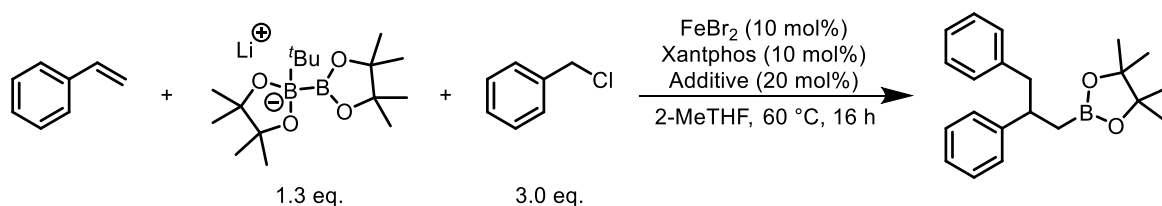
In a glovebox, an oven dried vial was charged with Xantphos (5.8 mg, 0.01 mmol) and FeBr₂ and was stirred at rt for 15 mins. In the following order: styrene (11.5 μL, 0.1 mmol), benzyl chloride (34.5 μL, 0.3 mmol), [B₂Pin₂][ᵗBuLi] (47.7 mg, 0.15 mmol) and 2-MeTHF (2.5 mL) were then added to the vial. The vial was sealed, heated to 60 °C and allowed to stir for 16 h. The reaction was quenched with sat. NH₄Cl (1.0 mL) and 1,3,5-trimethoxybenzene (8.4 mg, 0.05 mmol) was added. The organics were then extracted into CH₂Cl₂ (5.0 mL). The volatiles were then removed, and the reaction mixture was analysed by ¹H NMR and GCMS to observe the components of the reaction mixture.

General Procedure 23: DoE study
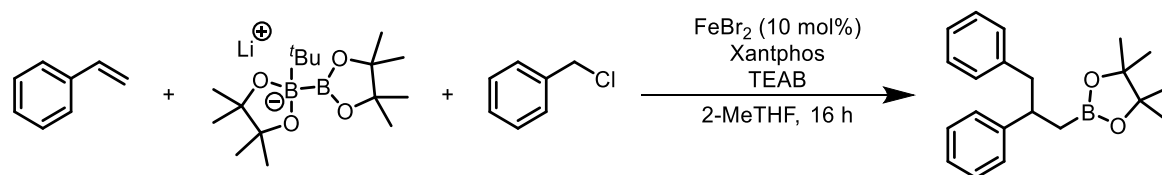
See Table 4.7 for amounts of reagents. In a glovebox, an oven dried vial was charged with Xantphos and FeBr₂ (500 μL, 0.02 M in 2-MeTHF, 0.01 mmol) and was stirred at rt for 15 mins. In the following order: styrene (11.5 μL, 0.1 mmol), benzyl chloride, [B₂Pin₂][ᵗBuLi], TEAB and 2-MeTHF were then added to the vial. The vial was sealed, heated to 60 °C and allowed to stir for 16 h. The following day, the reaction was quenched with sat. NH₄Cl (1.0 mL) and then extracted into DCM (5.0 mL). The reaction was quenched with sat. NH₄Cl (1.0 mL) and 1,3,5-trimethoxybenzene (8.4 mg, 0.05 mmol) was added. The organics were then extracted into CH₂Cl₂ (5.0 mL). The volatiles were then removed, and the reaction mixture was analysed by ¹H NMR and GCMS to observe the components of the reaction mixture.

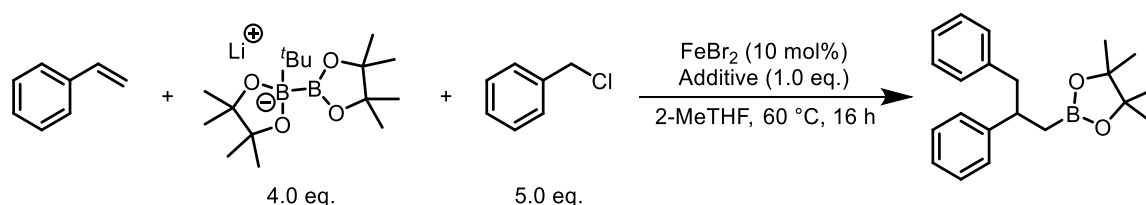## General procedure 24: Robustness screen

4.0 eq.   5.0 eq.

In a glovebox, an oven dried vial was charged with: FeBr₂ (250 μL, 0.02 M, 0.005 mmol), styrene (5.7 μL, 0.05 mmol), benzyl chloride (28.8 μL, 0.25 mmol), [B₂Pin₂][ᵗBuLi] (63.6 mg, 0.2 mmol), additive (0.1 mmol) and 2-MeTHF (1.25 mL). The vial was sealed, heated to 60 °C and allowed to stir for 16 h. The reaction was quenched with sat. NH₄Cl (1.0 mL) and dodecane (11.4 μL, 0.05 mmol) was added. The organics were then extracted into CH₂Cl₂ (5.0 mL) and an aliquot was taken to analyse by GC and GCMS to observe the components of the reaction mixture.

.

6.4.3 Substrate scope

General Procedure 25: Alkene scope
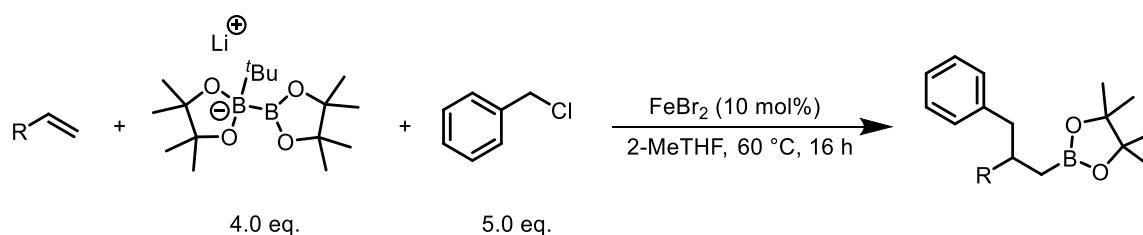
In a glovebox, an oven Schlenk tube was charged with: FeBr₂ (2.5 mL, 0.02 M in 2-MeTHF, 0.05 mmol), alkene (0.5 mmol), benzyl chloride (287.7 μL, 2.5 mmol), [B₂Pin₂][ᵗBuLi] (636 mg, 2.0 mmol), and 2-MeTHF (12.5 mL). The Schlenk tube was sealed, taken outside of the glovebox, heated to 60 °C and allowed to stir for 16 h. The reaction was quenched with sat. NH₄Cl (5.0 mL) and then extracted into DCM (3 x 15 mL) and dried over MgSO₄. The volatiles were then removed and the crude was analysed by ¹H NMR and GCMS. The product was then purified by flash column chromatography (100% hexane to 25% EtOAc in Hexane).

2-(2,3-diphenylpropyl)-4,4,5,5-tetramethyl-1,3,2-dioxaborolane, 67
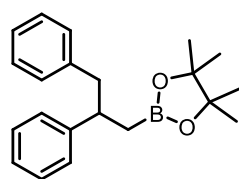
Isolated as a colourless oil, 71%. **¹H NMR** (400 MHz, Chloroform-*d*) δ 7.24 – 7.09 (m, 8H), 7.06 – 7.00 (m, 2H), 3.13 (m, 1H), 2.96 – 2.78 (m, 2H), 1.21 – 1.15 (m, 2H), 1.06 (s, 6H), 1.04 (s, 6H); **¹³C NMR** (101 MHz, Chloroform-*d*) δ 146.6, 140.9, 129.5, 128.1, 128.1, 127.7, 126.0, 125.9, 83.1, 46.3, 43.7, 24.8, 24.7 (signal of carbon directly bonded to boron was not detected because of quadrupolar relaxation); **¹¹B NMR** (128 MHz, Chloroform-*d*) δ 33.58; **HRMS (m/z)**: (+EI) calculated for C₂₀H₂₄BO₂ [M-Me]⁺: 307.1864. Found: 307.1862. Spectroscopic data in accordance with literature.[302]

4,4,5,5-tetramethyl-2-(3-phenyl-2-(p-tolyl)propyl)-1,3,2-dioxaborolane, 76
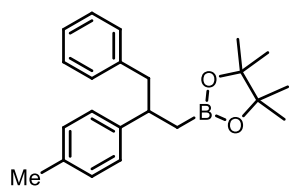
Isolated as a colourless oil, 54%. **¹H NMR** (400 MHz, Chloroform-*d*) δ 7.22 – 7.17 (m, 2H), 7.16 – 7.12 (m, 1H), 7.07 – 7.01 (m, 6H), 3.11 (dq, *J* = 9.2, 7.1 Hz, 1H), 2.93 – 2.78 (m, 2H), 2.29 (s, 3H), 1.21 – 1.15 (m, 1H), 1.08 (s, 6H), 1.07 (s, 6H); **¹³C NMR** (101 MHz, Chloroform-*d*) δ 143.7, 141.1, 135.3, 129.5, 128.8, 128.1, 127.5, 125.8, 83.1, 46.3, 43.2, 24.8, 24.7, 21.1 (signal of carbon directly bonded to boron was not detected because of quadrupolar relaxation); **¹¹B NMR** (128 MHz, Chloroform-*d*) δ 33.36; **HRMS (m/z)**: (+EI) calculated for $C_{21}H_{26}BO_2$ [M-CH₃]⁺: 321.2020. Found: 321.2018; **IR (neat) ν$_{max}$**: 2979, 1365, 1322, 1274, 1143, 967, 848, 764 cm⁻¹.

2-(2-(4-methoxyphenyl)-3-phenylpropyl)-4,4,5,5-tetramethyl-1,3,2-dioxaborolane, 77
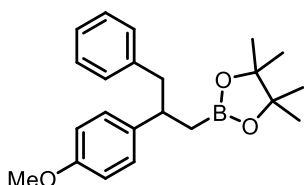
Isolated as a colourless oil, 61%. **¹H NMR** (400 MHz, Chloroform-*d*) δ 7.22 – 7.16 (m, 2H), 7.15 – 7.11 (m, 1H), 7.07 – 6.99 (m, 4H), 6.80 – 6.71 (m, 2H), 3.76 (s, 3H), 3.08 (dq, *J* = 9.3, 7.3 Hz, 1H), 2.83 (d, *J* = 7.3 Hz, 2H), 1.19 – 1.10 (m, 2H), 1.07 (s, 6H), 1.06 (s, 6H); **¹³C NMR** (101 MHz, Chloroform-*d*) δ 157.9, 141.0, 138.8, 129.5, 128.6, 128.1, 125.8, 113.5, 83.1, 55.4, 46.5, 42.9, 24.87, 24.74 (signal of carbon directly bonded to boron was not detected because of quadrupolar relaxation); **¹¹B NMR** (128 MHz, Chloroform-*d*) δ 33.67; **HRMS (m/z)**: (+EI) calculated for $C_{22}H_{29}BO_3$ [M]⁺: 352.2204. Found: 352.2204; Spectroscopic data in accordance with literature.[302]

2-(2-(4-fluorophenyl)-3-phenylpropyl)-4,4,5,5-tetramethyl-1,3,2-dioxaborolane, 78
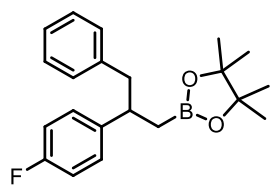
Isolated as a colourless oil, 68%. **¹H NMR** (400 MHz, Chloroform-*d*) δ 7.22 – 7.16 (m, 2H), 7.16 – 7.12 (m, 1H), 7.07 (ddd, *J* = 8.5, 5.4, 2.6 Hz, 2H), 7.03 – 6.96 (m, 2H), 6.94 – 6.84 (m, 2H), 3.19 – 3.06 (m, 1H), 2.93 – 2.70 (m, 2H), 1.27 – 1.13 (m, 2H), 1.08 (s, 6H), 1.06 (s, 6H); **¹³C NMR** (101 MHz, Chloroform-*d*) δ 161.3 (d, *J* = 243.17 Hz), 142.1 (d, *J* = 3.10 Hz), 140.5, 129.4, 129.0 (d, *J* = 7.77 Hz), 128.1, 125.9, 114.8 (d, *J* = 20.92 Hz), 83.1, 46.5, 43.1, 24.8, 24.7 (signal of carbon directly bonded to boron was not detected because of quadrupolar relaxation); **¹¹B NMR** (128 MHz, Chloroform-*d*) δ 33.56; **¹⁹F NMR** (377 MHz, Chloroform-d) δ -117.73 (tt, *J* = 8.7, 5.5 Hz); **HRMS (m/z)**: (+EI) calculated for $C_{20}H_{23}BFO_2$ [M-CH₃]⁺: 325.1770. Found: 325.1768; Spectroscopic data in accordance with literature.[289]

4,4,5,5-tetramethyl-2-(3-phenyl-2-(4-(trifluoromethyl)phenyl)propyl)-1,3,2-dioxaborolane, 79
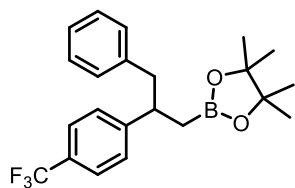
Isolated as a colourless oil, 65%. **^{1}H NMR** (400 MHz, Chloroform-*d*) δ 7.49 – 7.44 (m, 2H), 7.24 (d, *J* = 8.0 Hz, 2H), 7.22 – 7.11 (m, 3H), 7.02 – 6.98 (m, 2H), 3.20 (dq, *J* = 9.1, 6.9 Hz, 1H), 2.96 – 2.77 (m, 2H), 1.24 – 1.16 (m, 2H), 1.07 (s, 6H), 1.05 (s, 6H); **^{13}C NMR** (101 MHz, Chloroform-*d*) δ 150.7 (q, *J* = 1.4 Hz), 140.2, 129.4, 128.4, 128.2, 128.0, 126.1, 125.6, 125.1 (q, *J* = 3.8 Hz), 83.3, 45.9, 43.7, 24.8, 24.7 (signal of carbon directly bonded to boron was not detected because of quadrupolar relaxation); **^{11}B NMR** (128 MHz, Chloroform-*d*) δ 33.58; **^{19}F NMR** (377 MHz, Chloroform-d) δ -62.27; **HRMS (m/z)**: (+EI) calculated for $C_{21}H_{23}BF_3O_2$ [M-CH$_3$]$^+$: 375.1738. Found: 375.1736; **IR (neat) ν_{max}**: 2981, 1372, 1325, 1275, 1257, 1123, 1068, 845 cm^{-1}.

4,4,5,5-tetramethyl-2-(3-phenyl-2-(thiophen-2-yl)propyl)-1,3,2-dioxaborolane, 80
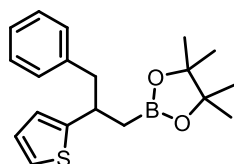
Isolated as a colourless oil, 46%. **^{1}H NMR** (400 MHz, Chloroform-*d*) δ 7.25 – 7.13 (m, 4H), 7.11 – 7.02 (m, 3H), 6.83 (dd, *J* = 5.1, 3.5 Hz, 1H), 6.69 (dt, *J* = 3.5, 1.0 Hz, 1H), 3.45 (dq, *J* = 8.8, 7.2 Hz, 1H), 2.92 (d, *J* = 7.2 Hz, 2H), 1.28 – 1.22 (m, 2H), 1.13 (s, 6H), 1.11 (s, 6H); **^{13}C NMR** (101 MHz, Chloroform-*d*) δ 150.8, 140.5, 129.5, 128.2, 126.3, 126.1, 123.5, 122.6, 83.2, 47.0, 39.1, 24.9, 24.87 (signal of carbon directly bonded to boron was not detected because of quadrupolar relaxation); **^{11}B NMR** (128 MHz, Chloroform-*d*) δ 33.60; **HRMS (m/z)**: (+EI) calculated for $C_{18}H_{22}BO_2S$ [M-CH$_3$]$^+$: 316.1428. Found: 316.1427; **IR (neat) ν_{max}**: 2989, 2918, 1442, 1371, 1275, 1258, 1066, 842 cm^{-1}.

4-(1-phenyl-3-(4,4,5,5-tetramethyl-1,3,2-dioxaborolan-2-yl)propan-2-yl)aniline, 81
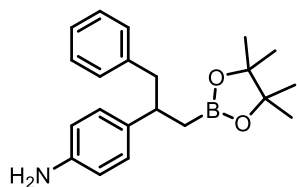
Isolated as a yellow oil, 52%. **^{1}H NMR** (400 MHz, Chloroform-*d*) δ 7.23 – 7.13 (m, 2H), 7.15 – 7.08 (m, 1H), 7.06 – 6.98 (m, 2H), 6.96 – 6.89 (m, 2H), 6.60 – 6.51 (m, 2H), 3.52 (b, 2H), 3.03 (dq, *J* = 9.3, 7.1 Hz, 1H), 2.86 – 2.78 (m, 2H), 1.29 – 1.20 (m, 2H), 1.08 (s, 6H), 1.07 (s, 6H); **^{13}C NMR** (101 MHz, Chloroform-*d*) δ 144.3, 141.2, 136.9, 129.5, 128.4, 128.0, 125.7, 115.1, 83.0, 46.6, 42.9, 24.9, 24.7 (signal of carbon directly bonded to boron was not detected because of quadrupolar relaxation); **^{11}B NMR** (128 MHz, Chloroform-*d*) δ 33.79; **HRMS (m/z)**: (+ESI) calculated for $C_{21}H_{29}NBO_2$ [M+H]$^+$: 338.2286 Found: 338.2281; **IR (neat) ν_{max}**: 3376, 2979, 1516, 1371, 1276, 1144, 848, 784 cm^{-1}.

4,4,5,5-tetramethyl-2-(2-(naphthalen-2-yl)-3-phenylpropyl)-1,3,2-dioxaborolane, 82
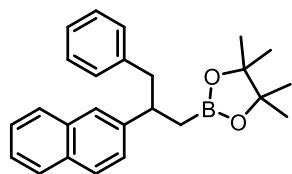
Isolated as a colourless oil, 73%. **¹H NMR** (400 MHz, Chloroform-*d*) δ 7.82 – 7.78 (m, 1H), 7.78 – 7.73 (m, 2H), 7.61 (d, *J* = 1.7 Hz, 1H), 7.47 – 7.36 (m, 3H), 7.24 – 7.11 (m, 4H), 7.11 – 7.07 (m, 2H), 3.36 (dq, *J* = 9.1, 7.2 Hz, 1H), 3.01 (qd, *J* = 13.3, 7.2 Hz, 2H), 1.38 – 1.27 (m, 2H), 1.05 (s, 6H), 1.04 (s, 6H); **¹³C NMR** (101 MHz, Chloroform-*d*) δ 144.2, 140.8, 133.6, 132.3, 129.5, 128.1, 127.7, 127.7, 127.6, 126.4, 125.9, 125.9, 125.7, 125.1, 83.1, 46.0, 43.8, 24.8, 24.7 (signal of carbon directly bonded to boron was not detected because of quadrupolar relaxation); **¹¹B NMR** (128 MHz, Chloroform-*d*) δ 34.25; **HRMS (m/z)**: (+EI) calculated for $C_{25}H_{29}BO_2$ [M]⁺: 372.2255. Found: 372.2252. Spectroscopic data in accordance with literature.[289]

methyl 4-(1-phenyl-3-(4,4,5,5-tetramethyl-1,3,2-dioxaborolan-2-yl)propan-2-yl)benzoate, 83
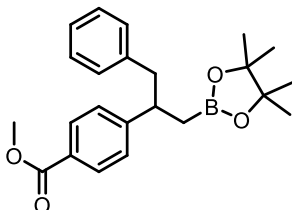
Isolated as a colourless oil, 45%. **¹H NMR** (400 MHz, Chloroform-*d*) δ 7.95 – 7.85 (m, 2H), 7.21 – 7.11 (m, 5H), 7.01 – 6.95 (m, 2H), 3.89 (s, 3H), 3.25 – 3.14 (m, 1H), 2.94 – 2.81 (m, 2H), 1.21 (m, 2H), 1.07 (s, 6H), 1.04 (s, 6H); **¹³C NMR** (101 MHz, Chloroform-*d*) δ 167.4, 152.2, 140.3, 129.5, 129.4, 128.2, 127.9, 127.8, 126.1, 83.2, 52.1, 45.9, 43.9, 24.8, 24.7 (signal of carbon directly bonded to boron was not detected because of quadrupolar relaxation); **¹¹B NMR** (128 MHz, Chloroform-*d*) δ 33.44; **HRMS (m/z)**: (+EI) calculated for $C_{23}H_{29}BO_4$ [M+]⁺: 380.2153. Found: 380.2152; **IR (neat) ν_max**: 2998, 1717, 1275, 1251, 764, 750 cm⁻¹.

4,4,5,5-tetramethyl-2-(2,2,3-triphenylpropyl)-1,3,2-dioxaborolane, 84
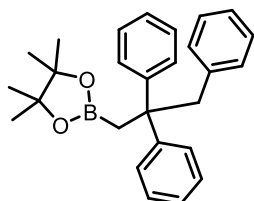
Isolated as a colourless oil, 32%. **¹H NMR** (400 MHz, Chloroform-*d*) δ 7.25 – 7.19 (m, 4H), 7.19 – 7.13 (m, 6H), 7.11 – 7.08 (m, 1H), 7.07 – 7.02 (m, 2H), 6.63 (d, *J* = 6.9, 2H), 3.64 (s, 2H), 1.55 (s, 2H), 1.04 (s, 12H); **¹³C NMR** (101 MHz, Chloroform-*d*) δ 150.1, 138.8, 131.2, 128.3, 127.7, 127.2, 125.8, 125.7, 82.9, 48.6, 45.3, 24.8 (signal of carbon directly bonded to boron was not detected because of quadrupolar relaxation); **¹¹B NMR** (128 MHz, Chloroform-*d*) δ 33.43; **HRMS (m/z)**: (+EI) calculated for $C_{26}H_{28}BO_2$ [M-CH₃]⁺: 383.2177. Found: 383.2175. Spectroscopic data in accordance with literature.[302]

4,4,5,5-tetramethyl-2-(2-methyl-2,3-diphenylpropyl)-1,3,2-dioxaborolane, 85
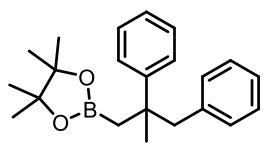
Isolated as a colourless oil, 38%. **^{1}H NMR** (400 MHz, Chloroform-*d*) δ 7.31 – 7.27 (m, 2H), 7.26 – 7.22 (m, 2H), 7.18 – 7.14 (m, 1H), 7.14 – 7.09 (m, 3H), 6.89 – 6.74 (m, 2H), 2.95 (q, *J* = 12.4 Hz, 2H), 1.44 (s, 3H), 1.12 (m, 2H), 1.07 (s, 6H), 1.03 (s, 6H); **^{13}C NMR** (101 MHz, Chloroform-*d*) δ 149.0, 139.1, 130.8, 127.8, 127.5, 126.7, 125.9, 125.6, 82.8, 52.4, 40.5, 26.6, 24.9, 24.6 (signal of carbon directly bonded to boron was not detected because of quadrupolar relaxation); **^{11}B NMR** (128 MHz, Chloroform-*d*) δ 33.23; **HRMS (m/z)**: (+EI) calculated for $C_{21}H_{26}BO_2$ [M-CH$_3$]$^+$: 321.2020 Found: 321.2020. Spectroscopic data in accordance with literature.[302]

General Procedure 26: Diboron screen
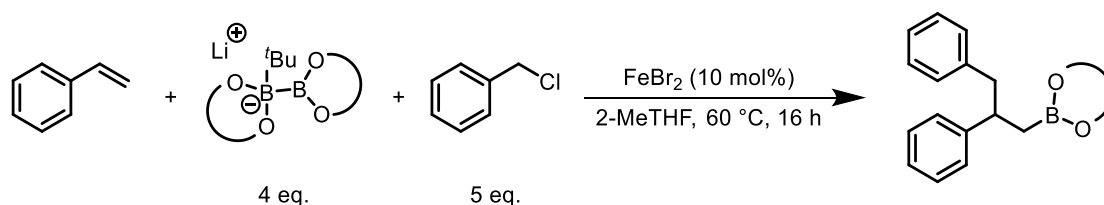
In a glovebox, an oven dried Schlenk tube was charged with FeBr$_2$ (2.5 mL, 0.02 M in 2-MeTHF, 0.05 mmol), styrene (57.5 μL, 0.5 mmol), benzyl chloride (287.7 μL, 2.5 mmol) and 2-MeTHF (7.5 mL).

In a separate Schlenk tube, diboron reagent (2.0 mmol) was dissolved in 2-MeTHF (5.0 mL). Both Schlenk tubes were sealed and taken out of the glovebox. The iron Schlenk tube was heated to 60 °C and stirred.

The Schlenk tube containing the diboron solution was cooled to -40 °C and stirred, ^{t}BuLi (1.17 mL, 1.7 M in hexane, 2.0 mmol,) was then added dropwise to the solution. The reaction mixture was left to stir for 30 mins, before being brought slowly to RT and left to stir for a further 30 mins. This solution was then added in one portion to the iron Schlenk tube and left to stir for 16 h at 60 °C.

The following day, the reaction was quenched with sat. NH$_4$Cl (5.0 mL) and then extracted into DCM (3 x 15 mL) and dried over MgSO$_4$. The volatiles were then removed, and the crude was analysed by ^{1}H NMR and GCMS. The product was then purified by flash column chromatography (100% hexane to 25% EtOAc in Hexane).

(2,3-diphenylpropyl)-5,5-dimethyl-1,3,2-dioxaborinane, 101
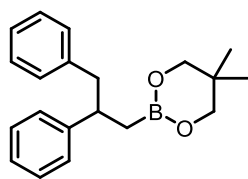
Isolated as a colourless oil, 44%. **^{1}H NMR** (400 MHz, Chloroform-*d*) δ 7.26 – 7.08 (m, 8H), 7.08 – 6.98 (m, 2H), 3.42 (s, 4H), 3.12 (p, *J* = 7.5 Hz, 1H), 2.85 (qd, *J* = 13.2, 7.5 Hz, 2H), 1.22 – 1.01 (m, 2H), 0.75 (s, 6H); **^{13}C NMR** (101 MHz, Chloroform-*d*) δ 147.5, 141.2, 129.6, 128.2, 128.0, 127.6, 125.8, 125.8, 71.9, 46.3, 43.6, 31.6, 29.9, 21.8 (signal of carbon directly bonded to boron was not detected because of quadrupolar relaxation); **^{11}B NMR** (128 MHz, Chloroform-*d*) δ 30.48; **HRMS (m/z)**: (ESI+) calculated for $C_{12}H_{17}BNaO_3$ [M+Na]$^+$: 243.1168. Found: 243.1170; **IR (neat) ν$_{max}$**: 2987, 1275, 1257, 1101, 764, 751 cm^{-1}.

References

1   R. L. R. F. Haber, *Z. Elektrochem. Angew. Phys. Chem*, 1913, **19**, 53.

2   C. Torborg and M. Beller, *Adv. Synth. Catal.*, 2009, **351**, 3027–3043.

3   X. F. Wu, P. Anbarasan, H. Neumann and M. Beller, *Angew. Chem. Int. Ed.*, 2010, **49**, 9047–9050.

4   C. Glaser, *Ber. Dtsch. Chem. Ges*, 1869, **2**, 422–424.

5   C. Glaser, *Ann. Chem. Pharm*, 1870, **154**, 137–171.

6   F. Ullmann and J. Bielecki, *Ber. Dtsch. Chem. Ges.*, 1901, **34**, 2174–2185.

7   F. Ullmann and P. Sponagel, *Ber. Dtsch. Chem. Ges.*, 1903, **38**, 2211–2212.

8   R. J. P. Corriu, *J. Organomet. Chem.*, 2002, **653**, 20–22.

9   M. S. Kharasch and E. K. Fields, *J. Am. Chem. Soc.*, 1941, **63**, 2316–2320.

10   C. F. Fuchs, G. Herbert and M. S. Kharasch, *J. Am. Chem. Soc.*, 1941, **65**, 504–507.

11   M. S. Kharasch and C. F. Fuchs, *J. Am. Chem. Soc.*, 1943, **65**, 504–507.

12   H. Meerwein, E. Büchner and K. van Emster, *J. Prakt. Chem.*, 1939, **152**, 237–266.

13   M. Kharasch and G. Sosnovsky, *J. Am. Chem. Soc.*, 1958, **80**, 756–756.

14   Corriu R. and Masse J., *J. Chem. Soc. Chem. Commun.*, 1972, **3**, 144a.

15   K. Tamao, K. Sumitani and M. Kumada, *J. Am. Chem. Soc.*, 1972, **94**, 4374–4376.

16   K. Tamao, Y. Kiso, K. Sumitani and M. Kumada, *J. Am. Chem. Soc.*, 1972, **94**, 9268–9269.

17   R. F. Heck, *J. Am. Chem. Soc.*, 1968, **90**, 5538–5542.

18   R. F. Heck, *J. Am. Chem. Soc.*, 1968, **90**, 5542–5546.

19   R. F. Heck, *J. Am. Chem. Soc.*, 1968, **90**, 5518–5526.

20   R. F. Heck, *J. Am. Chem. Soc.*, 1968, **90**, 5531–5534.

21   R. F. Heck, *J. Am. Chem. Soc.*, 1968, **90**, 5546–5548.

22   R. F. Heck, *J. Am. Chem. Soc.*, 1968, **90**, 5526–5531.

23   R. F. Heck, *J. Am. Chem. Soc.*, 1968, **90**, 5535–5538.

24   K. F. Heck and J. P. Nolley, *J. Org. Chem.*, 1972, **37**, 2320–2322.

25   A. M. Thomas, A. Sujatha and G. Anilkumar, *RSC Adv.*, 2014, **4**, 21688–21698.

26   K. Sonogashira, Y. Tohda and N. Hagihara, *Tetrahedron Lett.*, 1975, **7950**, 4467–4470.

27   M. Yamamura, I. Moritani and S. I. Murahashi, *J. Organomet. Chem.*, 1975, **91**, 3–6.

28   S. I. Murahashi, M. Yamamura, K. ichi Yanagisawa, N. Mita and K. Kondo, *J. Org. Chem.*, 1979, **44**, 2408–2417.

29   D. Milstein and J. K. Stille, *J. Org. Chem.*, 1979, **44**, 1613–1618.

30   E. Negishi, A. O. King and N. Okukado, *J. Org. Chem.*, 1977, **42**, 1821–1823.

31   N. Miyaura and A. Suzuki, *Chem. Rev.*, 1995, **95**, 2457–2483.

32   N. Miyaura and A. Suzuki, *J. Chem. Soc. Chem. Commun.*, 1979, **19**, 866–867.

33   Y. Hatanaka and T. Hiyama, *J. Org. Chem.*, 1988, **53**, 918–920.

34   S. D. Roughley and A. M. Jordan, *J. Med. Chem.*, 2011, **54**, 3451–3479.

35   K. C. Nicolaou, P. G. Bulger and D. Sarlah, *Angew. Chem. Int. Ed.*, 2005, **44**, 4442–4489.

36   P. Nuss and M. J. Eckelman, *PLoS One*, 2014, **9**, e101298–e101310.

37   Daily metal price, https://www.dailymetalprice.com/ . Accessed on 31/03/2022.

38   M. M. Reddy, K. H. Reddy and M. U. Reddy, *Pharm. Regul. Aff.*, 2016, **5**, 1–8.

39   C. E. Garrett and K. Prasad, *Adv. Synth. Catal.*, 2004, **346**, 889–900.

40   S. Shi, G. Meng and M. Szostak, *Angew. Chem. Int. Ed.*, 2016, **55**, 6959–6963.

41   S. K. Gurung, S. Thapa, B. Shrestha and R. Giri, *Org. Chem. Front.*, 2015, **2**, 649–653.

42   S. B. Tailor, M. Manzotti, G. J. Smith, S. A. Davis and R. B. Bedford, *ACS Catal.*, 2021, **11**, 3856–3866.

43   G. Vavon and P. Mottez, *C. R. Acad. Sci.*, 1944, **218**, 557–559.

44   J. D. Sears, P. G. N. Neate and M. L. Neidig, *J. Am. Chem. Soc.*, 2018, **140**, 11872–11883.

45   M. Tamura and J. Kochi, *J. Am. Chem. Soc.*, 1971, **93**, 1487–1489.

46   G. Cahiez and H. Avedissian, *Synthesis (Stuttg).*, 1998, **08**, 1199–1205.

47   A. Fürstner, A. Leitner, M. Méndez and H. Krause, *J. Am. Chem. Soc.*, 2002, **124**, 13856–13863.

48   R. B. Bedford, D. W. Bruce, R. M. Frost and M. Hird, *Chem. Commun.*, 2005, 4161–4163.

49   N. J. Wolford, S. B. Muñoz, P. G. N. Neate, W. W. Brennessel and M. L. Neidig, *Chem. Eur. J.*, 2021, **27**, 13651–13658.

50   D. J. Cardenas, *Angew. Chem. Int. Ed.*, 2003, **42**, 384–387.

51   T. Nagano and T. Hayashi, *Org. Lett.*, 2004, **6**, 1297–1299.

52   M. Nakamura, K. Matsuo, S. Ito and E. Nakamura, *J. Am. Chem. Soc.*, 2004, **126**, 3686–3687.

53   R. Martin and A. Fürstner, *Angew. Chem. Int. Ed.*, 2004, **43**, 3955–3957.

54   R. B. Bedford, M. Betham, D. W. Bruce, A. a Danopoulos, R. M. Frost and M. Hird, *Top. Curr. Chem.*, 2006, **219**, 1104–1110.

55   X. Wei, I. Abdiaj, C. Sambiagio, C. Li, E. Zysman-colman, J. Alcazar and T. Noel, *Angew. Chem. Int. Ed.*, 2019, **58**, 13030–13034.

56   K. Machitani, Y. Tanaka, Y. Nishiyama, A. Fujii, A. Saito and H. Mori, *J. Flow Chem.*, 2020,

10, 491–495.

57   G. Cahiez, G. Lefèvre, A. Moyeux, O. Guerret, E. Gayon, L. Guillonneau, N. Lefèvre, Q. Gu and E. Zhou, *Org. Lett.*, 2019, **21**, 2679–2683.

58   E. Bisz, M. Kardela, A. Piontek and M. Szostak, *Catal. Sci. Technol.*, 2019, **9**, 1092–1097.

59   X. Ma, H. Wang, Y. Liu, X. Zhao and J. Zhang, *ChemCatChem*, 2021, **13**, 5134–5140.

60   P. G. N. Neate, B. Zhang, J. Conforti, W. W. Brennessel and M. L. Neidig, *Org. Lett.*, 2021, **23**, 5958–5963.

61   S. H. Carpenter, T. M. Baker, S. B. Muñoz, W. W. Brennessel and M. L. Neidig, *Chem. Sci.*, 2018, **9**, 7931–7939.

62   M. Nakamura, S. Ito, K. Matsuo and E. Nakamura, *Synlett*, 2005, 1794–1798.

63   R. B. Bedford, M. Huwe and M. C. Wilkinson, *Chem. Commun.*, 2009, 600–602.

64   J. Clifton, E. R. M. Habraken, P. G. Pringle and I. Manners, *Catal. Sci. Technol.*, 2015, **5**, 4350–4353.

65   K. Wang, S. Chen, Y. Li, D. Li and H. Bao, *Chinese J. Org. Chem.*, 2021, **41**, 2707–2714.

66   K. Zhu, J. Dunne, M. P. Shaver and S. P. Thomas, *ACS Catal.*, 2017, **7**, 2353–2356.

67   R. Loska, C. Rao Volla and P. Vogel, *Adv. Synth. Catal.*, 2008, **350**, 2859–2864.

68   G. W. Waldhart and N. P. Mankad, *J. Organomet. Chem.*, 2015, **793**, 171–174.

69   H. Xiong, Y. Li, B. Qian, R. Wei and H. Bao, *Org. Lett.*, 2019, 8–11.

70   C. M. Rao Volla and P. Vogel, *Tetrahedron Lett.*, 2008, **49**, 5961–5964.

71   M. Carril, A. Correa and C. Bolm, *Angew. Chem. Int. Ed.*, 2008, **47**, 4862–4865.

72   K. S. Sindhu, A. P. Thankachan, A. M. Thomas and G. Anilkumar, *ChemistrySelect*, 2016, **1**, 556–559.

73   D. N. Sawant, P. J. Tambade, Y. S. Wagh and B. M. Bhanage, *Tetrahedron Lett.*, 2010, **51**, 2758–2761.

74   T. Hatakeyama, Y. Yoshimoto, T. Gabriel and M. Nakamura, *Org. Lett.*, 2008, **10**, 5341–5344.

75   X. Xie, X. Xu, H. Li, X. Xu, J. Yang and Y. Li, *Adv. Synth. Catal.*, 2009, **351**, 1263–1267.

76   T. Hatakeyama, Y. Okada, Y. Yoshimoto and M. Nakamura, *Angew. Chem. Int. Ed.*, 2011, **50**, 10973–10976.

77   R. Agata, S. Kawamura, K. Isozaki and M. Nakamura, *Chem. Lett.*, 2019, **48**, 238–241.

78   S. Kawamura, K. Ishizuka, H. Takaya and M. Nakamura, *Chem. Commun.*, 2010, **46**, 6054–6056.

79   R. B. Bedford, P. B. Brenner, E. Carter, J. Clifton, P. M. Cogswell, N. J. Gower, M. F.

Haddow, J. N. Harvey, J. A. Kehl, D. M. Murphy, E. C. Neeve, M. L. Neidig, J. Nunn, B. E. R. Snyder and J. Taylor, *Organometallics*, 2014, **33**, 5767–5780.

80   W. J. Shi, H. W. Zhao, Y. Wang, Z. C. Cao, L. S. Zhang, D. G. Yu and Z. J. Shi, *Adv. Synth. Catal.*, 2016, **358**, 2410–2416.

81   R. B. Bedford, M. A. Hall, G. R. Hodges, M. Huwe and M. C. Wilkinson, *Chem. Commun.*, 2009, 6430–6432.

82   T. Hatakeyama, T. Hashimoto, Y. Kondo, Y. Fujiwara, H. Seike, H. Takaya, Y. Tamada, T. Ono and M. Nakamura, *J. Am. Chem. Soc.*, 2010, **132**, 10674–10676.

83   T. Hatakeyama, T. Hashimoto, K. K. A. D. S. Kathriarachchi, T. Zenmyo, H. Seike and M. Nakamura, *Angew. Chem. Int. Ed.*, 2012, **51**, 8834–8837.

84   M. P. Crockett, C. C. Tyrol, A. S. Wong, B. Li and J. A. Byers, *Org. Lett.*, 2018, **20**, 5233–5237.

85   M. P. Crockett, A. S. Wong, B. Li and J. A. Byers, *Angew. Chem. Int. Ed.*, 2020, **59**, 5392–5397.

86   A. S. Wong, B. Zhang, B. Li, M. L. Neidig and J. A. Byers, *Org. Process Res. Dev.*, 2021, **25**, 2461–2472.

87   H. M. O'Brien, M. Manzotti, R. D. Abrams, D. Elorriaga, H. A. Sparkes, S. A. Davis and R. B. Bedford, *Nat. Catal.*, 2018, **1**, 429–437.

88   M. Jin, L. Adak and M. Nakamura, *J. Am. Chem. Soc.*, 2015, **137**, 7128–7134.

89   T. Iwamoto, C. Okuzono, L. Adak, M. Jin and M. Nakamura, *Chem. Commun.*, 2019, **55**, 1128–1131.

90   H. U. Blaser, *Rend. Lincei*, 2013, **24**, 213–216.

91   C. C. Tyrol, N. S. Yone, C. F. Gallin and J. A. Byers, *Chem. Commun.*, 2020, **56**, 14661–14664.

92   A. Piontek, E. Bisz and M. Szostak, *Angew. Chem. Int. Ed.*, 2018, **57**, 11116–11128.

93   N. Tewari, N. Maheshwari, R. Medhane, H. Nizar and M. Prasad, *Org. Process Res. Dev.*, 2012, **16**, 1566–1568.

94   R. Martin and S. L. Buchwald, *Acc. Chem. Res.*, 2008, **41**, 1461–1473.

95   R. B. Bedford, *Acc. Chem. Res.*, 2015, **48**, 1485–1493.

96   B. Bogdanovic and M. Schwickardi, *Angew. Chem. Int. Ed.*, 2000, **39**, 4610–4612.

97   A. Fürstner, R. Martin, H. Krause, G. Seidel, R. Goddard and C. W. Lehmann, *J. Am. Chem. Soc.*, 2008, **130**, 8773–8787.

98   R. B. Bedford, M. Betham, D. W. Bruce, S. A. Davis, R. M. Frost and M. Hird, *Chem.*

Commun., 2006, 1398.

99   R. B. Bedford, P. B. Brenner, E. Carter, P. M. Cogswell, M. F. Haddow, J. N. Harvey, D. M. Murphy, J. Nunn and C. H. Woodall, *Angew. Chem. Int. Ed.*, 2014, **53**, 1804–1808.

100   V. Wowk, L. Rousseau and G. Lefèvre, *Organometallics*, 2021, **40**, 3253–3266.

101   R. S. Smith and J. K. Kochi, *J. Org. Chem.*, 1976, **41**, 502–509.

102   S. B. Muñoz, S. L. Daifuku, W. W. Brennessel and M. L. Neidig, *J. Am. Chem. Soc.*, 2016, **138**, 7492–7495.

103   C. J. Adams, R. B. Bedford, E. Carter, N. J. Gower, M. F. Haddow, J. N. Harvey, M. Huwe, M. Á. Cartes, S. M. Mansell, C. Mendoza, D. M. Murphy, E. C. Neeve and J. Nunn, *J. Am. Chem. Soc.*, 2012, **134**, 10333–10336.

104   R. B. Bedford, T. Gallagher, D. R. Pye and W. Savage, *Synth.*, 2015, **47**, 1761–1765.

105   T. Hashimoto, T. Hatakeyama and M. Nakamura, *J. Org. Chem.*, 2012, **77**, 1168–1173.

106   S. L. Daifuku, M. H. Al-Afyouni, B. E. R. Snyder, J. L. Kneebone and M. L. Neidig, *J. Am. Chem. Soc.*, 2014, **136**, 9132–9143.

107   S. L. Daifuku, J. L. Kneebone, B. E. R. Snyder and M. L. Neidig, *J. Am. Chem. Soc.*, 2015, **137**, 11432–11444.

108   J. L. Kneebone, W. W. Brennessel and M. L. Neidig, *J. Am. Chem. Soc.*, 2017, **139**, 6988–7003.

109   R. Agata, H. Takaya, H. Matsuda, N. Nakatani, K. Takeuchi, T. Iwamoto, T. Hatakeyama and M. Nakamura, *Bull. Chem. Soc. Jpn.*, 2018, **92**, 381–390.

110   D. Noda, Y. Sunada, T. Hatakeyama, M. Nakamura and H. Nagashima, *J. Am. Chem. Soc.*, 2009, **131**, 6078–6079.

111   N. J. Bakas, J. D. Sears, W. W. Brennessel and M. L. Neidig, *Angew. Chem. Int. Ed.*, , DOI:10.1002/anie.202114986.

112   G. Cahiez, V. Habiak, C. Duplais and A. Moyeux, *Angew. Chem. Int. Ed.*, 2007, **46**, 4364–4366.

113   K. Ding, F. Zannat, J. C. Morris, W. W. Brennessel and P. L. Holland, *J. Organomet. Chem.*, 2009, **694**, 4204–4208.

114   S. B. Muñoz, S. L. Daifuku, J. D. Sears, T. M. Baker, S. H. Carpenter, W. W. Brennessel and M. L. Neidig, *Angew. Chem. Int. Ed.*, 2018, **57**, 6496–6500.

115   A. M. Messinis, S. L. J. Luckham, P. P. Wells, D. Gianolio, E. K. Gibson, H. M. O'Brien, H. A. Sparkes, S. A. Davis, J. Callison, D. Elorriaga, O. Hernandez-Fajardo and R. B. Bedford, *Nat. Catal.*, 2019, **2**, 123–133.

References

116   L. Rousseau, N. Touati, L. Binet, P. Thu and G. Lefe, *Inorg. Chem.*, 2021, **60**, 7991–7997.

117   S. H. Kyne, G. Lefe, C. Ollivier, M. Petit, R. Cladera and L. Fensterbank, *Chem. Soc. Rev.*, 2020, **49**, 8501–8542.

118   C. L. Sun, H. Krause and A. Fürstner, *Adv. Synth. Catal.*, 2014, **356**, 1281–1291.

119   G. Bauer, M. D. Wodrich, R. Scopelliti and X. Hu, *Organometallics*, 2015, **34**, 289–298.

120   T. Hatakeyama and M. Nakamura, *J. Am. Chem. Soc.*, 2007, **129**, 9844–9845.

121   Y. Y. Chua and H. A. Duong, *Chem. Commun.*, 2014, **50**, 8424–8427.

122   X. Yu, H. Zheng, H. Zhao, B. C. Lee and M. J. Koh, *Angew. Chem. Int. Ed.*, 2021, **60**, 2104–2109.

123   L. Yet, *Privileged Structures in Drug Discovery: Biaryls*, Wiley, Hoboken, 1st Ed., 2018.

124   A. Taheri Kal Koshvandi, M. M. Heravi and T. Momeni, *Appl. Organomet. Chem.*, 2018, **32**, 1–59.

125   V. L. Budarin, P. S. Shuttleworth, J. H. Clark and R. Luque, *Curr. Org. Synth.*, 2011, **7**, 614–627.

126   M. J. Buskes and M.-J. Blanco, *Molecules*, 2020, **25**, 3493–3515.

127   R. K. Arvela, N. E. Leadbeater, M. S. Sangi, V. A. Williams, P. Granados and R. D. Singer, *J. Org. Chem.*, 2005, **70**, 161–168.

128   P. Orecchia, D. S. Petkova, R. Goetz, F. Rominger, A. S. K. Hashmi and T. Schaub, *Green Chem.*, 2021, **23**, 8169–8180.

129   S. Ge and J. F. Hartwig, *Angew. Chemie*, 2012, **124**, 13009–13013.

130   S. K. Gurung, S. Thapa, A. Kafle, D. A. Dickie and R. Giri, *Org. Lett.*, 2014, **16**, 1264–1267.

131   S. D. Ramgren, L. Hie, Y. Ye and N. K. Garg, *Org. Lett.*, 2013, **15**, 3950–3953.

132   J. H. Li, J. L. Li and Y. X. Xie, *Synthesis (Stuttg).*, 2007, 984–988.

133   S. Thapa, B. Shrestha, S. K. Gurung and R. Giri, *Org. Biomol. Chem.*, 2015, **13**, 4816–4827.

134   Y. P. Budiman, A. Friedrich, U. Radius and T. B. Marder, *ChemCatChem*, 2019, **11**, 5387–5396.

135   H. A. Duong, W. Wu and Y. Y. Teo, *Organometallics*, 2017, **36**, 4363–4366.

136   S. Asghar, S. B. Tailor, D. Elorriaga and R. B. Bedford, *Angew. Chem. Int. Ed.*, 2017, **56**, 16367–16370.

137   C. R. LeBlond, A. T. Andrews, Y. Sun and J. R. Sowa, *Org. Lett.*, 2001, **3**, 1555–1557.

138   N. Shahnaz, B. Banik and P. Das, *Tetrahedron Lett.*, 2013, **54**, 2886–2889.

139   E. Silarska, A. M. Trzeciak, J. Pernak and A. Skrzypczak, *Appl. Catal. A Gen.*, 2013, **466**,

216–223.

140   L. Y. Xu, C. Y. Liu, S. Y. Liu, Z. G. Ren, D. J. Young and J. P. Lang, *Tetrahedron*, 2017, **73**, 3125–3132.

141   T. Hatakeyama, Y. Fujiwara, Y. Okada, T. Itoh, T. Hashimoto, S. Kawamura, K. Ogata, H. Takaya and M. Nakamura, *Chem. Lett.*, 2011, **40**, 1030–1032.

142   S. Kawamura and M. Nakamura, *Chem. Lett.*, 2013, **42**, 183–185.

143   R. B. Bedford, E. Carter, P. M. Cogswell, N. J. Gower, M. F. Haddow, J. N. Harvey, D. M. Murphy, E. C. Neeve and J. Nunn, *Angew. Chem. Int. Ed.*, 2013, **52**, 1285–1288.

144   M. Guisán-Ceinos, F. Tato, E. Buñuel, P. Calle and D. J. Cárdenas, *Chem. Sci.*, 2013, **4**, 1098–1104.

145   T. Agrawal and S. P. Cook, *Org. Lett.*, 2014, **16**, 5080–5083.

146   A. L. Silberstein, S. D. Ramgren and N. K. Garg, *Org. Lett.*, 2012, **14**, 3796–3799.

147   R. Agata, T. Iwamoto, N. Nakagawa, K. Isozaki, T. Hatakeyama, H. Takaya and M. Nakamura, *Synth.*, 2015, **47**, 1733–1740.

148   M. C. Perry, A. N. Gillett and T. C. Law, *Tetrahedron Lett.*, 2012, **53**, 4436–4439.

149   Z. Mo, Q. Zhang and L. Deng, *Organometallics*, 2012, **31**, 6518–6521.

150   S. K. Ghorai, M. Jin, T. Hatakeyama and M. Nakamura, *Org. Lett.*, 2012, **14**, 1066–1069.

151   Y. Y. Chua and H. A. Duong, *Chem. Commun.*, 2014, **50**, 8424–8427.

152   M. Jalal, B. Hammouti, R. Touzani, A. Aouniti and I. Ozdemir, *Mater. Today Proc.*, 2020, **31**, 122–129.

153   R. B. Bedford, M. Betham, D. W. Bruce, A. A. Danopoulos, R. M. Frost and M. Hird, *J. Org. Chem.*, 2006, **71**, 1104–1110.

154   L. Hintermann, *Beilstein J. Org. Chem.*, 2007, **3**, 2–6.

155   J. A. Przyojski, H. D. Arman and Z. J. Tonzetich, *Organometallics*, 2012, **31**, 3264–3271.

156   T. Hashimoto, S. Urban, R. Hoshino, Y. Ohki, K. Tatsumi and F. Glorius, *Organometallics*, 2012, **31**, 4474–4479.

157   H. Clavier and S. P. Nolan, *Chem. Commun.*, 2010, **46**, 841–861.

158   J. M. Berlin, K. Campbell, T. Ritter, T. W. Funk, A. Chlenov and R. H. Grubbs, *Org. Lett.*, 2007, **9**, 1339–1342.

159   L. Vieille-Petit, H. Clavier, A. Linden, S. Blumentritt, S. P. Nolan and R. Dorta, *Organometallics*, 2010, **29**, 775–788.

160   J. J. Dunsford, D. J. Evans, T. Pugh, S. N. Shah, N. F. Chilton and M. J. Ingleson, *Organometallics*, 2016, **35**, 1098–1106.

References

161   Q. Teng, W. Wu, H. A. Duong and H. V. Huynh, *Chem. Commun.*, 2018, **54**, 6044–6047.

162   M. Mayr, K. Wurst, K. H. Ongania and M. R. Buchmeiser, *Chem. Eur. J.*, 2004, **10**, 1256–1266.

163   S. K. Schneider, W. A. Herrmann and E. Herdtweck, *J. Mol. Catal. A Chem.*, 2006, **245**, 248–254.

164   I. Özdemir, S. Demir, B. Çetinkaya and E. Çetinkaya, *J. Organomet. Chem.*, 2005, **690**, 5849–5855.

165   T. Hatakeyama, S. Hashimoto, K. Ishizuka and M. Nakamura, *J. Am. Chem. Soc.*, 2009, **131**, 11949–11963.

166   Y. Chua and H. A. Duong, *Chem. Commun.*, 2016, **52**, 1466–1469.

167   J. A. Przyojski, K. P. Veggeberg, H. D. Arman and Z. J. Tonzetich, *ACS Catal.*, 2015, **5**, 5938–5946.

168   M. H. Al-Afyouni, K. L. Fillman, W. W. Brennessel and M. L. Neidig, *J. Am. Chem. Soc.*, 2014, **136**, 15457–15460.

169   N. J. Bakas and M. L. Neidig, *ACS Catal.*, 2021, **11**, 8493–8503.

170   E. Bisz, M. Koston and M. Szostak, *Green Chem.*, 2021, **23**, 7515–7521.

171   E. Bisz, M. Kardela and M. Szostak, *ChemCatChem*, 2019, 5733–5737.

172   M. E. Garner, S. Hohloch, L. Maron and J. Arnold, *Organometallics*, 2016, **35**, 2915–2922.

173   J. L. Martinez, S. L. Lutz, H. Yang, J. Xie, J. Telser, B. M. Hoffman, V. Carta, M. Pink, Y. Losovyj and J. M. Smith, *Science (80-.)*, 2020, **370**, 356–359.

174   J. J. Tang, X. Yu, Y. Yamamoto and M. Bao, *ACS Catal.*, 2021, **11**, 13955–13961.

175   L. M. Kumar, P. Mishra and B. R. Bhat, *Catal. Letters*, 2019, **149**, 1118–1124.

176   R. M. Ansari, L. K. Mahesh and B. R. Bhat, *Chinese J. Chem. Eng.*, 2019, **27**, 556–563.

177   L. M. Kumar, R. M. Ansari and B. R. Bhat, *Appl. Organomet. Chem.*, 2018, **32**, 1–8.

178   T. Kylmälä, A. Valkonen, K. Rissanen, Y. Xu and R. Franzén, *Tetrahedron Lett.*, 2009, **50**, 5692.

179   D. Bézier and C. Darcel, *Adv. Synth. Catal.*, 2009, **351**, 1732–1736.

180   L. M. Kumar and B. R. Bhat, *J. Organomet. Chem.*, 2017, **827**, 41–48.

181   R. M. Ansari and B. R. Bhat, *J. Chem. Sci.*, 2017, **129**, 1483–1490.

182   R. M. Ansari, L. M. Kumar and B. R. Bhat, *Russ. J. Coord. Chem. Khimiya*, 2018, **44**, 1–8.

183   A. Saroja and B. R. Bhat, *Ind. Eng. Chem. Res.*, 2019, **58**, 590–601.

184   S. B. Tailor, M. Manzotti, S. Asghar, B. J. S. Rowsell, S. L. J. Luckham, H. A. Sparkes and R. B. Bedford, *Organometallics*, 2019, **38**, 1770–1777.

185   S. B. Tailor and R. B. Bedford, *Catal. Letters*, 2020, **150**, 963–968.

186   M. Avanthay, R. B. Bedford, C. S. Begg, D. Böse, J. Clayden, S. A. Davis, J.-C. Eloi, G. P. Goryunov, I. V Hartung, J. Heeley, K. A. Khaikin, M. O. Kitching, J. Krieger, P. S. Kulyabin, A. J. J. Lennox, R. Nolla-Saltiel, N. E. Pridmore, B. J. S. Rowsell, H. A. Sparkes, D. V Uborsky, A. Z. Voskoboynikov, M. P. Walsh and H. J. Wilkinson, *Nat. Catal.*, 2021, **4**, 994–998.

187   J. K. Vinod, A. K. Wanner, E. I. James and K. Koide, *Nat. Catal.*, 2021, **4**, 999–1001.

188   Z. Novák, R. Adamik, J. T. Csenki, F. Béke, R. Gavaldik, B. Varga, B. Nagy, Z. May, J. Daru, Z. Gonda and G. L. Tolnai, *Nat. Catal.*, 2021, **4**, 991–993.

189   R. B. Bedford, M. Nakamura, N. J. Gower, M. F. Haddow, M. A. Hall, M. Huwe, T. Hashimoto and R. A. Okopie, *Tetrahedron Lett.*, 2009, 50, 6110–6111.

190   L. Xu, F. Y. Liu, Q. Zhang, W. J. Chang, Z. L. Liu, Y. Lv, H. Z. Yu, J. Xu, J. J. Dai and H. J. Xu, *Nat. Catal.*, 2021, **4**, 71–78.

191   T. Yoshida, L. Ilies and E. Nakamura, *ACS Catal.*, 2017, **7**, 3199–3203.

192   E. Vitaku, D. T. Smith and J. T. Njardarson, *J. Med. Chem*, 2014, **57**, 10257–10274.

193   Q. Lin, D. Meloni, Y. Pan, M. Xia, J. Rodgers, S. Shepard, M. Li, L. Galya, B. Metcalf, T. N. Yue, P. Liu and J. Zhou, *Org. Lett.*, 2009, **11**, 1999–2002.

194   A. M. Haydl, K. Xu and B. Breit, *Angew. Chem. Int. Ed.*, 2015, **54**, 7149–7153.

195   S. E. Webber, S. S. Canan-Koch, J. Tikhe, L. H. Thoresen, AGOURON PHARMA OP, Tricyclic Inhibitors of Poly(ADP-Ribose) Polymerases - US Patent 6,495,541B1, 2002.

196   S. E. Webber, S. S. Canan-Koch, J. Tikhe, L. H. Thoresen, AGOURON PHARMA OP, Tricyclic Inhibitors of Poly(ADP-Ribose) Polymerases - US Patent 6,977,298B2, 2005.

197   S. E. Webber, S. S. Canan-Koch, J. Tikhe, L. H. Thoresen, AGOURON PHARMA OP, Tricyclic Inhibitors of Poly(ADP-Ribose) Polymerases - US Patent 7,429,578B2, 2008.

198   L. Ürge, J. Alcazar, L. Huck and G. Dormán, *Annu. Rep. Med. Chem.*, 2017, **50**, 87–147.

199   Y. Lu, K. P. Cole, J. W. Fennell, T. D. Maloney, D. Mitchell, R. Subbiah and B. Ramadas, *Org. Process Res. Dev.*, 2018, **22**, 409–419.

200   M. O. Frederick and D. P. Kjell, *Tetrahedron Lett.*, 2015, **56**, 949–951.

201   M. Poratti and G. Marzaro, *Eur. J. Med. Chem.*, 2019, **172**, 143–153.

202   G. Erickson, J. Guo, M. McClure, M. Mitchell, M. C. Salaun and A. Whitehead, *Tetrahedron Lett.*, 2014, **55**, 6007–6010.

203   K. D. Collins and F. Glorius, *Nat. Chem.*, 2013, **5**, 597–601.

204   K. D. Collins, A. Rühling and F. Glorius, *Nat. Protoc.*, 2014, **9**, 1348–1353.

205   T. Gensch, M. Teders and F. Glorius, *J. Org. Chem.*, 2017, **82**, 9154–9159.

206   R. B. Bedford, P. B. Brenner, E. Carter, T. W. Carvell, P. M. Cogswell, T. Gallagher, J. N. Harvey, D. M. Murphy, E. C. Neeve, J. Nunn and D. R. Pye, *Chem. Eur. J.*, 2014, **20**, 7935–7938.

207   J. J. Dunsford, I. A. Cade, K. L. Fillman, M. L. Neidig and M. J. Ingleson, *Organometallics*, 2014, **33**, 370–377.

208   J. J. Dunsford, E. R. Clark and M. J. Ingleson, *Dalt. Trans.*, 2015, **44**, 20577–20583.

209   H. Motohashi, M. Kato and K. Mikami, *J. Org. Chem.*, 2019, **84**, 6483–6490.

210   A. A. Danopoulos, P. Braunstein, M. Wesolek, K. Y. Monakhov, P. Rabu and V. Robert, *Organometallics*, 2012, **31**, 4102–4105.

211   B. Blom, G. Tan, S. Enthaler, S. Inoue, J. D. Epping and M. Driess, *J. Am. Chem. Soc.*, 2013, **135**, 18108–18120.

212   H. Zhang, Z. Ouyang, Y. Liu, Q. Zhang, L. Wang and L. Deng, *Angew. Chem. Int. Ed.*, 2014, **53**, 8432–8436.

213   T. Hashimoto, R. Hoshino, T. Hatanaka, Y. Ohki and K. Tatsumi, *Organometallics*, 2014, **33**, 921–929.

214   Z. Mo, Z. Ouyang, L. Wang, K. L. Fillman, M. L. Neidig and L. Deng, *Org. Chem. Front.*, 2014, **1**, 1040–1044.

215   Z. Ouyang, J. Du, L. Wang, J. L. Kneebone, M. L. Neidig and L. Deng, *Inorg. Chem.*, 2015, **54**, 8808–8816.

216   T. Hashimoto, R. Hoshino, T. Hatanaka, Y. Ohki and K. Tatsumi, *Organometallics*, 2014, **33**, 2–10.

217   H. Zhang, Z. Ouyang, Y. Liu, Q. Zhang, L. Wang and L. Deng, *Angew. Chem. Int. Ed.*, 2014, **53**, 8432–8436.

218   F. A. Harraz, S. E. El-hout, H. M. Killa and I. A. Ibrahim, *J. Catal.*, 2012, **286**, 184–192.

219   A. Monfared, R. Mohammadi and S. Ahmadi, *RSC Adv.*, 2019, **9**, 3185–3202.

220   J. I. Ayogu and E. A. Onoabedje, *Chem. Open*, 2021, **10**, 430–450.

221   M. Szekeres, Y. T, K. Farkas and I. Földesi, *nanomaterials*, 2018, **8**, 776–795.

222   M. J. Bonder, Y. Zhang, K. L. Kiick, V. Papaefthymiou and G. C. Hadjipanayis, *J. Magn. Magn. Mater.*, 2007, **311**, 658–664.

223   J. F. Sonnenberg, N. Coombs, P. A. Dube and R. H. Morris, *J. Am. Chem. Soc.*, 2012, **134**, 5893–5899.

224   M. Neamtu, C. Nadejde, V. Hodoroaba and R. J. Schneider, *Sci. Rep.*, 2018, 1–11.

References

225   R. H. Crabtree, *Chem. Rev.*, 2012, **112**, 1536–1554.

226   R. Wolf, A. Jacobi and V. Wangelin, *Green Chem.*, 2015, **17**, 1408–1413.

227   E. V Anslyn and D. A. Dougherty, *Modern Physical Organic Chemistry*, University Science Books, Sausalito, 1st edn., 2006.

228   J. Burés, *Angew. Chem. Int. Ed.*, 2016, **55**, 16084–16087.

229   C. D. T. Nielsen and J. Burés, *Chem. Sci.*, 2019, **10**, 348–353.

230   J. Burés, *Angew. Chem. Int. Ed.*, 2016, **55**, 2028–2031.

231   R. Pagni, *J. Chem. Educ.*, 2006, **83**, 387.

232   L. P. Hammett, *J. Am. Chem. Soc.*, 1936, **125**, 96–103.

233   C. Hansch, A. Leo and R. W. Taft, *Chem. Rev.*, 1991, **91**, 165–195.

234   X. Creary and S. Mcdonald, *J. Org. Chem.*, 1987, **52**, 3254–3263.

235   A. Gualandi, L. Mengozzi and P. G. Cozzi, *Asian J. Org. Chem.*, 2017, **6**, 1160–1179.

236   C. Sandford, L. R. Fries, T. E. Ball, S. D. Minteer and M. S. Sigman, *J. Am. Chem. Soc.*, 2019, **141**, 18877–18889.

237   M. Ahlquist and P. Norrby, *Society*, 2007, 550–553.

238   A. Hedström, U. Bollmann, J. Bravidor and P. O. Norrby, *Chem. Eur. J.*, 2011, **17**, 11991–11993.

239   J. A. Cadge, J. F. Bower and C. A. Russell, *Angew. Chem. Int. Ed.*, 2021, **60**, 24976–24983.

240   M. Puri, S. Gatard, D. A. Smith and O. V. Ozerov, *Organometallics*, 2011, **30**, 2472–2482.

241   P. M. Pérez-García, A. Darù, A. R. Scheerder, M. Lutz, J. N. Harvey and M. E. Moret, *Organometallics*, 2020, **39**, 1139–1144.

242   M. R. Hurst, L. N. Zakharov and A. K. Cook, *Chem. Sci.*, 2021, **12**, 13045–13060.

243   S. E. Denmark, R. C. Smith and W. T. T. Chang, *Tetrahedron*, 2011, **67**, 4391–4396.

244   M. S. Driver and J. F. Hartwig, *J. Am. Chem. Soc.*, 1997, **119**, 8232–8245.

245   A. Hedström, Z. Izakian, I. Vreto, C. J. Wallentin and P. O. Norrby, *Chem. Eur. J.*, 2015, **21**, 5946–5953.

246   J. F. Hartwig, *Organotransition Metal Chemistry: From Bonding to Catalysis*, University Science Books, Sausalito, 6th Ed., 2010.

247   J. W. Grissom and T. L. Calkins, *J. Org. Chem.*, 1993, **58**, 5422–5427.

248   K. K. Wang, H. R. Zhang and J. L. Petersen, *J. Org. Chem.*, 1999, **64**, 1650–1656.

249   S. E. Lindahl, H. Park, M. Pink and J. M. Zaleski, *J. Am. Chem. Soc.*, 2013, **135**, 3826–3833.

250   L. Nurdin, W. E. Piers, J. Bin Lin and B. S. Gelfand, *Organometallics*, 2020, **39**, 2269–2277.

251   W. A. Pryor, J. tau Gu and D. F. Church, *J. Org. Chem.*, 1985, **50**, 185–189.

252   K. Furusawa, T. Kawamura, Y. Akutsu, M. Arai and M. Tamura, *Atmos. Environ.*, 1997, **31**, 3363–3367.

253   M. Rosselin, B. Tuccio, P. Pério, F. A. Villamena, P. Fabre and G. Durand, *Electrochim. Acta*, 2016, **193**, 231–239.

254   K. B. Bahari, D. J. Deodhar, M. M. Hesabi, J. Hill, M. Kosmirak, A. M'Hamedi and A. Morley, *J. Chem. Soc. Perkin Trans. 1*, 1994, **19**, 2393–2398.

255   M. Ochiai, T. Shu, T. Nagaoka and Y. Kitagawa, *J. Org. Chem.*, 1997, **62**, 2130–2138.

256   A. Nagaki, A. Miyazaki and J. I. Yoshida, *Macromolecules*, 2010, **43**, 8424–8429.

257   X. Zhang, *J. Mol. Struct.*, 2011, **1002**, 121–127.

258   R. M. Ward and J. M. Schomaker, *J. Org. Chem.*, 2021, **86**, 8891–8899.

259   M. Scherübl, C. G. Daniliuc and A. Studer, *Angew. Chem. Int. Ed.*, 2021, **60**, 711–715.

260   M. R. Brennan, D. Kim and A. R. Fout, *Chem. Sci.*, 2014, **5**, 4831–4839.

261   X. Jiang, J. Zhang and S. Ma, *J. Am. Chem. Soc.*, 2016, **138**, 8344–8347.

262   D. C. Eisenberg, C. J. C. Lawrie, A. E. Moody and J. R. Norton, *J. Am. Chem. Soc.*, 1991, **113**, 4888–4895.

263   L. N. Bochkarev, N. E. Molosnova, L. N. Zakharov, G. K. Fukin, A. I. Yanovsky and Y. T. Struchkov, *Acta Crystallogr. Sect. C Cryst. Struct. Commun.*, 1995, **51**, 489–491.

264   S. Oh and Y. Lee, *Organometallics*, 2016, **35**, 1586–1592.

265   M. Mohadjer Beromi, G. W. Brudvig, N. Hazari, H. M. C. Lant and B. Q. Mercado, *Angew. Chem. Int. Ed.*, 2019, **58**, 6094–6098.

266   H. Defrancesco, J. Dudley and A. Coca, *ACS Symp. Ser.*, 2016, **1236**, 1–25.

267   C. Sandford and V. K. Aggarwal, *Chem. Commun.*, 2017, **53**, 5481–5494.

268   J. W. B. Fyfe and A. J. B. Watson, *Chem*, 2017, **3**, 31–55.

269   H. C. Brown and G. Zweifel, *J. Am. Chem. Soc.*, 1959, **81**, 247.

270   K. Burgess and M. J. Ohlmeyer, *Chem. Rev.*, 1991, **91**, 1179–1191.

271   S. P. Thomas and V. K. Aggarwal, *Angew. Chem. Int. Ed.*, 2009, **48**, 1896–1898.

272   M. Suginome, *Chem. Rec.*, 2010, **10**, 348–358.

273   Y. Ye, J. Liu, B. Xu, S. Jiang, R. Bai, S. Li, T. Xie and X. Y. Ye, *Chem. Sci.*, 2021, **12**, 13209–13215.

274   R. L. Melen, L. C. Wilkins, B. M. Kariuki, H. Wadepohl, L. H. Gade, A. S. K. Hashmi, D. W. Stephan and M. M. Hansmann, *Organometallics*, 2015, **34**, 4127–4137.

275   S. C. Ren, F. L. Zhang, J. Qi, Y. S. Huang, A. Q. Xu, H. Y. Yan and Y. F. Wang, *J. Am. Chem. Soc.*, 2017, **139**, 6050–6053.

276   J. R. Sanzone, C. T. Hu and K. A. Woerpel, *J. Am. Chem. Soc.*, 2017, **139**, 8404–8407.

277   Y. Cheng, C. Mück-Lichtenfeld and A. Studer, *J. Am. Chem. Soc.*, 2018, **140**, 6221–6225.

278   J. A. Gurak, K. S. Yang, Z. Liu and K. M. Engle, *J. Am. Chem. Soc.*, 2016, **138**, 5805–5808.

279   K. S. Yang, J. A. Gurak, Z. Liu and K. M. Engle, *J. Am. Chem. Soc.*, 2016, **138**, 14705–14712.

280   Z. Liu, T. Zeng, K. S. Yang and K. M. Engle, *J. Am. Chem. Soc.*, 2016, **138**, 15122–15125.

281   T. Zeng, Z. Liu, M. A. Schmidt, M. D. Eastgate and K. M. Engle, *Org. Lett.*, 2018, **20**, 3853–3857.

282   O. Daugulis, J. Roane and L. D. Tran, *Acc. Chem. Res.*, 2015, **48**, 1053–1064.

283   Z. Liu, J. Chen, H. X. Lu, X. Li, Y. Gao, J. R. Coombs, M. J. Goldfogel and K. M. Engle, *Angew. Chem. Int. Ed.*, 2019, **58**, 17068–17073.

284   Z. Liu, H. Q. Ni, T. Zeng and K. M. Engle, *J. Am. Chem. Soc.*, 2018, **140**, 3223–3227.

285   W. Wang, C. Ding, Y. Li, Z. Li, Y. Li, L. Peng and G. Yin, *Angew. Chem. Int. Ed.*, 2019, **58**, 4612–4616.

286   W. Wang, C. Ding and G. Yin, *Synlett*, 2019, **30**, 1850–1854.

287   W. Wang, C. Ding, H. Pang and G. Yin, *Org. Lett.*, 2019, 2–5.

288   P. Zhang, C. Zou, Q. Zhao and C. Zhang, *Org. Chem. Front.*, 2021, **8**, 2589–2594.

289   Y. Li, H. Pang, D. Wu, Z. Li, W. Wang, H. Wei, Y. Fu and G. Yin, *Angew. Chem. Int. Ed.*, 2019, **58**, 8872–8876.

290   K. M. Logan, S. R. Sardini, S. D. White and M. K. Brown, *J. Am. Chem. Soc.*, 2018, **140**, 159–162.

291   H. Xu, P. B. White, C. Hu and T. Diao, *Angew. Chem. Int. Ed.*, 2017, **56**, 1535–1538.

292   S. R. Sardini, A. L. Lambright, G. L. Trammel, H. M. Omer, P. Liu and M. K. Brown, *J. Am. Chem. Soc.*, 2019, **141**, 9391–9400.

293   L. A. Chen, A. R. Lear, P. Gao and M. K. Brown, *Angew. Chem. Int. Ed.*, 2019, **58**, 10956–10960.

294   H. Li, J. Long, Y. Li, W. Wang, H. Pang and G. Yin, *European J. Org. Chem.*, 2021, **2021**, 1424–1428.

295   G. L. Trammel, R. Kuniyil, P. F. Crook, P. Liu and M. K. Brown, *J. Am. Chem. Soc.*, 2021, **143**, 16502–16511.

296   A. K. Simlandy, S. R. Sardini and M. K. Brown, *Chem. Sci.*, 2021, **12**, 5517–5521.

297   A. Parra, A. López, S. Díaz-Tendero, L. Amenós, J. L. G. Ruano and M. Tortosa, *Synlett*, 2015, **26**, 494–500.

References

298 I. Kageyuki, I. Osaka, K. Takaki and H. Yoshida, *Org. Lett.*, 2017, **19**, 830–833.

299 K. B. Smith, Y. Huang and M. K. Brown, *Angew. Chem. Int. Ed.*, 2018, **57**, 6146–6149.

300 S. Akiyama, N. Oyama, T. Endo, K. Kubota and H. Ito, *J. Am. Chem. Soc.*, 2021, **143**, 5260–5268.

301 H. Yoshida, I. Kageyuki and K. Takaki, *Org. Lett.*, 2013, **15**, 952–955.

302 I. Kageyuki, H. Yoshida and K. Takaki, *Synth.*, 2014, **46**, 1924–1932.

303 W. Su, T.-J. Gong, X. Lu, M.-Y. Xu, C.-G. Yu, Z.-Y. Xu, H.-Z. Yu, B. Xiao and Y. Fu, *Angew. Chemie*, 2015, **127**, 13149–13153.

304 F. Meng, F. Haeffner and A. H. Hoveyda, *J. Am. Chem. Soc.*, 2014, **136**, 11304–11307.

305 T. W. Butcher, E. J. McClain, T. G. Hamilton, T. M. Perrone, K. M. Kroner, G. C. Donohoe, N. G. Akhmedov, J. L. Petersen and B. V. Popp, *Org. Lett.*, 2016, **18**, 6428–6431.

306 J. C. Green, M. V. Joannou, S. A. Murray, J. M. Zanghi and S. J. Meek, *ACS Catal.*, 2017, **7**, 4441–4445.

307 Y. Huang, K. B. Smith and M. K. Brown, *Angew. Chem. Int. Ed.*, 2017, **56**, 13314–13318.

308 K. B. Smith, K. M. Logan, W. You and M. K. Brown, *Chem. Eur. J.*, 2014, **20**, 12032–12036.

309 K. Semba and Y. Nakao, *J. Am. Chem. Soc.*, 2014, **136**, 7567–7570.

310 K. M. Logan, K. B. Smith and M. K. Brown, *Angew. Chem. Int. Ed.*, 2015, **54**, 5228–5231.

311 T. Jia, P. Cao, B. Wang, Y. Lou, X. Yin, M. Wang and J. Liao, *J. Am. Chem. Soc.*, 2015, **137**, 13760–13763.

312 B. Chen, P. Cao, X. Yin, Y. Liao, L. Jiang, J. Ye, M. Wang and J. Liao, *ACS Catal.*, 2017, **7**, 2425–2429.

313 K. B. Smith and M. Kevin Brown, *J. Am. Chem. Soc.*, 2017, **139**, 7721–7724.

314 K. M. Logan and M. K. Brown, *Angew. Chem. Int. Ed.*, 2017, **56**, 851–855.

315 K. Semba, Y. Ohtagaki and Y. Nakao, *Tetrahedron Lett.*, 2021, **72**, 153059–153064.

316 K. Semba, Y. Ohtagaki and Y. Nakao, *Org. Lett.*, 2016, **18**, 3956–3959.

317 A. E. Allen and D. W. C. MacMillan, *Chem. Sci.*, 2012, **3**, 633–658.

318 S. M. Inamdar, V. S. Shinde and N. T. Patil, *Org. Biomol. Chem.*, 2015, **13**, 8116–8162.

319 N. Nakagawa, T. Hatakeyama and M. Nakamura, *Chem. Eur. J.*, 2015, **21**, 4257–4261.

320 D. J. Durand and N. Fey, *Chem. Rev.*, 2019, **119**, 6561–6594.

321 T. R. Kégl, R. M. B. Carrilho and T. Kégl, *J. Organomet. Chem.*, 2020, **924**, 121462–121469.

322 R. B. Bedford, P. B. Brenner, E. Carter, T. Gallagher, D. M. Murphy and D. R. Pye, *Organometallics*, 2014, **33**, 5940–5943.

323   V. Pace, P. Hoyos, L. Castoldi, P. Domínguez De María and A. R. Alcántara, *ChemSusChem*, 2012, **5**, 1369–1379.

324   C. J. Clarke, W. C. Tu, O. Levers, A. Bröhl and J. P. Hallett, *Chem. Rev.*, 2018, **118**, 747–800.

325   D. F. Aycock, *Org. Process Res. Dev.*, 2007, **11**, 156–159.

326   E. . Morgan, *Endeavour*, 1990, 14, 148.

327   A. H. Johnstone, *J. Chem. Technol. Biotechnol.*, 2007, **50**, 294–295.

328   J. R. Wagner, E. M. Mount and H. F. Giles, *Extrusion, Chapter 25 - Design of Experiments*, 2nd edn., 2014.

329   A. Sethuramiah and R. Kumar, *Statistics and Experimental Design in Perspective*, 2016.

330   R. Leardi, *Anal. Chim. Acta*, 2009, **652**, 161–172.

331   P. M. Murray, F. Bellany, L. Benhamou, D. K. Bučar, A. B. Tabor and T. D. Sheppard, *Org. Biomol. Chem.*, 2016, **14**, 2373–2384.

332   A. Nadin, C. Hattotuwagama and I. Churcher, *Angew. Chem. Int. Ed.*, 2012, **51**, 1114–1122.

333   M. D. Delost, D. T. Smith, B. J. Anderson and J. T. Njardarson, *J. Med. Chem.*, 2018, **61**, 10996–11020.

334   J. Wang, M. Sánchez-Roselló, J. L. Aceña, C. Del Pozo, A. E. Sorochinsky, S. Fustero, V. A. Soloshonok and H. Liu, *Chem. Rev.*, 2014, **114**, 2432–2506.

335   A. S. Travis, *Manufacture and Uses of the Anilines: A Vast Array of Processes and Products*, 2007.

336   L. Adak, T. Hatakeyama and M. Nakamura, *Bull. Chem. Soc. Jpn.*, 2021, **94**, 1125–1141.

337   H. A. Duong, W. Wu and Y.-Y. Teo, *Organometallics*, 2017, **36**, 4363–4366.

338   C. P. Delaney, V. M. Kassel and S. E. Denmark, *ACS Catal.*, 2019, 73–80.

339   Y. Makida, E. Marelli, A. M. Z. Slawin and S. P. Nolan, *Chem. Commun.*, 2014, **50**, 8010–8013.

340   Y. Na, S. Park, S. B. Han, H. Han, S. Ko and S. Chang, *J. Am. Chem. Soc.*, 2004, **126**, 250–258.

341   N. R. Srinivas, R. H. Barbhaiya and K. K. Midha, *J. Pharm. Sci.*, 2001, **90**, 1205–1215.

342   J. H. Kim and A. R. Scialli, *Toxicol. Sci.*, 2011, **122**, 1–6.

343   A. Pfaltz and W. J. Drury, *Proc. Natl. Acad. Sci. U. S. A.*, 2004, **101**, 5723–5726.

344   G. Desimoni, G. Faita and K. A. Jørgensen, *Chem. Rev.*, 2006, **106**, 3561–3651.

345   X. Liu, L. Lin and X. Feng, *Acc. Chem. Res.*, 2011, **44**, 574–587.

346   N. Kim, J. T. Han, D. H. Ryu and J. Yun, *Org. Lett.*, 2017, **19**, 6144–6147.

347   A. J. Arduengo, H. V. Rasika Diaz, L. V. Harlow and M. Kilne, *J. Am. Chem. Soc*, 1992,

114, 5530–5534.

348 H. Kinuta, M. Tobisu and N. Chatani, *J. Am. Chem. Soc.*, 2015, **137**, 1593–1600.

349 J. Berlin, R. Grubbs, S. Yann, and C. Stewart, Organometallic Ruthenium Complexes and Related Methods for the Preparation of Tetra-Substituted and Other Hindered Olefins, US 8008224 B2, 2011, .

350 J. A. Przyojski, H. D. Arman and Z. J. Tonzetich, *Organometallics*, 2012, **31**, 3264–3271.

351 J. Kim, J. Choi, K. Shin and S. Chang, *J. Am. Chem. Soc.*, 2012, **134**, 2528–2531.

352 J. Hu, Y. Zhao, J. Liu, Y. Zhang and Z. Shi, 2016, **4**, 8718–8722.

353 N. Dastbaravardeh, M. Schnürch and M. D. Mihovilovic, *Org. Lett.*, 2012, **14**, 1930–1933.

354 Q. Liu, W. Zhang, X. Zhao and Z. Zhao, *European J. Org. Chem.*, 2013, 1253–1261.

355 X. Yang and Z. Wang, *Organometallics*, 2014, **33**, 5863–5873.

356 J. Zeng, K. M. Liu and X. F. Duan, *Org. Lett.*, 2013, **15**, 5342–5345.

357 S. Wang, F. Ren, Y. Qiu and M. Luo, *J. Organomet. Chem.*, 2015, **788**, 27–32.

358 L. Huang, L. K. G. Ackerman, K. Kang, A. M. Parsons and D. J. Weix, *J. Am. Chem. Soc.*, 2019, **141**, 10978–10983.

359 F. Mo, D. Qiu, Y. Jiang, Y. Zhang and J. Wang, *Tetrahedron Lett.*, 2011, **52**, 518–522.

360 R. J. Key, J. M. M. Tengco, M. D. Smith and A. K. Vannucci, , DOI:10.1021/acs.organomet.9b00082.

361 V. G. Haensch, T. Neuwirth, J. Steinmetzer, F. Kloss, R. Beckert, S. Grafe, S. Kupfer and C. Hertweck, *Chem. Eur. J.*, 2019, **25**, 16068–16073.

362 M. Baghbanzadeh, C. Pilger and C. O. Kappe, *J. Org. Chem.*, 2011, **76**, 1507–1510.

363 F. Hu and X. Lei, *Tetrahedron*, 2014, **70**, 3854–3858.

364 C. I. Tra, C. M. L. Delpiccolo and E. G. Mata, 2014, 16–19.

365 K. Chen, W. Chen, X. Yi, W. Chen, M. Liu and H. Wu, *Chem. Commun.*, 2019, **55**, 9287–9290.

366 J. M. Quibell, G. Duan, G. J. P. Perry and I. Larrosa, *Chem. Commun.*, 2019, **55**, 6445–6448.

367 Y. Monguchi, T. Hattori, Y. Miyamoto, T. Yanase, Y. Sawama and H. Sajiki, *Adv. Synth. Catal.*, 2012, **354**, 2561–2567.

368 Y. Sun, H. Jiang, W. Wu, W. Zeng and X. Wu, *Org. Lett.*, 2013, **15**, 1598–1601.

369 A. Xia, X. Qi, X. Mao, X. Wu, X. Yang, R. Zhang, Z. Xiang and Z. Lian, *Org. Lett.*, 2019, **21**, 3028–3033.

370 M. A. Hussain and F. A. Khan, *Tetrahedron Lett.*, 2019, **60**, 151040.

371   R. K. Saunthwal, M. Patel and A. K. Verma, *J. Org. Chem.*, 2016, **81**, 6563–6572.

372   E. Bratt, O. Verho, M. J. Johansson and J.-E. Bäckvall, *J. Org. Chem.*, 2014, **79**, 3946–3954.

373   T. Markovic, B. N. Rocke, D. C. Blakemore, V. Mascitti and M. C. Willis, *Org. Lett.*, 2017, **19**, 6033–6035.

374   D. Xue, Z. Jia, C. Zhao, Y. Zhang and C. Wang, *Chem. Eur. J.*, 2014, **20**, 2960–2965.

375   M. Buden, J. F. Guastavino and R. A. Rossi, *Org. Lett.*, 2013, **15**, 1174–1177.

376   G. Ranjani and R. Nagarajan, *Org. Lett.*, 2017, **19**, 3974–3977.

377   P. Li, L. Wang, L. Zhang and G. Wang, *Adv. Synth. Catal.*, 2012, **354**, 1307–1318.

378   S. Zhu, Y. Xiao, Z. Guo and H. Jiang, *Org. Lett.*, 2013, **15**, 898–901.

379   W. Tang, W. Yuan, B. Zhao, H. Zhang, F. Xiong, L. Jing and D. Qin, *J. Organomet. Chem.*, 2013, **743**, 147–155.

380   R. Ambre, H. Yang, W. Chen, G. P. A. Yap and T. Jurca, *European J. Org. Chem.*, 2019, **2**, 3511–3517.

381   X. Li, J. Zhang, Y. Geng and Z. Jin, *J. Org. Chem.*, 2013, **78**, 5078–5084.

382   H. Ke, X. Chen and G. Zou, *J. Org. Chem.*, 2014, **79**, 7132–7140.

383   Z. Yiqing, Y. Wei, S. K. B. and B. M. Kevin, *Angew. Chem. Int. Ed.*, 2014, **53**, 3475–3479.

384   Y. Zhou, W. You, K. B. Smith and M. K. Brown, *Angew. Chem. Int. Ed.*, 2014, **53**, 3475–3479.

385   Y. Li, W. Liu, Q. Tian, Q. Yang and C. Kuang, *European J. Org. Chem.*, 2014, 3307–3312.